SCHOOL OF APPLIED CHEMISTRY

MODELLING AND KINETICS ESTIMATION IN GIBBSITE PRECIPITATION FROM CAUSTIC ALUMINATE SOLUTIONS

Tian Siong LI

"This thesis is presented as part of the requirements for the award of the Degree of Doctor of Philosophy of the Curtin University of Technology"

NOVEMBER 2000

I declare that the work as presented in this thesis, is my own except as acknowledged in the text, and has not been submitted either in whole or in part, for a degree at this or any other institution.

Tian Siong LI

ACKNOWLEDGEMENTS

I would like to thank a number of people for their help during the course of this research. I express my deepest gratitude to my supervisors Dr Dean Ilievski and Dr Andrew Rohl for giving me the opportunity to undertake this research with them, for their invaluable advice, direction, discussions and encouragement throughout the course of this research, and proof reading this thesis.

Special thanks also go to

Professor E.T. White for his valuable discussions on the subject of uncertainty estimation during his brief visit to CSIRO Minerals at Waterford in Perth;

Dr Iztok Livk for his involvement and contributions to the kinetics estimation studies in this research, particularly for performing the non-linear parameter optimisation in Chapter 9;

Staff of the Precipitation Technology group at CSIRO Minerals in Perth. Judy McShane and David Rossiter for performing a number of the batch and constant composition experiments studied in Chapters 5, 8 and 9; Dianne Bedell for her help in performing a number of the batch precipitation experiments, conducting liquor composition analysis and SEM analysis; and Mark Schibeci for his help in operating the Coulter counter multisizer; and

The Australian Postgraduate Award with stipend (APAWS) and the AJ Parker CRC for Hydrometallurgy Research Scholarship for financial support.

Finally, I would like to thank my family, particularly my parents, for giving me the opportunity to study in Australia, for their encouragement, help and support.

PUBLICATIONS FROM THESIS RESEARCH

Li, T.S. and Ilievski, D. 1999, 'Gibbsite crystallisation kinetics estimates from different crystalliser configurations', in the proceedings of the *14th International Symposium on Industrial Crystallisation*, Cambridge, UK, 1999, paper 128.

Li, T.S., Rohl, A.L. and Ilievski, D. 2000, 'Modelling a constant supersaturation precipitator', in *Mixing and crystallisation*, ed. B. Sen Gupta and S. Ibrahim, Kluwer Academic Publishers, Dordrecht, pp227-241.

Li, T.S., Rohl, A.L. and Ilievski, D. 2000, 'An investigation on the uncertainty in batch gibbsite precipitation experimental data', in the proceedings of the *28th Australasian Chemical Engineering Conference* (*Chemeca 2000*), Perth, Australia, 2000, paper 151.

Li, T.S., Livk, I. and Ilievski, D. 2000, 'The influence of crystalliser configuration on the accuracy and precision of gibbsite crystallisation kinetics estimates', *Chemical Engineering Science*, accepted for publication.

Li, T.S., Rohl, A.L. and Ilievski, D. 2000, 'Modelling non-stationary gibbsite precipitation systems: Sources of error and their propagation', *Chemical Engineering Science*, accepted for publication.

Li, T.S., Livk, I. and Ilievski, D. 2000, 'Influence of the estimation procedure on the accuracy and precision of aluminium trihydroxide crystallisation kinetics from dynamics data', *Industrial and Engineering Chemistry Research*, accepted for publication.

ABSTRACT

Precipitation of gibbsite from supersaturated caustic aluminate solutions has been investigated extensively due to its central role in the commercial Bayer plant, for extracting the alumina compound from bauxite. The primary focus of Bayer process simulation and optimisation is to help maximise the product recovery and the production of a product crystal size distribution (CSD) that meets the product specification and improves downstream process performance. The product CSD is essentially determined by the nucleation, growth and agglomeration kinetics, which occur simultaneously during the precipitation process. These processes are still poorly understood, owing to the high complexity of their mechanisms and of the structure of the caustic aluminate solutions.

This research focuses on the modelling and kinetics estimation aspects of simulating gibbsite precipitation. Population balance theory was used to derive different laboratory gibbsite precipitator models, and the discretised population balance models of Hounslow, Ryall & Marshall (1988) and Litster, Smit & Hounslow (1995) were employed to solve the resulting partial integro-differential equations. Gibbsite kinetics rates were determined from literature correlation models and also estimated from the CSD data using the, so-called, differential method. Modelling of non-stationary gibbsite precipitation systems showed that error propagated with the precipitation time scale. The main contribution to the observed error was found to be from the uncertainties in the kinetic parameter estimates, which are estimated from experimental data and used in the simulation. This result showed that care is required when simulating the CSD of non-stationary precipitators over longer time scales, and methods that produce precise estimates of the kinetics rates from the experimental data need to be used.

Kinetics estimation study from repeated batch gibbsite precipitation data showed that the uncertainty in the experimental data coupled with the error incurred from the

kinetic parameter estimation procedure used, resulted in large uncertainties in the kinetics estimates. The influences of the experimental design and the kinetics estimation technique on the accuracy and precision of estimates of the nucleation, growth and agglomeration kinetics for the gibbsite precipitation system were investigated. It was found that the operating conditions have a greater impact on the uncertainties in the estimated kinetics than does the precipitator configuration. The kinetics estimates from the integral method, i.e. non-linear parameter optimisation method, describe the gibbsite precipitation data better than those obtained by the differential method. However, both kinetics estimation techniques incurred significant uncertainties in the kinetics estimates, particularly toward the end of the precipitation runs where the kinetics rates are slow. The uncertainties in the kinetics estimates are strongly correlated to the magnitude of kinetics values and are dependent on the change in total crystal numbers and total crystal volume.

Batch gibbsite precipitation data from an inhomogeneously-mixed precipitator were compared to a well-mixed precipitation system operated under the same operating conditions, i.e. supersaturation, seed charge, seed type, mean shear rate and temperature. It was found that the gibbsite agglomeration kinetic estimates were significantly different, and hence, the product CSD, but the gibbsite growth rates were similar. It was also found that a compartmental model approach cannot fully account for the differences in suspension hydrodynamics, and resulted in unsatisfactorily CSD predictions of the inhomogeneously-mixed precipitator. This is attributed to the coupled effects of local energy dissipation rate and solids phase mixing on agglomeration process.

TABLE OF CONTENTS

LIST OF FIGURES

LIST OF TABLES

CHAPTER 1

INTRODUCTION

Precipitation of gibbsite, a polymorph of aluminium trihydroxide, from caustic aluminate solutions is arguably the most important step of the Bayer process employed in commercial alumina plants, for recovering alumina from bauxite. The Bayer process has been in use since its development by Karl Joseph Bayer back in 1888. The gibbsite precipitation process is extraordinarily slow and is a critical factor controlling the rate of alumina production from an operating alumina plant.

The main considerations in the precipitation process are (1) the recovery of the crystalline product from the caustic aluminate solutions, and (2) the product crystal size distribution (CSD). These two factors affect the economics of the process. Hence, the primary focus of Bayer process simulation is to meet these requirements. Predicting the product yield is relatively simple, generally done via mass and energy balances, but predicting the product CSD is more difficult, as the product CSD is determined by the simultaneous occurrence of a number of processes, i.e. nucleation, growth and agglomeration.

The two important steps in developing the precipitator model for predicting the product CSD, are the formulation and solution of the mathematical model capable of describing the process, and the estimation of the kinetics rates to be incorporated in the model. The population balance (PB) theory has been widely used for deriving mathematical models for laboratory and industrial precipitators.

Most crystallisation and precipitation simulation studies rely on empirical models of the kinetics, due to a lack of understanding of their mechanisms. The empirical models usually correlate the kinetics rates to the process variables that are the most influential on the kinetic mechanisms.

Despite enormous efforts invested into studying the gibbsite precipitation system in the last few decades, the fundamental understanding of the process mechanisms involve in the precipitation remains incomplete. This is attributed to the complex structure of the caustic aluminate solutions, intricate process mechanisms, the induction period phenomenon, and the difficulty of measuring the mechanisms accurately. The best known studies undertaken to investigate the mechanisms of nucleation, growth and agglomeration in gibbsite precipitation system are the experimental studies of Misra (1970), Misra and White (1971a; 1971b), Sakamoto, Kanehara & Matsushita (1971), White and Wright (1971), Brown (1972a; 1972b; 1975), Low (1975), Halfon and Kaliaguine (1976a; 1976b), White and Bateman (1988), Ilievski (1991), Veesler and Boistelle (1993; 1994), Ilievski and White (1994a; 1994b; 1995) and Ilievski and Hounslow (1995). However, much of the work is qualitative and some findings are contradictory. Most of the experimental studies were performed in batch operation, even though the common commercial Bayer plants are continuous operation. The batch operation has several advantages over the continuous operation, it is less complex to perform, requires less inventories of materials, less time and investment, and large number of data of different conditions (i.e. supersaturation) can be obtained in a single run. Hence, batch configuration is often employed in the laboratory research for kinetics studies.

There are differences and contradictions between the gibbsite kinetics estimates reported by different authors. White and Bateman (1988), Veesler and Boistelle (1994) and Muhr et al. (1997) all reported the discrepancy in the published gibbsite growth rates. Low (1975) and Ilievski and White (1994a; 1994b; 1995) reported different gibbsite agglomeration mechanisms. Similarly, the experimental gibbsite secondary nucleation studies of Misra and White (1971a), Halfon and Kaliaguine (1976a) and Loh, Ang & Kirke (1988) showed some contradictions. Li, Livk & Ilievski (2000a) proposed that these differences may be due to inconsistencies in the methods used by those authors to estimate the respective kinetics.

The current work is motivated by the need to explain the differences in precipitation kinetic parameters reported in the literature for this system, and to investigate the effect of uncertainties in the kinetic parameters on CSD simulation. The specific issues under consideration in the current research are

(1) the applicability of the PB theory in describing well-mixed gibbsite precipitation system;
(2) the uncertainty in the experimental precipitation data, and consequently the uncertainties in the kinetics estimates;
(3) the impact of the uncertainties in the kinetics estimates on CSD simulation;
(4) the influence of the precipitator configuration and kinetics estimation technique on the accuracy and precision of the kinetics estimates;
(5) the influence of an inhomogeneous suspension on gibbsite precipitation, i.e. precipitation kinetics and product CSD; and
(6) options for incorporation of hydrodynamics into the precipitator model.

This thesis comprises four parts. The first part consists of Chapters 2 to 4, which give a review of the gibbsite precipitation system, PB theory, precipitator modelling and precipitation kinetics estimation techniques. The second part, consisting of Chapters 5 and 6, demonstrates the applicability of the PB model to simulate well-mixed precipitation system with different configurations, and investigates the issue of error propagation in modelling the precipitators. Chapters 7 to 9 focus on kinetics estimation issues such as, the uncertainty in the experimental precipitation data, and the influence of precipitator configuration and estimation technique on the accuracy and precision of the kinetics estimates. Finally, Chapters 10 and 11 include a review on mixing models and an experimental study of an inhomogeneously-mixed suspension batch gibbsite precipitation, respectively.

The work undertaken in this thesis was part of a larger AJ Parker Cooperative Research Centre for Hydrometallurgy effort to improve precipitator modelling and kinetics estimation. Work not performed by the author is acknowledged where appropriate in the text.

CHAPTER 2

BAYER PRECIPITATION OF ALUMINIUM TRIHYDROXIDE

2.1 INTRODUCTION

Aluminium trihydroxide, $Al(OH)_3$, is one of the two groups of crystalline aluminium hydroxides reported in the literature. The other group is the monohydrates, AlO(OH). The four main polymorphic forms of the trihydroxides are gibbsite (γ-$Al(OH)_3$), bayerite, d-$Al(OH)_3$ and nordstrandite, and the two common polymorphs of the monohydrates are boehmite and diaspore (Misra 1970; Schoen and Roberson 1970).

Precipitation of aluminium hydroxide from supersaturated caustic aluminate solutions (i.e. under Bayer precipitation conditions) has been studied and reported extensively in the literature. Misra (1970) and Ilievski (1991) reviewed most of the studies prior to the 1990s. Under the Bayer process conditions, bayerite, gibbsite and boehmite may be present. Reports have been made on the conditions such as, pH and temperature that favour one form over the others, their stability and inter-conversion processes (Oomes, de Boer & Lippens 1961; Ginsberg, Huttig & Stiehl 1962; Chistyakova 1964; Schoen and Roberson 1970; Sato 1984; van Straten and de Bruyn 1984).

The aluminium trihydroxide precipitation experiments conducted in the current work and those used from other sources were generated under Bayer conditions at temperatures between 60-80 °C. Numerous experimental studies on aluminium trihydroxide precipitation have reported that gibbsite is the trihydroxide polymorph forms primarily at the temperature ranges between 40-100 °C (Ginsberg, Huttig &

Stiehl 1962; Sakamoto 1963; Sato 1984; van Straten and de Bruyn 1984; Lee et al. 1997). This chapter reviews briefly the current state of knowledge of the precipitation of gibbsite from supersaturated caustic aluminate solutions.

2.2 PRECIPITATION OF GIBBSITE

In order for a precipitation to occur, a solution must be supersaturated, that is the concentration of the solute must in excess of the saturation or equilibrium concentration. Bulk precipitation will not take place if the solution is saturated or undersaturated. The equilibrium concentration of a solution at any given temperature is determined from the solubility curve.

2.2.1 Solubility of $Al(OH)_3$ in Caustic Aluminate Solutions

Caustic aluminate solutions are commonly prepared by the dissolution of aluminium hydroxide in aqueous sodium hydroxide solutions. There have been numerous studies on speciation in these solutions, using various analytical techniques such as, potentiometry, Infra-red, nuclear magnetic resonance, Raman, UV-Vis and X-ray diffraction spectroscopies (Lippincot, Psellos & Tobin 1952; Moolenaar, Evans & McKeever 1970; Zámbó 1986; Radnai et al. 1998; Sipos et al. 1998), and molecular dynamic modelling (Gale et al. 1998; Watling et al. 1998). There still remains considerable uncertainty in regards to which aluminate species exist in the caustic aluminate solutions. In general, many investigators agree that $Al(OH)_4^-$ ions exist in dilute caustic aluminate solutions, and the dissolution of aluminium trihydroxide may be represented by

$$Al(OH)_3 + OH^- \; Al(OH)_4^- \qquad (2.1)$$

However, there is evidence that species such as, AlO_2^-, $AlO(OH)_2$, $Al_2O(OH)_6^{2-}$ and other poly-aluminium species exist in caustic aluminate solutions (Moolenaar, Evans & McKeever 1970; Zámbó 1986; Radnai et al. 1998). The existence of some of the species depends on the solution concentrations.

Solubility studies of $Al(OH)_3$ in caustic aluminate solutions have been performed by Pearson (1955), Misra (1970), McCoy and Dewey (1982), Chaubal (1990) and Rosenberg and Healy (1996). The equilibrium aluminate species concentration is determined by temperature and caustic concentration. The aluminate species concentration, A, is expressed as g L^{-1} Al_2O_3, and the caustic concentration, C, is expressed as either g L^{-1} Na_2O or g L^{-1} Na_2CO_3 following the common terminology used in either European or North America industrial practice, respectively. Misra (1970) extensively reviewed the solubility studies of caustic aluminate solutions, and derived the following correlation from the available solubility data for synthetic caustic aluminate liquor in the literature,

$$A^* = C\exp\left(6.2106 - \frac{2486.7}{T} + \frac{1.08753C}{T}\right) \tag{2.2}$$

where A^* is the equilibrium aluminate species concentration in g L^{-1} Al_2O_3, C is the caustic concentration in g L^{-1} Na_2O and T is the temperature in K. This correlation is derived for the caustic concentration range of 30-230 g L^{-1} Na_2O and the temperature range of 298-373 K, and it has a 95% confidence limits of ±15%.

Rosenberg and Healy (1996) derived a more compliant $Al(OH)_3$ solubility correlation that is applicable for both synthetic and plant liquors, which has the form

$$A^* = 0.96197C\left(1 + \frac{10^{(-9.2082\sqrt{I}(1+\sqrt{I})+0.8743I-0.2149I^{\frac{3}{2}})}}{\exp(\frac{\Delta G}{RT})}\right)^{-1} \tag{2.3}$$

where C is the caustic concentration in g L^{-1} Na_2CO_3, ΔG is the Gibbs energy of dissolution and has a value of –30.96 kJ mol^{-1}, R is the ideal gas constant and T is the temperature. The ionic strength, I, in the caustic aluminate solution can be evaluated from the simplified expression derived by Rosenberg and Healy (1996). For the caustic aluminate liquor containing sodium carbonate as impurity, the ionic strength, I, can be expressed as

$$I = 0.01887C + 0.01911SC \quad (2.4)$$

where SC is the concentration of sodium carbonate in g L^{-1}.

2.2.2 Precipitation Mechanisms

Precipitation of gibbsite from caustic aluminate solution involves process mechanisms such as, nucleation, growth and agglomeration. These mechanisms often take place simultaneously. Apart from these mechanisms, other processes such as, breakage or attrition may also occur during the precipitation process.

2.2.2.1 Nucleation

Nucleation is the process of formation of new crystals in solution, and can be classified as either primary or secondary. Primary nucleation describes the nucleation mechanisms when no solute crystals are present, and is termed homogeneous when nucleation occurs spontaneously in a solution free of any particles, and termed heterogeneous when non-solute particles are present. Secondary nucleation on the other hand describes the nucleation mechanism that requires the presence of suspended solute crystals.

It has been reported that the nucleation is strongly dependent on the supersaturation (i.e. concentration driving force), which is closely linked to the solubility of the precipitation system. At high solubilities and low supersaturation, the nucleation mechanism is likely to be secondary or heterogeneous, and at low solubilities and high supersaturation homogeneous nucleation is favoured (Mersmann 1995). However, spontaneous homogeneous nucleation will not occur unless the supersaturation is above the metastable limit. Supersaturated solutions above this limit are said to be labile (i.e. unstable) and are termed metastable if below this limit, and require seeding to promote precipitation (Mullin 1993).

Nucleation is not well understood in most precipitation processes. Many of the difficulties are due to the lack of suitable techniques and instrumentation to accurately measured the negligible size of nuclei, and preparation of impurities free solution. Qualitative fundamental studies on nucleation in the Bayer precipitation

have been performed by Pearson (1955), Kuznetsov (1963), Scott (1963), Glastonbury (1969), Misra and White (1971a; 1971b), Brown (1972a; 1972b; 1975; 1977), Halfon and Kaliaguine (1976a), Loh, Ang & Kirke (1988) and Rossiter et al. (1998). However, the knowledge of the nucleation mechanism remains limited and contradictory.

Several explanations have been suggested to explain the secondary nucleation mechanism in gibbsite precipitation. Pearson (1955) and Scott (1963) stated that broken fragments formed by attrition of the seed crystals could be the main source of new crystals. Misra and White (1971b) argued that this is only valid at high agitation intensity, and does not explain the generation of fines at low temperature and agitation rates. Brown (1972a; 1972b) suggested that nucleation depends on supersaturation and initial seeding (i.e. total seed surface area), and the nucleation mechanism is closely associated with crystal growth via a surface nucleation mechanism. Brown (1977) further proposed that the aluminium ion clusters diminish in size as temperature rises, and the breakdown of clusters is completed above 75 °C. Misra and White (1971a), Brown (1975; 1977), Loh, Ang & Kirke (1988) and Ilievski (1991) all reported that there is negligible nucleation at temperature above 75 °C. Misra and White (1971a) proposed the following relation for gibbsite secondary nucleation

$$B^o = k_b s^2 A_T \tag{2.5}$$

which has a square dependence on supersaturation, $s = (A\text{-}A^*)$, and a first order dependence on the total crystal surface area, A_T. The nucleation rate constant, k_b, depends on the precipitation environment. However, this correlation was derived based on five experimental data sets. Misra and White (1971a) stated that further experiments need to be done in order to assess if the reported empirical orders of the supersaturation and the total surface area above are appropriate to describe gibbsite secondary nucleation in general.

2.2.2.2 Growth

Crystal growth is the process where solute is deposited from a supersaturated solution onto crystal surfaces. The growth process is believed to involve two successive steps, which are (1) transportation of the solute or solute cluster from bulk solution to the crystal surface and (2) surface reaction that integrates the new material into the crystal lattice (King 1973; Chaubal 1990). The growth rate can be a mass transfer step or a surface reaction step (i.e. surface integration). In most cases, one of the steps is rate controlling. In those where both steps offer significant resistance, Garside (1971) introduced an effectiveness factor, η_r, defined in Equation (2.6), as a measure of the relative importance of each. As η_r approaches 1, the surface integration step becomes dominant.

$$\eta_r = \frac{\text{measured growth rate}}{\text{growth rate if surface integration controlled}} \tag{2.6}$$

In practice, the commonly used empirical model for the growth rate is expressed as

$$G = k_g s^g \tag{2.7}$$

where k_g and g are the growth rate constant and the empirical order of the supersaturation, s = (A-A^*), respectively. Note that the growth rate is normally defined as the change in crystal size with time (see Chapter 3 for further details).

There are a large number of studies on gibbsite crystal growth reported in the literature. Gibbsite growth is extraordinary slow (i.e. a few microns per hour) and exhibits a marked dependence on temperature, supersaturation (Pearson 1955; Misra and White 1971a; King 1973; Veesler and Boistelle 1993; Ilievski and White 1994a), and caustic concentration (White and Bateman 1988). In general, gibbsite growth is correlated to the temperature and supersaturation according to the relation in Equation (2.7), and the growth rate constant, k_g, is expressed as an Arrhenius equation to give

$$G = k_G \exp\left(-\frac{\Delta E}{RT}\right) s^2 \tag{2.8}$$

which has a square dependence on supersaturation, ΔE is the activation energy, R is the gas constant, and T is the temperature. The term k_G may be a function of process conditions and chemical species in the solution. Misra and White (1971a) and White and Bateman (1988) reported that the growth of gibbsite is surface reaction controlled, due to the low growth rate at high supersaturation, the high growth rate activation energies, and the negligible effect of agitation on the growth rate. Misra and White (1971a) found that gibbsite growth rate is independent of crystal size, that is, crystals growth at relatively similar rates irrespective of their sizes. White and Wright (1971) showed that size dispersion effects in gibbsite precipitation are negligible.

A number of gibbsite growth rate equations have been reported in the literature, in which supersaturation are expressed in different functional forms of concentration. The most frequently used expression is the concentration difference, $(A\text{-}A^*)$, where A and A^* are aluminate and equilibrium aluminate concentrations, respectively. Table 2.1 shows some of the supersaturation expressions used in the published gibbsite growth rate equations.

Table 2.1. Published supersaturation expressions and activation energies for gibbsite growth rates.

Source	s	ΔE (kJ mol^{-1})
Misra and White (1971a)	$(A\text{-}A^*)$	59.9 ± 6
King (1973)	$(A\text{-}A^*)/FC$	53.2 ± 12
Low (1975)	$(A\text{-}A^*)$	62.4 ± 12
Overbey and Scott (1978)	$(A\text{-}A^*)/(C+A^*)$	83.1
Mordini and Cristol (1982)	$C(A\text{-}A^*)$	79
White and Bateman (1988)	$(A/C\text{-}A^*/C)/C^{1/4}$	70.7 ± 7
Audet and Larocque (1989)	$(A\text{-}A^*)$	77.3 ± 6
Veesler and Boistelle (1994)	$A/A^*\text{-}1$	120.7
Muhr et al. (1997)	$(A\text{-}A^*)$	67.9
Cornell et al. (1999)	$\ln(A/A^*)^{\dagger}$	141
Harris et al. (1999)	$(A\text{-}A^*)$	51 ± 5

Note: † The empirical order of the supersaturation is 3;
C is caustic concentration; and
FC is free caustic concentration.

There is large variation in the reported activation energy, ΔE, for the growth rate equations in Table 2.1. This is likely due to the uncertainty in the experimental measurements, and the different supersaturation expressions used. These large variations in ΔE result in different k_G values in Equation (2.8), and hence, the growth rates. Ilievski and White (1994a) collected the available growth rate data for pure caustic aluminate liquors in the literature, and re-structured the Arrhenius equation centred at temperature of 70 °C and caustic concentration of 100 g L^{-1} Na_2O, and derived the following correlation

$$G = \frac{15}{\sqrt{C/100}} \exp\left[-7600\left(\frac{1}{T} - \frac{1}{343.16}\right)\right] s^2 \qquad (2.9)$$

where the supersaturation is expressed as

$$s = \left(\frac{A - A^*}{C}\right) \qquad (2.10)$$

The 95% confidence limits of the correlation are within ±50%, and ΔE has a value of 63.2 kJ mol^{-1}.

Veesler and Boistelle (1993) pointed out that the solubility of the aluminate is greatly affected by the caustic concentration. Thus expressing the supersaturation in terms of concentration differences in the growth rate equation limits its applicability to the specific range of caustic concentration used to derive the rate equation. Hence, that may be why the published growth rate equations are not applicable to a wider caustic concentration range. They reconciled the differences between the published growth rates at different caustic concentrations by normalising the caustic effect using the relative concentration, $(A\text{-}A^*)/A^*$. They showed that all growth rates measured at different caustic concentrations lie on a single curve when the supersaturation is expressed in relative concentration.

A number of microscopic studies of gibbsite crystal growth have been reported. Lee and Parkinson (1999) investigated the growth of single gibbsite crystals by *in situ* optical microscopy. They found that growth of the (110) prismatic face is via spiral growth. The basal face grows via the birth and spread mechanism when the relative supersaturation is above 0.67 and via spiral growth below this value. Freij et al. (1999) investigated the kinetics and surface evolution of single crystals growing at 80 °C, using both *in situ* optical microscopy and *ex situ* atomic microscopy techniques. They found that at a low relative supersaturation of 0.43, the basal face grows via a step flow mechanism, via birth and spread at a relative supersaturation of 1.0, and by both mechanisms at a relative supersaturation of 0.71.

Harris et al. (1999) employed the dynamic light scattering technique to characterise nucleation and growth processes in unseeded synthetic Bayer liquors. The technique is based on the variations of the light intensity scattered from crystals in a suspension over time. Information on the numbers and diameters of the crystals may be obtained by monitoring the intensity of the scattered light and short-term fluctuations in it, respectively. Comparisons were made between gibbsite nuclei growth in the nanometer range and gibbsite crystal growth in the micrometer range. They concluded that the growth of nuclei less than 200 nm is dominated by agglomeration or Ostwald ripening and larger nuclei are by single crystal growth. Roach, Cornell & Griffin (1998) reported on the application of a new scanning electron microscopic technique, known as charge contrast imaging, which enables the growth history of a gibbsite crystal to be studied. They suggested that growth of gibbsite on different faces can be directly measured and the presence of secondary nucleation can also be detected.

2.2.2.3 Agglomeration

Agglomeration is the process where smaller particles collide and adhere, eventually forming a stable new particle or agglomerate. It is the dominant size enlargement mechanism in gibbsite precipitation system, due to the extraordinary slow growth rate. The agglomeration of gibbsite crystals in caustic aluminate solutions has been studied by Misra (1970), Sakamoto, Kanehara & Matsushita (1971), Low (1975), Halfon and Kaliaguine (1976b), Ilievski and White (1994b; 1995), Veesler, Roure &

Boistelle (1994), Ilievski and Hounslow (1995) and Seyssiecq et al. (1998). The mechanism for gibbsite agglomeration is not well understood, but it is believed to be a two sequential step process, suggested by the experimental results of Misra (1970) and Low (1975), which are

(1) shear induced collisions between particles lead to the formation of loosely bound aggregates; and
(2) cementation of loose aggregates by deposition from solution, which eventually forming a stable agglomerate.

White (1988) reported that gibbsite crystal agglomeration is favoured by low agitation level, high supersaturation, high seed charge and fines crystal sizes. He also stated that it is difficult to generate agglomerates larger than 50 μm in practice, and that larger agglomerates increase their size by further crystal growth. Scott (1963) and Low (1975) reported that agglomeration is favoured at high growth rates, which suggests the importance of the cementation process.

The mechanism of agglomeration is described by the agglomeration kernel, $\beta(t,v,\xi)$. There are different forms of the agglomeration kernel to describe the different process conditions thought to cause the agglomeration. Sastry (1975) proposed that the agglomeration kernel consist of two terms as

$$\beta(t,v,\xi) = \beta_o f(v,\xi) \tag{2.11}$$

The term β_o depends on operating conditions (eg. supersaturation, fluid viscosity, temperature and stirrer speed) which controls the extent of agglomeration. While the term $f(v,\xi)$ is a function of crystal sizes v and ξ, which controls the shape of the resultant crystal size distribution (CSD).

In the literature, a number of theoretical and empirical models have been proposed to describe the agglomeration mechanisms under different process environments. The common models are those describing collision mechanisms under the condition of

Brownian motion, laminar shear, turbulent diffusion, turbulent inertia, gravitational settling, and some empirical kernels derived for analytical convenience. Some of the proposed agglomeration kernels are shown in Table 2.2.

Table 2.2. Some of the proposed agglomeration kernels published in the literature.

Agglomeration kernel	Description
$\beta_o(v^{1/3}+\xi^{1/3})(v^{-1/3}+\xi^{-1/3})$	Brownian motion (Smoluchowski 1917)
$\beta_o(v^{1/3}+\xi^{1/3})^3$	Laminar Shear (Smoluchowski 1917) Turbulent Diffusion (Low 1975)
$\beta_o(v^{1/3}+\xi^{1/3})^2\lvert v^{1/3}-\xi^{1/3}\rvert$	Gravitational settling, L>50μm (Berry 1967)
$\beta_o(v-\xi)^2/(v+\xi)$	Semi empirical kernel (Thompson 1968)
$\beta_o(v^{1/3}+\xi^{1/3})^2\lvert v^{2/3}-\xi^{2/3}\rvert$	Gravitational settling, L<50μm (Drake 1972)
$\beta_o(v^{1/3}+\xi^{1/3})^2(v^{2/3}-\xi^{2/3})$	Turbulent Inertia (Drake 1972)
β_o	Size independent or random coalescence
$\beta_o(v.\xi)$	Product kernel
$\beta_o(v+\xi)$	Sum kernel
$\beta_o(v^{1/3}+\xi^{1/3})^\gamma$	Empirical kernel, 2 parameter (Ilievski 1991)
$\beta_o(v^{1/3}+\xi^{1/3})^\gamma.(v^{-1/3}+\xi^{-1/3})^\lambda$	Empirical kernel, 3 parameter (Ilievski 1991)

These kernels are described in detail in Drake (1972), Hartel and Randolph (1986a; 1986b), Ilievski and White (1994a) and Smit, Hounslow & Paterson (1994). A number of investigations have tried to infer an agglomeration kernel that best describes the agglomeration mechanism involved. The approaches employed for selecting the agglomeration kernel include (1) finding a kernel that best fits the experimental CSD (Hartel and Randolph 1986b; Hounslow 1990c; Ilievski and White 1994a; 1995; Ilievski and Hounslow 1995); (2) using self-preserving theory (Ilievski and White 1994a); and (3) using the inverse problem method (Muralidar and Ramkrishna 1986).

Low (1975) derived a model for gibbsite agglomeration by theoretical considerations of particle collisions in a turbulent flow system. He proposed that the collisions of particles entrained within the turbulent eddies are due to diffusion, which is similar to the laminar shear model of Smoluchowski (1917). His agglomeration model has a strong dependency on the crystal size. Halfon and Kaliaguine (1976b) assumed a

functional form for their agglomeration model and then determined the parameters of best fit. Their model shows gibbsite agglomeration is independent of crystal size. Perhaps the most extensive studies on characterising the gibbsite agglomeration kernel and thus the agglomeration mechanism are those of Ilievski and White (1994a; 1995) and Ilievski and Hounslow (1995). They utilised three independent methods, which include

(1) determining which agglomeration kernel consistently results in the best fit to 200 sets of data available;
(2) matching the shape of the self-preserving CSD with functional forms derived from population balance models with different agglomeration kernels; and
(3) a novel technique employing doped gibbsite "tracer" crystals, and a two dimensional population balance model.

They demonstrated that gibbsite agglomeration is either size independent, or that the size dependency is so weak that it may be considered size independent for modelling purposes.

Halfon and Kaliaguine (1976b) derived a correlation model for the agglomeration kernel from batch experimental data at 60 °C and found that the agglomeration kernel has a fourth order dependence on supersaturation.

$$\beta = k_A s^4 \tag{2.12}$$

where k_A is the agglomeration rate constant and depends on the hydrodynamic conditions. Remillard, Cloutier & Methot (1980) also inferred that the agglomeration kernel has a fourth order dependence on supersaturation in their studies of alumina precipitation. Ilievski and White (1994b) proposed a correlation model for gibbsite agglomeration,

$$\beta = k_H s^4 \left(\frac{P}{V}\right)^{-1.4} \tag{2.13}$$

where $k_H = 0.05 \pm 0.01$, s is supersaturation in g $L^{-1}Al_2O_3$/ g $L^{-1}Na_2O$ and P/V is the power per unit volume in kg s^{-3} m^{-1}. The 95% confidence limits on the estimates are ± 70%. This correlation is applicable between the P/V range of 22-1420 kg s^{-3} m^{-1}, the temperatures range of 75-78 °C and s of 0.93-0.99 g $L^{-1}Al_2O_3$/ g $L^{-1}Na_2O$.

The agglomeration kernels proposed in Table 2.2 do not reveal the mechanism on how the loose aggregates are held together in supersaturated solutions to form stable agglomerates through cementation. One explanation is that loose aggregates are held together by van der Waals forces with short range repulsion due to the hydration barrier layer or the electrical double layer, or both. Thus, increasing the solution ionic strength may increase the aggregation rate (Hartel and Randolph 1986b; Hounslow 1990c; Ilievski 1991; David, Marchal & Marcant 1995).

Mumtaz et al. (1997) stated that when crystals collide in a supersaturated solution, they temporarily adhere to each other, and due to precipitation at the point of contact, a bridge between the crystals is formed. This bridge must withstand the stress induced by hydrodynamic drag in order to form stable agglomerates. They reported that the cementation process is diffusion controlled, and agglomeration is dependent on shear rate and solution ionic strength. They also suggested that not all shear induced collisions are successful in forming an aggregate, and incorporated an overall aggregation efficiency of collisions, η, to the shear induced agglomeration kernel as

$$\beta = \eta \beta_o f(v, \xi) \tag{2.14}$$

2.2.2.4 Crystal Breakage and Attrition

Crystal breakage is the process where crystals rupture into two or more parts, resulting in the parent crystal losing its identity. Attrition, on the other hand, is the chipping off of small fragments from the crystal surface following collisions between crystals, as well as between crystal and impeller and finally between crystal and precipitator wall. But in this case the parent crystal retains its identity (Misra 1970).

Crystal breakage is only significant at very high agitation rates, and in practice, the agitation rates employed in both the laboratory and in industrial precipitators are kept as low as possible to avoid breakage. This is because it is difficult to distinguish between fines generated by nucleation and the fragments resulting from crystal breakage, and hence, complicates the CSD analysis in the precipitation process.

2.2.3 Induction Period

Ilievski, Zheng & White (1989) reported that during the precipitation of gibbsite from seeded supersaturated caustic aluminate solutions in a laboratory precipitator, there is a period where no noticeable change in the solution supersaturation and solids content is observed. This period is referred to as the induction period, and is also defined as the period between the seed addition to the liquor and the onset of measurable precipitation (Smith and Woods 1993).

The induction time has been proposed to be a period of surface preparation (Brown 1972a; 1972b; 1977; Halfon and Kaliaguine 1976a). Ilievski, Zheng & White (1989) showed that the induction period can be reduced by seeding fresh liquor with growing crystals, a technique referred to as cross-fertilisation. This further suggests that the seed surface is conditioned during the induction period.

Brown (1972a; 1972b) found from his scanning electron microscopy (SEM) studies that a fine structure can be seen developing on the crystal surface during the induction period. Smith and Woods (1993) provided SEM micrographs that clearly indicate the appearance of precipitated material onto seed crystal surfaces during the induction period. Lee, Parkinson & Tsukamoto (1999) employed the dynamic light scattering technique to investigate the kinetics of gibbsite crystal growth during the induction period. They suggested that crystal growth follows the polynuclear birth and spread model during the induction period before the onset of secondary nucleation.

The mechanism of the induction phenomenon is not clear. Misra (1970), Misra and White (1971b), Brown (1972a; 1972b; 1977), Ilievski, Zheng & White (1989), Smith and Woods (1993) and Smith, Austin & Ilievski (1995) have studied the induction

time in seeded caustic aluminate solutions. The induction time has been reported to depend on the initial supersaturation, initial seed surface and temperature. Brown (1972a) reported that impurities lengthen the induction time by impeding the absorption of aluminate ions on the surface. Brown (1977) derived a correlation model for the induction time,

$$\log_{10}\theta = C(I) - 3\times10^{-4}T^2 - 0.76A_o^{0.3} - 4.8\log_{10}s \qquad (2.15)$$

where θ is the induction time in minutes, $C(I)$ is a function of impurity type and concentration, T is the temperature in °C, A_o is the seed surface area in $m^2\ L^{-1}$, and s is the supersaturation.

Brown (1972a; 1972b) noted that the induction period is most noticeable when seed charges are low and supersaturation is high. He also suggested that the generation of nuclei coincides with the end of the induction period. This theory is supported by the increase in turbidity that corresponds to the birth of nuclei at the end of the induction period (Smith and Woods 1993). Ilievski, Zheng & White (1989) performed an experimental study to deduce an induction time model that incorporated the effects of supersaturation, surface area and temperature, which they found to be

$$\theta = \exp(K_\theta)A_o^\alpha s^\varepsilon \exp\left(\frac{p}{T+273}\right) \qquad (2.16)$$

with K_θ = -29 ± 5, α = -0.4 ± 0.04, ε = - 3.5 ± 0.3, p = 11000 ± 2000 K. The errors are the 95% confidence levels. They then combined the effect of supersaturation and temperature to relate the induction time to the initial growth rate G_o, which is calculated from Equation (2.9). The correlation model becomes

$$\theta = \exp(K_g)A_o^\alpha G_o^g \qquad (2.17)$$

where K_g = 9 ± 0.5, α = -0.4 ± 0.04 and g = -1.7 ± 0.2.

2.3 CONCLUSIONS

Precipitation of aluminium trihydroxide under Bayer conditions has been reviewed. Most reported findings agreed that gibbsite is the most likely trihydroxide polymorph formed under the Bayer precipitation conditions between 40-80 °C. Despite the long history of the Bayer precipitation process and the considerable research effort devoted to investigate this particular precipitation system, a fundamental understanding of the precipitation process remains incomplete. The lack of understanding of this process can be attributed to the highly complex nature of caustic aluminate solutions, and the complexity of the precipitation phenomena involved. These are demonstrated by the inconclusive findings reported in the literature in regards to which aluminate species exist in the caustic aluminate solutions, and the unexplained mechanisms for nucleation, growth and agglomeration and the induction time period.

CHAPTER 3

POPULATION BALANCE MODELLING OF PRECIPITATION SYSTEMS

3.1 INTRODUCTION

Modelling of dispersed phase particulate systems such as, aerosols, colloids or precipitation requires the properties of the particles that characterise the systems to be specified. A particle is characterised by properties such as, size, shape, surface area, mass, and composition. In precipitation systems, we are interested in how the crystal size and total number of crystals change with time. As the system involves large numbers of crystals with different sizes, a mathematical formulation, known as the crystal size distribution, is often used to describe how crystals are distributed with respect to their size. In addition, a mathematical theory capable of describing the behaviour of the crystal population during the precipitation processes is also needed.

The population balance theory is the mathematical framework widely used in modelling particulate systems. It is derived from the law of conservation of particle numbers. According to the concept for particulate systems introduced by Hulburt and Katz (1964), a crystal in the particle phase space is characterised by its internal coordinates, i.e. its properties, and its external coordinates, which define its location in space. If a number of internal properties vary between crystals, then it is difficult to characterise the system and a multi-dimensional distribution is required. Fortunately, the chemical composition of a system of particulates generally does not vary from crystal to crystal. Randolph and Larson (1988) suggested that if the shapes of all crystals are roughly uniform, then the system can be described by a one-

dimensional size distribution function. Before discussing the population balance theory, it is necessary to clarify crystal size and introduce the concept of crystal size distribution.

3.2 CRYSTAL SIZE

Crystal size depends on the method of crystal measurement and is generally expressed in terms of some equivalent dimension such as, diameter of a sphere, or a linear dimension according to the measuring techniques. Some crystal size definitions are volume diameter, surface diameter, projected area diameter, sieve diameter, or maximum chord. Allen (1981) provided a good description of many particle measurement techniques. The crystal size used in precipitation studies is either diameter, L, or volume, v. Both have merit, as will be discussed later. These two size properties are related through a volume shape factor, k_v, as

$$v = k_v L^3 \tag{3.1}$$

3.2.1 Crystal Size Distribution

The crystals in a precipitator have a range of sizes, which can be described by a crystal size distribution (CSD). A CSD simply indicates the amount of crystals in each size range. This amount can be either in terms of the number or the mass. In precipitation systems, it is desirable to account for the number of crystals, hence, a number size distribution is considered in the modelling process. The CSD may be expressed as a number density function, a cumulative number oversize, or a cumulative number undersize. If the size is taken as linear size L, then the number density function is $n(L)$ and is defined as

$$n(L) = \frac{dN(L)}{dL} \tag{3.2}$$

where $dN(L)$ is the differential number, in the differential neighbourhood of L. Multiplying Equation (3.2) with dL will give the number of crystals within the size interval L to $L + dL$ in a given volume of slurry. The cumulative number undersize,

$CUS(L)$, and cumulative number oversize, $COS(L)$, are the number per unit slurry volume of crystals smaller and greater than size L, respectively. The inter-relationships between all these distributions are

$$CUS(L) = \int_0^L n(L)dL \tag{3.3}$$

and

$$COS(L) = \int_0^\infty n(L)dL - CUS(L) \tag{3.4}$$

According to Equation (3.2), if the internal coordinate is taken as volume, v, then,

$$n(v) = \frac{dN(v)}{dv} \tag{3.5}$$

Comparing Equation (3.5) to Equation (3.2), the differential number dN is the same, as v and L are related according to Equation (3.1), from which it follows

$$\frac{n(L)}{n(v)} = \frac{dv}{dL} = 3k_v L^2 \tag{3.6}$$

3.2.2 Moments of a Crystal Size Distribution

It is sometimes convenient to consider the moments of a CSD in precipitation system analysis. There are two types of moments, these are (1) Moments about the origin, i.e. $L = 0$, defined as

$$\mu_j = \int_0^\infty L^j n(L)dL \tag{3.7}$$

and (2) Moments about the mean, μ_1, defined as

$$m_j = \int_0^\infty (L - \mu_1)^j n(L)dL \tag{3.8}$$

Representation of the CSD in the moment form reduces the complexity of modelling precipitation systems. The moments are related to the physical and statistical properties of the precipitation system. For example, in the precipitation system with a population of N_T crystals, the physical and statistical properties of the system are summarised in Table 3.1. For further details see Randolph and Larson (1988).

Table 3.1 Summary of the relationships between moments and the physical and statistical properties of a precipitation system.

Physical properties of a precipitation system	**Moment Relations**
Total number of crystals, N_T	μ_0 or m_0
Total crystal length, L_T	μ_1
Total crystal surface area, A_T	$k_a\mu_2$
Total crystal volume, V_T	$k_v\mu_3$
Total crystal mass, M_T	$\rho_s k_v\mu_3$
Statistical properties of a CSD	
Mean crystal size, L_{10}	μ_1/μ_0
Variance, σ^2	$(m_2/m_0-(m_1/m_0)^2)$
Coefficient of variance, CV	$(m_0 m_2/m_1^2-1)^{0.5}$

Randolph and Larson (1988) showed that various useful mean size can be determined from the following relation:

$$L_{jk} = \left(\frac{\mu_j}{\mu_k}\right)^{\frac{1}{j-k}} \tag{3.9}$$

For example, L_{30} is the volume mean size, L_{32} is the volume surface mean or Sauter mean, and L_{43} is the mass mean size.

3.3 POPULATION BALANCE THEORY

The mathematical description of particulate systems in particle phase space, otherwise known as the population balance (PB), has been used to describe systems of particles undergoing different internal processes. The PB theory was pioneered by Hulburt and Katz (1964), and then elaborated by Randolph and Larson (1988). The PB is a continuity statement in particle phase space, and expressed in terms of the number density distribution, n, as

$$\frac{\partial n}{\partial t} + \nabla.(nv) = B - D \tag{3.10}$$

where t is time, v is the velocity vector, which represents the rate of change of position in phase space involving both the external and internal coordinates. The external coordinates give the spatial location of particles, and the internal coordinates refer to those particle properties independent of position such as, particle size, chemical activity or particle age. The terms B and D represent the birth and death functions at a point in phase space, which can account for processes such as, nucleation, agglomeration and breakage.

The above equation is a microscopic form of the PB model, as it describes the particulate system at a microscopic level. The macroscopic PB model is of more practical use, and was derived by Randolph and Larson (1988). For a well-mixed system of volume V, with k entering and leaving streams, each with a volumetric flow rate of Q_i and number density function of n_i, the PB model has the form

$$\frac{\partial n}{\partial t} + \nabla \cdot v_i n + n\frac{d(\log V)}{dt} = B - D - \frac{1}{V}\sum_{i=1}^{k} Q_i n_i \tag{3.11}$$

where v_i is the internal velocity. This is the generic form of the population balance equation (PBE) used in modelling particulate systems. In modelling precipitation processes, it allows the incorporation of different processes such as, nucleation, growth and agglomeration, as well as different modes of operations to completely describe the system being modelled. The internal coordinate in Equation (3.11) is taken as particle size, i.e. linear size or volume.

3.3.1 Nucleation

Nucleation is a birth process, creating particles of negligible size. If the nuclei are of the same size, L_o, then the nucleation birth term, B_N, is

$$B_N = B^o \delta(L - L_o) \tag{3.12}$$

where B^o is the nucleation rate, and $\delta(L\text{-}L_o)$ is the Dirac delta function, which is defined as

$$\delta(L-L_o)=\begin{cases} 1 & L=L_o \\ 0 & L\neq L_o \end{cases} \tag{3.13}$$

This formulation is used frequently in modelling precipitation systems involving nucleation processes.

3.3.2 Growth

Growth is accounted for explicitly in the PB model and is defined as the velocity along the size, x, axis:

$$G=\frac{dx}{dt} \tag{3.14}$$

McCabe's ΔL law, which states growth is independent of linear crystal size, is valid for most solution precipitation systems (Mullin 1993). In such a case, using the linear size L, simplifies the PB model. However, some systems do exhibit size dependent growth (Canning and Randolph 1967; Abegg, Stevens & Larson 1968; Budz, Jones & Mullin 1987; Yokota and Kubota 1996). There are a number of possible explanations for the size dependent growth. One is attributed to the bulk diffusion effects in which growth rate increases with crystal size, because of an inverse relationship between solubility and size (Garside, Phillips & Shah 1976). The other explanation is that the number of surface active sites, or dislocations increases with crystal size (Mullin 1993).

Growth rate dispersion is another phenomenon that violates McCabe's ΔL law. It is found that in some systems, crystals of the same size exhibit different growth rates under the same precipitation conditions (White and Wright 1971; Graside 1979). This phenomenon is thought to occur because different crystals experience different environments in the precipitator (Randolph and Larson 1988) or because of inherent structural differences of the crystals (Zumstein and Rousseau 1987a). Two growth

rate dispersion mechanisms have been proposed. Firstly, the random fluctuation growth dispersion (Randolph and White 1977), where under constant conditions the growth rate of individual crystal vary with time. Secondly, the intrinsic growth dispersion (Randolph and Larson 1988), where under constant conditions each crystal grows at a constant rate, which is different to the other crystals. It is quite frequently argued that most systems that exhibit apparently size dependent growth are actually experiencing growth rate dispersion (Girolami and Rousseau 1985; Ilievski and White 1996).

3.3.3 Agglomeration

Hulburt and Katz (1964) developed a PB binary collision model for agglomeration using volume as the internal coordinate. The birth of particles of sizes within the interval v to $v + dv$ due to the agglomeration of particles of sizes $v-\xi$ and ξ is

$$B_A(t,v) = \frac{1}{2}\int_0^v \beta(t,v-\xi,\xi)n(t,v-\xi)n(t,\xi)d\xi \tag{3.15}$$

The factor 1/2 is included as the integral counts each collision twice. The death of particles of size v due to agglomeration with any particle of size ξ is expressed as

$$D_A(t,v) = n(t,v)\int_0^\infty \beta(t,v,\xi)n(t,\xi)d\xi \tag{3.16}$$

where $\beta(t,v,\xi)$ is the agglomeration kernel, which is a measure of the frequency of collisions between particles of volumes v and ξ that are successful in producing an agglomerate.

The above formulation has found extensive use in the description of agglomeration in the field of atmospheric aerosols (Ramabhadran, Patterson & Seinfeld 1976; Gelbard and Seinfeld 1978a; 1978b), and in precipitation systems (Hartel and Randolph 1986b; Hounslow, Ryall & Marshall 1988; Ilievski and White 1994a; 1995). Sastry

(1975) proposed that the kernel consists of two factors as discussed in Chapter 2, i.e. Equation (2.11), and it is now common practice to view the kernel in this manner.

3.3.4 Choice of Internal Coordinates

Two internal coordinates that can be used in PB formulation are length L and volume v. In modelling systems without an agglomeration term, using length can greatly simplify the PBE. On the other hand, if the system solely involves agglomeration, then using volume leads to a simpler PBE. If both growth and agglomeration take place simultaneously, then choosing the internal coordinate becomes rather difficult. The reason, as explained by Hounslow (1990c) and Ilievski (1991), is that in length coordinate the agglomeration term becomes extremely complicated, whereas in volume coordinate the growth term becomes highly non-linear. This problem is best illustrated by the following example of a well-mixed, constant volume, batch precipitation system with simultaneous growth and agglomeration taking place. The PB model yields

$$\frac{\partial n}{\partial t}+\frac{\partial (Gn)}{\partial x}=B_A-D_A \tag{3.17}$$

where x is the internal coordinate, and B_A and D_A are the respective birth and death terms due to agglomeration. If the internal coordinate L is used, then the PBE becomes

$$\frac{\partial n(t,L)}{\partial t}+G\frac{\partial n(t,L)}{\partial L}=B_A(t,L)-D_A(t,L) \tag{3.18}$$

Hounslow, Ryall & Marshall (1988) showed that the birth and death terms can be expressed in terms of L as

$$B_A(t,L)=\frac{L^2}{2}\int_0^L \frac{\beta(t,[L^3-\lambda^3]^{\frac{1}{3}},\lambda)n(t,[L^3-\lambda^3]^{\frac{1}{3}})n(t,\lambda)}{(L^3-\lambda^3)^{\frac{2}{3}}}\,d\lambda \tag{3.19}$$

and

$$D_A(t,L) = n(t,L)\int_0^{\infty} \beta(t,L,\lambda)n(t,\lambda)d\lambda \tag{3.20}$$

where L and λ are linear crystal sizes.

If the volume v is used as the internal coordinate, the growth rate is no longer size independent. For volume equivalent crystal diameter, the volumetric growth rate, G_v, can be expressed in terms of the linear growth rate, G, as

$$G_v = 3k_v^{\frac{1}{3}} G v^{\frac{2}{3}} \tag{3.21}$$

The PBE then becomes

$$\frac{\partial n(t,v)}{\partial t} + 3k_v^{\frac{1}{3}} G \frac{\partial (n(t,v)v^{\frac{2}{3}})}{\partial v} = B_A(t,v) - D_A(t,v) \tag{3.22}$$

where $B_A(t,v)$ and $D_A(t,v)$ are expressed in equations (3.15)-(3.16). It can be seen that neither choice of the internal coordinates result in a simpler form of the PBE.

3.4 THE MOMENT FORM OF THE PBE

Sometimes knowledge of the complete CSD is unnecessary. Rather some average or total quantities from the CSD are sufficient. The moment transform, defined in section 3.2.2 is one method for estimating such averaged properties of a particulate system. Randolph and Larson (1988) provided a clear description of the use of moment transformation in the solution of the PBE. The moment transformation converts the intractable PBE into a set of ordinary differential equations. The j^{th} moment of a distribution is defined in Equation (3.7). With the application of a moment transformation, the PBE (3.11) is converted into a set of ordinary differential equations as

$$\frac{d\mu_j}{dt} = 0^j B^o + jG\mu_{j-1} + \overline{B}_j - \overline{D}_j + \frac{1}{V}\left(\sum_i Q_i^{in}\mu_{j,i}^{in} - \sum_i Q_i^{out}\mu_{j,i}^{out}\right) \quad (3.23)$$

where $j = 0,1,2,...k$, and k is the order of the moments. B^o is the nucleation rate, and $\overline{B}_j$ and $\overline{D}_j$ are moment transformed birth and death terms, given as

$$\overline{B}_j = \int_0^\infty L^j B(t,L)dL \quad (3.24)$$

and

$$\overline{D}_j = \int_0^\infty L^j D(t,L)dL \quad (3.25)$$

The zeroth, first, second and third moments are related to total number, N_T, length, L_T, area, A_T, and volume, V_T of crystals per unit volume of suspension, respectively. Hounslow, Ryall & Marshall (1988) showed that $\overline{B}_j$ and $\overline{D}_j$ can be simplified for a size independent kernel, i.e. $\beta(t,L,\lambda) = \beta_0$, in Equation (2.11). In that case, $\overline{B}_j$ can be evaluated if $j/3$ is an integer. Hence, for $j = 0$, 3 and 6, $\overline{B}_j$ are given as

$$\overline{B}_0 = \frac{1}{2}\beta\mu_0^2\,;\ \overline{B}_3 = \beta\mu_0\mu_3\,;\ \text{and}\ \overline{B}_6 = \beta\mu_3^2 \quad (3.26)$$

The term $\overline{D}_j$ for a size independent kernel is

$$\overline{D}_j = \beta\mu_0\mu_j \quad (3.27)$$

3.5 SOLUTION METHODS FOR THE PBE

Establishing the PB model for a given system is simple, but solving the PBE is relatively difficult. The solution of the PBE involves finding the number density function, n, that satisfies the governing equation (3.11) and the initial and boundary

conditions. Considerable attention has been focused on methods for solving the PBE in the published literature. Pulvermacher and Ruckenstein (1974), Gerald and Seinfeld (1978a) and Ramkrishna (1985) provided a thorough discussion on this matter. A brief overview on the solution methods for the PBE reported in the literature is presented in the following sections.

3.5.1 Analytical Solutions

The resulting PBE describing the system being modelled is often a non-linear partial integro-differential equation. Analytical solutions for the PBEs are generally unavailable, except for special cases, eg. agglomeration or growth is the sole kinetic factor involved in the process. In the presence of both agglomeration and growth, the situation becomes more difficult as demonstrated earlier. Some of the special cases for which analytical solutions have been reported in the literature are provided in Table 3.2.

Table 3.2. Some of the analytical solutions published in the literature in the fields of aerosols and precipitation.

Source	Mechanism
Aerosols	
Ramabhadran, Patterson & Seinfeld (1976)	coagulation and growth by condensation
Gelbard and Seinfeld (1978a)	coagulation and growth of multi-component aerosol
Gelbard and Seinfeld (1978b)	coagulation; coagulation and growth
Precipitation – MSMPR	
Randolph and Larson (1988)	growth and nucleation; size dependent growth
Hounslow (1990a)	size (in)dependent agglomeration
Tavare and Patwardhan (1992)	agglomeration, growth and nucleation
Hostomsky and Jones (1993)	nucleation and agglomeration
Lee and Saleeby (1994)	agglomeration and size dependent growth
Saleeby and Lee (1994)	agglomeration and size independent growth
Saleeby and Lee (1995)	agglomeration and random growth rate dispersion

Analytical solutions obtained in the literature are limited to simple growth functions, (eg. size independent or linear size dependent), simple agglomeration kernels (eg. size independent kernel or sum kernel), and simple seed distribution (eg. exponential distribution). It should be noted that analytical solutions obtained for aerosols are in terms of volume. In the case of simultaneous agglomeration and growth, a volume independent growth is assumed. This assumption may be valid for growth by condensation in aerosols, but its applicability to precipitation systems is doubtful.

In precipitation systems, most analytical solutions (in length coordinate) are found for steady state mixed suspension mixed product removal (MSMPR) systems. However, some analytical solutions for MSMPR precipitation system using volume coordinate are also reported (Tavare and Patwardhan 1992; Lee and Saleeby 1994; Saleeby and Lee 1994; 1995). For those PBEs that can be dealt with analytically, the Laplace transform method is often employed because it handles the partial differential and integral equation forms well. In the cases where the inverse Laplace transforms are not straightforward to evaluate, or involve a complex integral inversion, approximation techniques have been used to obtain the analytical solutions. These include Picard's method (Hounslow 1990a), Taylor series (Lui and Thompson 1992; Lee and Saleeby 1994) or reversion method (Saleeby and Lee 1994; 1995).

3.5.2 Similarity Solution

The similarity approach of solving the PBE for an aggregation system is based on the similarity theory developed by Swift and Friedlander (1964). This approach has been used widely in the aerosol aggregation systems (Wang and Friedlander 1967; Pulvermacher and Ruckenstein 1974; Ramabhadran and Seinfeld 1975; Lee 1983), and to lesser extent in other fields (Ramabhadran 1975; Sastry 1975; Skrtic, Markovic & Fuerdi-Milhofev 1984; Ilievski and White 1994a). The similarity approach reduces the PBE to an ordinary integro-differential equation in terms of a dimensionless particle volume, and then is solved accordingly. This approach has not been applied to systems involving other mechanisms or continuous systems.

3.5.3 Method of Moments

Moment transformation of the PBE into ordinary differential equation as discussed in section 3.4 provides an alternative approach to solve the PBE. The resulting moment equations can be expressed in terms of the physical properties of the precipitation system. Important moment equations are those of zeroth, first, second and third moments. In this research, crystal length or diameter is used as the internal coordinate in modelling the gibbsite precipitation system, due to simultaneous growth and agglomeration being involved. The presence of the agglomeration in the precipitation process results in both first and second moment equations containing complex intractable integral terms (see Hounslow, Ryall & Marshall 1988). The treatment of

the moment equations is restricted to precipitation processes involving simultaneous size independent agglomeration and growth, or nucleation.

3.5.3.1 MSMPR System

In an unseeded steady state MSMPR system involving simultaneous agglomeration, growth and nucleation, the resulting zeroth and third moment equations are

$$\mu_0 = \frac{\sqrt{1+2\beta B^o \tau^2} - 1}{\beta \tau} \tag{3.28}$$

and

$$\frac{\mu_3}{\mu_2} = L_{32} = 3G\tau \tag{3.29}$$

Equations (3.28)-(3.29) reveal the relations between the measurable variables (i.e. μ_0, μ_2 and μ_3) and the operating variables (i.e. β, B^o, G and τ) in the steady state system.

3.5.3.2 Dynamic Systems

In a batch system with agglomeration and growth occurring, the zeroth moment is

$$\frac{d\mu_0}{dt} = -\frac{1}{2}\beta\mu_0^2 \tag{3.30}$$

which implies that the change in the total number of crystals depends only on crystal agglomeration and the number of crystals. Similarly, the resulting third moment is

$$\frac{d\mu_3}{dt} = 3G\mu_2 \tag{3.31}$$

The change in total crystal volume depends on the growth rate and total crystal surface area, and not directly on crystal agglomeration.

In the case of simultaneous agglomeration, growth, and nucleation taking place in a batch system, the zeroth moment equation becomes

$$\frac{d\mu_0}{dt} = B^o - \frac{1}{2}\beta\mu_0^2 \tag{3.32}$$

Equation (3.32) indicates that nucleation affects the change in total crystal numbers, along with agglomeration and the total crystal numbers. The third moment equation in this case is equivalent to Equation (3.31), as the contribution to the total crystal volume by nucleation is negligible.

Generally, it is impossible to obtain an analytical solution for the batch system as the operating variables continuously change with time. If the agglomeration kernel can be kept constant for an extended time interval, then the analytical solution for Equation (3.30) can be found with the initial condition, $\mu_0(t)\big|_{t=0} = \mu_0(0)$, as shown

$$\frac{1}{\mu_0(t)} = \frac{1}{\mu_0(0)} + \frac{1}{2}\beta t \tag{3.33}$$

where $\mu_0(0)$ is the total seed crystal numbers added initially.

Similarly, for a special case, where time-invariant nucleation rate and agglomeration kernel can be assumed in Equation (3.32), the analytical solution is found to be (see Appendix 1)

$$\mu_0(t) = \sqrt{\frac{2B^o}{\beta}}\left(\frac{\kappa\exp\left(\sqrt{2B^o\beta}t\right)-1}{1+\kappa\exp\left(\sqrt{2B^o\beta}t\right)}\right) \tag{3.34}$$

where

$$\kappa = \frac{\sqrt{B^o} + \sqrt{\frac{\beta}{2}}\mu_0(0)}{\sqrt{B^o} - \sqrt{\frac{\beta}{2}}\mu_0(0)} \tag{3.35}$$

and

$$\mu_0(t)\big|_{t\to\infty} \approx \sqrt{2B^o/\beta} \tag{3.36}$$

The latter result implies that the total number of crystals eventually depends on the balance of nucleation and agglomeration kinetics, as time becomes large. With the addition of nucleation process, the analytical solution becomes a complex function of operating variables compared to Equation (3.33). This implies that deducing the kinetics rates in the latter system is much more complicated.

3.5.4 Numerical Methods

The majority of numerical methods are well covered in the reviews of Gerald and Seinfeld (1978b), Ramkrishna (1985) and Seigneur et al. (1986). The numerical methods generally employed to solve the PBE are the method of weighted residuals, the finite element method and the discretisation method.

3.5.4.1 Weighted Residuals/Finite Element Methods

In the method of weighted residuals, the solution of the PBE is approximated by a linear combination of chosen basis functions as

$$n(t,L) = \sum_{i=1} a_i(t)\phi_i(L) \tag{3.37}$$

where $\phi_i(L)$ are some known functions on the interval $[0,\infty)$. The unknown coefficients $a_i(t)$ are determined by substituting Equation (3.37) into the governing PBE to define a residual. The equation is then multiplied by weight functions and integrated over the domain of interest. Rawlings, Miller & Witkowski (1993) reported that the limitations of the weighted residuals method are that an efficient set of basis functions, $\phi_i(L)$, cannot always be found, convergence can be slow, and exhibits oscillatory behaviour if a discontinuity exists in the solution.

Ramkrishna (1973) and Singh and Ramkrishna (1975) proposed the use of problem-specific polynomials (PSP) as trial functions in the weighted residuals method for solving the PBE. Sampson and Ramkrishna (1985) further suggested the use of root shifted PSP as improvement of the PSP in the collocation method. Bhatia and Chakraborty (1992) developed a modified weighted residuals method in which they combined expansions based on limiting forms of the true solution to solve the PBE.

This method converts the PBE into a system of algebraic equations and solves accordingly. But it is applicable to steady state precipitation system only.

In the finite element method, the size domain is subdivided into elements, and the assumed solution is approximated by basis functions on each element. Rawlings, Miller & Witkowski (1993) reported that this method converges slower than the weighted residuals method, but it can be tailored to handle discontinuity and a sharply changing CSD. Gelbard and Seinfeld (1978a) combined the collocation method with finite element method, and incorporated piecewise cubic polynomial into the collocation formulation, which gives excellent agreement between the numerical results and analytical solutions. The drawbacks of their method are the high computation time required for determining the coefficients of the polynomials, and the complexity in implementing the method in a code. Nicmanis and Hounslow (1998) developed a finite element algorithm for solving the MSMPR PBE, which combines both collocation and the Galerkin methods. They emphasised that the Galerkin method must be used in the growth problem in order to obtain a well-conditioned system.

Wulkow, Gerstlauer & Nieken (1999) developed a method called the adaptive Galerkin h-p method for solving the PBE. This method is based on a generalised finite element scheme, with self-adaptive grid and order construction, and a Rothe's type time discretisation. They emphasised that the method has an automatic error control for time and property discretisation. This method seems to be promising for solving the PBE, but no in depth details are given. The method has been implemented in a software package called PARSIVAL, and is commercially available.

3.5.4.2 Discretisation Methods

The discretisation method, which is sometimes referred to as the discretised population balance (DPB), transforms the continuous PBE into a number of sub-equations. The number of sub-equations generated depends on the number of size intervals selected. These equations are written as ordinary differential equations,

describing the rate of change of the number of particles in each discretised size interval. The generic form of the DPB is

$$\frac{dN_i}{dt} = \left(\frac{dN_i}{dt}\right)_A + \left(\frac{dN_i}{dt}\right)_G + \left(\frac{dN_i}{dt}\right)_B + \left(\frac{dN_i}{dt}\right)_F \tag{3.38}$$

The change in particle numbers in the i^{th} size interval, N_i, is directly the result of the change in numbers in that particular interval due to agglomeration, growth, nucleation and net-flow term, respectively in Equation (3.38). Hence, the essence of the discretisation method is to derive the formulation to each of the discretised terms.

A large number of discretisation methods have been reported in the literature (Gelbard, Tambour & Seinfeld 1980; Sastry and Gaschignard 1981; Batterham, Hall & Barton 1981; Marchal et al. 1988; Hounslow, Ryall & Marshall 1988; Landgrebe and Pratsinis 1990; David et al. 1991; Litster, Smit & Hounslow 1995; Wynn 1996). These methods vary in their choice of discretisation of the size domain (linear, geometric or arbitrary), their assumptions about the shape of the size distribution within each interval, and the choice of average values of properties in each interval.

Hounslow, Ryall & Marshall (1988) reviewed the discretisation techniques published in the literature prior to the 1990s, and noted that most of the authors fail to test their discretisation methods. Some of them result in significant error in the prediction of total crystal numbers and volume. In addition, not all of them are simple to solve. Hounslow then developed a discretisation method based on the criterion that the moments of the DPB should be consistent with those of the continuous PB. Litster, Smit & Hounslow (1995) and Wynn (1996) further extended Hounslow's discretised agglomeration model to allow for an adjustable size discretisation ratio and improved convergence.

Hill and Ng (1996) developed a discretised agglomeration model, which correctly predicts total crystal numbers and volume, and is applicable to equal size intervals and geometric size intervals of any ratio. For an equal size interval, a single set of equations is produced, while for geometric intervals, the proposed method becomes

unattractive to use as the geometric ratio decreases toward 1. This is because the discretised agglomeration model to be solved is no longer unique, and more terms are involved at larger size range. Kumar and Ramkrishna (1996a; 1996b) developed a fixed pivot technique to solve the agglomerative PBE, where the discretised size can be geometric with varying coarseness, and a more flexible pattern; fine in some size ranges and coarse elsewhere. They claimed that this technique has the same accuracy as the Litster's discretised agglomeration model but is computationally more efficient. However, the fixed pivot discretised agglomeration model over-predicts the crystal numbers over the larger size domain, due to the steeply non-linear gradients in the number density over the discretised interval. They further introduced a moving pivot technique, which has the same feature as the fixed pivot technique, but is more accurate in predicting the crystal numbers over large size ranges. Kumar and Ramkrishna (1997) extended their previous model by including discretised growth and nucleation models. The growth term is solved by a technique that combines both the moving pivot method and the method of characteristics in order to avoid oscillatory behaviour of the numerical solution.

In the current research, Hounslow's discretisation method, and hence, those of Litster, Smit & Hounslow (1995) and Wynn (1996) will be adopted to solve the PBEs of interest. This approach is simple to implement and computationally efficient.

3.6 HOUNSLOW'S DISCRETISED POPULATION BALANCE MODEL

The main challenge of a discretisation method is to derive an accurate formulation for each of the discretised terms in Equation (3.38) that are efficient to solve.

3.6.1 Discretised Net-Flow Term

The formulation of the net-flow term is straightforward, and can be expressed as

$$\left(\frac{dN_i}{dt}\right)_F = \frac{1}{V}\left(\sum_{j=1} Q_j^{in} N_{i,j}^{in} - \sum_{j=1} Q_j^{out} N_{i,j}^{out}\right) \tag{3.39}$$

The right hand side of Equation (3.39) is the net crystal numbers that flow in and out of the i^{th} size interval and V is the system working volume.

3.6.2 Discretised Nucleation Model

Nuclei are usually considered to occur at the smallest discretised size interval, which is equivalent to the smallest detectable size of the particle size analyser. Hounslow, Ryall & Marshall (1988) defined the discretised nucleation model as

$$\left(\frac{dN_i}{dt}\right)_B = \begin{cases} B^o & i=1 \\ 0 & i>1 \end{cases} \tag{3.40}$$

where B^o is the nucleation rate. This model assumes that nuclei of the same size as the mean first size interval, $\overline{L}_1$, are generated.

3.6.3 Discretised Growth Models

Hounslow, Ryall & Marshall (1988) developed size independent discrete growth terms that satisfy the criterion

$$\frac{d\mu_j}{dt} = jG\mu_{j-1} \tag{3.41}$$

Two discretised growth models were developed; a two-term and a three-term discretised model. The two-term growth model is given as

$$\left(\frac{dN_i}{dt}\right)_G = \frac{G}{(r-1)L_i}\left(rN_{i-1} - N_i\right) \tag{3.42}$$

where $r = L_{i+1}/L_i = 2^{1/3}$ is the geometric size discretisation ratio. The terms L_i and L_{i+1} are the lower and upper bounds of the i^{th} size interval, respectively. This model predicts the zeroth moment correctly, but overpredicts all other moments. However, we are generally interested in the first four moments (i.e. μ_j and $j = 0$, 1,2 and 3).

The degree of over prediction of the moments can be reduced if the discretised size resolution is increased. Following Litster, Smit & Hounslow (1995), the geometric size discretisation ratio is defined as

$$r = \frac{L_{i+1}}{L_i} = 2^{\frac{1}{3q}} \tag{3.43}$$

where q is the size resolution parameter and an integer greater than zero. The effect of discretised size resolution on the over prediction can be investigated by increasing q. Hounslow, Ryall & Marshall (1988) showed that the two-term growth model over predicts the j^{th} moment by a factor of

$$\varphi_{j,q} = \left(\frac{1+r}{2}\right)\left(\frac{r^j - 1}{r-1}\right)\frac{1}{j} \tag{3.44}$$

The over prediction factor of the j^{th} moment, $\varphi_{j,q}$, for any q in Equation (3.44), is the ratio of the resultant moments from the two-term growth model to the moments in Equation (3.41). It has a value greater than one, and equals to one if the moments match exactly. Table 3.3 shows the over prediction factor of the j^{th} moment at different q.

Table 3.3. The over prediction factor of the j^{th} moment at different q for the two-term growth model.

q	$\varphi_{1,q}$	$\varphi_{2,q}$	$\varphi_{3,q}$
1	1.13	1.28	1.45
2	1.06	1.13	1.20
3	1.04	1.08	1.13
4	1.03	1.06	1.09
5	1.02	1.05	1.07
6	1.02	1.04	1.06
7	1.02	1.03	1.05
8	1.01	1.03	1.04

The values of $\varphi_{j,q}$ reduce significantly as the q value increases, particularly those of the third moment (i.e. from 45% at q = 1 down to 4% at q = 8). This demonstrates that the two-term growth model becomes accurate with finer size resolution.

The three-term growth model has the form

$$\left(\frac{dN_i}{dt}\right)_G = \begin{cases} \dfrac{2G}{(1+r)L_1}\left(\left(1-\dfrac{r^2}{r^2-1}\right)N_1 - \dfrac{r}{r^2-1}N_2\right) & i=1 \\ \dfrac{2G}{(1+r)L_i}\left(\dfrac{r}{r^2-1}N_{i-1} + N_i - \dfrac{r}{r^2-1}N_{i+1}\right) & i\neq 1 \end{cases} \tag{3.45}$$

This model ensures correct prediction of the first three moments (i.e. j = 0,1 and 2), but overpredicts the third moment marginally, that is, 1.8% with q = 1 and becomes negligible as q increases. Hounslow, Ryall & Marshall (1988) and Hounslow (1990a) found that the numerical solution obtained from the three-term growth model gives satisfactory agreement with the analytical solutions of the size dependent and size independent growth systems. They further stated that this growth model will cause numerical oscillations if the number of particles in the first size interval falls to zero. To overcome this problem, they suggested that for seeded systems, replacing any negative values of N_i with zero will provide the correct solution. Similarly, for a system that involves growth and nucleation, the three-term discretized growth model above will lead to oscillations in the CSD. Hounslow, Ryall & Marshall (1988) pointed out that the two-term growth model should be used for systems with unseeded nucleation.

3.6.4 Discretised Agglomeration Model

Hounslow, Ryall & Marshall (1988) considered that crystal agglomeration is a result of four binary contact mechanisms, as summarised in Table 3.4.

Table 3.4. Binary contact mechanisms proposed by Hounslow, Ryall & Marshall (1988) for developing the discretised agglomeration model.

Mechanism	Birth or Death in size interval i	Collision between	
		Particle 1	Particle 2
1	Birth	i-1	1 to i-2
2	Birth	i-1	i-1
3	Death	i	1 to i-1
4	Death	i	i to ∞

It is assumed that the size independent agglomeration kernel is constant within each size interval. A geometric discretised size ratio of $v_{i+1}/v_i = 2$ is used. This is equivalent to a linear size ratio of $L_{i+1}/L_i = 2^{1/3}$. The contribution of each of the four mechanisms is summed over all crystals and the formulation is derived to ensure that the resultant zeroth and third moments of the discretised agglomeration model satisfy the criteria,

$$\frac{d\mu_0}{dt} = -\frac{1}{2}\beta\mu_0^2; \quad \text{and} \quad \frac{d\mu_3}{dt} = 0 \tag{3.46}$$

Hounslow, Ryall & Marshall (1988) stated that the zeroth moment equation of the discretised agglomeration model satisfies the above criterion but a volume correction factor is required to ensure the third moment equation is in agreement with the criterion. Hence, the discretised agglomeration model has the following form

$$\begin{aligned}\left(\frac{dN_i}{dt}\right)_A = {} & N_{i-1}\sum_{j=1}^{i-2} 2^{j-i+1}\beta_{i-1,j}N_j + \frac{1}{2}\beta_{i-1,i-1}N_{i-1}^2 \\ & - N_i\sum_{j=1}^{i-1} 2^{j-i}\beta_{i,j}N_j - N_i\sum_{j=i}^{\infty}\beta_{i,j}N_j\end{aligned} \tag{3.47}$$

This model gives excellent agreement with the analytical solutions for both size dependent and independent agglomeration kernels in the batch and steady state systems.

3.7 LITSTER'S DISCRETISED AGGLOMERATION MODEL

A drawback of the Hounslow's discretised agglomeration model above is that it fixes the discretisation domain at $v_{i+1}/v_i = 2$. In practice, it is frequently desirable to use a much finer discretisation. In addition, the method results in considerable error in higher-order moments of the CSD (i.e. $j > 3$), which leads to inaccuracies in prediction of the shape of the CSD (Ilievski, White & Hounslow 1993). Another problem with the method is that larger size intervals occur at the larger end of the CSD.

Litster, Smit & Hounslow (1995) developed an improved version of the original Hounslow's discretised agglomeration model. In this version, the geometric size discretisation is adjustable, and the geometric ratio is $v_{i+1}/v_i = 2^{1/q}$, or length ratio, $L_{i+1}/L_i = 2^{1/(3q)}$, as discussed in section 3.6.3. It takes advantage of the greater resolution in the measured CSD possible with modern particle size analysis devices. This new model is similar to the original version, simple to solve and correctly predicts the total crystal numbers and volume. As in the original discretised agglomeration model, agglomeration is considered as a result of binary contact. In this finer size discretisation, five types of interaction need to be considered; three birth types and two death types. Details on the interactions between particles that are added and removed from a size interval are given in Litster, Smit & Hounslow (1995). Wynn (1996) further improved the accuracy and convergence of the discretised agglomeration model of Litster, Smit & Hounslow (1995), leading to the following form

$$\begin{aligned}\left(\frac{dN_i}{dt}\right)_A = &\sum_{j=1}^{i-S_1} \beta_{i-1,j-1} N_{i-1} N_j \frac{2^{(j-i+1)/q}}{2^{1/q}-1} \\ &+ \sum_{p=2}^{q} \sum_{j=i-S_{p-1}}^{i-S_p} \beta_{i-p,j} N_{i-p} N_j \frac{2^{(j-i+1)/q} - 1 + 2^{-(p-1)/q}}{2^{1/q}-1} \\ &+ \frac{1}{2} \beta_{i-q,i-q} N_{i-q}^2 \\ &+ \sum_{p=1}^{q-1} \sum_{j=i+1-S_p}^{i+1-S_{p+1}} \beta_{i-p,j} N_{i-p} N_j \frac{-2^{(j-i)/q} + 2^{1/q} - 2^{-p/q}}{2^{1/q}-1} \\ &- \sum_{j=1}^{i-S_1+1} \beta_{i,j} N_i N_j \frac{2^{(j-i)/q}}{2^{1/q}-1} \\ &- \sum_{j=i-S_1+2}^{\infty} \beta_{i,j} N_i N_j\end{aligned} \tag{3.48}$$

where

$$S_p = \mathrm{Int}\left[1 - \frac{q \ln(1-2^{-p/q})}{\ln 2}\right] \tag{3.49}$$

and S_1 corresponding to the S_p value at $p = 1$.

This equation reduces to Hounslow's discretised agglomeration model when $q = 1$. Litster, Smit & Hounslow (1995) showed that for a large q value, the discretised agglomeration model is able to predict correctly (1) cumulative number and volume distributions, (2) self-preserving CSD, and (3) higher-order moments of the CSD. As the value of q increases, the computational time increases. They further suggested that for a trade off between accuracy and computational time, a value of 3 or 4 for q is reasonable. Wynn (1996) observed that the improvement in convergence for the modified discretised agglomeration model is effective only for $q > 4$.

3.8 CONCLUSIONS

The population balance theory that describes dispersed phase particulate systems has been introduced. This mathematical framework is widely used in modelling precipitation systems, undergoing processes such as, nucleation, growth and agglomeration. Establishing the PBE to describe any precipitation system is straightforward, but solving it is relatively difficult. The degree of complexity for solving the PBE depends on the internal processes involved. Solution methods for the PBE have been reviewed. The most frequently used method for solving the PBE for precipitation systems involving simultaneous nucleation, growth and agglomeration is the discretisation method. The DPB models of Hounslow and Litster will be adopted in this research to solve the resulting PBEs.

CHAPTER 4

PRECIPITATION KINETIC PARAMETER ESTIMATION

4.1 INTRODUCTION

Modelling of precipitators requires knowledge of the precipitation mechanisms that take place during the precipitation process; namely, nucleation, crystal growth and agglomeration. These precipitation mechanisms essentially determine the product CSD, an important product quality parameter that is necessary to control in order to meet product quality specifications. The formulation of a PB model for most precipitation configurations is simple, but obtaining the right kinetic expressions for the nucleation, growth and agglomeration is more difficult. A further complication is that these processes occur simultaneously during the precipitation run, making it very difficult to analyse their contribution to the product CSD and to deduce their rates. In addition, they may interact with each other.

In practice, precipitation kinetics rates are usually determined from experimental data via parameter estimation procedures. Kinetic parameter estimation methods have been reviewed by Tavare (1991; 1995a), Rawlings, Miller & Witkowski (1993) and Ilievski and White (1996). This chapter provides a brief review of the practical experimental techniques used to generate the precipitation data and methods for determining the kinetics from these precipitation data.

4.2 EXPERIMENTAL TECHNIQUES FOR PRECIPITATION

A number of experimental techniques have been reported in the literature for generating precipitation data. These include continuous, batch and semi-batch precipitation experiments, and are described below.

4.2.1 Continuous Precipitation

The mixed suspension mixed product removal (MSMPR) precipitation configuration has been used widely in precipitation kinetics studies. The precipitation experiment is carried out in a well-mixed vessel with uniform suspension and representative product removal. Supersaturation can be generated by cooling, heating, evaporating the liquor, or by chemical reaction. There are several disadvantages in performing MSMPR experiments, firstly, it is time consuming, i.e. a long time is required to reach a steady state (Ilievski 1991). Secondly, it is difficult to achieve a true steady state, as the apparatus is highly sensitive to small upsets, and can be unstable and oscillate continuously (Randolph and Larson 1988). Thirdly, it requires a large inventory of material. Finally, only one kinetic measurement can be obtained per run, and the transient data is discarded. The precipitation experiment should be performed such that sampling does not significantly disturb the system. Randolph and Larson (1988) stated that sample volume should be less than 10% of the vessel volume.

4.2.2 Batch Precipitation

Batch precipitation experiments are an attractive alternative to the MSMPR system. The major advantages of batch precipitation are its operational simplicity, i.e. a large number of kinetics data points are obtained in a single run, and significantly less liquor inventory and development time are required. However, the results can be difficult to interpret because the conditions in the precipitator are constantly changing. The precipitation experiment usually starts with supersaturated liquor at the nominated temperature, and the system is desupersaturated (i.e. the solute concentration is decreased) as the precipitation run proceeds. The solution or solids data can be taken regularly at different times during the batch run.

4.2.3 Semi-Batch Precipitation

Semi-batch precipitation experiments have the facility to measure a large number of kinetic responses in a single run, and to control certain precipitation conditions (Ilievski and White 1996). A commonly used semi-batch mode is the constant composition precipitation experiment (Seyssiecq et al. 1998; Ilievski 2000), where the solute concentration is monitored and maintained by an on-line feedback controller via conductivity probe. This system is transient in nature and does not reach steady state.

4.2.4 Precipitation Data Measurement

The available experimental data in precipitation experiments consists of both solution and solids measurements. The solute concentration and product CSD characterise the state of the precipitator, and are vital for the estimation of kinetic parameters.

4.2.4.1 Solution Measurement

The solute concentration of the precipitation system can be determined by taking liquor samples during the precipitation run and analysed via chemical analysis (eg. titration). Other analytical techniques for the determination of solute concentration include refractometer (Skidar and Randolph 1976; Helt and Larson 1977), densitometer (Ploss, Tengler & Mersmann 1984; Riebel, Kofler & Löffler 1990; Redman and Rohani 1994), temperature float method (Wang, Zeng & Qian 1989), and conductivity measurement (Smith and Woods 1993; Nallet, Mangin & Klein 1998). The solute concentration profile or "desupersaturation curve" represents important data for estimating kinetics rates, particularly the crystal growth rate.

4.2.4.2 Solids Measurement

Solids samples from the precipitator can be sampled for the determination of CSD and solids content. The solids content is determined by recovering and weighing the dry solids. The crystal sizing techniques reported in the literature include sieves, electrozone principle methods (eg. Coulter counter) and light scattering devices (eg. Malvern and Microtrac). On-line CSD measurement from a laser light scattering particle size analyser has also been used (Felton and Brown 1980; Randolph, White & Low 1981; Jager et al. 1991). Rawlings, Miller & Witkowski (1993) reported that the information of the CSD can also be obtained from transmittance measurement, i.e. the fraction of light transmitted by crystal slurry, using a spectrophotometer. According to the Beer-Lambert law, they stated that

$$\text{transmittance} = \frac{I}{I_0} = \exp(-\kappa l) \tag{4.1}$$

where I is the intensity of undiffracted light that passes through the suspension of crystals and I_0 is the intensity of the incident light. κ is the slurry turbidity, and l is

the flow cell width. Rawlings, Miller & Witkowski (1993) further stated that for non-spherical particles, the turbidity can be transformed to

$$\kappa = 3k_a \int_0^\infty L^2 n(t,L) dL \tag{4.2}$$

which gives a direct relationship between the transmittance and the second moment of the CSD, and k_a is the surface shape factor.

4.3 KINETIC PARAMETER ESTIMATION METHODS

A large number of methods have been developed for extracting the kinetics rates from steady state and dynamic experimental precipitation data. These methods are discussed in the following sections.

4.3.1 Methods for Steady State Precipitation Data

4.3.1.1 Classical Graphical Method for a MSMPR System

The application of the laboratory MSMPR precipitator for determining the precipitation kinetics has been widely reported. The description of the use of the MSMPR system for simultaneous determination of growth and nucleation rates is treated in Randolph and Larson (1988). For an unseeded, steady state, perfectly mixed precipitator, with size independent growth and nucleation occurring, the steady state PBE of the MSMPR precipitator has the form

$$n(L) = \frac{B^o}{G} \exp\left(-\frac{L}{G\tau}\right) \tag{4.3}$$

where $n(L)$ is the crystal number density function, B^o is the nucleation rate, G is the growth rate, L is the linear crystal size and τ is the mean residence time. The growth and nucleation rates can be determined from the experimental CSD data using a semi-logarithmic plot of Equation (4.3), which should give a straight line. The growth rate is determined from the slope of the semi-log plot, and the nucleation rate is calculated from the intercept.

However, most MSMPR precipitation systems generally do not yield straight lines. An upward curvature in the fine end of the CSD has been often reported (Garside and Shah 1980; Randolph and Larson 1988; Hostomsky and Jones 1991). Ilievski and White (1996) reported that the curvature could be either due to size dependent growth, growth rate dispersion, agglomeration, or non-representative sampling, or combination of the above phenomena. Similarly, they also stated that any downward curvature at the coarse end may be due to agglomeration and non-representative sampling.

4.3.1.2 Cumulative Weight Method

A drawback of the above graphical technique is the inaccuracy in determining the nucleation rate that results from the uncertainty in the CSD measurement, particularly, at the fine end of the CSD and the extrapolation of the CSD to size zero. Zumstein and Rousseau (1987b) used the cumulative weight data instead of the number density data to estimate the nucleation rate, in order to minimise the effect of these uncertainties. They fitted the experimental cumulative weight data with a non-linear regression model to determine the parameter $G\tau$. The nucleation rate is then estimated from

$$B^o = \frac{M_T}{6\rho_s k_v \tau (G\tau)^3} \tag{4.4}$$

where M_T is the total crystal mass, ρ_s is the solute density and k_v is the volume shape factor.

4.3.1.3 Non-linear Parameter Fitting Method

Non-linear fitting of experimental CSD data with a suitable function has also been employed. Sowul and Epstein (1981) used an exponential function of the form

$$n(t,L) = c\exp(-aL)\exp\left(-\frac{b\tau}{t}\right) \tag{4.5}$$

to fit the MSMPR CSD data, and a, b and c are empirical constants.

The growth and nucleation rates can be determined from

$$G = \frac{b\tau}{at^2} \tag{4.6}$$

and

$$B^o = c\exp\left(-\frac{b\tau}{t}\right) \tag{4.7}$$

This approach can be time consuming, as it requires the determination of the empirical parameters that give the best fit between the empirical function and experimental CSD data.

4.3.1.4 Simultaneous Method for Agglomeration, Growth and Nucleation

All the methods described above are applicable for a MSMPR precipitation system with simultaneous size independent growth and nucleation. The MSMPR system with size dependent growth has been treated in Canning and Randolph (1967), Abegg, Stevens & Larson (1968), Randolph and White (1977) and Randolph and Larson (1988).

Hounslow (1990b) introduced a kinetic parameter estimation method for a steady state precipitation system where simultaneous agglomeration, growth and nucleation are occurring. He transformed and solved the dimensionless PBE describing the MSMPR system, and then combined the analytical solution of the dimensionless steady state PBE with the zeroth and third moment equations. The growth rate can be determined independently from

$$G = \frac{\mu_3}{3\tau\mu_2} \tag{4.8}$$

where μ_2 and μ_3 are the second and third moments of the CSD, respectively. The agglomeration kernel, β, is estimated from

$$\beta = \frac{\sqrt{1+2K}-1}{\mu_0\tau} \tag{4.9}$$

where μ_0 is the zeroth moment, and K is the aggregation parameter and is estimated from

$$K = \frac{2I_{Agg}}{I_{Agg}^2 - 2I_{Agg} + 1} \tag{4.10}$$

I_{Agg} is referred to as the index of aggregation, and it has a value between 0 (no aggregation) and 1 (complete aggregation of every crystal formed). For the steady state MSMPR system considered by Hounslow (1990b), I_{Agg} is determined as follows

$$I_{Agg} = 1 - CV^{-\frac{10}{3}} \tag{4.11}$$

where CV is the coefficient of variance of the CSD. The nucleation rate is then determined by

$$B^o = \frac{K}{\beta\tau} \tag{4.12}$$

4.3.2 Methods for Dynamic Precipitation Data

4.3.2.1 Solute Mass Balance Method

The crystal growth rate can be estimated from the desupersaturation curve using the solute mass balance (Ilievski and White 1996) and rearranged to give

$$G = -\frac{k_a}{3k_v\rho_s A_T}\frac{ds}{dt} \tag{4.13}$$

where A_T is the total crystal surface area and s is the solute concentration. The desupersaturation curve is usually numerically differentiated to estimate *ds/dt* at any time instant. This method assumes that nucleation contributes negligibly to the desupersaturation.

4.3.2.2 Initial Derivatives Method

Garside, Gibilaro & Tavare (1982) developed the method of initial derivatives, which fits the initial part of the desupersaturation curve with a second-degree polynomial as

$\Delta c = a_0 + a_1 t + a_2 t^2$, where Δc is the solute concentration (kg/ kg solvent) and t is time. The first and second derivatives of the fitted desupersaturation curve are evaluated at $t = 0$, i.e.

$$\left.\frac{d\Delta c}{dt}\right|_{t=0} = a_1; \text{ and } \left.\frac{d^2\Delta c}{dt^2}\right|_{t=0} = 2a_2 \tag{4.14}$$

The parameters in the empirical power law growth model, equivalent to Equation (2.7), are then determined according to

$$g = \frac{2k_a a_0}{3\rho_s k_v A_o L_o} + \frac{2a_0 a_2}{a_1^2} \tag{4.15}$$

and

$$k_g = -\frac{a_1}{A_o a_0^g} \tag{4.16}$$

where A_o and L_o are the seed surface area and seed mean size, respectively.

4.3.2.3 Cumulative CSD Method

Misra and White (1971a) employed a cumulative number oversize plot to estimate the growth rate. The growth rate is determined by the amount of lateral shift, ΔL, over a time period, Δt, i.e. $G = \Delta L/\Delta t$. This method is limited to systems with negligible agglomeration and breakage. Similarly, they estimated the nucleation rate from the measured crystal numbers according to

$$B^o = \left.\frac{\Delta N}{\Delta t}\right|_{L=0} \tag{4.17}$$

where ΔN is the net change in crystal numbers at zero size per unit volume at a given time interval, Δt. However, it is not possible to measure the nuclei at zero size. Misra and White (1971a) reported that the smallest detectable size of the orifice tube they used in the Coulter counter particle size analyser was 1.42 μm. They assumed that no agglomeration and breakage occurred, and that nuclei grow at the same rate as the larger crystals. In that case, it can be argued that the number of crystals measured

greater than 1.42 μm at any time must have been the number of crystals at some prior time, $t-\Delta t$, where Δt is the time required for nuclei to grow to the detectable size of 1.42 μm, and is determined from the relation,

$$\int_{t-\Delta t}^{t} G(t)dt = 1.42\mu\text{m} \tag{4.18}$$

and G is determined from the approach described above. However, they found that the scatter in the raw data led to a high degree of scatter in their estimates of nucleation rate.

4.3.2.4 Laplace/Fourier Transform Methods

Tavare and Garside (1982, 1986a) developed a method for estimating the kinetic parameters in the Laplace domain. For a batch precipitation with size independent growth and no agglomeration and breakage, the PB model gives

$$\frac{\partial n(t,L)}{\partial t} = -G\frac{\partial n(t,L)}{\partial L} \tag{4.19}$$

Taking the Laplace transform with respect to L, gives

$$\frac{d\overline{n}(t,s)}{dt} + \overline{G}s\overline{n}(t,s) - \overline{B}^{o} = 0 \tag{4.20}$$

where s is the Laplace transform variable with respect to size L. $\overline{B}^{o}$ and $\overline{G}$ are averaged values over a small time interval Δt. A plot of $\Delta\overline{n}(t,s)/\Delta t$ versus $s\overline{n}(t,s)$ should give a straight line, provided Δt is small. $\overline{G}$ and $\overline{B}^{o}$ are determined from the slope and intercept of the plot, respectively. Similarly, an equivalent Fourier transform method for estimating the kinetics is also described in Tavare (1986a).

4.3.2.5 Moments Matching Method

This method requires matching of the experimentally measured moments with those derived theoretically from the PBE for the precipitation system considered. The

moment of a distribution has been defined in Chapter 3. For a batch precipitation system with simultaneous nucleation and size independent growth occurring, application of this method yields the following moment equations for determining nucleation and growth rates,

$$\frac{d\mu_0}{dt} = B^o \tag{4.21}$$

$$\frac{d\mu_1}{dt} = G\mu_0 \tag{4.22}$$

The zeroth and first moments in equations (4.21) and (4.22) are determined from the experimental CSD data, and both time derivative terms are evaluated by numerical differentiation. The moments matching method is particularly sensitive to errors in the coarse size intervals, because the weighting favours the coarse size end.

Tavare and Garside (1993) applied the moments matching method to extract agglomeration, growth and nucleation kinetics from the experimental data, utilising the first three moment equations for a semi-batch precipitation system. They assumed that the growth rate was independent of crystal volume. However, there is some doubt about the validity of this assumption, and hence, the applicability of their approach to estimating the kinetics in a precipitation system.

Hounslow, Ryall & Marshall (1988) showed that for size independent growth, only those moments that are a multiple of 3 can be evaluated analytically. Hence, the zeroth, third and sixth moment equations can be employed to extract agglomeration, growth and nucleation kinetics from the experimental precipitation data. However, it needs to be emphasised that large uncertainty in using higher order moment equations can occur. This method and its problem will be discussed in detail in Chapter 9.

4.3.2.6 The Bramley, Hounslow & Ryall (1996) Method

Bramley, Hounslow & Ryall (1996) introduced a novel differential method for the determination of precipitation kinetics. Their method uses the discretised population

balance model of Hounslow, Ryall & Marshall (1988), and transforms it to derive the equations for the zeroth and third moments and the number of particles in the first size interval. Their method has the form

$$\dot{\mu}_0 = B_u + \Phi_0 \beta \tag{4.23}$$

$$\dot{\mu}_3 = \Phi_3 G + \overline{L}_1^3 B_u \tag{4.24}$$

$$\dot{N}_1 = \Phi_2 G + B_u + \Phi_1 \beta \tag{4.25}$$

where the coefficients Φ_0 , Φ_1 , Φ_2 and Φ_3 can be calculated from the experimental data and are defined as

$$\begin{aligned}\Phi_0 = &\sum_{i=1}^{n} N_{i-1} \sum_{j=1}^{i-2} 2^{j-i+1} f(\overline{L}_{i-1}, \overline{L}_j) N_j + \frac{1}{2} \sum_{i=1}^{n} f(\overline{L}_{i-1}, \overline{L}_{i-1}) N_{i-1}^2 \\ &- \sum_{i=1}^{n} N_i \sum_{j=1}^{i-1} 2^{j-i} f(\overline{L}_i, \overline{L}_j) N_j - \sum_{i=1}^{n} N_i \sum_{j=1}^{n} f(\overline{L}_i, \overline{L}_j) N_j\end{aligned} \tag{4.26}$$

$$\Phi_1 = -N_1 \sum_{j=1}^{n} f(\overline{L}_1, \overline{L}_j) N_j \tag{4.27}$$

$$\Phi_2 = \frac{2}{(1+r)L_1} \left(\left(1 - \frac{r^2}{r^2 - 1} \right) N_1 - \frac{r}{r^2 - 1} N_2 \right) \tag{4.28}$$

$$\begin{aligned}\Phi_3 = &\frac{2}{(1+r)L_1} \left(\left(1 - \frac{r^2}{r^2 - 1} \right) N_1 - \frac{r}{r^2 - 1} N_2 \right) \overline{L}_1^3 \\ &+ \sum_{i=2}^{n} \frac{2}{(1+r)L_i} \left(\frac{r}{r^2 - 1} N_{i-1} + N_i - \frac{r}{r^2 - 1} N_{i+1} \right) \overline{L}_i^3\end{aligned} \tag{4.29}$$

where $f(\overline{L}_i, \overline{L}_j)$ is the size dependent term of the agglomeration kernel, and $\overline{L}_i$ is the mean size of the i^{th} size interval. This approach is not restricted to only size independent agglomeration system as in the case of the moments matching method of Tavare and Garside (1993) described above.

The time derivative terms, $\dot{\mu}_0$, $\dot{\mu}_3$ and $\dot{N}_1$ are the rate of change in the zeroth moment, third moment and number in the first size interval, respectively. These terms are determined from the experimental data using a numerical differentiation scheme. The above system of linear equations (4.23)-(4.25) needs to be solved simultaneously in order to determine the values of the agglomeration kernel, β, the growth rate, G, and the source term rate, B_u. The source term rate in the above equations is the apparent nucleation rate, but is not necessarily the true nucleation rate. It is a measure of the rate of crystal numbers appearing in the first size interval (of mean size $\overline{L}_1$) of the particle size analyser.

The aforementioned methods for estimating kinetics from dynamic precipitation data involve estimation of the time derivative terms, and are referred to as the differential methods in the literature (Aoun et al. 1999; Livk, Pohar & Ilievski 1999). The error introduced by numerical differentiation will propagate through the kinetic parameter estimation methods, and can lead to large errors in the parameter estimates.

4.3.3 Non-Linear Parameter Estimation Method

The application of the non-linear parameter estimation method (or sometimes referred to as integral method) to determine precipitation kinetic parameters has increased since the 1980s (Tavare, Shah & Garside 1985; Beigler, Damiano & Blau 1986; Tavare 1986a; Qiu and Rasmouson 1990; 1991; Hostomsky and Jones 1991; Rawlings, Witkowski & Eaton 1992; Farrell and Tsai 1994; Miller and Rawlings 1994; Aoun et al. 1999). The method is complex and requires an iterative optimisation scheme to obtain the optimum kinetic parameter estimates. However, the optimisation scheme does not require model simplification. This method is potentially the most accurate and precise parameter estimation method available in the literature, as it avoids the numerical differentiation procedures of differential methods. However, to compensate for the accuracy and precision in the parameter estimates, this method has several drawbacks (Livk, Pohar & Ilievski 1999). Firstly, it is computationally intensive and time consuming. Secondly it can suffer from problems associated with solution convergence (i.e. multiple minima), and finally, if the optimisation problem is not well posed, then uniqueness of parameter estimates is in doubt. Several authors repeated their parameter optimisation procedure with

different sets of initial guess in order to ensure solution convergence, for the same experimental data set (Nallet, Mangin & Klein 1998).

The parameter estimation problem is posed as an optimisation problem:

$$\begin{aligned} &\min \quad \Phi(y^{\text{expt}}, y^{\text{model}}(\theta)) \\ &\text{Subject to} \quad \text{Precipitation Model} \end{aligned} \tag{4.30}$$

The aim is to minimise the objective function, $\Phi(\theta)$, with the optimum kinetic parameter values, θ, subject to the precipitation model and measurement data used. In order for the non-linear parameter optimisation scheme to be successful in estimating precipitation kinetic parameters, careful experimental design and selection of the objective function are required (Rawlings, Miller & Witkowski 1993). The usual form of the objective function used is

$$\Phi(\theta) = \sum_{i=1}^{m} \sum_{j=1}^{n} \omega_i (y_{i,j}^{\text{expt}} - y_{i,j}^{\text{model}}(\theta))^2 \tag{4.31}$$

which is the sum of squares difference between the experimental measurement and model prediction. $y_{i,j}^{\text{expt}}$ and $y_{i,j}^{\text{model}}$ are the i^{th} experimental measurement and model prediction, respectively, at the j^{th} sampling instant during the experiment. ω_i is the weighting assigned to the i^{th} measured variable, m, and n are the number of samples of each measured variable, and θ represents the kinetic parameters.

Tavare, Shah & Garside (1985) and Hostomsky and Jones (1991) employed the non-linear parameter optimisation method to estimate the nucleation, growth and agglomeration kinetics rates in the MSMPR system. Livk, Pohar & Ilievski (1999) incorporated a differential approach into the non-linear optimisation problem to determine growth, agglomeration and nucleation rates in batch gibbsite precipitation. They reduced the optimisation problem into three sub-problems, which can be solved sequentially using both solute concentration and CSD data.

4.4 UNCERTAINTY IN THE PARAMETER ESTIMATES

There is no doubt that the kinetics estimates determined from the experimental data will incur estimation uncertainty. However, the uncertainty bounds of the kinetics estimates are generally not reported in most of the parameter estimation studies in the literature. A number of investigators have found significant scatter in the parameter estimates using different parameter estimation methods on the same data (Nývlt and Broul 1982; Tavare 1986a; Jager et al. 1991). It has also found that different investigators studying the same precipitation system have published quite different kinetic parameters. For example, Rohani (1993) reported large discrepancies in the published nucleation and growth kinetics from different authors studying potassium chloride system. Yokota, Sato & Kubota (2000) also reported similar inconsistencies in the kinetic parameters for the potash alum system.

The inconsistency in the kinetic parameter values and the failure of some kinetic parameter estimation methods to obtain accurate values are related to the issues of proper experimental design, choice of measurement data used in determining the parameter, and uncertainty in the kinetic parameter estimates (Rawlings, Miller & Witkowski 1993). In precipitation systems, the choice of the measurable variables, namely, solute concentration and CSD data, is an important factor in determining the accuracy of the parameter values. Rawlings, Witkowski & Eaton (1992) showed that the use of solute concentration data alone is insufficient to determine the nucleation parameters accurately. This is not surprising given that nucleation contributes negligibly to the desupersaturation data, and hence, the solute concentration data is not sensitive enough to determine the nucleation rate. They further demonstrated that by using additional information (i.e. transmittance data in their case) in the objective function, the uncertainties in both growth rate and nucleation rate parameters were significantly reduced.

Uncertainty in the measured data can lead to large uncertainty in the kinetic parameter estimates through the parameter estimation procedure. The uncertainty in the parameter can be readily determined if many replicate experimental data sets are available. However, replicate data sets from precipitation experiments can be difficult to generate, due to the constraints on time or resources for carrying out large

number of experiments, or both. An alternative is to employ Monte Carlo simulations to generate replicate data sets, by adding random errors to the original data set, in accordance with the assumed measurement probability distribution. However, Monte Carlo simulations are time consuming when used with the non-linear parameter optimisation, because the estimation process is computationally intensive (Rawlings, Miller & Witkowski 1993). Bard (1974) stated that the uncertainty of the parameters in a non-linear parameter optimisation problem can be roughly determined from the diagonal elements of the covariance matrix, using the maximum likelihood method. The details are given in Bard (1974) and will not be treated here.

4.5 CONCLUSIONS

Experimental precipitation techniques and kinetic parameter estimation methods used to extract kinetics rates from the experimental precipitation data have been reviewed. There is no universal kinetic parameter estimation technique for determining the kinetics, as the techniques used will depend on which processes are present and the experimental setup employed. It should be borne in mind that all kinetic parameter estimation techniques incur uncertainty in the kinetic parameter estimates. This originates from uncertainty in the measurement data, which is being propagated by the kinetic parameter estimation techniques used to extract the kinetic parameters.

CHAPTER 5

MODELLING WELL-MIXED GIBBSITE PRECIPITATION SYSTEMS

5.1 INTRODUCTION

This chapter focuses on modelling the CSD in well-mixed gibbsite precipitation experiments conducted in a constant composition semi-batch configuration under the conditions such that, agglomeration and growth were occurring, and nucleation was negligible; and a batch configuration under the conditions where simultaneous agglomeration, growth and nucleation took place. The PB theory is adopted here to model both experimental rigs. The Hounslow's discretisation method is used to solve the resulting PBEs. Gibbsite kinetics rates are determined from correlations published in the literature and from the experimental data by matching the moments of the CSD or by the Bramley's method. The suitability of the developed precipitator models to describe the experimental systems being modelled is validated by comparing the CSD predictions to the corresponding experimental gibbsite precipitation data. In addition, the quality of the CSD predictions made in the constant composition system, using the kinetics from correlation models is compared with those using kinetics estimated by the moments matching method.

5.2 THE EXPERIMENTAL GIBBSITE PRECIPITATION DATA

The gibbsite precipitation experiments reported in this chapter were performed by Ilievski, McShane & Rudman (1997). Two different precipitation configurations were used: a constant composition semi-batch system and a batch system. A schematic of the experimental precipitation system is depicted in Figure 5.1.

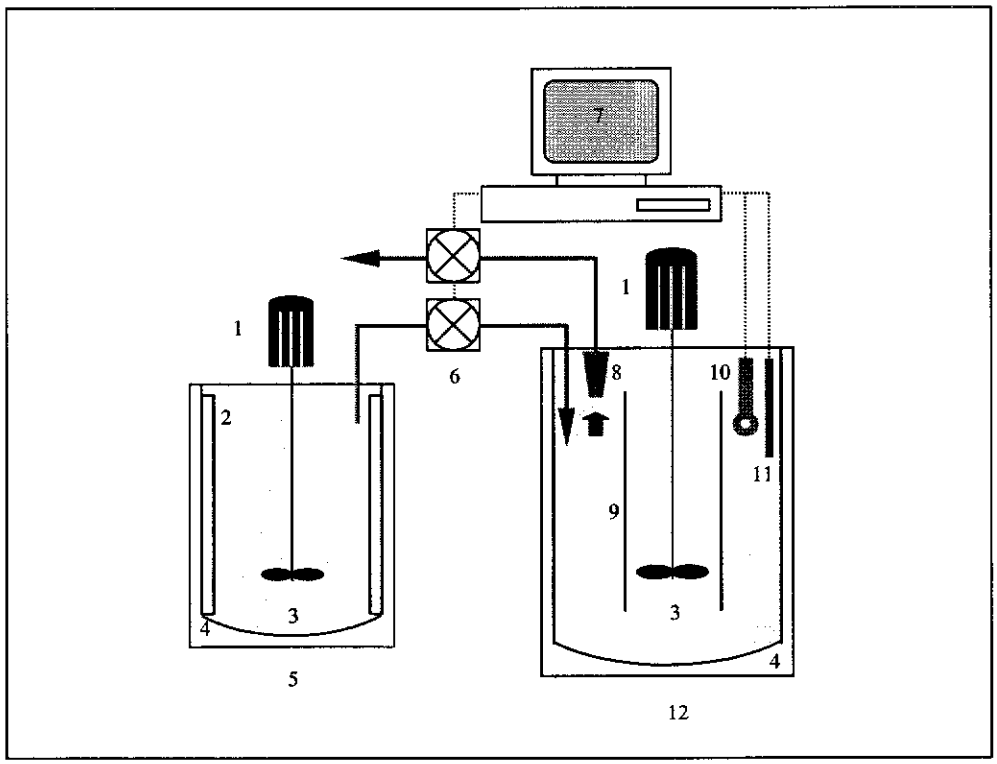

Figure 5.1. Schematic of the constant composition experimental precipitation unit of Ilievski, McShane & Rudman (1997): 1, overhead stirring motor; 2, baffles; 3, impeller; 4, water jacket; 5, liquor feed tank; 6, peristaltic pump; 7, computer monitoring system; 8, clear liquor or solids withdrawal system; 9, draft tube with spoilers; 10, conductivity probe; 11, turbidity probe; and 12, precipitator.

In both of the batch and constant composition precipitation experiments, a 4-litre stainless steel precipitator and an on-line computer monitoring system was used. In the constant composition configuration, the liquor feeding and withdrawal systems were also utilised. Ilievski, McShane & Rudman (1997) reported that the liquor composition was kept constant by maintaining the set point conductivity. Deviations from the set point conductivity result in the feed pump being activated, which in turn feeds liquor of an appropriate composition to the precipitator at a rate regulated by feedback control. The conductivity was monitored on-line and shown to be proportional to the aluminate concentration. The precipitator was operated in a semi-batch mode with clear liquor flow (i.e. solids are retained). The clear liquor removal rate was at the same volumetric flow rate as the feed addition. Details of the development of the constant composition precipitator and its validation are reported in Ilievski (2000).

The constant composition precipitation experiment was conducted at a constant temperature of 80 °C and agitated at 800 rpm by an IKA EUROSTAR overhead stirring motor with a 86 mm Lightnin® A310 axial impeller. The caustic aluminate solution was prepared by digesting technical grade gibbsite crystals in a hot aqueous sodium hydroxide solution, and made up to a supersaturation ratio *A/C* of 0.6 (expressed in g L^{-1} Al_2O_3/ g L^{-1} Na_2CO_3). A seed charge of 15 g L^{-1} (Alcoa C31 gibbsite) was used. An important feature of this constant composition precipitation experiment is that the precipitator was operated under conditions where the agglomeration and growth kinetics are expected to be constant, and negligible nucleation and crystal breakage are expected (Ilievski, McShane & Rudman 1997).

Ilievski, McShane & Rudman (1997) periodically sampled the suspension for determination of liquor composition, magma density and CSD. They demonstrated that the particulate phase sampling was representative. The CSD were determined using a Coulter® counter multisizer II, which measures particle population and spherical volume equivalent diameter. The liquor composition was determined using a Watts-Utley titration (Watts and Utley 1956). Their experimental data were checked for mass balance consistency. Figure 5.2 shows that the aluminate species concentration, *A*, during the course of the constant composition precipitation experiment, constant with time at 111 ± 2 g L^{-1} Al_2O_3.

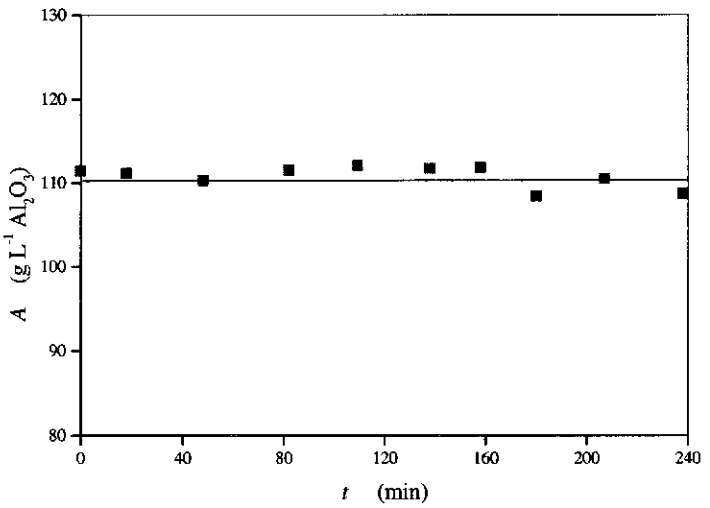

Figure 5.2. Aluminate species concentration, *A*, during the constant composition precipitation run (from the data of Ilievski, McShane & Rudman 1997).

The batch precipitation experiment was carried out isothermally at 60 °C and agitated at 800 rpm in the same precipitator vessel used in the constant composition experiment described above. An initial supersaturation ratio *A/C* of 0.7 and a seed charge of 20 g L^{-1} were employed. Under these operating conditions, agglomeration, growth and nucleation occurred simultaneously during the precipitation run. Figure 5.3 shows the typical desupersaturation curve obtained in the batch precipitation experiment.

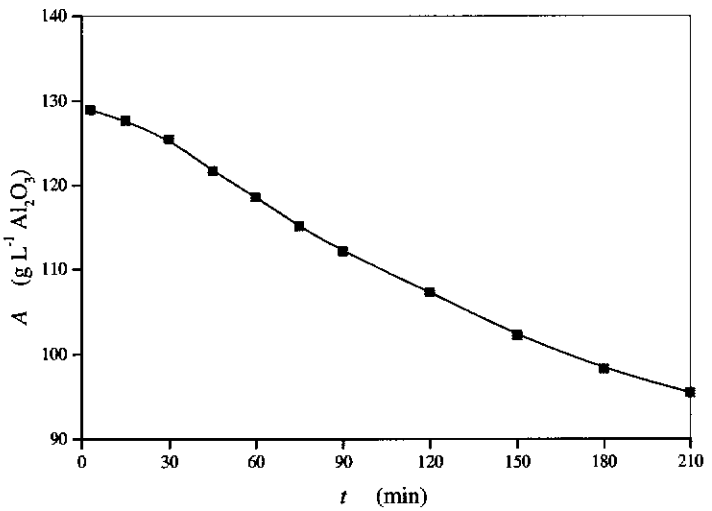

Figure 5.3. Typical desupersaturation curve from the batch precipitation run (from the data of Ilievski, McShane & Rudman 1997).

5.3 MODELLING THE CONSTANT COMPOSITION PRECIPITATION EXPERIMENT

5.3.1 Constant Composition Precipitator Model

The PB model for the experimental constant composition, semi-batch precipitator described above is

$$\frac{\partial n}{\partial t} + G\frac{\partial n}{\partial L} = B_A - D_A \tag{5.1}$$

The term n is the crystal number density function, t is the time, G is the linear growth rate, and L is the crystal size. B_A and D_A are the birth and death terms due to agglomeration, respectively as described in Chapter 3.

The assumptions made in deriving the above PB model are (1) the precipitation system is well-mixed; (2) constant precipitator working volume; (3) no crystals withdrawn from the precipitator; (4) no nucleation and crystal breakage; (5) size independent crystal growth; and (6) agglomeration occurring.

Ilievski and White (1994a) and Ilievski and Hounslow (1995) showed that gibbsite agglomeration can be considered independent of crystal size for modelling purposes. Hence, for a size independent agglomeration kernel, B_A given in Equation (3.19) can be expressed as

$$B_A = \frac{\beta L^2}{2} \int_0^L \frac{n(t,[L^3 - \lambda^3]^{\frac{1}{3}}) n(t,\lambda)}{(L^3 - \lambda^3)^{\frac{2}{3}}} d\lambda \tag{5.2}$$

which represents the appearance of crystals into the size range L to $L + dL$ due to agglomeration of crystals of sizes $L - \lambda$ and λ. Similarly, D_A is

$$D_A = \beta\, n(t,L) \int_0^\infty n(t,\lambda) d\lambda \tag{5.3}$$

which is the disappearance of crystals in the size range L to $L + dL$ as they agglomerate with crystals of any size, λ.

5.3.2 Discretised Constant Composition Precipitator Model

The PB model equations (5.1), (5.2) and (5.3) above are intractable and the DPB was used to solve them. For the constant composition experiment considered here, the DPB for the i^{th} size interval, i.e. Equation (3.38) can be written as

$$\frac{dN_i}{dt} = \left(\frac{dN_i}{dt}\right)_A + \left(\frac{dN_i}{dt}\right)_G \tag{5.4}$$

where N_i is the number of crystals per unit volume of slurry in the i^{th} size interval. The terms on the right hand side of Equation (5.4) are the rate of change in crystal numbers in the i^{th} size interval due to crystal agglomeration and growth, respectively,

and can be represented by equations (3.47) and (3.42) or (3.45). A size discretisation ratio, $r = \sqrt[3]{2}$ was used. A fourth-order Runge-Kutta numerical technique has been used to solve the DPB equations in a computer code written in Visual Basic.

5.3.3 Experimental Data Transformation

The experimental CSD data could not be used directly in the DPB model because the measured size intervals did not follow a $\sqrt[3]{2}$ progression. Two approaches were considered for transforming the CSD data into the correct form, i.e. to estimate the crystal numbers in each discretised interval. These are outlined below.

5.3.3.1 Approximation from Absolute Particle Numbers

In this approach, the crystal numbers in each size interval are determined by summing all the numbers from the raw data that fall within the lower and upper bounds of the discretised interval. At the extremes, a linear approximation function is applied to estimate the fractional number portion of the measured size interval that falls within the discretised size intervals. The details of this approach are illustrated below. Consider the bounds of the measured size intervals to be denoted as x_j and those for the discretised size intervals as L_i, and the number within size x_j to x_{j+1} denoted as Y_j and the number within size L_i to L_{i+1} as N_i, as shown in Figure 5.4.

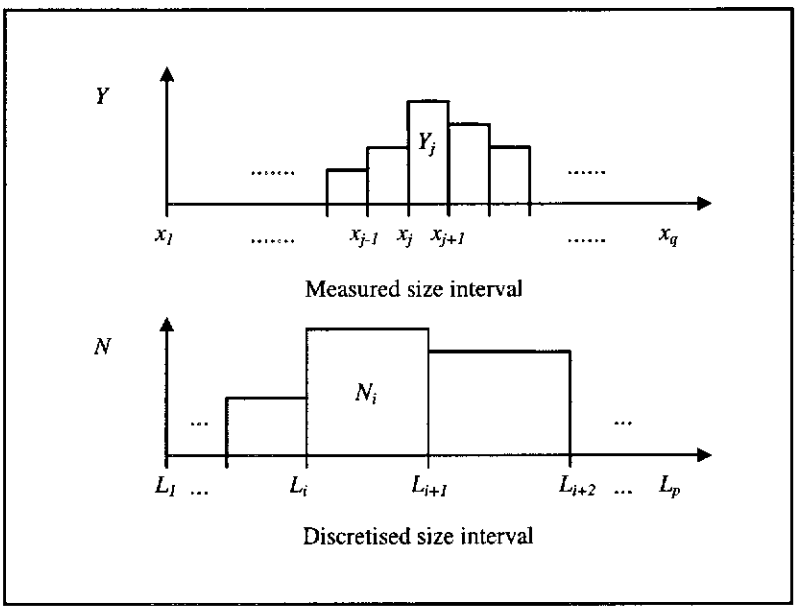

Figure 5.4. A comparison of the experimentally measured and discretised size intervals.

The number, N_i, in the size interval L_i to L_{i+1} is estimated according to equations (5.5) and (5.6),

$$N_i = \begin{cases} \sum_{j=1}^{k_1+M_1-1} Y_j + \left(\frac{L_2 - x_{k_1+M_1}}{x_{k_1+M_1+1} - x_{k_1+M_1}} \right) Y_{k_1+M_1} & i=1 \\ \left(\frac{x_{k_i} - L_i}{x_{k_i} - x_{k_i-1}} \right) Y_{k_i-1} + \sum_{j=k_i}^{k_i+M_i-1} Y_j + \left(\frac{L_{i+1} - x_{k_i+M_i}}{x_{k_i+M_i+1} - x_{k_i+M_i}} \right) Y_{k_i+M_i} & i \neq 1 \end{cases} \quad (5.5)$$

where

$$k_i = \begin{cases} 1 & i=1 \\ k_{i-1} + M_{i-1} + 1 & i \neq 1 \end{cases} \quad (5.6)$$

M_i is defined such that

$$M_i = \left\{ \mathrm{Int}\left(\frac{L_{i+1} - x_i^o}{h} \right) : L_i \leq x_i^o < L_{i+1}; i = 1,2,..p \right\} \quad (5.7)$$

The term h is the width of the equally spaced measured size intervals. x_i^o is the starting measured size that falls between the discretised interval of L_i to L_{i+1}. This formulation however is valid only for a discretisation ratio greater than the experimentally measured size interval width. Hence, if a finer size discretisation ratio, i.e. $r < h$, is desired, then the next approach should be employed.

5.3.3.2 Approximation from Particle Number Density

In this approach, the number density, n_i, in each discretised size interval, with the geometric mean of $\overline{L_i} = \sqrt{L_i L_{i+1}}$ is approximated from the experimental number density, y_i, of measured size interval of x_j to x_{j+1}, using linear or cubic spline functions. The number, N_i, in the discretised size interval is then estimated by multiplying the number density with the discretised size width of (L_{i+1} - L_i). This approach is only suitable for narrow discretised size interval widths.

5.3.4 Constant Composition Kinetic Parameter Estimation

The agglomeration kernel, β, and growth rate, G, were determined from the correlation models of Ilievski and White (1994a; 1994b) discussed in Chapter 2, i.e. equations (2.13) and (2.9), respectively. Similarly, β and G were also estimated by matching the zeroth and third moment formulations of Equation (5.1) with the experimental data. In this experimental system, it can be assumed that (a) the nucleation rate can be ignored, (b) the agglomeration kernel and the growth rate are independent of crystal size, and dependent only on supersaturation and temperature, and (c) the precipitator operation is isothermal and at constant supersaturation. Hence, the resulting zeroth and third moment equations are identical to equations (3.30) and (3.31) discussed in Chapter 3.

The zeroth moment equation (3.30) can be solved analytically for a time-invariant β to give (see Appendix 1)

$$\frac{1}{\mu_0(t)} = \frac{1}{\mu_0(0)} + \frac{1}{2}\beta t \tag{3.33}$$

where $\mu_0(t)$ is the total crystal numbers in the precipitator at time t, and is measured experimentally. $\mu_0(0)$ is the number of seed crystals added initially. The value of β is estimated from the slope of the plot of $1/\mu_0(t)$ against t using linear regression, as shown in Figure 5.5.

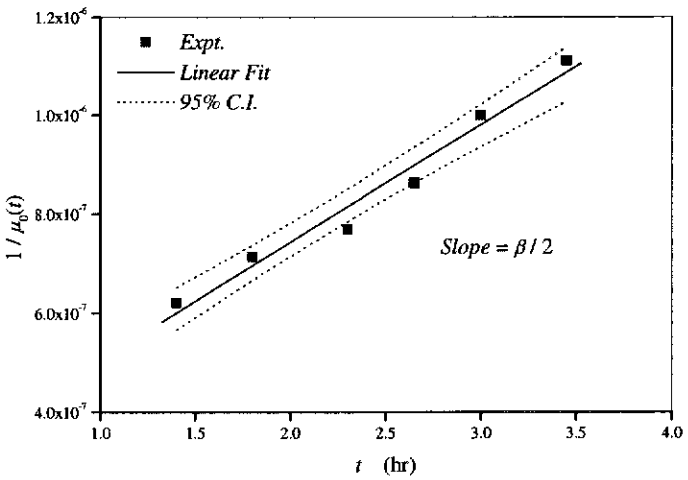

Figure 5.5. Linear least squares fit to the experimental data. Plot of $1/\mu_0(t)$ against time, t.

Similarly, G can be estimated from a linear least squares fit to Equation (3.31), as shown in Figure 5.6, where the terms $d\mu_3(t)/dt$ and $\mu_2(t)$ are obtained by transforming the experimental CSD data, according to

$$\mu_j(t) = \sum_{i=1}^{n} \overline{L}_i^j N_i(t) \tag{5.8}$$

where j denotes the order of the moments. Equation (5.8) is the discrete form of the moments of the CSD in Equation (3.7). As noted in Li, Rohl & Ilievski (2000), the linear behaviour of figures 5.5 and 5.6 confirms the assumptions of size independent agglomeration and growth, and indeed, the other model assumptions.

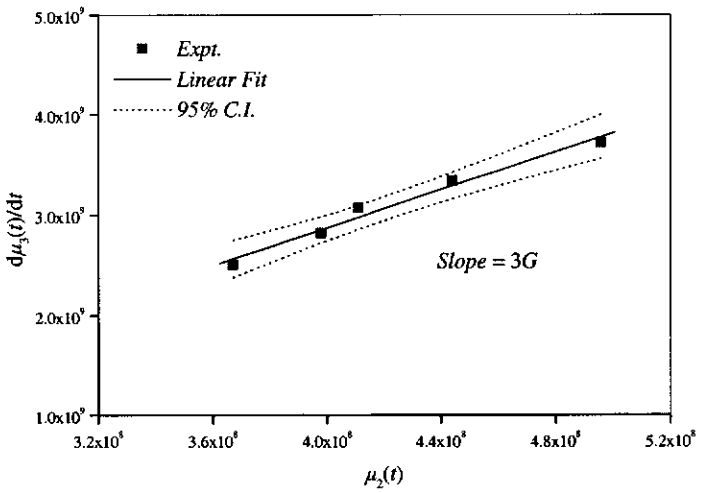

Figure 5.6. Linear least squares fit to the experimental data. Plot of $d\mu_3(t)/dt$ against $\mu_2(t)$.

The β and G estimates from the correlation models and the moments matching method were different. For the constant composition experimental conditions reported here, the β estimate from the correlation model was 1.02×10^{-7} mL hr^{-1}, which is significantly lower than the value of 4.63×10^{-7} mL hr^{-1} estimated from the zeroth moment matching. The G estimate from the correlation model was 4.80 μm hr^{-1} compared to the value of 2.44 μm hr^{-1} from the third moment matching.

5.4 CONSTANT COMPOSITION SIMULATION RESULTS

5.4.1 Comparison of Constant Composition Data to Model Prediction

In the context of this chapter, the DPB model using β and G estimates from the correlation models and from the moment equations are referred as CModel and MModel, respectively. The prefixes 2G and 3G are used to denote the use of either the two-term or three-term growth models in the DPB model, i.e. Equation (3.42) or (3.45). A comparison of the CSD predictions made at different simulation times from the 2GMModel and 3GMModel, with the experimental CSD is presented in Figure 5.7, which shows that the CSD predictions by the 3GMModel give better agreement to the experimental CSD than those from the 2GMModel. The 2GMModel results in more crystals in the larger size ranges.

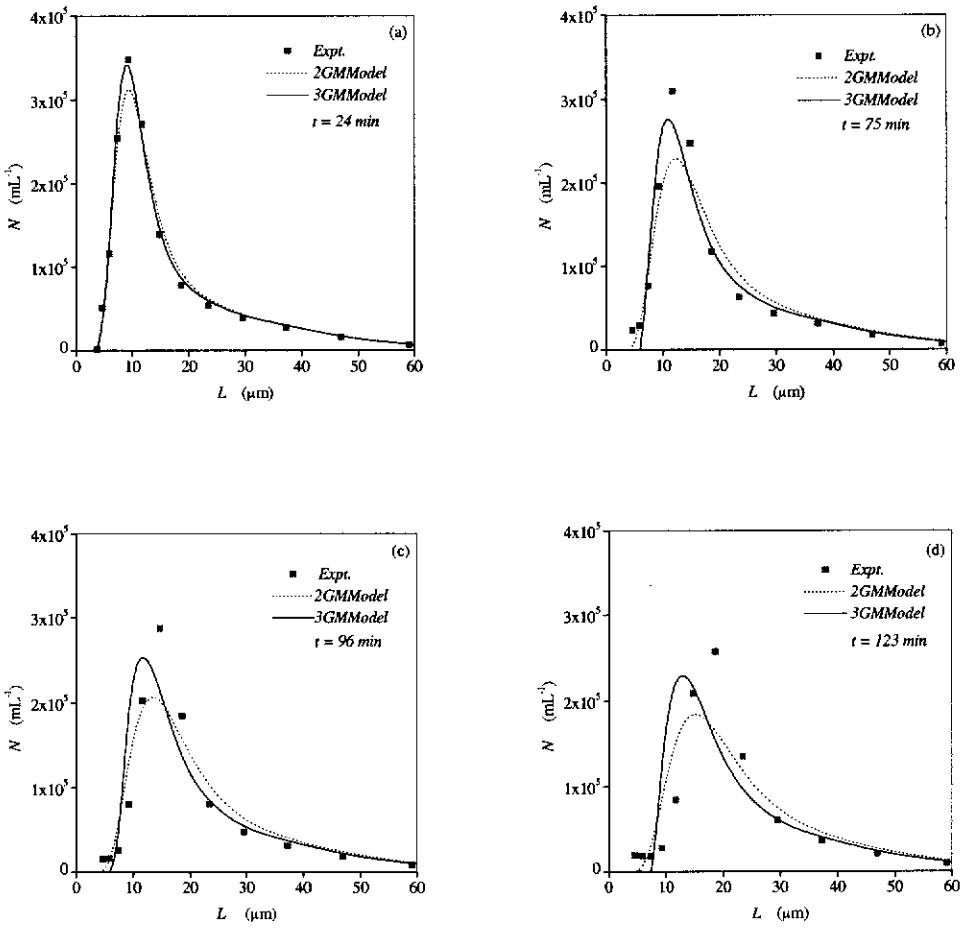

Figure 5.7. Comparisons of the experimental data and model predictions, by the 2GMModel and 3GMModel at different simulation times. (a) 24 minutes; (b) 75 minutes; (c) 96 minutes; and (d) 123 minutes.

Figure 5.8 shows the comparison of the CSD predictions from the 3GCModel and 3GModel (this model will be explained in details later on) to the experimental CSD. It can be seen that poorer CSD predictions were obtained from the 3GCModel compared to the experimental CSD, than those from either of the MModels in Figure 5.7. This is expected since the kinetics used in the MModel are essentially the best fit parameters to the experimental data, assuming that the form of the model is correct. The main source of the discrepancy between the CModel predictions and the experimental data is due to the low β estimate predicted by the agglomeration correlation.

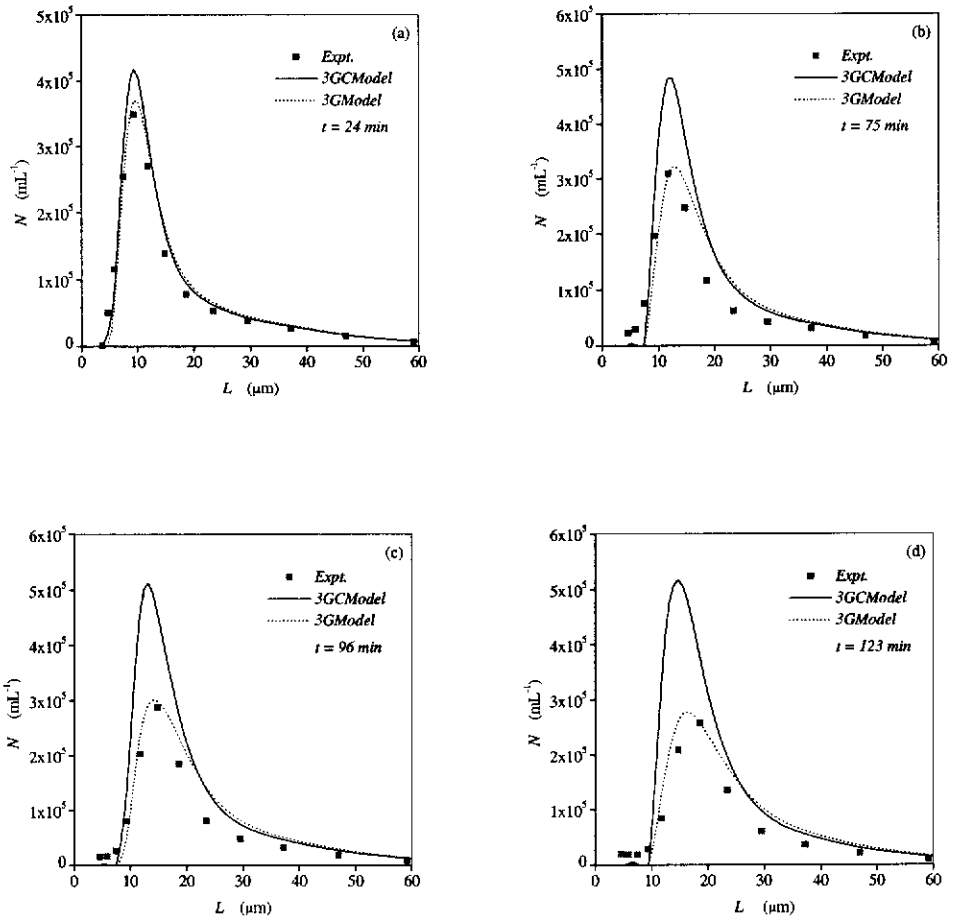

Figure 5.8. Comparisons of the experimental data and model predictions, by the 3GCModel and 3GModel at different simulation times. (a) 24 minutes; (b) 75 minutes; (c) 96 minutes; and (d) 123 minutes.

As the effect of crystal agglomeration on the product CSD is great compared to that from crystal growth (due to the extraordinary slow gibbsite growth), the effect of crystal growth cannot be observed clearly from the CSD predictions made by the 3GCModel in Figure 5.8. However, the effect of crystal growth on the product CSD can be observed by using the β estimate from the zeroth moment matching and G estimate from the correlation model. This approach is referred to as 3GModel in Figure 5.8, which shows the resultant CSD predictions are of the same shape as the experimental CSD but shifted to larger sizes as in the 3GCModel. This clearly indicates that the G estimate from the correlation model is too high.

Figure 5.9 shows the predictions of the total number of crystals, $\mu_0(t)$, by different models. The CModel predicts significantly higher number of crystals. In contrast, the MModel gives a much better prediction, and the relative error is less than 7% in the MModel compared to up to 85% for the CModel.

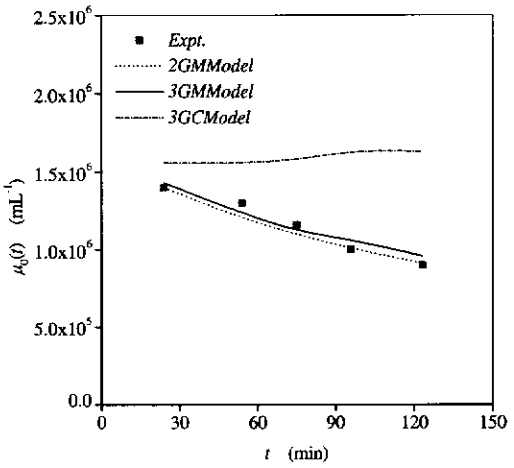

Figure 5.9. Comparisons of the experimental and predicted total crystal numbers, $\mu_0(t)$, by the 2GMModel, 3GMModel, and 3GCModel.

The results clearly demonstrate that the literature correlation models for the gibbsite agglomeration and growth are not accurate in describing the gibbsite precipitation data being modelled. It is important to recognise the high statistical uncertainties quoted for the correlation models; the 95% confidence limits on the agglomeration

and growth correlation models are ± 70% and ± 50%, respectively. In contrast, the moment equations estimate the kinetics directly from the experimental data being measured and are expected to provide better estimates.

5.4.2 Error Propagation

It can be observed in Figure 5.7 that the CSD predictions are continuously drifting away from the experimental data as the simulation time increases. This, as reported by Li, Rohl & Ilievski (2000), suggests propagation of error in the DPB model. To put the error propagation in clearer context, two simulations are presented. In the first, hereafter referred to as the "seed" approach, all the transient CSD predictions are made starting at time $t = 0$ (after accounting for the induction time). In the second approach, hereafter referred to as the "preceding" approach, the transient CSD at sample time t_{i+1} is predicted using the experimental CSD at the preceding sample time of t_i as the starting distribution. If error propagation is significant then we expect the "seed" approach simulations to show greater deviation with time than the "preceding" approach simulation. This is seen to be the case in Figure 5.10, which compares the experimental CSDs with the predicted product CSDs at different simulation times, from both the "seed" and "preceding" approaches.

To quantify the deviations between the model predictions and the experimental data, the sum of squares error, SSE, given by Equation (5.9), is used to measure the goodness of fit of the DPB model predictions to the experimental data.

$$SSE(t) = \sum_i \left(\frac{N_i^{\text{expt}}(t)}{\mu_0^{\text{expt}}(t)} - \frac{N_i^{\text{model}}(t)}{\mu_0^{\text{model}}(t)} \right)^2 \tag{5.9}$$

where the superscripts "expt" and "model" denote the experimental and predicted quantities, i.e. the crystal numbers in the i^{th} size interval, N_i, and the total crystal numbers, μ_0, respectively. The normalised SSE defined above ensures that the decrease in crystal numbers with time, due to the agglomeration of crystals, does not bias the SSE estimate.

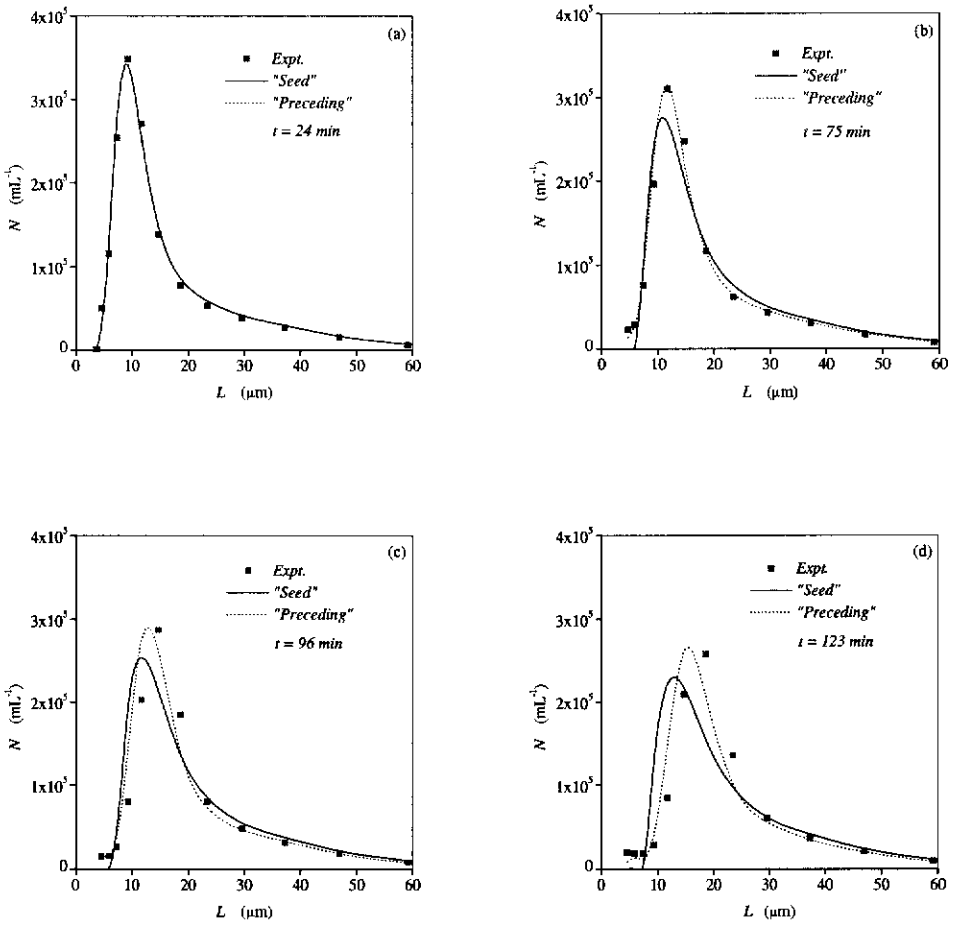

Figure 5.10. Comparisons of the experimental data and model predictions, by the 3GMModel at different simulation times, with the "seed" and "preceding" approaches. (a) 24 minutes; (b) 75 minutes; (c) 96 minutes; and (d) 123 minutes.

Figure 5.11 shows the difference in the SSE between the "seed" and "preceding" approaches using the 3GMModel. The differences in the SSE continuously increase with time, which clearly demonstrates that the error in the DPB model propagates with time. The extent of the propagation of error may be exacerbated by the coarse discretised size used in the discretisation method, and will be discussed in Chapter 6. In general, the DPB model of the constant composition precipitator is capable of accurately predicting the product CSD over short time intervals, i.e. up to 75 minutes for this particular precipitation data. The approach of starting with the seed CSD and predicting product CSDs over longer time periods will need to be assessed in view of the propagation of error.

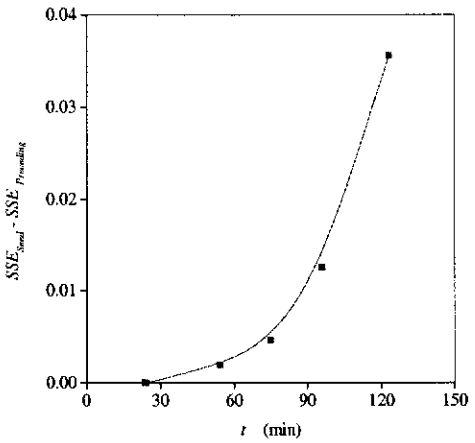

Figure 5.11. The difference in the sum of squares error between the "seed" and "preceding" approaches, using the 3GMModel, for the constant composition experiment.

5.5 MODELLING THE BATCH PRECIPITATION EXPERIMENT

5.5.1 Batch Precipitator Model

The PB model for the batch precipitator considered has the form

$$\frac{\partial n}{\partial t} + G\frac{\partial n}{\partial L} = B_A - D_A + B_N \tag{5.10}$$

The model assumptions made are the same as those assumed in deriving the constant composition precipitator model, with the exception that nucleation is occurring in this case, and is described by the term B_N.

5.5.2 Discretised Batch Precipitator Model

The DPB for the i^{th} size interval in this batch system is written as

$$\frac{dN_i}{dt} = \left(\frac{dN_i}{dt}\right)_A + \left(\frac{dN_i}{dt}\right)_G + \left(\frac{dN_i}{dt}\right)_B \tag{5.11}$$

The terms on the right hand side of Equation (5.11) are the discretised agglomeration, growth and nucleation terms as given in Chapter 3. As mentioned in Chapter 4, the true nucleation rate cannot be determined, as the particle size analyser

is unable to detect the negligibly small nuclei. The source term rate, B_u, is usually adopted as a measure of the apparent nucleation rate (i.e. replacing B^o by B_u in Equation (3.40)). This term affects only the crystal numbers in the first discretised size interval, the smallest measurable size of the particle size analyser. Hence, the discretised source term is defined as

$$\left(\frac{dN_i}{dt}\right)_B = \begin{cases} B_u & i=1 \\ 0 & \text{Otherwise} \end{cases} \tag{5.12}$$

5.5.3 Batch Kinetic Parameter Estimation

The method of Bramley, Hounslow & Ryall (1996) was applied to estimate the β, G and B_u from the experimental data simultaneously. Equations (4.23)-(4.25) can be rearranged to give

$$B_u = \frac{\dot{N}_1 - \frac{\Phi_2}{\Phi_3}\dot{\mu}_3 - \frac{\Phi_1}{\Phi_0}\dot{\mu}_0}{\left(1 - \frac{\Phi_2}{\Phi_3}\bar{L}_1^3 - \frac{\Phi_1}{\Phi_0}\right)} \tag{5.13}$$

$$G = \frac{\dot{\mu}_3 - \bar{L}_1^3 B_u}{\Phi_3} \tag{5.14}$$

$$\beta = \frac{\dot{\mu}_0 - B_u}{\Phi_0} \tag{5.15}$$

It should be noted that all the parameters in the above equations are time dependent. The terms Φ_0, Φ_1, Φ_2 and Φ_3 are given in Chapter 4, and can be determined from the experimental CSD data. Similarly, the time derivative terms, $\dot{\mu}_0$, $\dot{\mu}_3$ and $\dot{N}_1$ are determined from the experimental data using a numerical differentiation scheme.

The estimates of β, G and B_u for the batch system are shown in Figure 5.12, as a function of supersaturation, A/A^*, where A^* is determined using the solubility correlation of Misra (1970), in Equation (2.2). The β and G estimates from the correlation models of Ilievski and White (1994a; 1994b) are also presented for

comparison. It should be mentioned that the kinetics rates presented here are those after the induction time.

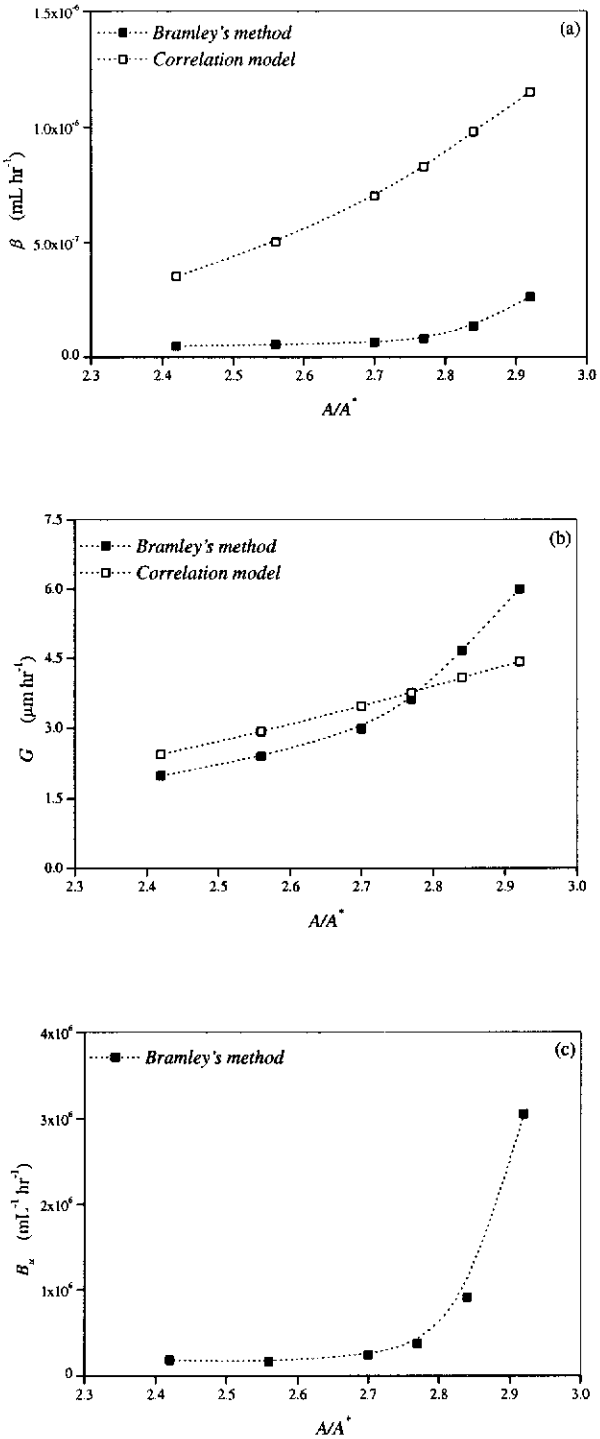

Figure 5.12. Kinetics estimates determined from correlation models and by the Bramley's method. (a) Agglomeration kernel, β; (b) growth rate, G; and (c) source term rate, B_u.

Figure 5.12 shows typical kinetic behaviour in a batch system, where the rates decrease as the system is desupersaturated, and illustrates the dependency of the kinetics on the supersaturation. The β estimates from the correlation model are significantly higher than those from the Bramley's method. These results are opposite to those in the constant composition experiment, where the β estimate is significantly lower than the zeroth moment matching method. The discrepancy may be due to the temperature effect on the agglomeration rate constant, k_H, in the correlation model in Equation (2.13). This gibbsite agglomeration correlation model was derived for the temperatures between 75-78 °C, which are significantly higher than the 60 °C employed in the batch precipitation experiment considered here.

The G estimates from the Bramley's method drop rapidly as the batch system is desupersaturated, compared to the gradual decrease in G estimates from the correlation model. However, the G estimates from the correlation model do not show great deviation to those from the Bramley's method except at high A/A^* values.

5.6 BATCH SIMULATION RESULTS

The CSD predictions from both the 2GMModel and 3GMModel using the kinetics estimates from the Bramley's method are shown in Figure 5.13. It can be seen that the 3GMModel gives better CSD predictions than the 2GMModel, which is similar to the findings obtained from modelling the constant composition experiment. However, it should be emphasised here that this result is for the discretisation ratio of $\sqrt[3]{2}$, and if this discretisation ratio is reduced the accuracy of the two-term growth model will improve, as discussed in Chapter 3, section 3.6.3.

Figure 5.14 again shows that the "preceding" approach gives better CSD prediction than the "seed" approach. This result further supports the likelihood of significant error propagation in the DPB precipitator models. Figure 5.15 shows the difference in the SSE between the "seed" and "preceding" approaches for the batch system increases with time as in the constant composition case.

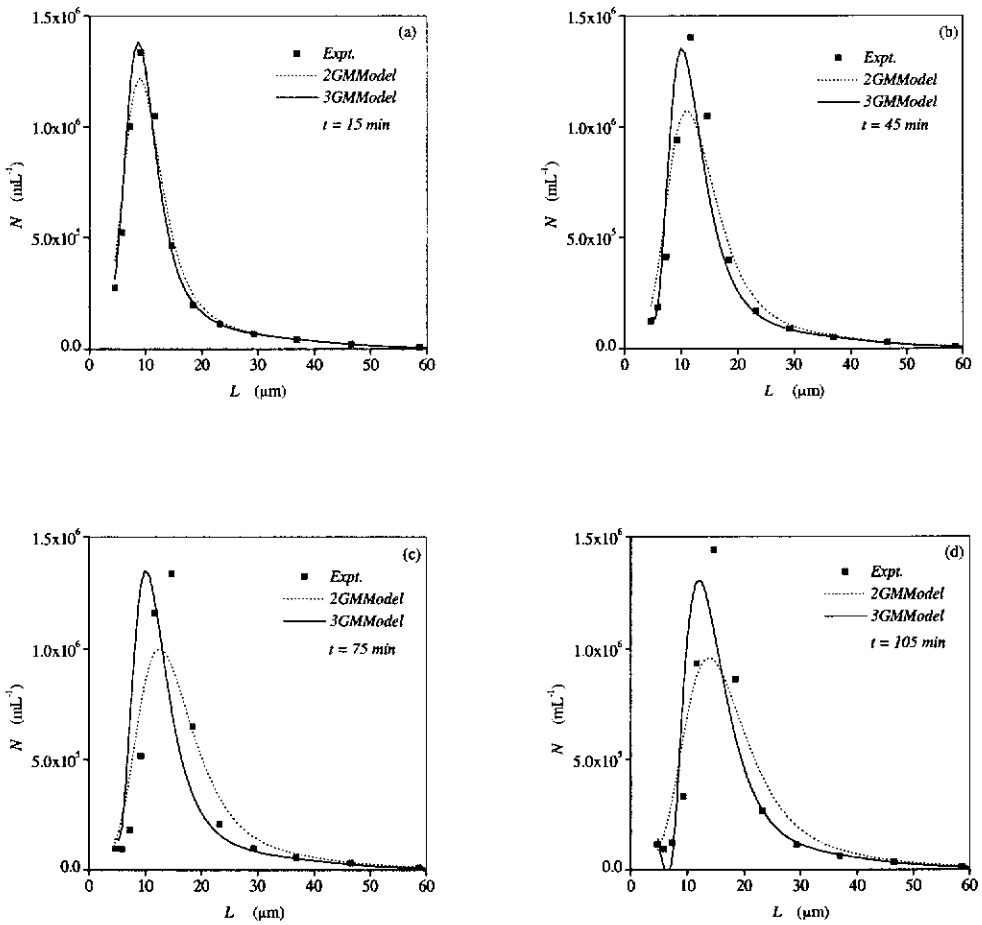

Figure 5.13. Comparisons of the experimental data and model predictions, by the 2GMModel and 3GMModel at different simulation times. (a) 15 minutes; (b) 45 minutes; (c) 75 minutes; and (d) 105 minutes.

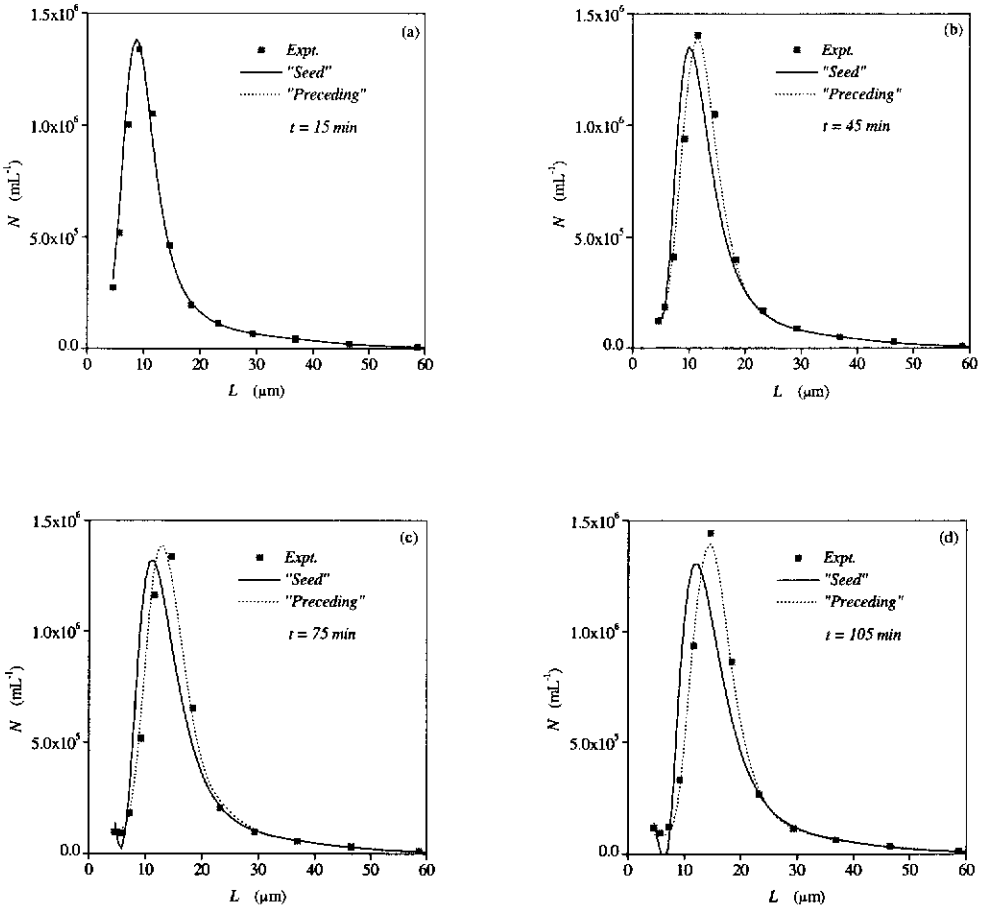

Figure 5.14. Comparisons of the experimental data and model predictions, by the 3GMModel at different simulation times, with the "seed" and "preceding" approaches.
(a) 15 minutes; (b) 45 minutes; (c) 75 minutes; and (d) 105 minutes.

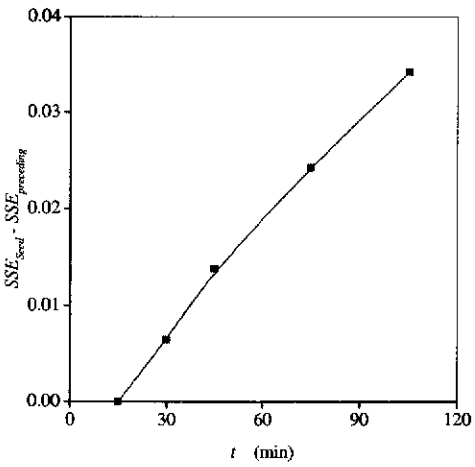

Figure 5.15. The difference in the sum of squares error between the "seed" and "preceding" approaches, using the 3GMModel for the batch experiment.

5.7 CONCLUSIONS

The PB theory was used to model both well-mixed, constant composition, and well-mixed batch gibbsite precipitators. Comparisons between model predicted CSDs and the experimental CSDs in the constant composition system have shown that the CSD predictions using agglomeration and growth kinetics correlations from the literature were poor, and good agreement was achieved if the kinetics were estimated by the moments matching method. This highlights that the current correlation models are unsuitable for describing the precipitation data being modelled. It was found that the three-term growth model is more accurate than the two-term growth model in modelling both precipitation systems considered when a discretisation ratio of $\sqrt[3]{2}$ was used.

The SSE of the model predictions in both experimental systems increases monotonically with time, which puts a time constraint on modelling the product CSD accurately. The progressive deviation between the experimental and predicted CSDs is believed to be due to the propagation of error in the DPB model. The propagation of error is a potential problem, which may be significant in precipitator modelling. It is assessed further in Chapter 6.

CHAPTER 6

MODELLING WELL-MIXED NON-STATIONARY GIBBSITE PRECIPITATION SYSTEMS: SOURCES OF ERROR AND THEIR PROPAGATION

6.1 INTRODUCTION

This work follows the findings of the previous chapter, where it was found that, using the DPB model, the transient CSD predictions are in good agreement with the experimental CSDs initially but deviate with time. These deviations in the CSD predictions with time have also been observed in other constant composition and batch experimental data sets, as reported by Li, Rohl & Ilievski (2000). Depending on its magnitude, this accumulated or propagated error may have a significant impact on the simulation of non-stationary precipitators. Furthermore, it may compromise precipitator control in cases where predictive control methods using PB models are employed. This chapter addresses the issue of error propagation in the DPB precipitator models. The specific aims are to identify the sources of this error, establish if they are significant and to investigate how they may be reduced.

The constant composition semi-batch system was chosen to study the impact of error propagation on precipitator modelling. The reason for selecting this experimental configuration instead of the batch configuration is that constant agglomeration and growth kinetics can be used in the simulation of the transients for all sample times, which reduces the complexity of the investigation greatly.

6.2 SOURCES OF ERROR IN THE SIMULATION

As noted by Li, Rohl & Ilievski (2000), there are a number of possible explanations for the progressive drift observed between the predicted and experimental CSDs for the non-stationary precipitator. These include: (1) the PB model correctly represents the precipitation processes at the beginning of the run but not at later times; (2) a systematic error in particulate sampling and measurement, i.e. it was not representative at later times; (3) errors in the numerical solution such as, finite domain error, numerical diffusion and discretisation errors being propagated; and (4) uncertainty in the estimated kinetic parameters, arising from random errors in the experimental data, being propagated through the DPB model.

The first possibility can be discounted because the "preceding" approach simulations did not show significant deviations at the later sample times, as shown in Chapter 5. Further, the estimated growth and agglomeration kinetics from the moments matching method do not change during the precipitation experiment, which is consistent with the moments form of the model. The second possibility is also unlikely because an extensive study on this system was conducted to ensure that sampling is representative, and to minimise the sampling and sizing error (Ilievski, McShane & Rudman 1997). The relative contributions of the other potential error sources are discussed below.

6.2.1 Random Error in the Experimental CSD

The sources of error in the experimental CSD data are:

(1) sampling and sample preparation, which can be reduced by iso-kinetically taking large samples and minimising the number of sub-sampling and sample preparation steps;
(2) error associated with operation of the Coulter Counter multisizer, which can be reduced by using the appropriate orifice tube and sample volume, good calibration, and low coincidence; and
(3) counting statistics, which can be reduced by increasing the number of particles counted.

Li, Rohl & Ilievski (2000) reported on unpublished CSIRO reproducibility data, and estimated that the 95% probable error in the measured zeroth moment and third moment ranged from 4-10% and 5-20%, respectively. A reproducibility study of batch precipitation experiments reported in Chapter 7 gives comparable estimates.

6.2.2 Finite Domain Error and Numerical Diffusion

Finite domain error, termed by Gelbard and Seinfeld (1978a), is unavoidable in numerical techniques, and is incurred because the computation is carried out on a finite rather than an infinite domain. The failure to count particles beyond the size domain leads to particles outside the size domain being wrongly assigned to size intervals within the domain. Gelbard and Seinfeld (1978a) suggested that this error can be minimised in the DPB model by adding extra size intervals beyond the specified size domain, to account for any particles from outside the specified domain. Finite domain error is not a significant concern in the current work because prediction of total crystal numbers was found to be accurate (see Figure 5.9).

Kumar and Ramkrishna (1997) reported that the discretised growth model of Hounslow, Ryall & Marshall (1988) overpredicts in the tail region of the distribution due to numerical diffusion. This is a term they used to describe the errors that occur when the discretised growth partial differential equation corresponds to a different original equation with a diffusion term. The extent of this error for the finer size discretisation is not known. If this error is significant, it will affect the higher order moment predictions, i.e. over-predict the higher moments, as the moment calculation is weighted towards the larger size intervals. Figure 6.1 does not show significant over prediction of the CSD tail, suggesting numerical diffusion is not a concern.

6.2.3 Contribution of Discretisation Error to Model Error

The coarse size discretisation ratio used in the DPB model may have contributed to the observed error propagation. The Hounslow's discretised growth models can be used with finer size discretisation ratios. However, the Hounslow's discretised agglomeration model is restricted to use with a size discretisation ratio of $\sqrt[3]{2}$. For a finer size discretisation ratio, the agglomeration model of Litster discussed in Chapter 3 can be employed.

The extent of the discretisation error was assessed by varying the discretised size resolution, q. Figure 6.1 shows the comparisons between the CSD predictions made for q = 1,2 and 4, together with the experimental data. The "seed" approach and the kinetics estimates determined from the constant composition precipitation data in Chapter 5 were used in these simulations. It should be noted that in order to compare the simulation results for different q on a common basis, the CSDs are presented in number density, n_i, which is determined from the number, N_i, according to

$$n_i(\overline{L}_i) = \frac{N_i}{(2^{\frac{1}{3q}} - 1)L_i} \tag{6.1}$$

where $\overline{L}_i$ is the geometric mean for the i^{th} size interval.

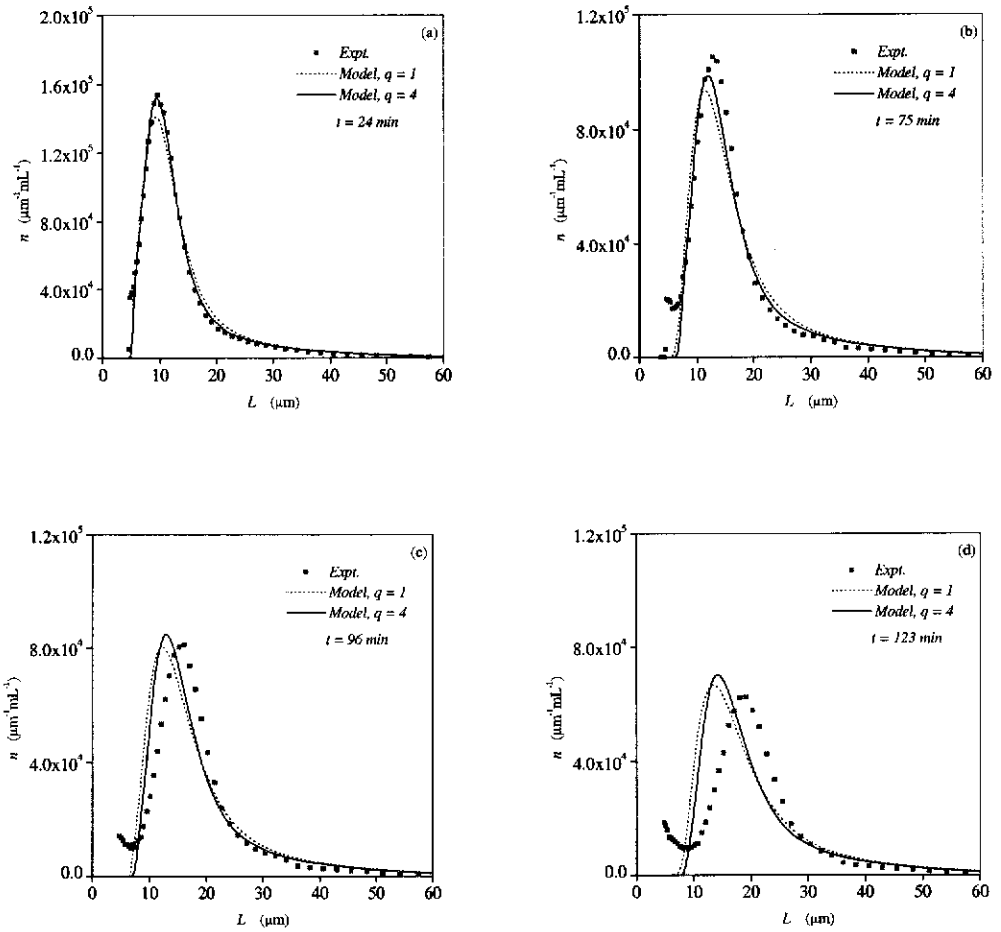

Figure 6.1. Effect of increasing the size discretisation resolution, q, on the predicted CSDs.

Figure 6.1 shows that there is little change in the appearance of the predicted CSDs between $q = 1$ and $q = 4$. This suggests that by increasing q cannot fully account for the deviation between the predicted and experimental CSDs. Figure 6.2 shows the SSE, i.e. Equation (5.9), between model predictions and experimental data with time, for $q = 1$, 2 and 4. This figure shows that using finer discretisation intervals does decrease the magnitude of the SSE, but, in all cases, the SSE increases with time.

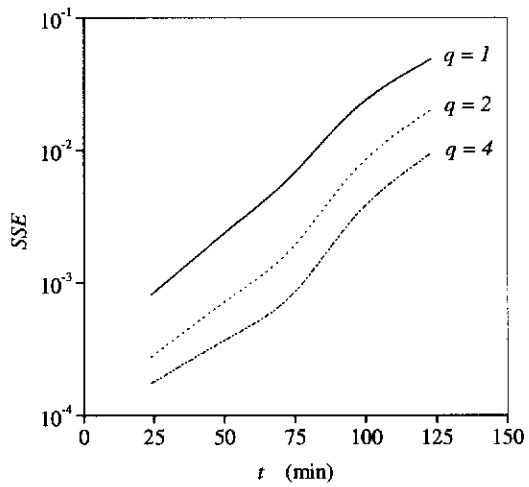

Figure 6.2. Comparisons of sum of squares error between the experimental data and model predictions, for $q = 1$, 2 and 4.

The separate contributions to the error arising from discretisation of the agglomeration and growth terms were assessed by comparing numerical solutions for the agglomeration only and growth only cases with the analytical solutions.

6.2.3.1 Error Contribution from the Discretised Agglomeration Model (DAModel)

The DPB model for the agglomeration only case is given in Chapter 3, i.e. equations (3.48) and (3.49). The equivalent continuous PB model is

$$\frac{\partial n}{\partial t} = B_A - D_A \tag{6.2}$$

The analytical solution to Equation (6.2) with the seed CSD of

$$n_{seed} = \frac{N_o}{v_o} \exp\left(-\frac{v}{v_o}\right) \tag{6.3}$$

N_o is the seed numbers and v_o is the mean seed size (in volume coordinate), is shown by Gelbard and Seinfeld (1978a) to be

$$n = \frac{4N_o}{v_o(\tau+2)^2} \exp\left(-\frac{2v/v_o}{\tau+2}\right) \tag{6.4}$$

where $\tau = N_o \beta\, t$, is the dimensionless time. Equation (6.4) is integrated from v_i to $2^{1/q} v_i$, to give the number N_i, within size interval v_i to v_{i+1},

$$N_i = \frac{2N_o}{\tau+2}\left[\exp\left(-\frac{2\tilde{L}_i^3}{\tau+2}\right) - \exp\left(-\frac{2^\alpha \tilde{L}_i^3}{\tau+2}\right)\right] \tag{6.5}$$

where $\tilde{L}_i^3 = v_i / v_o$ is the dimensionless length and $\alpha = 1+1/q$, see Appendix 4.

The analytical and numerical solutions, with $q = 1$ and 3, are presented in Figure 6.3. The value of β used was estimated from the constant composition experimental data shown in Chapter 5. The DAModel predicted CSD results were then transformed into number densities using Equation (6.1). Figure 6.3 shows that agreement between analytical and numerical solutions is excellent, particularly when $q = 3$, where both solutions virtually fall on the same curves at each simulation time, t.

A plot showing the SSEs of each of these comparisons on a log-linear scale is presented in Figure 6.4. The SSE is seen to increase initially with time and then plateau, for each discretisation resolution, q. The SSE decreases for larger q values, implying, as expected, that the relative magnitude of the error associated with the discretised agglomeration model is reduced as the discretisation interval is made finer. However, examination of the CSDs showed that the improvement is very small between $q = 1$ and $q = 3$. The results suggest that the error arising from

discretisation of the agglomeration term does not significantly contribute to the deviations observed in Figure 6.1.

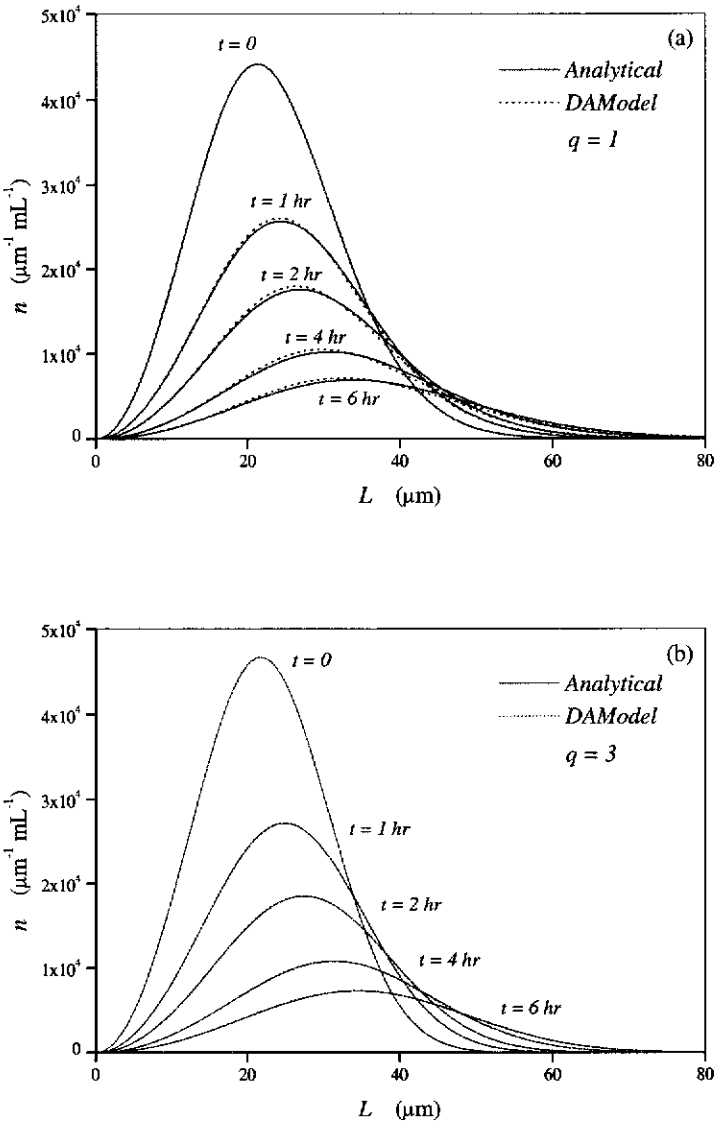

Figure 6.3. Comparisons of analytical and numerical solutions for the semi-batch system with a constant, size independent agglomeration kernel only. (a) $q = 1$; and (b) $q = 3$.

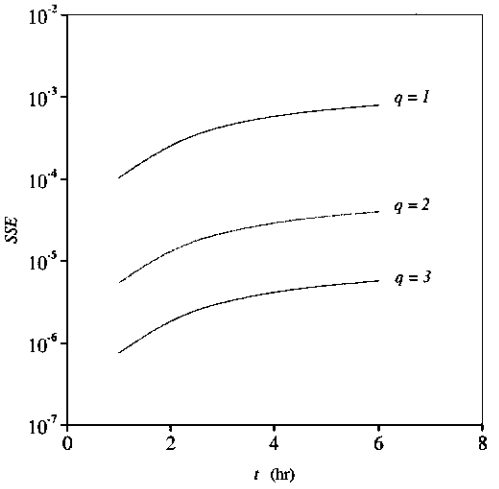

Figure 6.4. SSE between the analytical and numerical estimates of the number density for the agglomeration only case; for q = 1, 2 and 3.

6.2.3.2 Error Contribution from the Discretised Growth Model (DGModel)

The DPB model for growth only is given by Equation (3.45). The equivalent continuous PB model for the constant supersaturation, semi-batch system with size independent growth only is

$$\frac{\partial n}{\partial t} = -G\frac{\partial n}{\partial L} \tag{6.6}$$

It can be shown that an analytical solution of the form

$$n = n_{seed}(L - Gt) \tag{6.7}$$

satisfies Equation (6.6), see Appendix 5.

Two different functional forms for the seed CSD were considered: an exponential distribution and bell-shape distribution, both having length as the internal coordinate. These functional forms are commonly encountered in the experimental gibbsite precipitation studies (Li, Rohl & Ilievski 2000). The following functional form can be used to describe both distributions

$$n_{seed} = \frac{\gamma N_o}{L_o}\left(\frac{L}{L_o}\right)^{\gamma-1} \exp\left(-\left(\frac{L}{L_o}\right)^{\gamma}\right) \tag{6.8}$$

where L_o is the seed mean size. γ defines the seed CSD form, i.e. $\gamma = 1$ for the exponential function and $\gamma = 3$ for the bell-shaped Weibull function, respectively. For a constant growth rate, Equation (6.7) gives

$$n = \begin{cases} 0 & L \le Gt \\ \dfrac{\gamma N_o}{L_o}\left(\dfrac{L-Gt}{L_o}\right)^{\gamma-1} \exp\left(-\left(\dfrac{L-Gt}{L_o}\right)^{\gamma}\right) & L > Gt \end{cases} \tag{6.9}$$

The number, N_i, within size interval of L_i to L_{i+1} is obtained by integrating Equation (6.9) from L_i to $2^{1/3q}L_i$, which gives

$$N_i = \begin{cases} 0 & L_i \le Gt \\ N_o\left[\exp\left(-\left(\dfrac{L_i-Gt}{L_o}\right)^{\gamma}\right) - \exp\left(-\left(\dfrac{rL_i-Gt}{L_o}\right)^{\gamma}\right)\right] & L_i > Gt \end{cases} \tag{6.10}$$

Clearly, for a semi-batch system with size independent growth only, the CSD will shift laterally towards larger size domain as time increases. The G values used were estimated from the experimental precipitation data in Chapter 5. The analyses for the two different seed types are discussed separately.

6.2.3.2.1 Exponential Seed CSD (γ=1)

The seed CSD used in the experiment shown in Figure 6.1 was approximately exponential. The analytical and the numerical solutions for $q = 3$ are presented in Figure 6.5. Most of the discrepancy is in the smaller sizes, up to the mode of the CSD. This discrepancy was greater in $q = 1$ (not presented here). As time increases, errors in the smaller size range become more severe. The discontinuity at $L = Gt$ in Equation (6.9) for $\gamma = 1$ is the main cause of problems in the numerical solution.

Kumar and Ramkrishna (1997) have reported on the problem of locating a discontinuity when using numerical techniques.

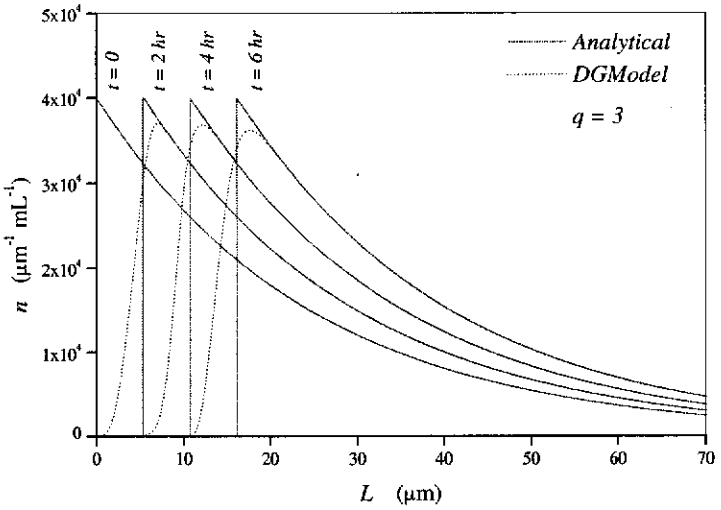

Figure 6.5. Comparisons of analytical and numerical solutions for a semi-batch system with constant, size independent growth only and an exponential seed CSD, for $q = 3$.

6.2.3.2.2 Bell-Shaped Seed CSD ($\gamma = 3$)

Figure 6.6 shows that the agreement between the analytical and numerical solutions, for $q = 3$, is better at earlier times. The agreement for $q = 1$ was significantly poorer than that for $q = 3$, and is not shown here. The slight over-prediction of the tail of the distributions may be due to numerical diffusion, but the effect is very small. The small peak observed at the smaller sizes is due to the numerical instability introduced by the three-term growth discretisation model. This problem is associated with the minimum size, L_1, used in the model. If the discretised size intervals are too narrow at the smaller size domains, the numerical solution shows oscillation. As q increases, a larger L_1 is needed to avoid this oscillation in the smaller size intervals. Hounslow (1990a) showed that there is a clear defined "no-go" region in which inaccurate solutions are obtained due to L_1 being too small. Kumar and Ramkrishna (1997) proposed a method of combining the discretization technique and the method of characteristics, to overcome this numerical instability, and although the method seems promising, it cannot easily be combined with the agglomeration discretisation models used here.

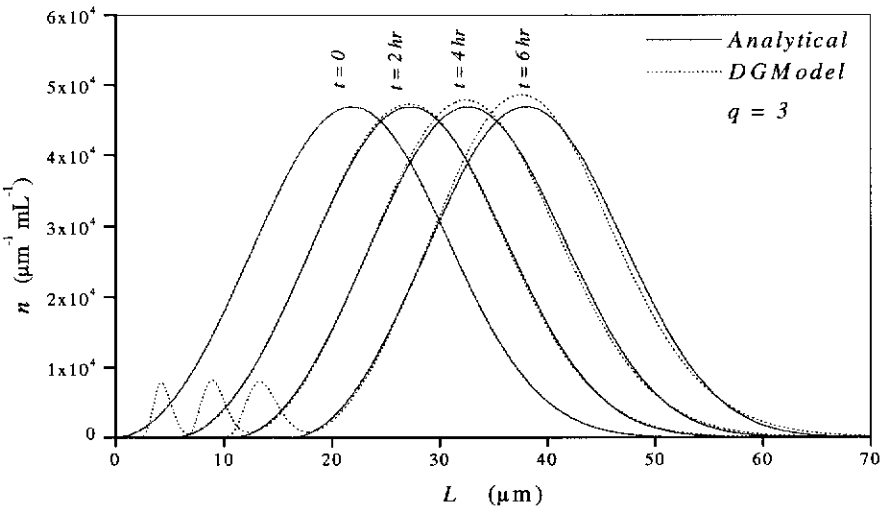

Figure 6.6. Comparisons of analytical and numerical solutions for a semi-batch system with constant, size independent growth only and a bell-shaped seed CSD, for $q = 3$.

The SSEs between the analytical and numerical solutions, for both the exponential and Weibull seed functions were observed to increase monotonically with time as shown in Figure 6.7, in contrast to the "agglomeration only" case, which tended to plateau with time.

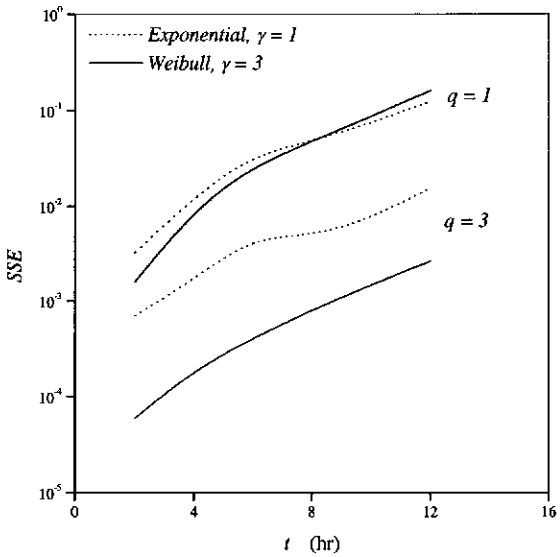

Figure 6.7. Comparisons of sum of squares error between analytical and numerical solutions for the growth only case with both exponential and Weibull seed CSDs; for $q = 1$ and 3.

The results suggest that error associated with the growth term discretisation will contribute more to error propagation than the agglomeration term discretisation. However, these errors introduced by the growth term discretisation cannot fully explain the differences between the predicted and experimental CSDs.

6.3 CONTRIBUTION OF KINETIC PARAMETER UNCERTAINTY TO MODEL ERROR

6.3.1 Error in Agglomeration and Growth Kinetics Estimates

The error in the experimental data will be propagated into the estimated moments, i.e. μ_0, μ_2 and μ_3, which are then used to estimate the kinetic parameters. The kinetic parameters, β and G may be viewed as random variables, which are assumed to be normally distributed, with mean values estimated from the slopes of the linear regressions shown in Chapter 5 and with standard distributions σ_A and σ_G estimated from the regression statistics. The 95% probable error in β and G were estimated to be ± 16% and ± 30%, respectively, using Student's t distribution with the appropriate degrees of freedom. The larger uncertainty in G relative to β, is most likely a consequence of the numerical differentiation of $d\mu_3(t)/dt$ required for the estimation of G. It was found that the uncertainty in G was influenced by the numerical technique used. Given the limited number of experimental data points, sophisticated numerical differential schemes could not be used. Best fit curves to the experimental data were used to help estimate $d\mu_3(t)/dt$.

6.3.2 Monte Carlo Simulation of Error in DPB Model

A Monte Carlo approach was used to simulate the uncertainty in CSD prediction resulting from the uncertainties in β and G estimates. 1000 pairs of β and G parameters were generated using the Gaussian random number generator in Microsoft Excel™. The means and standard deviations for these Gaussian error distributions of β and G were obtained from the linear regression, as described above. The CSD was then simulated for each parameter pair. The "mean" CSD was the same as the model predicted CSD, given earlier. The 95% confidence limits on the CSD predictions were estimated from the spread of the predicted number in a given

size interval at a given sample time. As seen in Figure 6.8, the estimated 95% confidence limits spread with time, as expected for error propagation.

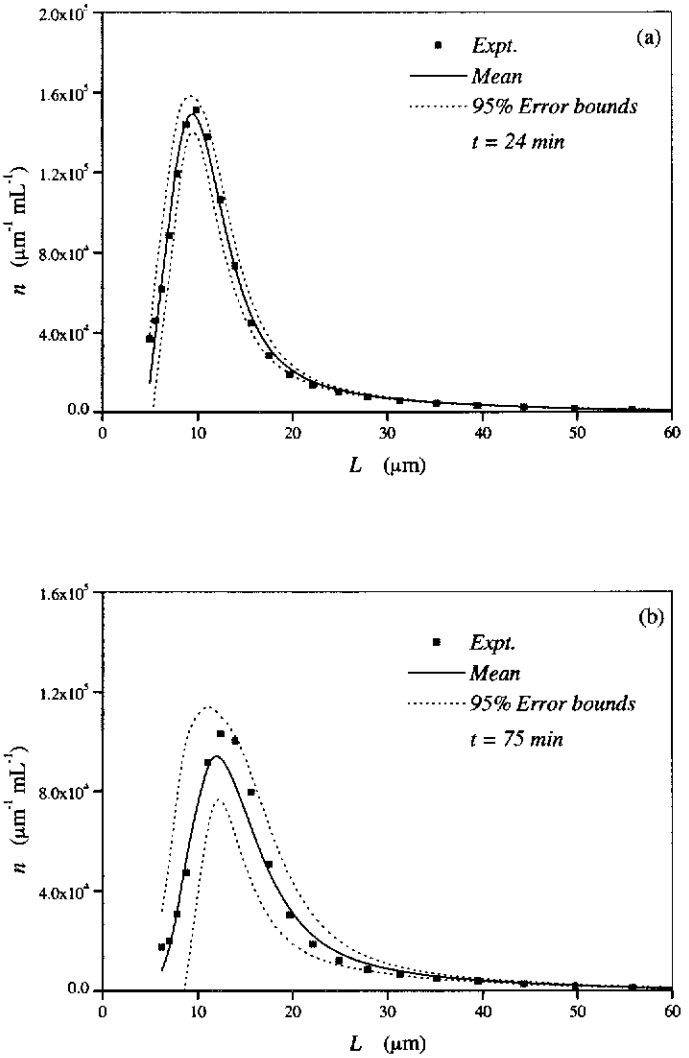

Figure 6.8. The 95% probable error bounds, estimated by Monte Carlo simulation, on the number density propagated from the errors in β and G. (a) t = 24 minutes; and (b) t = 75 minutes.

Figure 6.9 shows the 95% confidence limits on the predicted zeroth and third moments broaden with time as the simulation proceeded. These results also show that the drift between the predicted and experimental CSDs with time could be explained by propagation of the error in the two kinetic parameters in the DPB model. The kinetic parameters, β and G, are clearly the main contributors to the uncertainty in the predicted CSD. Reducing the uncertainties in β and G requires both

high precision experimental data and simple, accurate kinetics estimation methods. These important issues are treated in Chapters 7,8 and 9.

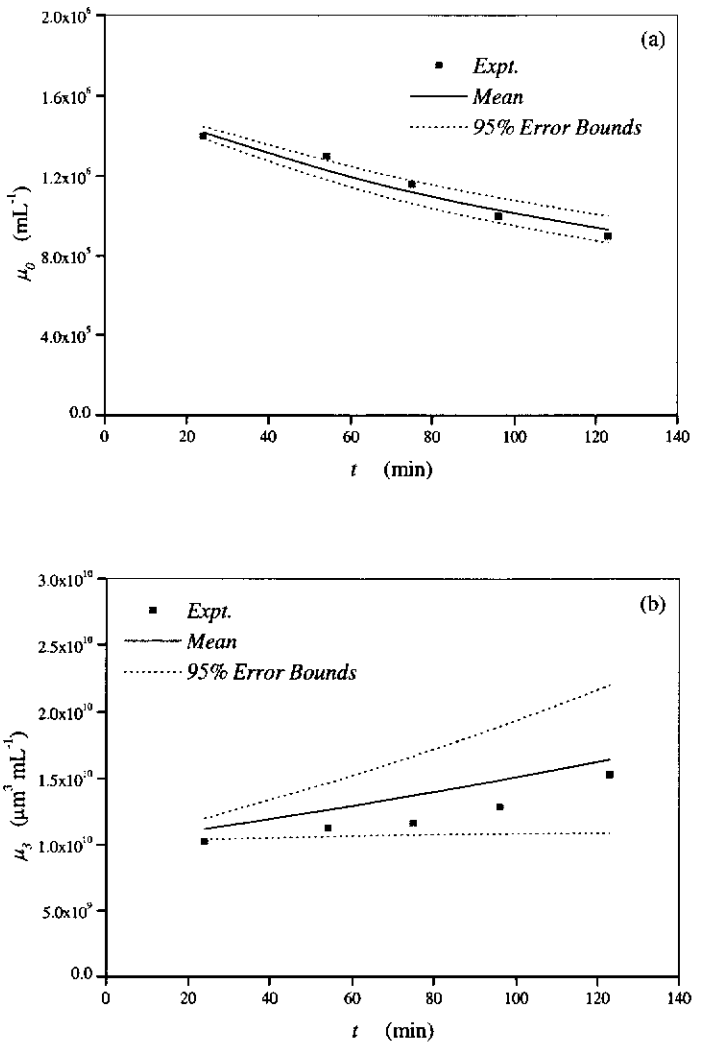

Figure 6.9. The 95% probable error bounds from Monte Carlo simulation on the (a) zeroth moment, μ_0, and (b) third moment, μ_3, propagated from the errors in β and G.

6.4 RELATIVE CONTRIBUTIONS FROM ERROR IN THE AGGLOMERATION AND GROWTH KINETICS ESTIMATES

6.4.1 Isolating Agglomeration and Growth Contributions in the Experimental Data

Ilievski (1991) applied results developed by White (1971) and introduced a method that allows the separate contributions of the agglomeration and growth kinetics on the

CSD to be isolated. The resultant experimental "agglomeration only" CSD can be compared to the CSD predicted from the discretised agglomeration model.

In this non-nucleating, semi-batch solids retention system with size independent growth and no growth dispersion, agglomeration is the only process to alter the shape of the CSD. Growth only shifts the CSD laterally by ΔL over time Δt. White (1971) developed a technique to estimate this lateral shift using the moments of the PBE. The essence of this technique is as follows. The change in the third moment with time, for a size independent growth only system is

$$\frac{d\mu_3'}{dt} = 3G\mu_2' \tag{6.11}$$

where $'$ denotes the normalised moment. The normalised second moment, μ'_2, can be expressed in terms of the distribution variance, σ^2 and the mean μ'_1 as

$$\mu_2' = \sigma^2 + \mu_1'^2 \tag{6.12}$$

Rearranging these equations and integrating from $\overline{L} - \Delta L$ to $\overline{L}$, the expression for the growth adjustment term ΔL (i.e. lateral shift) becomes (see Appendix 6)

$$\Delta\mu_3' = \Delta L^3 - 3\mu_1'\Delta L^2 + 3\mu_2'\Delta L \tag{6.13}$$

where $\Delta\mu_3'$ is the change in the third moment. ΔL is obtained by solving Equation (6.13); μ_1', μ_2' and $\Delta\mu_3'$ are determined experimentally. Subtracting this lateral shift, ΔL, from the experimental CSD removes the growth contribution, and the resulting CSD will be due nominally to agglomeration alone. Other assumptions inherent in using Equation (6.13) to remove the growth contribution are (i) any agglomeration takes place first followed by growth, and (ii) the variance of the CSD does not change with time. The inaccuracy introduced by Equation (6.13) is expected to be small, because the gibbsite growth kinetics are slow (Ilievski and White 1994a).

6.4.2 Comparison of the Predicted and Experimental "Agglomeration Only" CSD

The DPB model for the precipitator with only agglomeration occurring is given by Equation (3.47). Figure 6.10 shows the comparison between the "agglomeration only" CSD (i.e. adjusted with ΔL removed) and the CSD predicted by DAModel, with $q = 1$ and using the β estimate from Chapter 5.

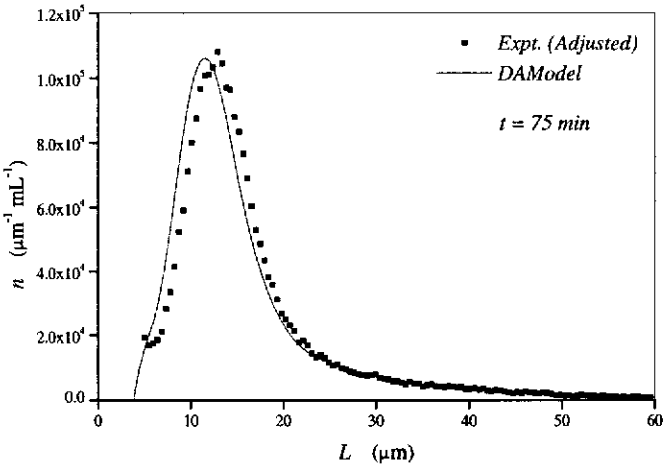

Figure 6.10. Comparison of the adjusted experimental and model predicted CSDs from the discretised agglomeration model (DAModel).

The simulation was carried out only for a CSD with the same variance. For the experimental run considered here, constant CSD variance only applied over limited sample times, between t = 54 to t = 75 minutes. As can be seen, reasonable agreement is observed, although it seems that ΔL is slightly underestimated in this case. The result indicates that the discretised agglomeration model does accurately predict the agglomeration contribution to the shape of the product CSD. The equivalence of the areas under the adjusted experimental CSD and the DAModel CSD is consistent with the discretised agglomeration model's ability to predict total crystal numbers, as already seen in Figure 6.9(a). However, it should be noted that the applicability of this approach to cases where the CSD variance changes significantly and the growth kinetics are fast is doubtful. This result suggests that, for this data, the error in the growth kinetics has a greater contribution to the deviations observed in the full CSD simulation. This highlights the need for accurate and

precise estimates of the growth kinetics, and reconciliation of the third moment of the CSD with the experimental solids concentration should always be conducted.

6.5 CONCLUSIONS

The well-mixed, constant supersaturation, semi-batch gibbsite precipitation system was used to investigate the source of the propagated error in the DPB model. It was found that using a finer discretisation resolution can reduce the SSE between the predicted and experimental CSDs but the improvement is small. The agglomeration term discretisations of Hounslow, Ryall & Marshall (1988) and Litster, Smit & Hounslow (1995) were both found to be quite precise and accurate. The discretised growth model is less accurate but accuracy can be significantly improved with higher q values (i.e. finer discretisation resolution). Investigation of the possible sources of error has shown that the error in the DPB model prediction is most strongly influenced by the uncertainty in the estimates of the agglomeration and the growth rate parameters used in the simulation. To minimise the extent of propagation of these uncertainties, both high precision experimental data and simple, accurate kinetics estimation methods are required. These will be considered in Chapters 7, 8 and 9.

CHAPTER 7

AN INVESTIGATION ON THE UNCERTAINTIES IN BATCH GIBBSITE PRECIPITATION DATA AND KINETIC PARAMETER ESTIMATES

7.1 INTRODUCTION

In Chapter 6, it was observed that the uncertainties in the kinetics estimates have been shown to be a significant source of error in CSD simulations. Clearly, the uncertainty in the experimental precipitation data contributes to the uncertainty in the kinetic parameter estimates generated from that data. This chapter focuses on the uncertainties in batch gibbsite precipitation experimental data and kinetics estimates. The objectives are to assess the reproducibility of the experimental data from repeated batch precipitation experiments, to quantify the uncertainty in the experimental data, and to determine the uncertainties in kinetic parameter estimates.

7.2 BATCH GIBBSITE PRECIPITATION EXPERIMENTS

Six repeated batch gibbsite precipitation experiments were performed in this study. The experiments were conducted following procedure developed at CSIRO Minerals. The same 4-litre precipitator was used in all experiments. Precipitation experiments were carried out isothermally at 80 °C and agitated at 480 rpm. An initial liquor composition with an A/C ratio of 0.7, and a seed charge of 15 g L^{-1} was used. The experimental batch precipitation set-up used is equivalent to the batch configuration described in Chapter 5.

7.2.1 Experimental Precipitation Procedure

The precipitator was preheated with water at 80 °C circulated around the water jacket of the precipitator. A Julabo MS12 water circulator was used as the heat source to maintain the circulating water temperature. The temperature reading was within ±0.5%. The synthetic liquor was poured into the precipitator prior to the precipitation run and the precipitator was closed with the stainless steel lid, to minimise carbon dioxide intake by the liquor from the atmospheric and evaporation losses during the run. The liquor was kept suspended in the precipitator with an IKA EUROSTAR overhead stirrer at the nominated stirrer speed. A 86 mm Lightnin A310 impeller was used. The conductivity and temperature, and turbidity readings were monitored on-line through the conductivity and turbidity probes, respectively.

The precipitation run is ready to proceed once steady readings for the conductivity and temperature, and turbidity are stabilised. The gibbsite seed crystals were fed into the precipitator through the port in the precipitator lid. During the precipitation run, liquor and particulate samples were taken regularly via the port in the lid. The samples were then analysed for liquor composition, solids content and CSD. The precipitation experiments reported here were run for 2.5 hours.

7.2.2 Liquor Preparation

An initial caustic concentration of 200 g L^{-1} Na_2CO_3 (i.e. combined aluminate and free hydroxide) was used to determine the amount of technical grade gibbsite seed crystals (Alcoa C31 gibbsite) and the AR grade sodium hydroxide pellets required for making up the synthetic liquor. The gibbsite crystals were digested in a hot aqueous sodium hydroxide solution, once the hydrate was completely dissolved, hot aqueous sodium carbonate solution was added. Sodium carbonate solution was added to simulate the plant liquor, which normally contains carbonate as impurities. The amount of sodium carbonate added was 40 g L^{-1} liquor. The solution was filtered through a 0.45 μm membrane filter in a stainless steel pressure vessel, to remove any residual crystals, i.e. undissolved gibbsite crystals. The filtered solution was then weighed and made up to the required volume with hot deionised water.

7.2.3 Seed Preparation

The gibbsite crystals used in making up the synthetic liquor and those used as seed in the precipitation experiments were from the same source (Alcoa C31 gibbsite). A QuantaChrome sieving riffler was used to prepare representative gibbsite seed samples for the precipitation experiments, where the bulk gibbsite seed was cut to the required weight. The riffled seed samples used in this experimental study were within 14.93 ± 0.08 g L^{-1}, which is in good agreement with the nominated seed charge of 15 g L^{-1}. The representative seed samples generated by the sieving riffle have an exponential CSD function (see Figure 7.4(a)), which was determined using the Coulter counter multisizer II.

7.2.4 Liquor and Particulate Sampling

Liquor and particulate samples were withdrawn periodically for analysis during the precipitation runs. Hence, proper particulate sampling technique is necessary to ensure unbiased results. In practice, accurate suspension sampling is rather difficult to achieve. Ideally, isokinetic withdrawal of the slurry is desired. There should be no change in the fluid flow direction ahead of the sample tube, such that the liquid and crystals of all sizes experience the same conditions at the entrance to the sampling device (Ilievski 1991; MacTaggart, Nasr-El-Din & Masliyah 1993). In order to achieve such a withdrawal condition, the sampling rate and the width of the sampling tube are important factors. It was recommended that the withdrawal velocity should be close to the circulation velocity at the point of entrance such that settling does not occur (Randolph and Larson 1988), and the internal diameter of sampling tube should be at least 5 times that of the largest crystal diameter (Nývlt et al. 1985).

In the current work a sampling pipette tip of 1.0 mm inner diameter was used, and the largest product crystal was approximately 100 μm. In addition, a draft tube with spoilers was used to direct the flow upward, since sampling at an upright position helps ensure isokinetic conditions. Both liquor and particulate samples were sampled with a micropipette, which is designed for high accuracy liquid sampling. The samples taken for liquor composition analysis and solids content determination were immediately filtered through a 0.45 μm membrane in a vacuum filter. The filtrate was collected in a vial with a small drop of gluconate solution (with concentration of

400 g L^{-1}) to halt the precipitation process. The filtrate was then taken for liquor composition analysis. The solids were thoroughly rinsed with hot deionised water in the vacuum filter prior to being collected in a watchglass and dried in an oven at 60 °C. This drying temperature was well below the temperature necessary to cause decomposition of crystals (Ilievski 1991). The solids content was measured by weighing the dry solids. Similarly, particulate samples taken for CSD determination also had gluconate solution added to halt the precipitation process in the samples. These samples were sized immediately after the precipitation run finished.

7.2.5 Liquor Analysis

The liquor composition was determined with an inflection point titrimetric method, originally developed by Watts and Utley (1956). This analysis method relies on the presence of carbonate ions in the liquor to determine the total caustic, *C*, and aluminate species, *A*, content of caustic aluminate liquors. The liquor analysis was performed on an automated Metrohm titrator, specifically set up for caustic aluminate liquor analysis at CSIRO Minerals, Waterford. The analyses were performed by CSIRO Minerals analytical services.

7.2.6 CSD Measurement

The Coulter counter multisizer II was employed to determine the CSD. This particle size analyser measures a volume equivalent diameter. The Coulter counter multisizer was operated following the procedure described in Ilievski, McShane & Rudman (1997) for the orifice tube selection, selection of a suitable electrolyte solution, and obtaining a representative sample volume for analysis. A 200 μm orifice tube was used to analyse the CSD, which covers the size range of 3.7-128 μm. The electrolyte solution contained 0.9% NaCl by weight to ensure good electrical conductivity. A small amount of 0.25% decon solution is used as a dispersant in the crystal sizing operation. The electrolyte and decon solutions were filtered through a 0.2 μm membrane filter prior to the CSD analysis, to remove any residual matter which may interfere with the accuracy of the analysis. Prior to crystal sizing, the Coulter counter was calibrated with blank electrolyte. The Coulter counter multisizer is linked to an on-line computer, which allows easy access and manipulation of the CSD data.

The main sources of error in crystal sizing are sampling from the precipitator and sampling at the orifice tube. The samples required for crystal sizing operation were obtained from the precipitator directly without the sub-sampling procedure. The required sample volume for analysis depended on the precipitation conditions, precipitation time, seed charge, and seed type. As these factors determine the crystal concentration in the precipitator, the sampling volume at each sampling time has to be determined by trial and error for any given operating conditions, in order to ensure that the crystal concentration is within the range recommended in the Coulter counter manual.

7.3 TRANSIENT PRECIPITATION DATA

7.3.1 Liquor Composition

The initial aluminate and caustic concentrations in the liquor averaged for the six experiments were 139 ± 1.0 g L^{-1} and 197 ± 2.0 g L^{-1}, respectively. Figures 7.1 and 7.2 show the aluminate, *A*, and caustic, *C*, concentrations, and their spreads, during the precipitation runs. The error bars indicate that the standard deviations in *A* and *C* are relatively constant during the precipitation runs, and are within 1.0% and 2.0% of the averaged values, respectively.

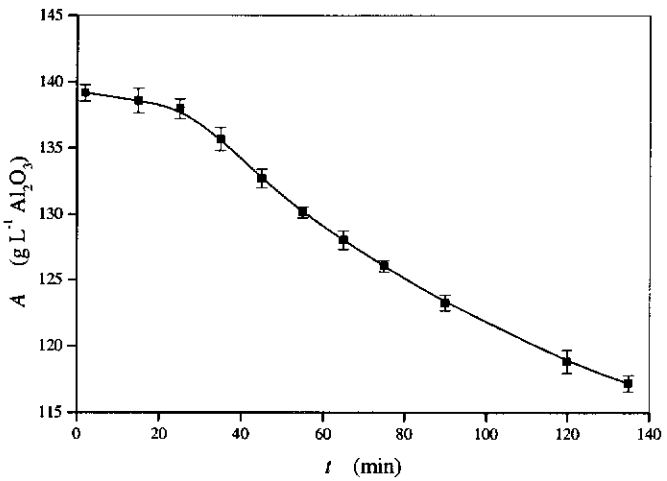

Figure 7.1. Transient aluminate species concentration, *A*, during the precipitation runs.

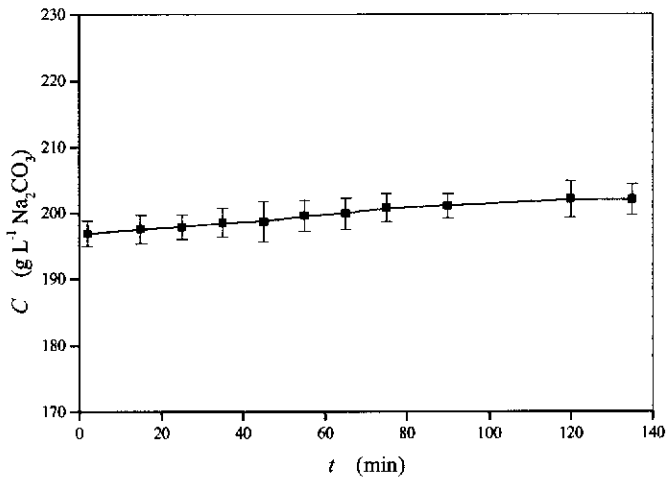

Figure 7.2. Transient caustic concentration, C, during the precipitation runs.

7.3.2 Total Mass Content

The total mass content, m, in this experimental study was determined from the Coulter counter data, solids content (see section 7.2.4, p100), and titration data. The mass determined from the Coulter counter data is according to

$$m(t) = \rho_s k_v \mu_3(t) \tag{7.1}$$

where ρ_s is the hydrate density, k_v is the volume shape factor, taken to be $\pi/6$ and $\mu_3(t)$ is the third moment of the CSD. The mass determined from the titration data is according to the following mass balance

$$m(t) = m(0) + \phi\big(A(0) - A(t)\varepsilon(t)\big) \tag{7.2}$$

where $m(0)$ is the seed charge mass, ρ_L is the liquor density, ϕ is the conversion factor from Al_2O_3 to $Al(OH)_3$ and $\varepsilon(t)$ is the change in liquor volume with time due to deposition of solute from solution to solids phase. $A(0)$ and $A(t)$ are the initial and transient aluminate species concentrations, respectively.

Figure 7.3 shows the total mass content determined from the three techniques. It was found that the total masses obtained from the solids content are marginally higher than those measured from the Coulter counter data and titration data; except at the beginning of the precipitation process where the Coulter counter data gives the highest m. Nevertheless, the differences are within the data spread (i.e. standard deviation) in each of the measurement techniques, which was ± 7%. The consistency in m from solids content, Coulter counter and titration measurements shows that the particulate phase sampling error between the experiments is relatively small.

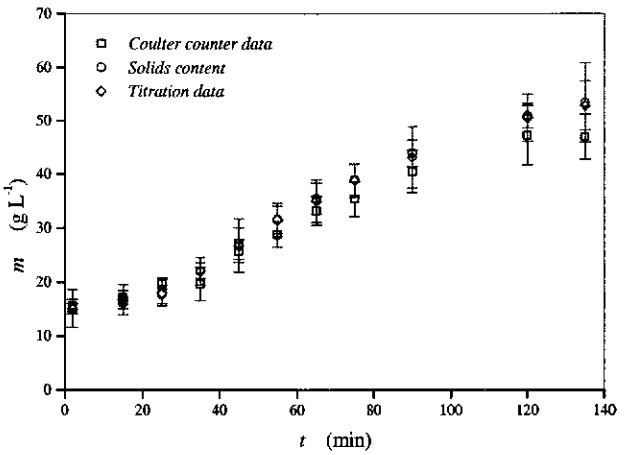

Figure 7.3. Comparisons of the total mass content, m, determined from Coulter counter data, solids content and titration data.

7.3.3 Reproducibility of the CSD Data

Comparisons of seed CSD between the batch precipitation experiments in Figure 7.4(a), demonstrates that the sampling technique employed in the experiments gives reproducible CSD data. Figure 7.4(b) shows poorly reproducible CSD data was obtained at the sampling times of 15 and 35 minutes into the precipitation run, which are normally within the induction period of the precipitation process. The induction time was determined from both desupersaturation curves (see Figure 7.1) and conductivity measurements, and is approximately 30-35 minutes for the precipitation conditions employed here. The main discrepancy in the CSD data is at the smaller size intervals. However, beyond the induction period, reproducible CSD data are again obtained, as shown in Figure 7.4(c) for CSD data at sampling times of 55 minutes and 90 minutes (see Appendix 7 for the reproducibility of the CSD at other

sampling times). The poorly reproducible CSD data during the induction period may be due to some complex mechanistic activities affecting the precipitation mechanisms.

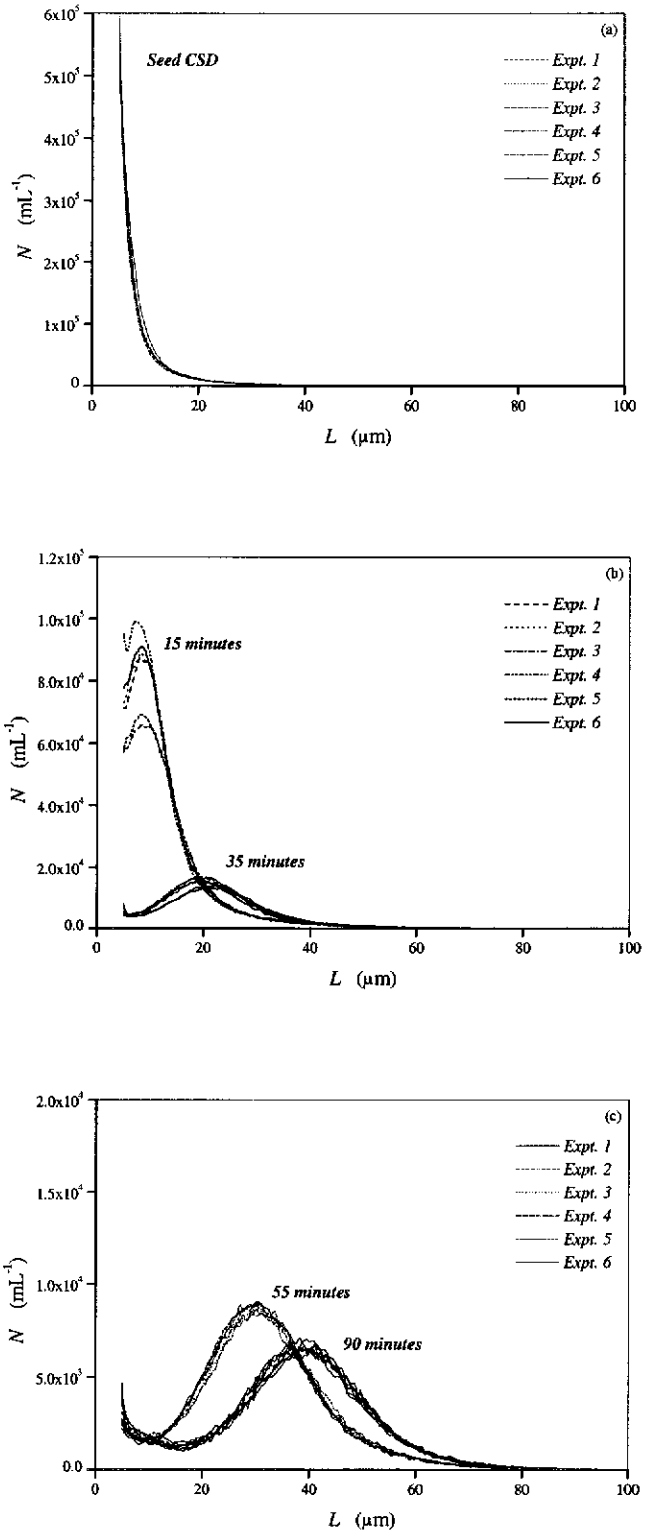

Figure 7.4. Comparisons of transient CSD data between batch precipitation experiments. (a) Seed CSD; (b) at 15 and 35 minutes; and (c) at 55 and 90 minutes.

Other experimental data of interest are the total crystal numbers, μ_0, third moment, μ_3, and crystal numbers in the first size interval, N_1. These quantities are determined from the CSD data. Figures 7.5(a)-(c) show the transient μ_0, μ_3, and N_1 data, respectively. The error bars show the standard deviations in the data.

These transient data reveal precipitation kinetics trends during the precipitation run. The steep decrease in the μ_0 in Figure 7.5(a) indicates that the agglomeration kinetics is particularly fast initially and then slows down substantially as the liquor is being desupersaturated. This corresponds to the flat region in the figure. In Figure 7.5(b), the μ_3 changes negligibly initially followed by a rapid increase and then plateaus as the supersaturation is exhausted. This essentially reflects the growth rate behaviour, as the μ_3 has no contribution from agglomeration and negligible contribution from the source term rate. Figure 7.5(c) shows that the change in N_1 follows the trend of the change in μ_0 in Figure 7.5(a).

7.3.4 Uncertainty in the Experimental CSD Data

CSDs together, in particular, the μ_0, μ_3, and N_1, are critical data required in kinetic parameter estimation techniques used in this work, as reported in Chapter 4. It was observed that the measured CSDs vary considerably during the induction period, and become reproducible as the precipitation proceeds beyond this period. The uncertainty in the crystal numbers in each size interval was evaluated from the six replicate data sets, using the standard deviation of the data.

The uncertainty can be quantified either in terms of relative uncertainty, $\hat{\sigma}$, or the probable error, δ. The relative uncertainty is the ratio of the standard deviation and the mean of the data, whereas, the probable error is determined by multiplying the relative uncertainty with a $t_{\alpha/2,\nu}$ factor, and is determined from Student's t probability distribution, with (1-α)% confidence limits and ν degrees of freedom. For the 95% confidence limits of the data in this study, $t_{\alpha/2,\nu} = 2.571$ with $\alpha = 0.05$ and $\nu = 5$. The 95% probable error will exacerbate the magnitude of the uncertainty in the data, due to the small sample of six data sets.

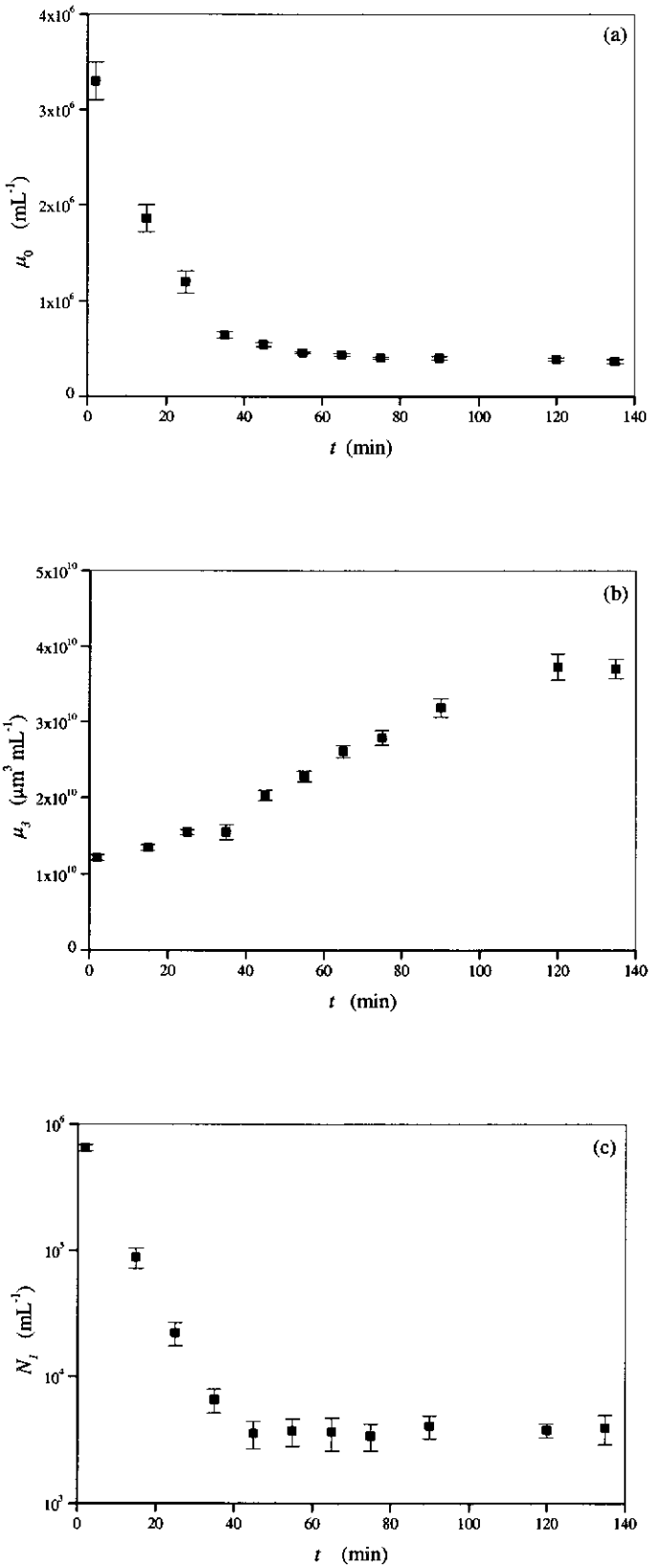

Figure 7.5. Transient batch precipitation data. (a) Total crystal numbers, μ_0; (b) third moment, μ_3; and (c) numbers in the first size interval, N_1.

It should be noted that the uncertainty in the crystal numbers in each size interval vary with time, as the crystal numbers in a size interval are changing continuously due to the precipitation. Figure 7.6 shows the evolution of the CSD (normalised values from the replicate data sets, i.e. $N' = N_i/\mu_0$) during the precipitation run. As can be seen, the seed CSD undergoes dramatic changes.

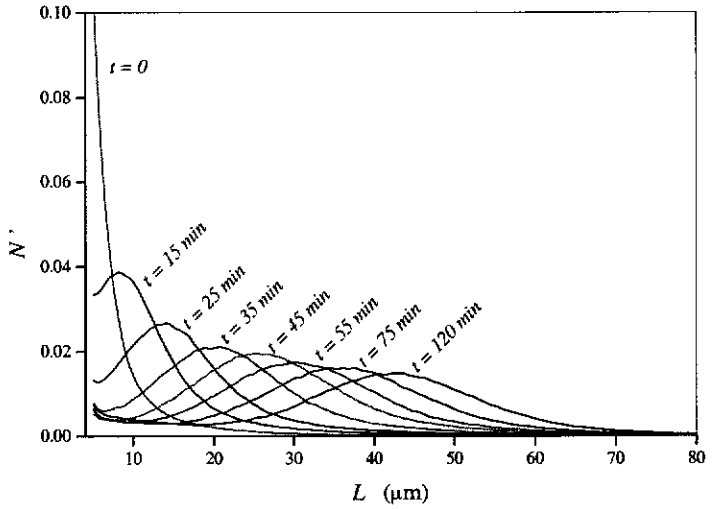

Figure 7.6. Evolution of the CSD during the batch precipitation experiments, expressed as normalised number, $N' = N_i/\mu_0$.

Figure 7.7(a) shows the relative uncertainty, $\hat{\sigma}_N$, in each size interval at different sampling times (not all CSD data are shown in Figure 7.6 in order to avoid congestion). It is observed that the uncertainties in the larger size intervals are particularly large compared to those at the smaller size ranges. This can be attributed to the significantly fewer crystals present in the larger size range as shown in Figure 7.6. The uncertainty in each size interval for size intervals smaller than 80 μm is approximately 5-20%. The uncertainty in each size interval is expected to be inversely proportional to the crystal numbers. This is demonstrated in Figure 7.7(a), where the uncertainty in the larger size range is reduced marginally as the CSD shifts toward the larger size intervals, during the course of precipitation run (i.e. from t = 0 to 120 minutes). Similarly, the uncertainty in the smaller size range increases marginally, as the crystal numbers in these size intervals are reduced over time.

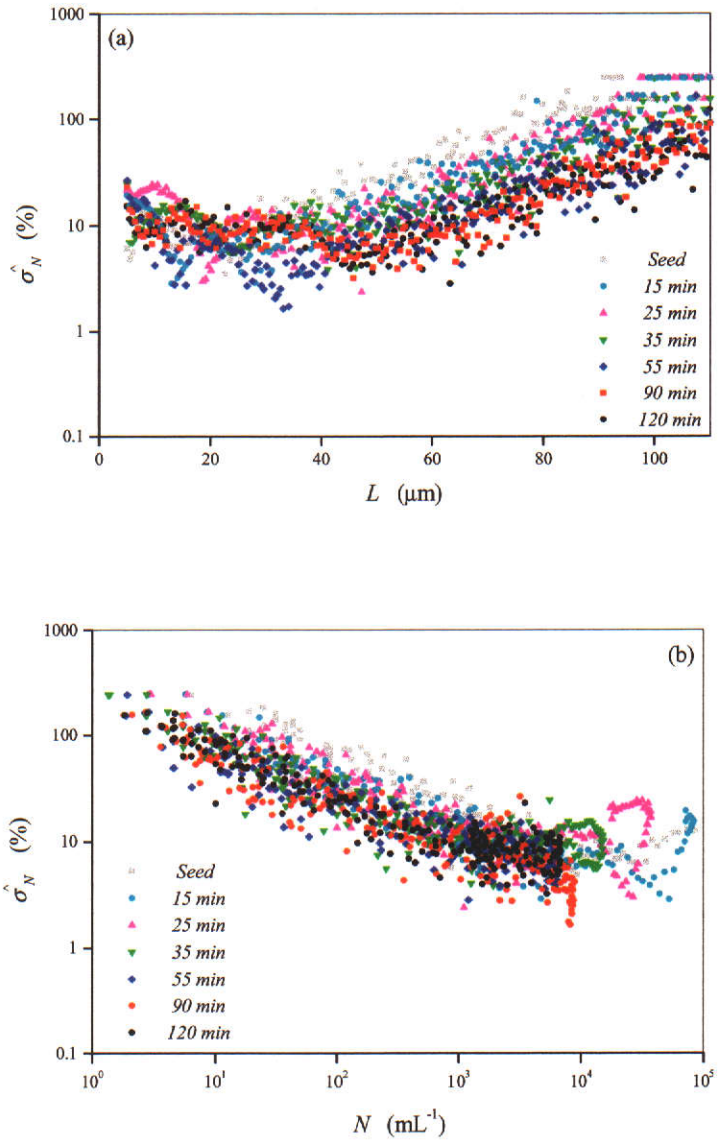

Figure 7.7. The relative uncertainty in the CSD data, (a) in each size interval and (b) as a function of crystal number counts.

This is further demonstrated by Figure 7.7(b), which shows that the highest uncertainty corresponds to the lowest crystal number counts, and vice-versa. A linear correlation exists between the relative uncertainty and the crystal numbers, for crystal number counts up to 10^4 mL^{-1}. The uncertainty is quite scattered for crystal number counts beyond 10^4 mL^{-1}, and there are not enough data to establish a trend of the uncertainty over this range. The observed uncertainty may not only depend on crystal number counts, other factors that may contribute to the uncertainty include

sampling errors, sizing error due to coincidence and minor variations between precipitation experiments.

Figure 7.8 shows the uncertainties in μ_0, μ_3 and N_1 for the six data sets. The uncertainties in μ_0 and μ_3 are of similar order, which are scattered around 5%. It can be seen that the uncertainty in μ_0 during the induction period (i.e. less than 35 minutes) of the precipitation process is marginally larger. The uncertainty in N_1 is significantly higher, at around 25%. The uncertainties in μ_0 and μ_3 do not vary significantly with time during the precipitation runs.

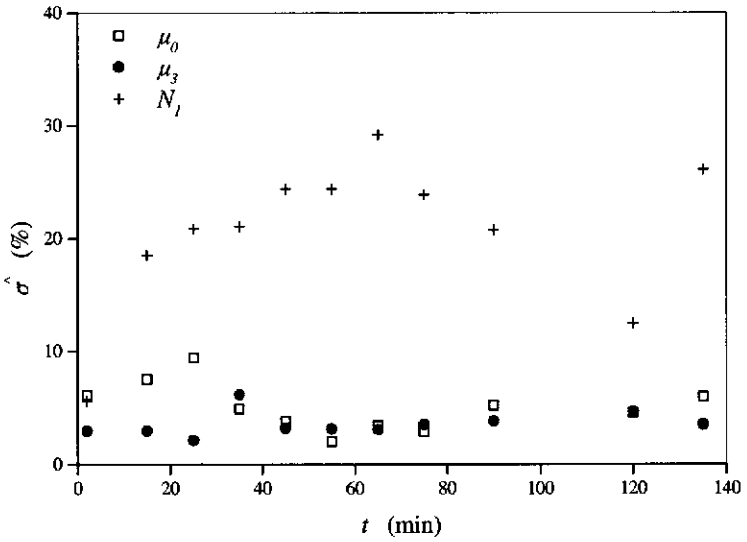

Figure 7.8. The estimated uncertainties in the experimentally measured total crystal numbers, μ_0, third moment, μ_3, and crystal numbers in the first size interval, N_1.

7.4 KINETIC PARAMETER ESTIMATION

Under the precipitation conditions used in this experimental study, crystal agglomeration and growth are the dominant precipitation mechanisms (Ilievski, McShane & Rudman 1997). However, the field of view effect complicates the kinetics estimation procedure. This is because the Coulter counter multisizer can only measure crystals larger than the minimum detectable size of 3.7 μm for the 200 μm orifice tube used. There is a continuous movement of smaller crystals into the

field of view of the Coulter counter multisizer with time. Hence, a source term rate was used to account for this phenomena, which is defined as a measure of crystal numbers appearing in the first size interval as discussed in Chapter 4. The source term rate in this experimental study is likely to be a result of agglomeration and growth of small gibbsite crystals into the detectable size.

The Bramley's method was used to estimate the agglomeration kernel, β, growth rate, G, and source term rate, B_u, simultaneously from the precipitation data. Numerical differentiation techniques were employed to determine the time derivative terms in equations (4.23)-(4.25). The β, G and B_u estimates are shown in Figures 7.9(a)-(c), as a function of supersaturation, A/A^*. The aluminate species solubility correlation of Rosenberg and Healy (1996) was used to determine A^*. The kinetic parameter estimates were determined from sampling times of 25 minutes onwards. The error bars indicate the relative uncertainties in both the kinetic parameter estimates and A/A^*. In Figure 7.9, the highest and lowest A/A^* values correspond to the early stage and the end of the precipitation run, respectively. The figures show that the kinetics are slow during the induction period, but increase toward the end of the induction period. Beyond this period, the precipitation kinetics decrease as the liquor is desupersaturated.

7.4.1 Uncertainties in the Kinetic Parameter Estimates

The relative uncertainties in the kinetics estimates (defined as the ratio of the standard deviation and mean of the six kinetics estimates) are plotted as a function of time in Figure 7.10. Generally, the uncertainty in each of the kinetic parameter increases with the precipitation time, except at early times for the G and B_u estimates (i.e. within the induction period of the precipitation run).

The uncertainty in the kinetics estimates is likely to be determined by two factors, firstly, the relative change in the total crystal numbers, third moment and crystal numbers in the first size interval, and secondly, the relative magnitude of the kinetics rates. The first factor determines the accuracy of the time derivative terms in equations (4.23)-(4.25), which are generally evaluated by numerical differentiation techniques, and the latter factor affects the sensitivity of the kinetics estimates.

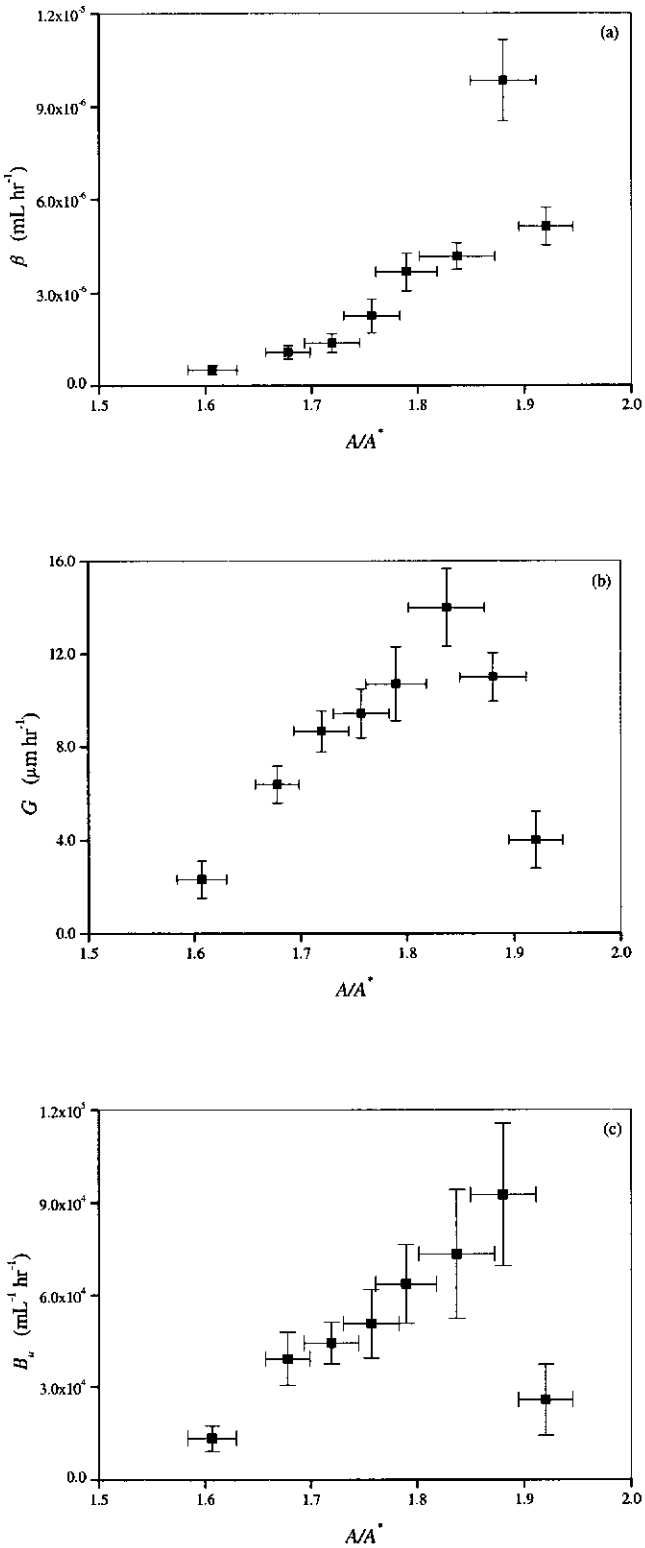

Figure 7.9. Kinetics estimates determined by the Bramley's method. (a) Agglomeration kernel, β; (b) growth rate, G; and (c) source term rate, B_u.

Larger uncertainty at the end of the precipitation run can be explanied by the lower kinetics rates as the system is desupersaturated, and larger errors introduced by the numerical differentiation as the relative changes in the μ_0, μ_3 and N_1, are relatively small (i.e. corresponding to the flat regions in figures 7.5(a)-(c)). The large uncertainties observed during the early stage of the precipitation run correspond to the estimates within or in the vicinity of the induction period, where the G and B_u are relatively slow (see figures 7.9(b) and (c)) and the change in the μ_3 is small. Larger uncertainty in the B_u may also be due to the large uncertainty in N_1.

From Figure 7.10, the relative uncertainties in the kinetics estimates are typically within 30%, which are relatively high for β and G estimates given that the uncertainty in the experimental μ_0 and μ_3 data are relatively small, i.e. 5%. This suggests that the numerical differentiation technique used in determining the time derivatives terms introduces significant errors, particularly at the sampling times toward the end of the precipitation runs. The accuracy of the kinetic estimates is not only influenced by the uncertainty in the experimental data, but also depends on the form of the transient experimental data.

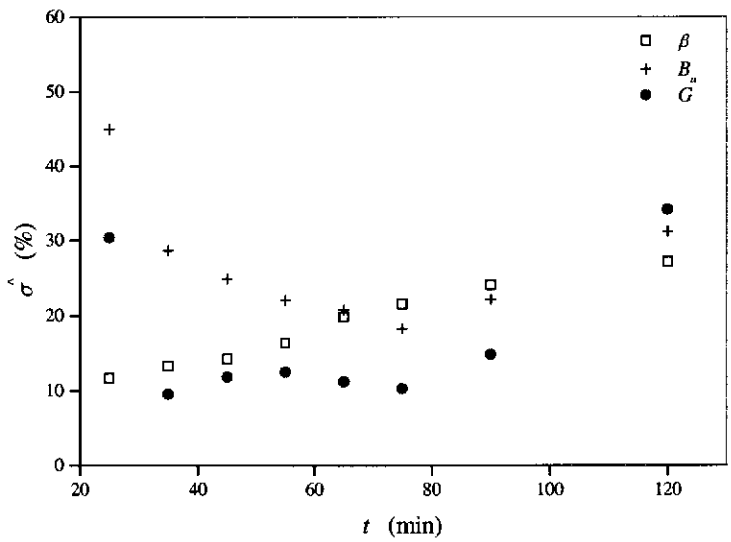

Figure 7.10. Estimated relative uncertainties of the kinetic parameters from six replicate experimental data sets.

7.4.2 Kinetic Parameter Estimates Validation via CSD Simulation

The DPB model was used to simulate the CSD of two randomly chosen experimental data sets (Batch#32 to Batch#37 in Appendix 8). A discretisation ratio of $2^{1/18}$ was used and the simulations were carried out between the sampling times of 55 to 120 minutes. A comparison of the experimental CSD and model predictions using the estimated kinetics will help to assess the adequacy of the kinetics estimates. Figures 7.11 and 7.12 show the comparisons of the experimental and predicted CSD from "seed" and "preceding" approaches, described in Chapter 5. The "preceding" approach simulations show excellent agreement with the experimental data. This shows that the kinetics estimates from the Bramley's method are adequate. As discussed from the findings in Chapter 5, the predicted CSDs from the "seed" approach are in good agreement with the experimental CSDs initially, then deviate with time.

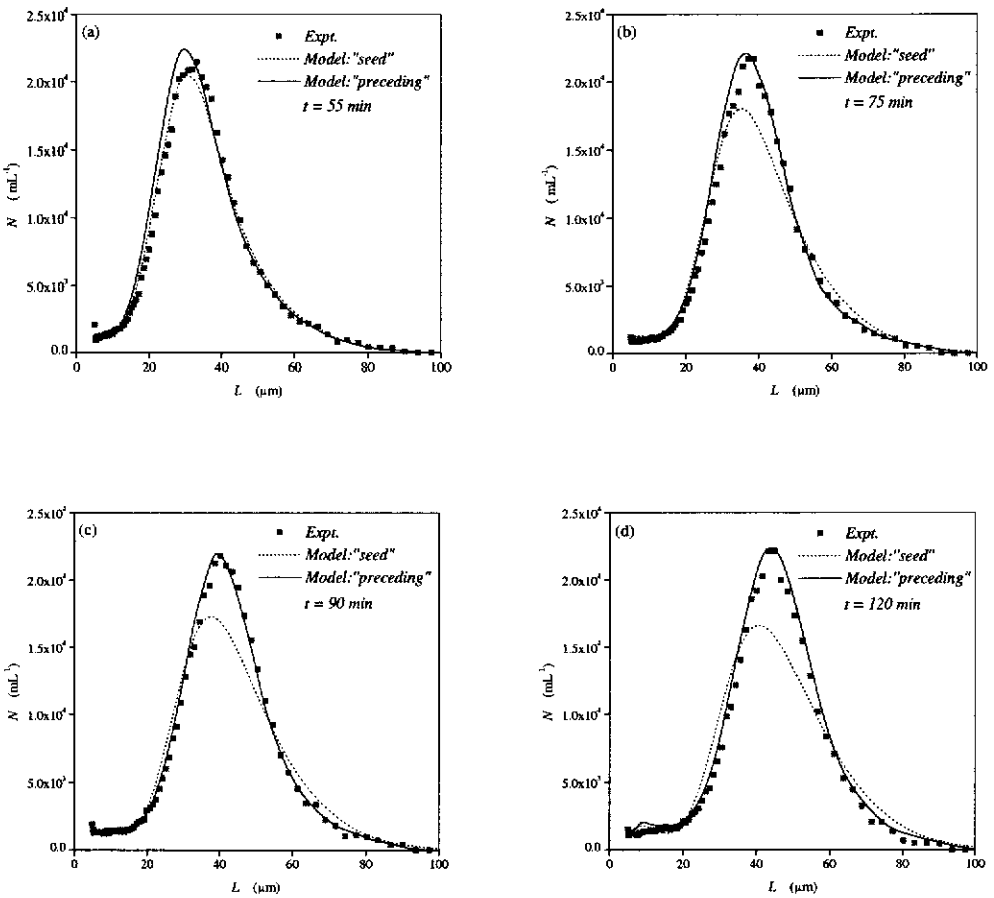

Figure 7.11. Comparisons between the experimental data (Batch#34) and model predictions using the estimated kinetics with the "seed" and "preceding" approaches at different sampling times. (a) 55 minutes; (b) 75 minutes; (c) 90 minutes; and (d) 120 minutes.

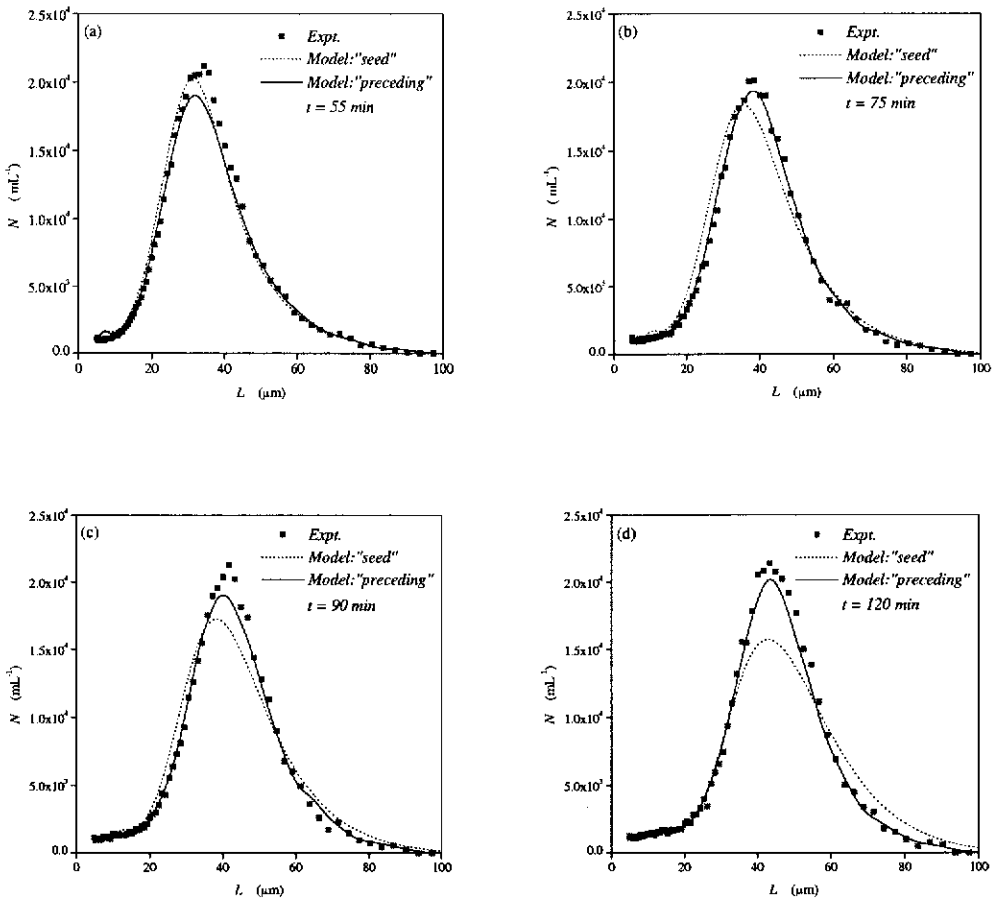

Figure 7.12. Comparisons between the experimental data (Batch#37) and model predictions using the estimated kinetics with the "seed" and "preceding" approaches at different sampling times. (a) 55 minutes; (b) 75 minutes; (c) 90 minutes; and (d) 120 minutes.

7.5 MONTE CARLO SIMULATION OF KINETIC PARAMETER UNCERTAINTY

The uncertainty in the kinetics estimates determined previously are based on six replicate data sets, which is not large enough to give an accurate estimation of the uncertainty limits. To establish statistically significant uncertainty estimates, at least 30 sets of experimental data should be used. Obviously it is not feasible to perform a large number of repeated experiments. Hence, a Monte Carlo approach was employed to further investigate the uncertainty in the kinetics estimates. 1000 sets of replicate experimental data were generated using the built-in random number generator in Microsoft Excel™. A standard normal distribution function with mean, $\mu = 0$ and standard deviation, $\sigma = 1$ was used as a basis to generate the random data,

z. The crystal numbers in each size interval, N_i, were then determined from the generated random data, z, according to Equation (7.3),

$$N_i = \overline{N}_i + z\sigma_{N_i} \tag{7.3}$$

The resultant computer-generated crystal numbers, N_i, in each size interval were normally distributed with mean, $\overline{N}_i$, and standard deviation, σ_{N_i}. The mean and standard deviation for each sampling time were estimated from the batch experimental data sets. Bramley's method was then used to determine the kinetics estimates of the 1000 data sets. The uncertainties for the kinetics estimates between sampling times of 35-120 minutes were determined from the resultant spread.

The relative uncertainty for each of the kinetic parameters is plotted in Figure 7.13. The trend with precipitation time resembles that determined from the six replicate data sets. The uncertainties also increase with precipitation time, and are within 30%. This shows that the estimates from the six data sets give a rough estimation of the uncertainties, except at the early stage of the precipitation run.

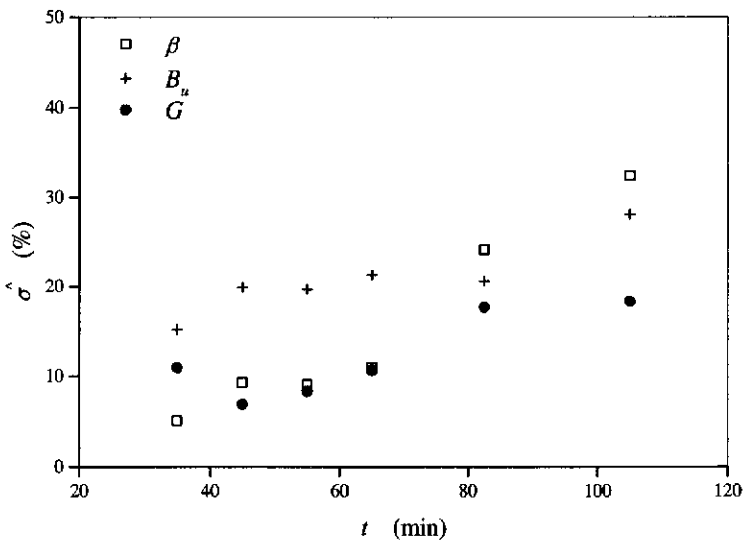

Figure 7.13. Kinetic parameter uncertainty profiles determined by Monte Carlo simulation.

7.6 THE EFFECT OF SIZE DISCRETISATION RATIO ON THE KINETIC PARAMETER ESTIMATES

Bramley's method requires that the experimental size interval be transformed into the discretised size interval that follows a geometric size discretisation ratio of $r = 2^{1/3}$, as discussed in Chapter 5. An investigation was conducted to assess if the discretised size ratio will affect the accuracy and precision of the kinetics estimates.

The kinetics estimates reported above were determined using a modification of the Bramley's method with $r = 2^{1/3q}$ and $q = 2$. Here, the discretisation ratios with $q = 1,4$ and 6 were used. The differences between the kinetics estimates were found to be within $\pm$ 2% for the β and G estimates, but higher for the B_u, which were $\pm$ 4%. This latter result is expected as the uncertainty in the N_1 is influenced greatly by the discretised size width. In comparison, the μ_0 and μ_3, which determine β and G kinetics estimates, respectively are not greatly affected. Hence, the differences in the kinetics estimates observed here are primarily due to the differences in the CSD content for each discretisation ratio, as different size discretisation ratios will result in a different number of discretised size intervals, and crystal numbers in each discretised size interval.

Monte Carlo simulation was also performed to investigate the effect of the discretisation size ratio on the uncertainties in the kinetics estimates. Because of the intensive computing time required to perform the Monte Carlo simulation, this study was restricted to determine the uncertainties of the parameter estimates for two sampling times only.

Figures 7.14(a)-(b) show the uncertainties in the kinetic parameters at sampling times of 45 and 55 minutes, respectively. The discretisation ratio with $q = 1$ resulted in the largest uncertainties in β and G estimates, and the lowest uncertainty in the B_u estimates. The differences in the uncertainties between $q = 2$ to 6 are within 3%, which indicates the influence of $q > 2$ on the kinetics estimates uncertainties is not significant, compared to the uncertainties in the kinetics estimates themselves.

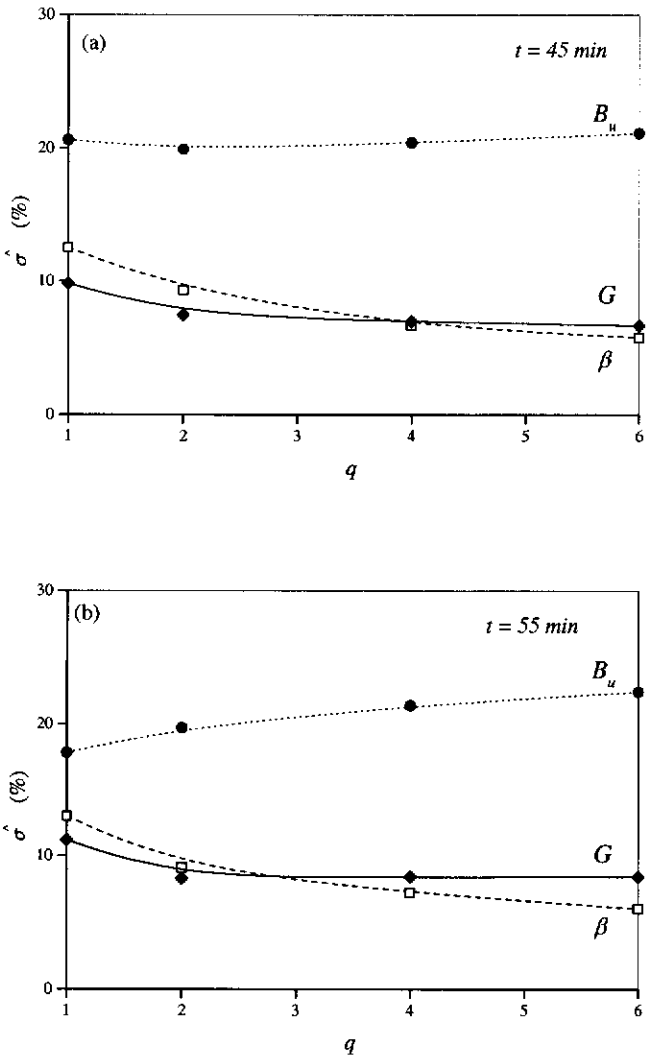

Figure 7.14. Kinetic parameter uncertainty as a function of size discretisation resolution, q. (a) 45 minutes; and (b) 55 minutes.

If the crystal numbers in each size interval are assumed to be independent random variables, then, the uncertainties in μ_0 and μ_3 can be evaluated according to

$$\delta_\psi = \sqrt{\sum_{i=1}^{n} \left(\frac{\partial \psi}{\partial N_i} \right)^2 \delta N_i^2} \qquad (7.4)$$

where ψ represents the quantities such as, μ_0, μ_3 and N_1, and δN_i is taken to be the standard deviation of the crystal numbers in the discretised size interval.

Figure 7.15 shows the plot of the ratio of the uncertainties, $\varphi = \delta_\psi(q = i) / \delta_\psi(q = 1)$ against q, for sampling times of 45 and 55 minutes. It can be seen that the ratio of the uncertainties in μ_0 and μ_3 are consistently less than 1, which means that higher order discretisation (i.e. larger q) improves the precision in the estimates of these parameters. On the other hand, the ratio of the uncertainty of N_1 is consistently greater than 1, which shows that $q = 1$ leads to the lowest uncertainty in the first size interval. Hence, larger uncertainties in β and G estimates with $q = 1$ can be explained by the larger uncertainties in μ_0 and the μ_3. Similarly, that the uncertainty in the B_u increases with q, can be explained by the increase in the uncertainty in N_1 with q.

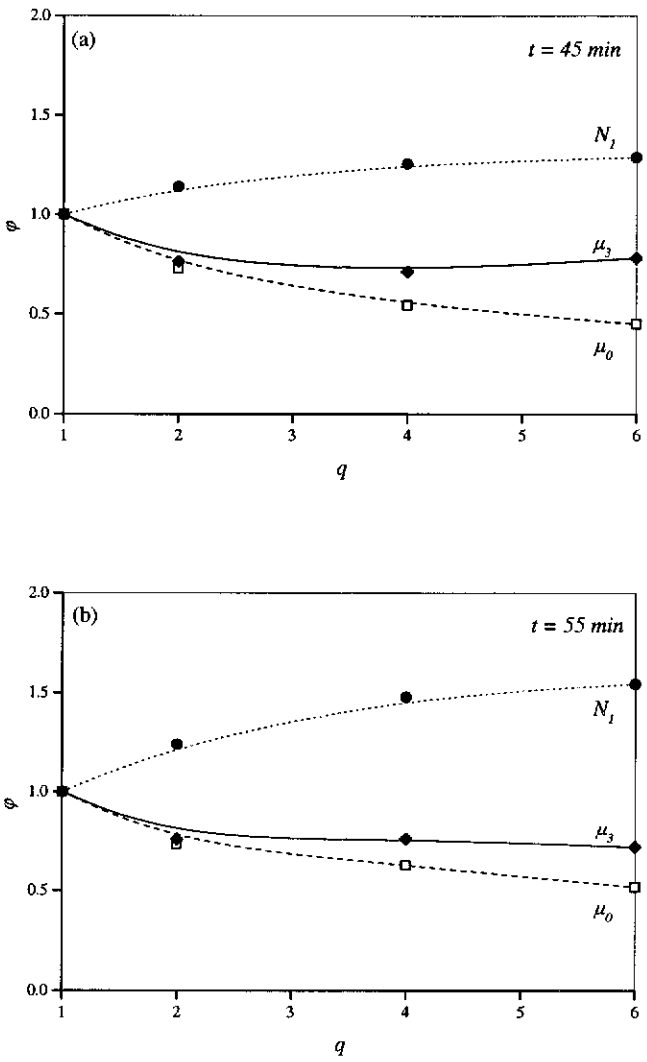

Figure 7.15. The relative uncertainties in the transformed experimental total crystal numbers, μ_0, third moment, μ_3, and crystal numbers in the first size interval, N_1, resulted from different size discretisation resolutions. (a) 45 minutes; and (b) 55 minutes.

7.7 CONCLUSIONS

An investigation into the uncertainty in batch gibbsite precipitation data and precipitation kinetics estimates was undertaken both experimentally, based on six repeated experiments, and theoretically using Monte Carlo and statistical analysis. Analysis of the transient liquor composition showed that the variation in the liquor composition is negligible. The consistency in the total mass content calculated from Coulter counter data, solids content and mass balance using titration data showed that the particulate phase sampling error is small.

Comparisons of the transient CSD data demonstrated that reproducible data was attained after the induction period. The uncertainty in each size interval depends on the crystal numbers in that interval, which varies with time. The experimentally obtained total crystal numbers and third moment data were reproducible, and uncertainties were around 5%. The uncertainty in the crystal numbers in the first size interval was significantly higher. This study demonstrated that consistent and reliable batch gibbsite precipitation data can be obtained after the induction period using the experimental procedure employed.

For batch precipitator, uncertainties in the kinetics estimates appear to increase with precipitation time. Monte Carlo simulation also showed that the uncertainties in the kinetics parameter estimates increase with time. This is believed to be due to the changing magnitude of the kinetics values, the total crystal numbers and third moment. Further investigation showed that the discretised size ratio has little effect on the kinetics estimates and their uncertainty bounds.

It needs to be emphasised that the findings of this study only strictly apply to the precipitation conditions used. It is only an indication of the magnitude of the uncertainty in the data. The results should not be directly applied to other precipitation conditions, as the precipitation conditions employed determine the form of the CSD, and hence, the crystal numbers in each size interval.

CHAPTER 8

THE INFLUENCE OF PRECIPITATOR CONFIGURATION ON THE ACCURACY AND PRECISION OF GIBBSITE PRECIPITATION KINETICS ESTIMATES

8.1 INTRODUCTION

The objective of this chapter is to investigate the effect of laboratory experimental design on the accuracy and precision of the precipitation kinetics estimates. Three different configurations of the same precipitator vessel (i.e. batch and two modes of semi-batch operation) were considered. The logic of the approach taken is that the different precipitator configurations will produce different functional forms of the product CSDs. It is hypothesised that some functional forms of the CSD may be better suited for extracting accurate and precise kinetics estimates for a given kinetic parameter estimation procedure. The hypothesis follows Rawlings, Miller & Witkowski (1993), who reported that different experimental configurations strongly influence the information content of the data and that this should be a major consideration in parameter estimation problems.

The quality of the kinetics estimates will be evaluated by comparing the experimental CSD with the CSD predicted using the estimates. A Monte Carlo simulation is used to explore which of the precipitator configurations will lead to kinetics estimates with the lowest uncertainty, the purpose being to identify a preferred laboratory precipitator configuration for gibbsite kinetics studies.

8.2 THE GIBBSITE PRECIPITATION EXPERIMENTS

8.2.1 The Experimental Procedure

Precipitation of gibbsite from supersaturated caustic aluminate solution was performed in three different precipitation configurations: batch, semi-batch at constant composition with representative solids removal (CCRSR), and semi-batch at constant composition with classified solids removal (CCCSR). The experimental gibbsite precipitation data reported in this chapter for analysis were extracted from Ilievski et al. (1998). The set-up of the experimental precipitation systems considered here are equivalent to those described in Chapter 5. The same 4-litre stainless steel precipitator, fitted with a draft tube and a 86 mm A310 Ligthnin impeller, was used in all experiments. All runs were conducted at a nominal caustic concentration of 180 g L^{-1} Na_2CO_3. The range of measured caustic concentrations, across all the runs, was less than ± 2.5%.

In the constant composition experiments, the aluminate species concentration was 118 ± 1 g L^{-1} Al_2O_3, i.e. a supersaturation A/A^* of 2.84. The composition in the CCRSR and the CCCSR was maintained constant by feeding liquor of a higher aluminate species concentration and lower total caustic concentration at a rate regulated by feedback control based on on-line conductivity measurements. Figure 8.1 shows that the control strategy was effective in maintaining the aluminate species concentration constant with time for both semi-batch configurations. The desupersaturation of the aluminate species in the batch precipitator is shown for comparison. The initial aluminate species concentration for the batch experiment was 129 g L^{-1} Al_2O_3, i.e. $A/A^* = 2.93$. All the precipitation experiments were carried out at 60 °C, agitated at 800 rpm and with a seed charge of 20 g L^{-1}.

In the CCRSR and the CCCSR experiments, solids were removed from the overflow while the fresh liquor was fed to the precipitator, both at the same regulated flow rate. Ilievski et al. (1998) reported that the precipitator working volume remained essentially constant because the solids content was very low and the density change in the liquor due to precipitation was negligible.

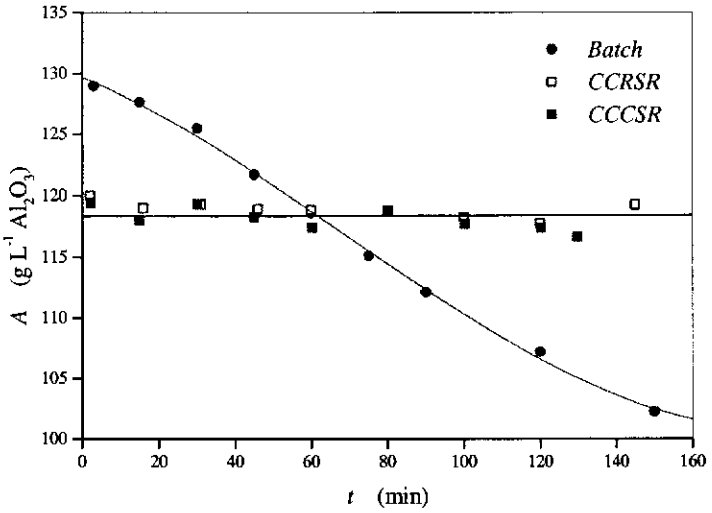

Figure 8.1. The concentration of the aluminate species, A, over the duration of the precipitation experiments (from the data of Ilievski et al. 1998).

For the CCRSR experiment, representative solids removal from the overflow was demonstrated by the observed good match between the overflow CSD with that sampled from the precipitator. Tracer studies on the same system, reported by Ilievski, Rudman & Metcalfe (1998) with the feed and withdrawal rates fixed continuously (i.e. 30 mL min^{-1}) at the CCRSR withdrawal pump setting, showed exponential residence time distribution functions for both the particulate and the liquor phases. An elutriator was used in the CCCSR experiment to remove fine crystals. The classification function, $h(L)$, was determined from analysis of the tank and overflow CSDs. $h(L)$ is 1 for the CCRSR system. For the CCCSR system employed, the best fit to the experimentally observed classification function was (Ilievski et al. 1998)

$$h(L) = \begin{cases} 2.02 - 0.133L & L < 15.2\,\mu m \\ 0 & \text{Otherwise} \end{cases} \qquad (8.1)$$

8.2.2 Experimental Data from the Different Precipitator Configurations

Figure 8.2 shows the transient total crystal numbers, μ_0, for each configuration. For the batch system, the μ_0 decrease quite rapidly initially and then plateau as the

supersaturation is consumed. For CCRSR and CCCSR configurations, the μ_0 decrease steadily with time. This is expected because the supersaturation is maintained constant in these systems. For the batch system, the slope of the curve in Figure 8.2, which is the rate of change of total crystal numbers, is directly related to the agglomeration kernel, β, and source term rate, B_u. Whereas, for the constant composition configurations, the rate of crystal numbers exiting the system also needs to be considered.

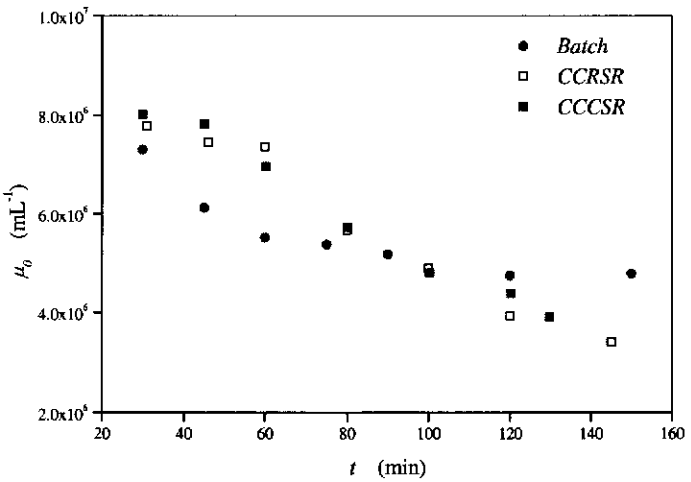

Figure 8.2. Measured transient total crystal numbers, μ_0, for the different precipitation systems (from the data of Ilievski et al. 1998).

Figure 8.3 shows the total crystal mass, m. The total crystal mass in the batch system is consistently higher than in the constant composition configurations because of solids removal in the latter. As expected, m is lower in the CCRSR system than in the CCCSR system because larger crystals are also being removed from the precipitator in the former system, compared to only fine crystals being removed from the latter. The slope of the curve for the batch configuration in Figure 8.3 is predominantly determined by the deposition rate due to crystal growth, G, because the B_u contributes negligible mass. The G in the batch system is continually changing with time because of desupersaturation. In contrast, the G in the constant composition experiments is time-invariant but the crystal mass removal rate also affects the corresponding curves in Figure 8.3.

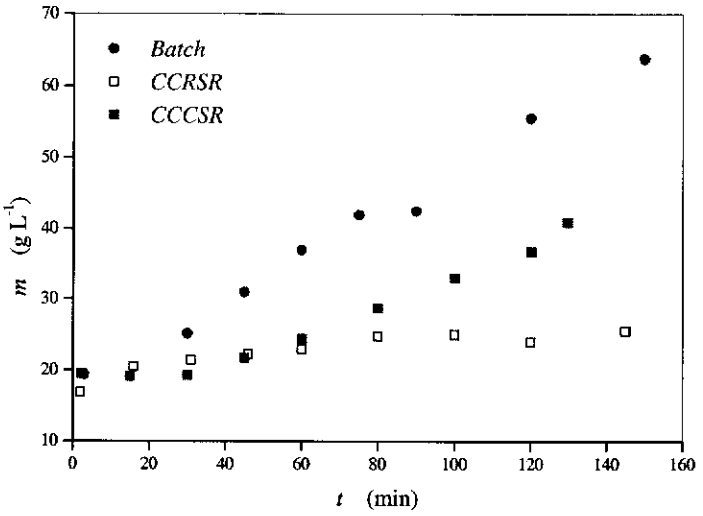

Figure 8.3. Measured transient total crystal mass, m, for each of the precipitator configurations (from the data of Ilievski et al. 1998).

Figure 8.4 shows the experimentally measured transient CSD for the different precipitator configurations. The CSDs are expressed as the normalised number in a size interval, $N' = N_i/\mu_0$, to enable meaningful comparison. N_i is the measured number of crystals per unit volume of slurry in the i^{th} size interval at a given time and μ_0 is the measured total crystal numbers at the same sample time. The measured CSD from the three configurations are significantly different, which was the reason for their selection.

Figure 8.4 shows that each of the product CSD have features that appear at the fines end. These may affect the kinetics estimates, particularly the nucleation source term. The cause of this feature is uncertain, though two possible sources are: (1) nuclei and seed crystals agglomerating and growing into the field of view of the particle size analyser, and (2) the presence of "inert" crystals which do not participate in the precipitation process (Ilievski and White 1994a). The "inert" crystals could be inactive gibbsite crystals, or impurity crystals contained in the industrial gibbsite seeds used in the experimental study. However, no work was done to test these hypotheses.

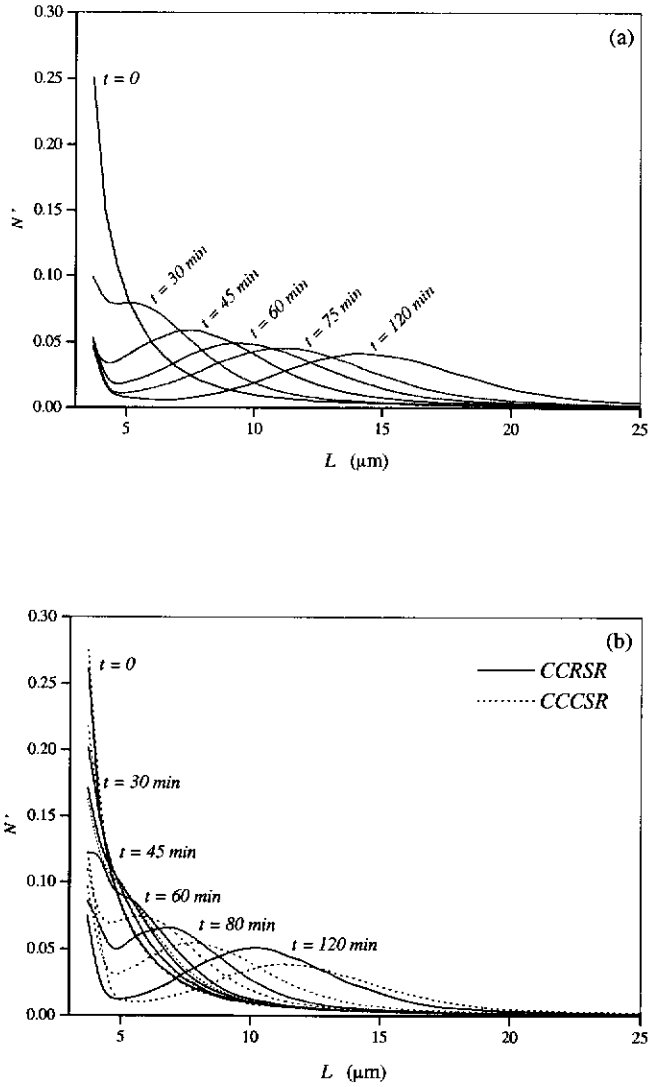

Figure 8.4. Evolution of the experimental CSD with time for the different precipitator configurations. (a) Batch; and (b) CCRSR and CCCSR (from the data of Ilievski et al. 1998).

8.3 KINETICS ESTIMATION FROM THE EXPERIMENTAL DATA

8.3.1 Kinetics Estimation Method

The Bramley's method introduced in section 4.3.2.6 is modified slightly to include flow terms for the two semi-batch precipitation configurations (i.e. representative removal and classified removal) to give

$$\dot{\mu}_0 = B_u + \Phi_0\beta - \frac{\bar{h}_0}{\tau} \tag{8.2}$$

$$\dot{\mu}_3 = \bar{L}_1^3 B_u + \Phi_3 G - \frac{\bar{h}_3}{\tau} \tag{8.3}$$

$$\dot{N}_1 = B_u + \Phi_1\beta + \Phi_2 G - \frac{N_1}{\tau} \tag{8.4}$$

The kinetic parameters β, G and B_u are obtained by solving equations (8.2)-(8.4) simultaneously, using the experimental data to determine the other quantities. N_1 is the number of crystals in the first size interval and τ is the mean residence time. The terms $\bar{h}_0$ and $\bar{h}_3$ are defined by

$$\bar{h}_j = \int_0^\infty L^j h(L) n(t,L) dL \tag{8.5}$$

where $n(t, L)$ is the number density. For the CCRSR system, $\bar{h}_0$ and $\bar{h}_3$ are the zeroth and third moments, respectively. For the CCCSR system considered here,

$$\bar{h}_j = 2.02\mu_j(15.2) - 0.133\mu_{j+1}(15.2) \tag{8.6}$$

where $\mu_j(x)$ is defined as

$$\mu_j(x) = \int_0^x L^j n(t,L) dL \tag{8.7}$$

8.3.2 Kinetics Estimates from the Different Precipitator Configurations

Figure 8.5 shows the estimates of β, G and B_u as a function of A/A^*, for each of the precipitator configurations considered. The batch system results show that the kinetics estimates are strongly correlated with supersaturation: the kinetics rates are fast initially and then decrease steeply as the supersaturation decreases. The evolution of the experimental CSD in Figure 8.4(a) also reflects such kinetics behaviour. Figure 8.5 shows good agreement in the β estimates between the constant

composition systems and the batch system, but greater deviations in the G and the B_u estimates. The maximum differences of 30%, 45% and 100% are obtained for the estimates of β, G and B_u, respectively.

Given that gibbsite crystal growth is independent of crystal size and suspension density (Misra and White 1971a), the observed differences in the measured growth rates are difficult to explain. Estimates of G using the magma density data were similar to the estimates from the CSD data, which is not surprising given that the experimental data was mass balance consistent. The estimated values of the G shown in Figure 8.5(b) agree well with the values predicted by the gibbsite growth correlation in Equation (2.9). For the operating conditions corresponding to the constant composition experiments, the correlation predicts values of the G in the range from 3.6 to 4.3 $\mu m\ hr^{-1}$. It is proposed that the observed deviations in the estimates between the batch and constant composition experiments are the result of uncertainty in the estimates.

The observed differences for the B_u may be an indication of its dependency on the surface area or solids content, which are different in each precipitator configuration. The alternative explanation is that there is a large uncertainty in the B_u estimates. This is consistent with the large variability observed for N_1 discussed in Chapter 7 and the subsequent effect on the uncertainty in the $\dot{N}_1$ term of Equation (8.4) obtained by numerical differentiation.

The hypothesis that the observed deviations in the estimates between the different precipitator configurations are due to uncertainty in the estimates is tested in the following sections by,

(1) dynamic simulation of the precipitators to check the match between the experimental CSD and that predicted using the estimated kinetics, and hence checking their validity; and
(2) Monte Carlo simulation to estimate the uncertainties in the kinetics estimates.

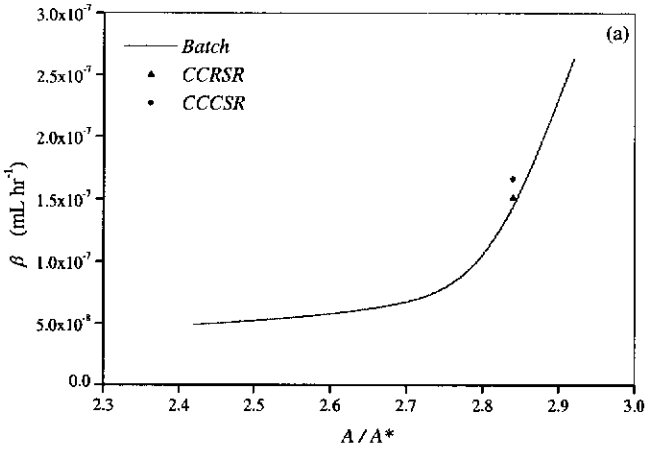

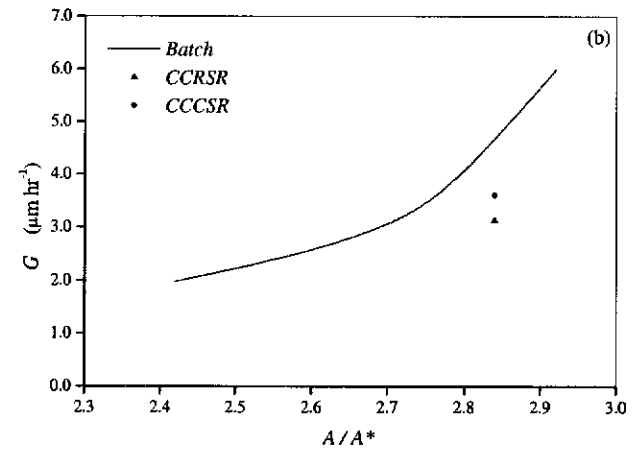

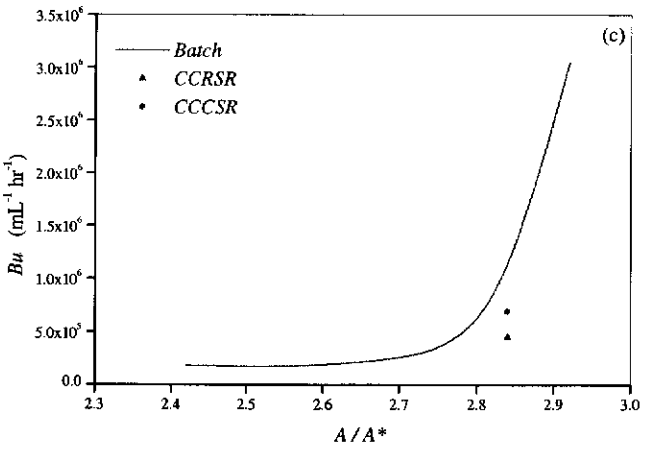

Figure 8.5. Kinetics estimates for the different precipitator configurations. (a) Agglomeration kernel, β; (b) growth rate, G; and (c) source term rate, B_u.

8.3.3 Kinetic Parameter Estimates Validation by Dynamic CSD Simulation

The CSDs were simulated by a DPB model, i.e. Equation (3.38). The discretised agglomeration, growth and source term formulations in equations (3.48), (3.42) and (5.12) were employed in the CSD simulation. The net-flow term for the CCRSR system is

$$\left(\frac{dN_i}{dt}\right)_F = -\frac{N_i}{\tau} \tag{8.8}$$

and for the CCCSR system is

$$\left(\frac{dN_i}{dt}\right)_F = \begin{cases} -\dfrac{h(\bar{L}_i)N_i}{\tau} & L_{i+1} < 15.2\mu\text{m} \\ 0 & L_{i+1} > 15.2\mu\text{m} \end{cases} \tag{8.9}$$

A size discretisation ratio of $2^{1/18}$ was used in the CSD simulations. The CSD predicted at 120 minutes are shown together with the corresponding experimental CSD in Figure 8.6. The experimental and simulated CSDs show good agreement in all three cases, indicating the adequacy of the respective kinetics estimates.

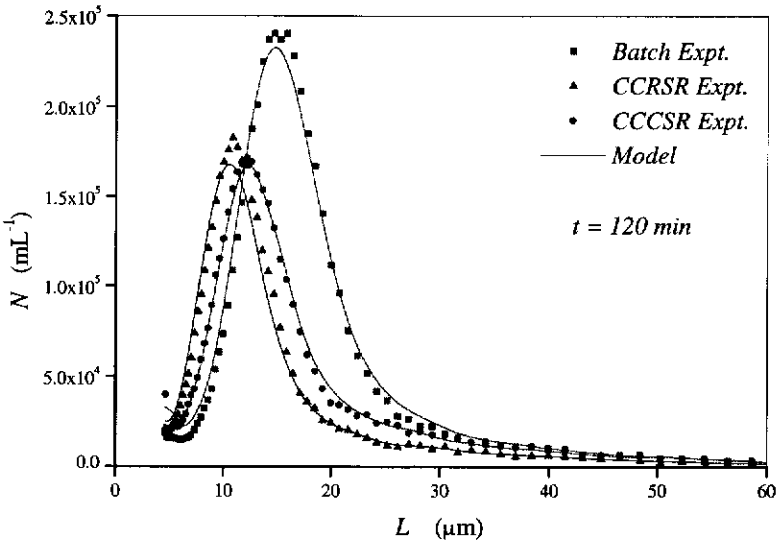

Figure 8.6. Comparisons between the experimental and predicted CSDs from the Batch, CCRSR and CCCSR configurations.

8.3.4 Uncertainties in the Kinetics Estimates from Monte Carlo Simulation

It is hypothesised that the observed discrepancies in the kinetics estimates between different precipitator configurations may be explained by the uncertainties associated with the kinetics estimates. A Monte Carlo simulation was used to determine the uncertainties in the kinetics estimates. It was assumed that the errors in the experimental data are independent and random. The main sources of variation in N_i are reported in Chapter 6. For each precipitator configuration, 1000 replicates set of experimental data were generated assuming that the N_i are normally distributed with a standard deviation of 10%. This is based on the unpublished CSIRO reproducibility data reported in Chapter 6, for a similar experimental configuration, which was found that the relative standard deviation in N_i for most of the size intervals to be within 4-10%.

Bramley's method was then applied to determine the kinetics estimates from each replicate data set. The 95% confidence limits on the relative uncertainties in the kinetics estimates, defined by Equation (8.10), are tabulated in Table 8.1 together with the mean kinetics estimates.

$$\delta_\theta = 1.96 \frac{\sigma_\theta}{\bar{\theta}} \tag{8.10}$$

where $\bar{\theta}$ is a vector containing the mean kinetic parameter values of $\bar{\beta}$, $\bar{G}$ and $\bar{B}_u$.

Table 8.1. The kinetics estimates and their 95% relative uncertainties limits for different precipitator configurations at the supersaturation ratio of $A/A^* = 2.84$.

Precipitator Configurations	$\bar{\beta} \pm \delta_\beta$ (mL hr^{-1})	$\bar{G} \pm \delta_G$ (μm hr^{-1})	$\bar{B}_u \pm \delta_{B_u}$ (mL^{-1} hr^{-1})
Batch	$1.3\times10^{-7} \pm 50\%$	$4.6 \pm 28\%$	$9.0\times10^{5} \pm 32\%$
CCRSR	$1.5\times10^{-7} \pm 68\%$	$3.2 \pm 25\%$	$4.5\times10^{5} \pm 35\%$
CCCSR	$1.7\times10^{-7} \pm 63\%$	$3.6 \pm 22\%$	$6.2\times10^{5} \pm 38\%$

Table 8.1 shows that the differences in estimates of β and G for the different precipitator configurations can be explained by the uncertainties in these estimates, provided the assumed uncertainty of 10% in N_i is not greatly overestimated. The large

large uncertainty in the β estimates is attributed to the relatively low values of the agglomeration kernel under the experimental conditions employed. The differences in the B_u estimates cannot be entirely explained by uncertainties. This result possibly reflects a dependency of the nucleation rate on solids content or surface area. The largest value of B_u is observed in the batch precipitator, where the solids content, m, is highest. The lowest is observed in the CCRSR precipitator, where m is lowest.

8.4 PARAMETER ESTIMATE SENSITIVITY TO PRECIPITATOR CONFIGURATION - CASE STUDY

The influence of the precipitator configurations on the uncertainties in the kinetics estimates was investigated by applying a Monte Carlo method to the simulated dynamic CSDs. The CSD simulation were performed by integrating Equation (3.38) together with the presumed correlations for β, G and B_u in Equation (8.11) and the CSD of the actual seed as an initial condition. The precipitation kinetics used in these studies are assumed to depend on supersaturation, $s = (A\text{-}A^*)$, as follows

$$\beta = k_\beta s^4; G = k_g s^2; \text{and } B_u = k_b s^2 \tag{8.11}$$

where k_β, k_g and k_b are the rate constants for agglomeration kernel, growth and source term rates, respectively. In the case of batch simulation, the supersaturation balance, stated for an isothermal case in Equation (8.12), was also taken into account (Li, Livk & Ilievski 2000a).

$$\varepsilon\phi\frac{ds}{dt} = -3\rho_s k_v \sum_{i=1}^{n} G\overline{L}_i^2 N_i - \rho_s k_v \overline{L}_1^3 B_u \tag{8.12}$$

where ε is the solids free volume fraction (volume of solution per volume of slurry) and ϕ is the conversion factor from Al_2O_3 to $Al(OH)_3$.

In this study a case with high agglomeration rate and low nucleation rate was considered. This case corresponds to gibbsite precipitation at a higher temperature

and lower agitation rates than reported here. The values of rate constant used in this study are $k_p = 1.55\times10^{-13}$, $k_g = 2.02\times10^{-3}$ and $k_b = 45.8$. The value of 70 g L^{-1} Al_2O_3 was taken as the initial supersaturation in the batch precipitation simulation. For both constant composition cases, three different values of *s*, namely, 41, 52 and 62 g L^{-1} Al_2O_3 were employed. Using a standard deviation of 10% for N_i, 1000 replicates of the simulated CSD data were generated. Bramley's method was then used to estimate the precipitation kinetics for all replicate data sets. It was assumed that in each replicate experiment data set, the CSD measurements at 7 sampling instants are available for determining the kinetics rates.

The uncertainties in the kinetic parameters as a function of supersaturation, estimated from repetitive data sets, are shown for each configuration in Figure 8.7. The points indicate uncertainties of the kinetics estimates that were evaluated for both constant composition cases carried out at that particular supersaturation. It is evident from the plots that the relative uncertainties vary with both supersaturation and configuration.

For the batch configuration, the relative uncertainties in the kinetics estimates decrease significantly with an increase in supersaturation as a consequence of an increase in the absolute values of the kinetics. A slightly more sluggish decrease can be observed for the constant composition cases. In addition, the results show that while the uncertainties for batch and constant composition configurations are similar at the high supersaturation value, the constant composition configuration tends to give smaller uncertainties than the batch one at the lower supersaturation values. However, deviations from this rule can be observed in the case of the agglomeration kernel. These are possibly due to factors associated with the evolution of the functional form of the CSD, which also impacts the values of uncertainties.

Finally, it should be noted that in both constant composition cases, the kinetics for each repetition were obtained as an average of 7 points from each experiment. Therefore, when comparing uncertainties of batch and constant composition cases in Figure 8.7, one should keep in mind that each constant composition case would demand 3 times as many measurements as the batch one.

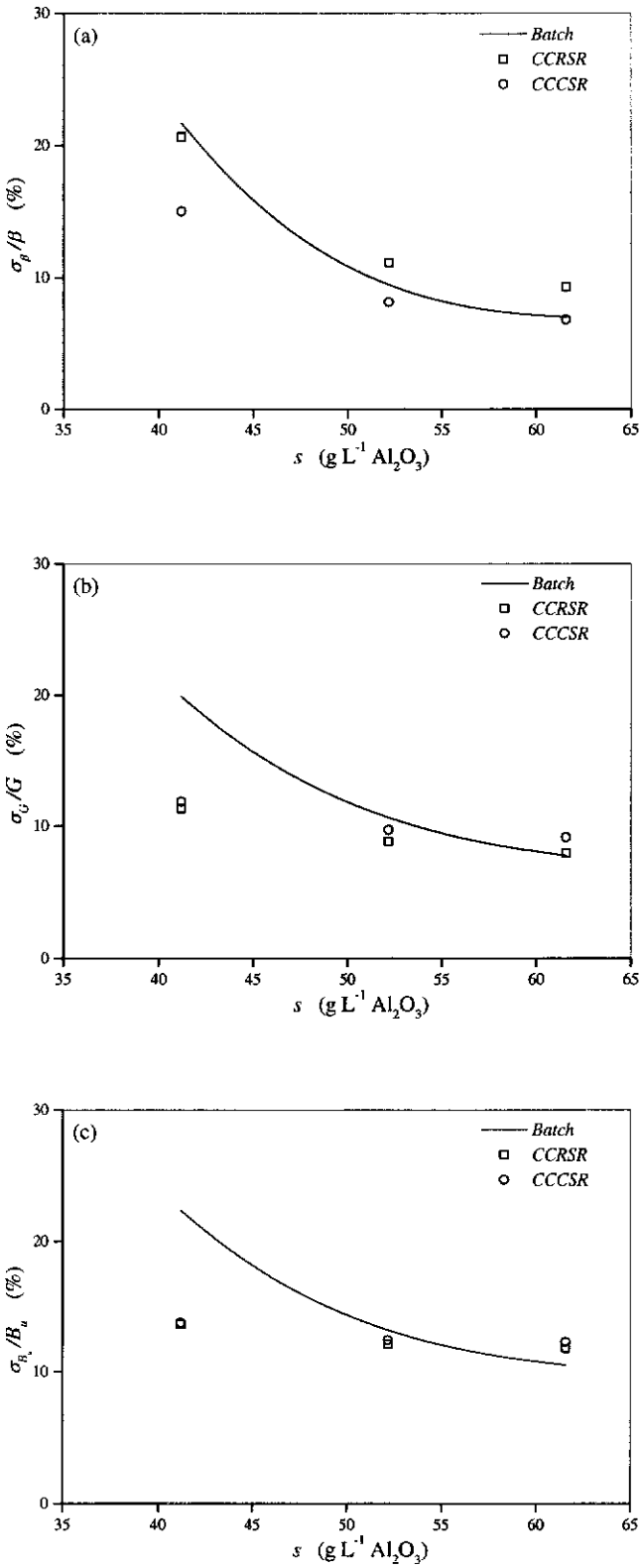

Figure 8.7. The relative uncertainties in kinetics estimates for the Case Study. (a) Agglomeration kernel, β; (b) growth rate, G; and (c) source term rate, B_u.

The uncertainties in the rate constants, estimated by applying Equation (8.11) to the estimated kinetics are presented in Table 8.2. They are consistently smaller than the uncertainties of the kinetics from which they were recovered.

Table 8.2. The uncertainties of the rate constants recovered from the estimated kinetics.

Precipitator Configurations	$\hat{\sigma}_{k_g}$	$\hat{\sigma}_{k_g}$	$\hat{\sigma}_{k_b}$
Batch	2.7%	3.1%	4.5%
CCRSR	3.4%	2.3%	3.9%
CCCSR	2.4%	2.4%	4.0%

It can be concluded that the most precise kinetics estimates are obtained under experimental conditions that promote the kinetics mechanisms, eg. high temperature and supersaturation. Hence, this factor appears to be a more important experimental design consideration than the precipitator configuration.

8.5 CONCLUSIONS

Gibbsite precipitation experiments were performed in three differently configured precipitators but with the same hydrodynamics, seed charge, supersaturation and temperature. Estimates of the agglomeration kernel, growth rate and nucleation source term rate obtained from the three configurations showed some variations. The differences in agglomeration kernel and growth rate estimates could be explained by uncertainties in their estimates. The differences between the source term rate estimates cannot be entirely explained by the uncertainties in the estimates and seem to be correlated to the differences in the suspension densities in the three configurations. A Monte Carlo simulation was used to investigate the sensitivity of uncertainties in the kinetic parameter estimates to the precipitator configuration and the operating conditions. Precipitator configuration appears to have less impact on uncertainties in the kinetic estimates than operating conditions, eg. supersaturation.

CHAPTER 9

THE ACCURACY OF GIBBSITE PRECIPITATION KINETICS ESTIMATES FROM DIFFERENT KINETICS ESTIMATION TECHNIQUES

9.1 INTRODUCTION

Precipitation kinetics estimation studies reported in the literature often encountered difficulties in generating accurate and reproducible kinetics estimates (Tavare 1986a; Rawlings, Miller & Witkowski 1993; Rohani 1993). As noted in Li, Livk & Ilievski (2000b), the poor reproducibility of precipitation kinetics estimates may be attributed to:

(1) random and systematic variations in the experimental data;
(2) differences in experimental design that affect the form and information content of the experimental data; and
(3) uncertainties associated with the parameter estimation procedures.

The uncertainty in the batch gibbsite precipitation data studied in this research has been treated in Chapter 7. The influence of precipitator configuration on the estimated gibbsite precipitation kinetics was investigated in Chapter 8. It was found that even at the same operating conditions, there were significant differences in the kinetics estimates. The differences can be explained by the uncertainties in the kinetics estimates (evaluated by Monte Carlo simulations), which are attributed to the interplay between the different forms of the data output (i.e. CSD) from the different configurations, uncertainty in the data, and the kinetic parameter estimation

procedure used. In addition, a kinetic parameter sensitivity analysis showed that operating conditions appears to be a more important factor in determining accurate kinetics estimates than the precipitator configuration.

The objective of this chapter is to establish whether the different kinetics estimation techniques when applied to the same gibbsite precipitation data will give the same results and, if not, which technique is the most reliable and has the lowest confidence limits on the estimates.

9.2 ESTIMATION OF PRECIPITATION KINETICS

Methods for the simultaneous determination of the kinetics of agglomeration, growth and nucleation source term from experimental precipitation data are reviewed in Chapter 4. The techniques that are based on the PB theory can be divided into two main categories. The first is referred to as the differential method, and uses directly the differential form of the PB based model together with the time derivatives of the precipitation data. The second is the so-called integral method, which uses the integrated PB based model and experimental precipitation data. The PB model of a non-stationary, well-mixed, constant volume precipitation system, with simultaneous agglomeration, growth and nucleation occurring is given by

$$\frac{\partial n}{\partial t} + G\frac{\partial n}{\partial L} = B_N + B_A - D_A + \frac{1}{V}\left(\sum Q_{in} n_{in} - \sum Q_{out} n_{out}\right) \qquad (9.1)$$

The underlying principle of the kinetics estimation procedures is to identify the functions of the kinetics that make the PBE (9.1), or its moment form, consistent with the dynamic experimental data. In this chapter, the differential and integral methods are considered in the estimation of kinetics.

9.2.1 Differential Methods

Most applications of this approach reported in the literature are based on the method of moment analysis (Tavare and Garside 1986; Tavare 1995a; Ilievski and White 1996). Four differential methods are considered here and are described below.

9.2.1.1 Generalised Method of Bramley, Hounslow & Ryall (1996)

The method of Bramley, Hounslow & Ryall (1996) for simultaneous determination of agglomeration kernel, β, growth rate, G, and source term rate, B_u, can be modified to the precipitator configuration described by Equation (9.1) to give

$$\dot{\mu}_0 = B_u + \Phi_0\beta + \frac{1}{V}\left(\sum Q_{in}\mu_{0,in} - \sum Q_{out}\mu_{0,out}\right) \tag{9.2}$$

$$\dot{\mu}_3 = \Phi_3 G + \overline{L_1}^3 B_u + \frac{1}{V}\left(\sum Q_{in}\mu_{3,in} - \sum Q_{out}\mu_{3,out}\right) \tag{9.3}$$

$$\dot{N}_1 = \Phi_2 G + B_u + \Phi_1\beta + \frac{1}{V}\left(\sum Q_{in}N_{1,in} - \sum Q_{out}N_{1,out}\right) \tag{9.4}$$

The above system of linear equations is solved at each time instant in order to determine the values of the kinetic parameters, β, G and B_u.

9.2.1.2 Moments Matching Method

The moments matching method constitutes finding the values of kinetics that reconcile the moments of the experimental CSD. The moment equations needed for the simultaneous determination of the β, G and B_u are those of the zeroth, third and sixth moments (see section 4.3.2.5). For the PBE (9.1) considered, these moment equations are given as

$$\dot{\mu}_0 = B_u - \frac{1}{2}\beta\mu_0^2 + \frac{1}{V}\left(\sum Q_{in}\mu_{0,in} - \sum Q_{out}\mu_{0,out}\right) \tag{9.5}$$

$$\dot{\mu}_3 = 3G\mu_2 + \frac{1}{V}\left(\sum Q_{in}\mu_{3,in} - \sum Q_{out}\mu_{3,out}\right) \tag{9.6}$$

$$\dot{\mu}_6 = 6G\mu_5 + \beta\mu_3^2 + \frac{1}{V}\left(\sum Q_{in}\mu_{6,in} - \sum Q_{out}\mu_{6,out}\right) \tag{9.7}$$

9.2.1.3 Simplified Moments Matching Method (SMM)

This method is a subset of the moments matching method and is only applicable for dynamic precipitation systems with constant kinetics, eg. constant composition precipitation system. Under the assumption of constant kinetics, B_u and β can be estimated from Equation (9.5) with linear regression analysis, similarly, G is determined from the linear least squares fit of Equation (9.6).

9.2.1.4 A Generalised Differential Method

Livk, Pohar & Ilievski (1999) posed the precipitation kinetics estimation problem as a non-linear optimisation with the objective function formulated in terms of time derivatives of measured precipitation properties. In the case where the β and G are all size independent, they reported that the non-linear optimisation problem reduces to a sequence of three algebraic equations that can be solved explicitly for G, β and B_u at each time instant. In such case, the technique becomes almost identical to the Bramley's method and leads to almost identical results, if the size discretisation scheme with $r = \sqrt[3]{2}$ is used. Although in this work only the Bramley's method will be thoroughly analysed, it is worth noting that both methods represent alternative approaches to the same differential method.

9.2.2 Integral Method

Estimation of precipitation kinetics using the integral method can be viewed as a non-linear parameter optimisation problem. The kinetic parameters are estimated by minimising a least square objective function (see Chapter 4), which is written as

$$\Phi(\theta) = \sum_{i=1}^{n} \sum_{j=1}^{m} \omega_i \left(N_{i,j}^{\text{expt}} - N_{i,j}^{\text{model}}(\theta)\right)^2 \tag{9.8}$$

where $N_{i,j}^{\text{expt}}$ and $N_{i,j}^{\text{model}}$ represent the experimental and model predicted crystal numbers in the i^{th} size interval taken at the j^{th} sampling time, respectively. ω_i is the weighting function. θ is the vector containing the set of unknown values of G, β, and B_u, at certain time instants during the precipitation run. $N_{i,j}^{\text{model}}$ is calculated using the

DPB model of Equation (9.1), i.e. Equation (3.38). In each step of the optimisation procedure, the DPB model equations are integrated together with the set of values of θ and initial conditions. The objective function is then evaluated and new set of values of θ is calculated. The high accuracy of this method results from the fact that the complete course of a process is predicted at each optimisation step. The main disadvantage of the integral method is the substantial computational effort required for the successive integration of the model equations (Li, Livk & Ilievski 2000b).

9.2.3 Validation of the Differential Estimation Techniques

The validity of each of the above differential techniques was assessed by applying them to a simulated CSD, generated using specified values of β, B_a and G. The hypothetical rates were chosen to be of the same order of magnitude as the estimated kinetic parameters from experimental precipitation data. A semi-batch, constant composition precipitator (i.e. constant kinetics) was selected as the test system because all the differential methods, including the SMM, can be compared.

The CSD was simulated using the DPB models of Hounslow, Ryall & Marshall (1988) and Litster, Smit & Hounslow (1995). A discretisation size scheme of $q = 2$ was used in the simulation. The DPB model was integrated together with the initial conditions using a fourth-order Runge-Kutta algorithm. A three-point numerical differentiation scheme was used to estimate the time derivative terms in the differential methods. Comparisons of the kinetics estimates and the true (hypothetical) kinetics are presented in Table 9.1.

Table 9.1. Comparisons of agglomeration kernel, source term rate and growth rate estimates determined from different differential methods.

	β ($mL\ hr^{-1}$)	B_a ($mL^{-1}\ hr^{-1}$)	G ($\mu m\ hr^{-1}$)
True Kinetic Rates	**1.12×10^{-6}**	**6.00×10^{4}**	**5.02**
Bramley's Method	1.12×10^{-6}	6.01×10^{4}	5.02
Moments Matching	1.31×10^{-6}	8.86×10^{4}	5.04
SMM	1.13×10^{-6}	6.10×10^{4}	5.04

Table 9.1 shows that the Bramley's method, and hence, the Livk's method provides the closest β, B_u and G estimates, followed by the SMM method. This result is expected as Bramley's method is based on a DPB model similar to that used to simulate CSD and the small deviations are primarily due to errors introduced by the numerical differentiation. The relatively poor quality of the estimates obtained from the moments matching method is most likely a consequence of the method's dependence on higher moments (i.e. μ_5 and μ_6), and in particular the numerical differentiation of μ_6. The higher moments weight towards the tail of the CSD, where the information content is relatively low. A relatively accurate estimate of G is obtained, suggesting that errors introduced by the numerical differentiation of μ_3 are not significant (provided accurate experimental data is available). The reasonable estimates obtained by the SMM method also supports the conclusion that it is the reliance on higher moments that compromises the kinetics estimates from the moments matching method. It can be concluded that the Bramley's method is preferred over the moments matching method.

9.3 GIBBISTE PRECIPITATION KINETICS

9.3.1 Gibbsite Precipitation Data

Gibbsite precipitation data reported here were extracted from the experimental study of Ilievski, McShane & Rudman (1997), which were generated from experiments performed in a batch configuration and a semi-batch, constant composition solids retention configuration (CCSR). These experimental configurations are similar to those reported in Chapter 5.

The precipitation experiments were conducted in a 4-litre precipitator at 80 °C, agitated at 600 rpm and a seed charge of 15 g L^{-1} (Alcoa C31 gibbsite). Initial supersaturation A/C ratios of 0.7 and 0.6 were employed in the batch and CCSR experiments, respectively. Figure 9.1 shows the transient zeroth moment, μ_0, number of crystals in the first size interval, N_1, and the third moment, μ_3, for both batch and CCSR precipitation experiments.

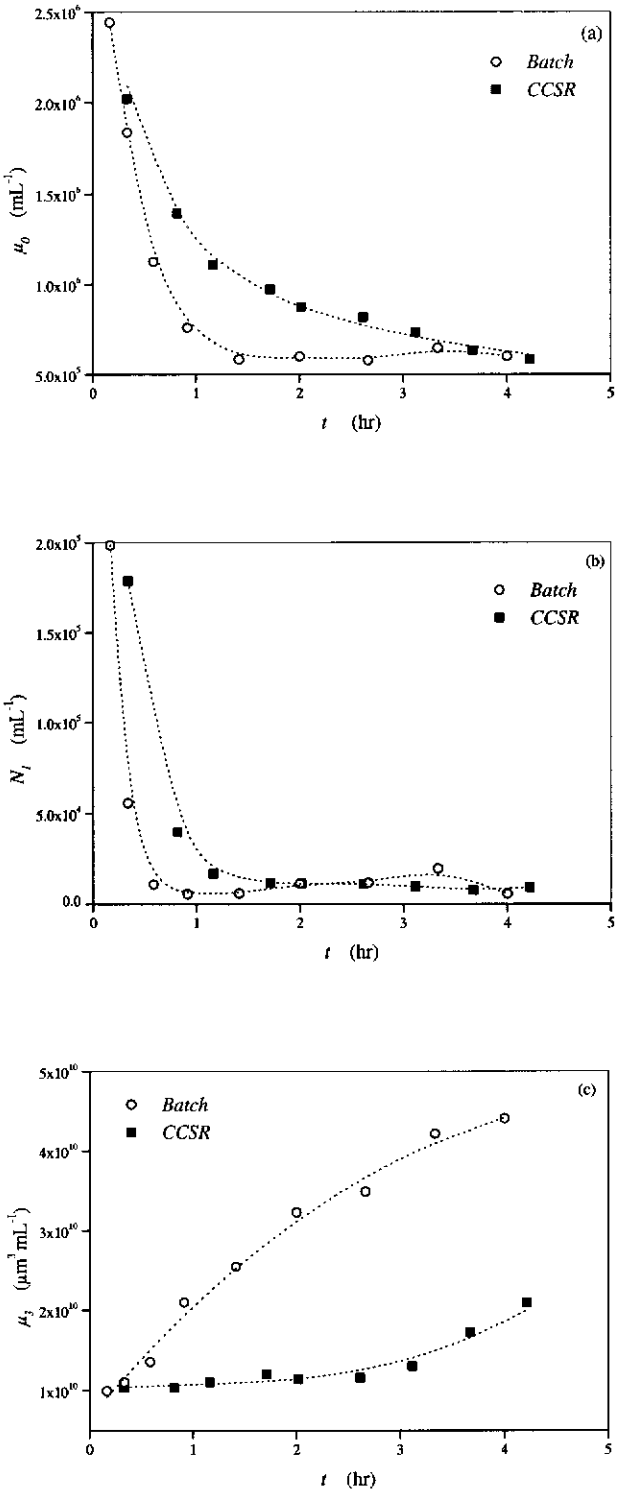

Figure 9.1. Transient batch and constant composition experimental data. (a) Total crystal numbers, μ_0; (b) crystal number in the first size interval, N_1; and (c) third moment, μ_3, (from the data of Ilievski, McShane & Rudman 1997).

9.3.2 Kinetics Estimates by the Different Techniques

The kinetics estimates and their uncertainty bounds generated from the non-linear parameter optimisation method (i.e. integral method) presented in the following sections were determined by Iztok Livk, and his contribution to the discussion in this chapter is gratefully acknowledged.

9.3.2.1 Batch Kinetics Estimates

The kinetics estimates from the differential and the integral methods are plotted in Figure 9.2 as functions of A/A^*. High supersaturation ratio values correspond to the early stages of the batch precipitation process. Figure 9.2 shows that Bramley's method and the integral method give different but comparable estimates of the kinetics. The two methods give almost identical estimates of G. The moments matching method, however, only gives reasonable G estimates and gives negative values for both β and B_u. The unrealistic estimates of β and B_u are a consequence of the dependence of this method on the fifth and sixth moments of the experimental CSD, which were observed to show a much larger scatter than the first, second and third moments.

9.3.2.2 Constant Composition Kinetics Estimates

Averaged kinetic estimates obtained by the differential and integral methods at a supersaturation of $A/A^* = 1.69$ are shown in Table 9.2. Again the moment matching method gives poor estimates for β and B_u. The values of β and B_u determined by the other methods are relatively consistent. In the case of G, all the methods give comparable estimates.

Table 9.2. Averaged agglomeration kernel, source term rate and growth rate estimated by the different methods from the constant composition precipitation data at $A/A^* = 1.69$.

	β (mL hr^{-1})	B_u (mL^{-1} hr^{-1})	G (μm hr^{-1})
Integral method	6.8×10^{-7}	4.3×10^{4}	3.6
Bramley's method	6.8×10^{-7}	5.6×10^{4}	3.0
Moments matching	-4.3×10^{-7}	-2.2×10^{5}	3.9
SMM	6.9×10^{-7}	5.6×10^{4}	3.6

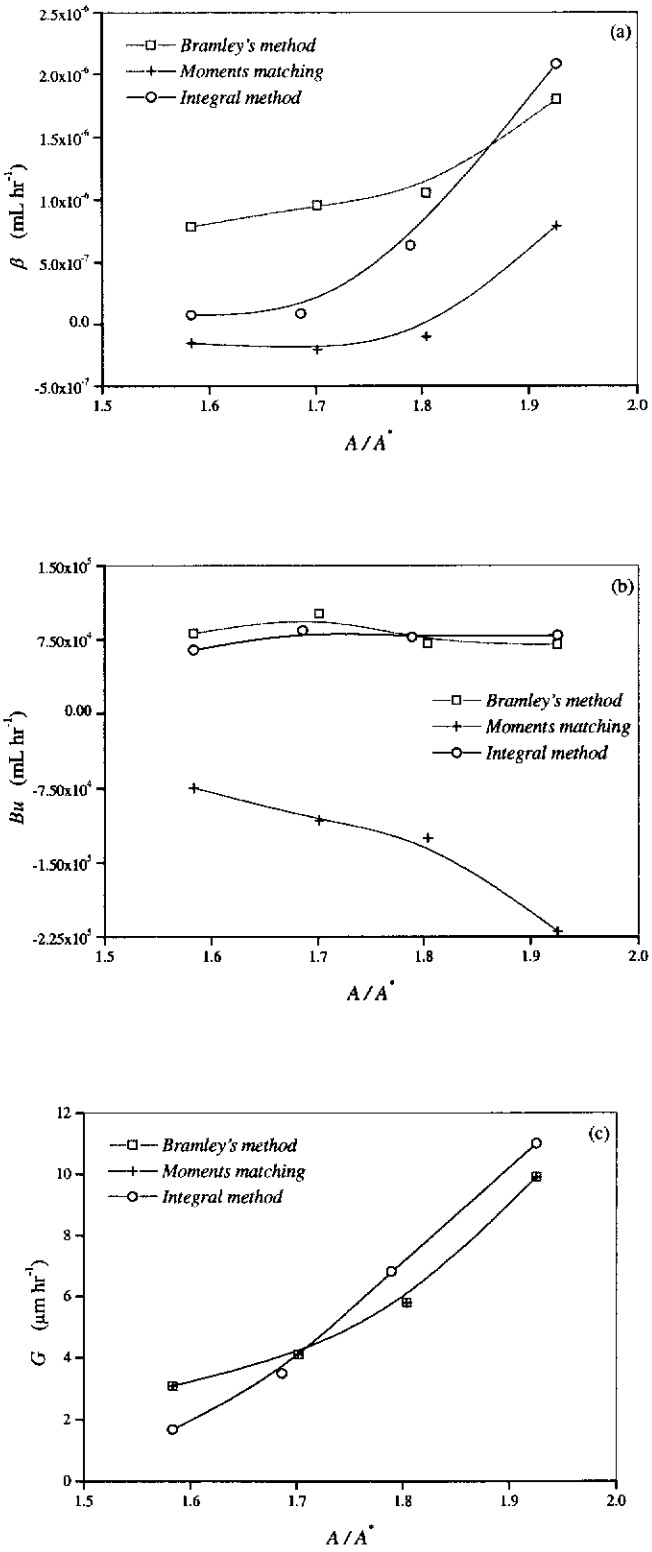

Figure 9.2. Precipitation kinetics determined by the differential and integral methods for batch experiment; (a) agglomeration kernel, β; (b) source term rate, B_u; and (c) growth rate, G.

9.3.3 Evaluation of the Estimation Methods by CSD Simulation

The different parameter estimation techniques were tested by comparing the experimental CSD with the CSD simulated using the kinetics estimates obtained from the respective techniques. Figure 9.3 shows that the CSD simulated using estimates obtained from the moments matching method are in very poor agreement with the experimental CSD. The estimates from the integral method appear to result in the best agreement.

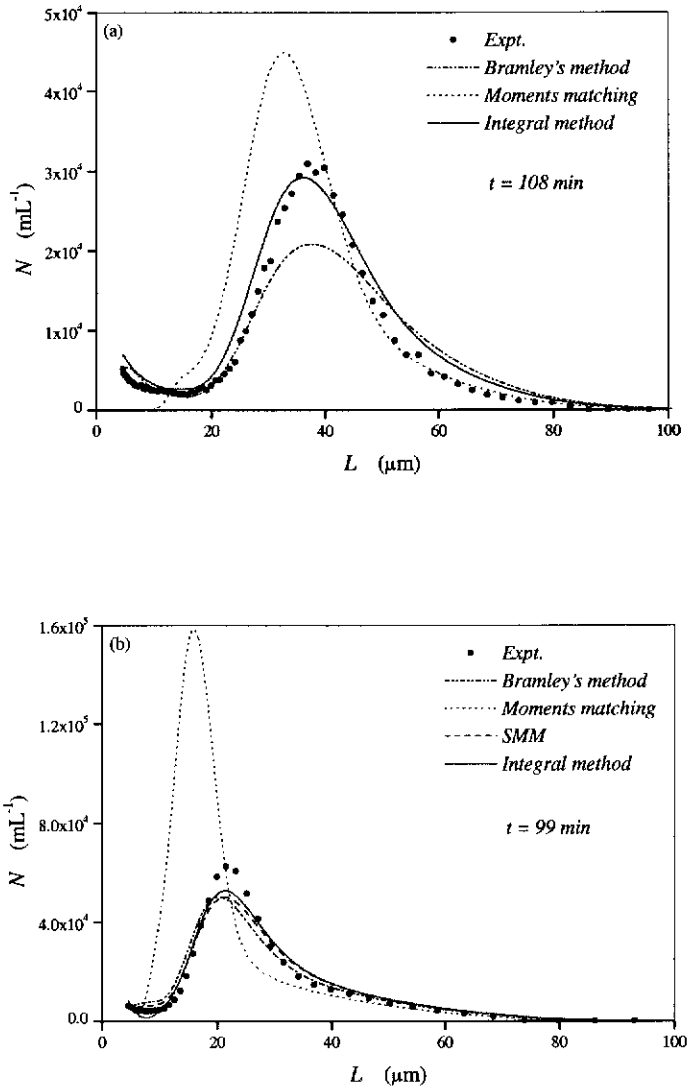

Figure 9.3. Comparisons between the experimental and predicted CSDs using the kinetics estimates from different techniques in different experimental configurations. (a) Batch; and (b) CCSR.

The difference between the experimental and predicted CSDs (i.e. SSE) was quantified using the definition given by Equation (9.8) with ω_i set to unity. Table 9.3 shows that the lowest SSE values are obtained with kinetics estimates from the integral method. As expected, the highest SSE was associated with the moments matching method. The estimates from Bramley's method give roughly 2-3 times the SSE values of those from the integral method. It is interesting to note that in the constant composition system, the estimate determined from the SMM method has a lower SSE value than the result from Bramley's method. This may be due to an additional source of error being introduced through Equation (9.4) in Bramley's method. The integral method gives the lowest SSE values is not entirely surprising since the same comparison is used by the integral method as a criterion in the estimation of precipitation kinetics.

Table 9.3. SSE between the experimental and predicted CSDs using the kinetics estimates from different kinetics estimation methods, in the batch and CCSR systems.

	SSE (Batch)	SSE (CCSR)
Integral method	**3.2×10^{8}**	**1.6×10^{8}**
Bramley's method	7.1×10^{8}	4.8×10^{8}
Moments matching	5.2×10^{9}	5.0×10^{10}
SMM	/	2.2×10^{8}

9.4 UNCERTAINTIES IN THE KINETICS ESTIMATES

9.4.1 Error in the Experimental Data

The kinetics estimation techniques reported here utilise the experimental CSD data described in section 9.3.1, the solids content and liquor titration data are used for mass balance consistency checks on μ_3. It is assumed that the uncertainty estimates in the experimental data from Chapter 7 can be satisfactorily applied to the precipitation data here, which was generated under similar operating conditions, but at a higher agitation rate (i.e. 600 rpm compared to 480 rpm).

9.4.2 Uncertainties in the Kinetics Estimates from the Differential Methods

9.4.2.1 Uncertainties in Batch Kinetics Estimates from Bramley's Method

The estimated values of kinetic rates can be considered as random variables and the probability distributions for each parameter estimate could be generated if sufficient replicate experiments were available. A Monte Carlo simulation was used to evaluate the uncertainties associated with the kinetics estimates. Using the experimental data's uncertainties from Chapter 7, 1000 computer-generated replicate data sets were obtained by loading the original data with random normally distributed errors. The Bramley's method was then applied to generate the kinetics estimates.

The relative uncertainties of these estimates are given in Figure 9.4 as functions of precipitation time. These uncertainty estimates, which are themselves random variables, did show scatter with time and have been smoothed to highlight the general trends. Figure 9.4 shows that the uncertainties in the agglomeration kernel estimates, $\hat{\sigma}_{\beta}$ and growth rate estimates, $\hat{\sigma}_{G}$, are low initially but increase steadily with precipitation time. The uncertainty in the source term rate estimates, $\hat{\sigma}_{B_u}$, on the other hand, shows a more complicated behaviour with time, i.e. plateaus with time.

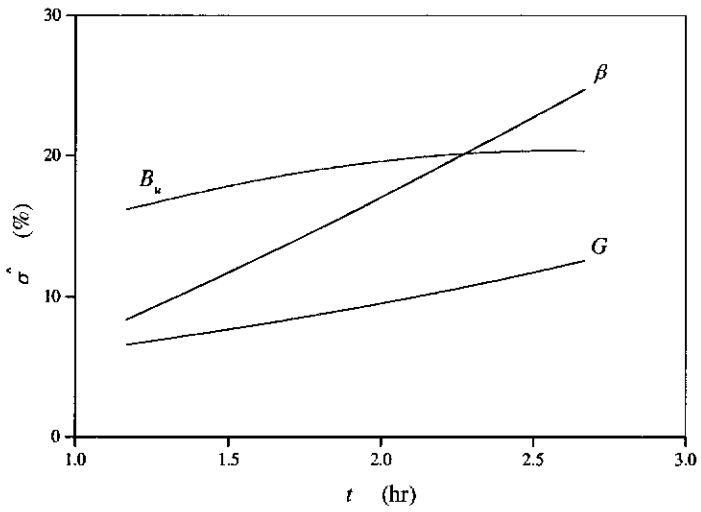

Figure 9.4. The relative uncertainties of the kinetics estimates obtained from a Monte Carlo analysis of batch precipitation experiments using the differential method of Bramley, Hounslow & Ryall (1996).

To explain the above results, two main factors, which determine the uncertainties of the kinetics estimates must be explored. As discussed in Chapter 7, these are the rate of change of crystal numbers and volume, and the relative magnitude of the β, G and B_u. The smaller values of $\hat{\sigma}_\beta$ and $\hat{\sigma}_G$ correspond to early stages of the precipitation run where the rates of change of total crystal numbers and volume are highest (see Figure 9.1). At these times the error introduced by numerical differentiation is the smallest. The consistent large $\hat{\sigma}_{B_u}$ values observed in Figure 9.4 may due to the large uncertainty in the crystal numbers in the first size interval as discussed in Chapter 7. Figure 9.4 is specific to the described experiment and should not be extrapolated to other conditions.

9.4.2.2 Uncertainties in Constant Composition Kinetics Estimates from the SMM

The uncertainties associated with the kinetic parameter estimates from the constant composition experiment obtained using the SMM method were estimated using the linear regression analysis. The corresponding relative uncertainty in β, G and B_u were 10%, 16% and 40%, respectively. Although the values of these uncertainties more or less indicate the deviation from the assumption of constant kinetics, it is noteworthy that they are in the same order of magnitude as those obtained by the Monte Carlo analysis in the previous section.

9.4.3 Uncertainties in the Kinetics Estimates from the Integral Method

Li, Livk & Ilievski (2000b) applied Monte Carlo simulation to evaluate the uncertainties of the estimates from the integral method. The same error structure as described above was used, but only 50 computer-generated replicate data sets were generated, due to the intensive computing requirements. The relative uncertainties of the batch and constant composition kinetics estimates obtained by the integral method using a Monte Carlo simulation are presented in Figure 9.5.

Again the uncertainties are typically small at the beginning of a precipitation run, and increasing towards the end. Li, Livk & Ilievski (2000b) suggested that this is mainly due to the fact that the kinetics values used in the final stage of the simulation have a lesser impact on the objective function value than the kinetics from the initial stage

of the simulation. Consequently, the sensitivity of the objective function with regard to the initial kinetics is larger than that to the kinetics from the final stage. The actual values of uncertainties also depend on the relative magnitude of the different kinetic parameters, in a similar manner to that observed with the differential method.

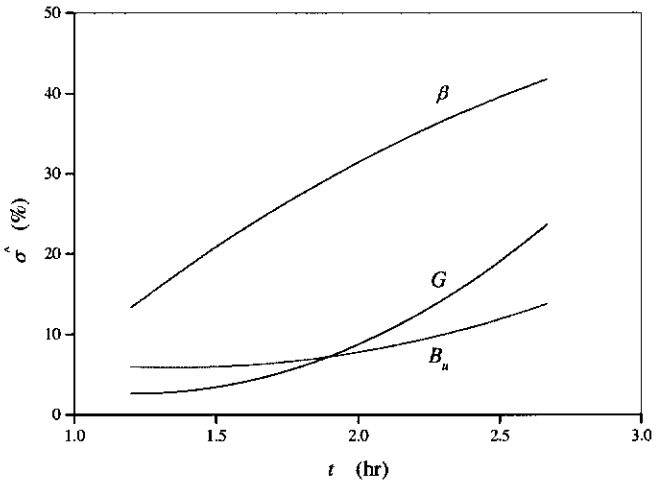

Figure 9.5. The relative uncertainties of the kinetics estimates obtained from the analysis of batch and constant composition experiments using the integral method.

9.5 CONCLUSIONS

The differential and integral techniques were employed to estimate gibbsite precipitation kinetics in batch and constant composition precipitation systems. Comparison of experimental and predicted CSDs showed that the kinetics estimates obtained from the integral method lead to better agreement than those obtained by the differential method. Both methods agree well in the case of growth rate, but deviate more in the case of agglomeration kernel and source term rate.

Uncertainties in the kinetics estimates have been evaluated for both estimation techniques using Monte Carlo simulation. It was found that the kinetics estimates from both the differential and integral methods have significant uncertainties. Both methods give comparable estimates of uncertainty in the growth rate estimates. The differential method resulted in lower uncertainty in the agglomeration kernel

estimates, but larger uncertainty in the source term rate estimates, than those from the integral method. The uncertainties of the estimates obtained by both methods increased toward the end of the precipitation runs.

The uncertainties of kinetics estimates are generally determined by the rate of change of a property, the relative magnitude of the kinetics rates and the nature of the optimisation problem. However, the number of replicate sets used (i.e. 50) in Monte Carlo simulation for the integral method may not be large enough to ensure an unbiased estimation of uncertainty intervals, compared to 1000 replicate sets used in the differential method.

The integral method is more accurate, but it requires substantial computational effort compared to the differential method, which is simple and rapid. Nevertheless, the differential and integral methods are complementary tools for precipitation kinetics estimation; differential methods can be used to help improve the efficiency of the integral method by providing an initial guess of the values of the kinetics rates. The final choice of what method to use, however, depends on the trade off between the computing power, accuracy desired and the quality of experimental data.

CHAPTER 10

MIXING IN PRECIPITATION SYSTEMS: A REVIEW

10.1 INTRODUCTION

In Chapter 11, precipitation kinetics estimation and modelling will be considered in a poorly-mixed precipitator. For this reason, the role of mixing in precipitation systems is reviewed. The geometry of a vessel, its internals (eg. baffles and draft tubes) and the mechanical forces generated by the stirrer, determine the hydrodynamic conditions in the vessel. In turn the hydrodynamic conditions in a vessel influence the fluid flow pattern, fluid velocity profile and the rate of mixing. Mixing on the other hand controls the interaction between fluids at both the macroscopic and microscopic levels. That is, it determines the spatial homogeneity of supersaturation, temperature, energy dissipation, and solids suspension in a vessel.

The assumption of "well-mixed" or "ideal-mixed" is commonly made for mixing in a stirred vessel. However, this assumption is generally only valid for smaller scale vessels. In precipitation processes, the chemical reactions or the process mechanisms such as, nucleation and growth are essentially molecular level processes, which require that the chemical species come in contact with each other and its environment at molecular level. It has been reported that nucleation is strongly dependent on supersaturation, if the nucleation time is fast compared to the mixing time, then nucleation can begin in an inhomogeneous supersaturation field, resulting in local nucleation. In addition, inhomogeneous suspension mixing in the vessel also subjects crystals to different supersaturation zones, which may affect secondary nucleation, growth and agglomeration kinetics.

10.1.1 Mixing Process

The mixing process is characterised by two independent mechanisms, known as macromixing and micromixing. The state of one mechanism does not define a corresponding level of the other. Micromixing is concerned with the mixing of fluids on the molecular level. Macromixing is generally defined as all the mixing processes other than micromixing, and is concerned with mixing due to the fluid velocity field, which controls macroscopic composition homogeneities in the fluid, and also determines the environment for micromixing.

10.1.2 Premixed and Unpremixed Systems

Baldyga and Bourne (1986) reported that two distinct systems can arise depending on how the reactants are fed into the vessel. Firstly, in premixed systems, a single stream of reactants is fed into the vessel, and mixing occurs between fluid elements of different age, and hence, different reactant concentrations. In unpremixed systems, two separate streams of different reactants are introduced into the vessel, and mixing between different species occurs. Mixing in this case is particularly important, because it precedes the chemical reaction.

Considerable research effort has been devoted to investigate unpremixed systems, which are commonly employed in fast chemical reaction systems. The unpremixed systems studied in the literature include consecutive-competing reactions, reaction between two miscible reactants from different feed streams, and point feed of one reactant to another. These include the work of Angst, Bourne & Sharma (1982a; 1982b), Baldyga and Bourne (1988), Bourne and Tovstiga (1988), Tavare (1989; 1994), Baldyga, Bourne & Yang (1993), Bourne, Gholap & Rewatkar (1995), and Fournier, Falk & Villermaux (1996a; 1996b).

10.2 DEVELOPMENT OF MIXING MODELS IN THE LITERATURE

Models that account for non-ideal mixing systems have been developed since the 1950s. Two branches of mixing models have been developed in parallel; those based on the chemical reaction engineering viewpoint and those from fluid turbulent theory. Numerous models based on the residence time distribution concept, and the concepts

of degree of segregation and mixing earliness have been developed (Curl 1963; Ng and Rippin 1965; Becker and Larson 1969; Costa and Trevissoi 1972; Ritchie and Tobgy 1978; Garside and Tavare 1985; Tavare 1992; 1995b).

Similarly, a large number of mechanistic models based on fluid turbulent theory have also been developed (Bourne 1983; Pohorecki and Baldyga 1983a; 1983b; 1988; Villermaux and David 1983; Rohani and Baldyga 1987; Baldyga and Bourne 1989a; 1989b). Others include the network-of-zones model (Mann and Mavros 1982; Knysh and Mann 1984; Mann 1986; Dudczak 1994; Mann, Ying & Edwards 1994; Mann et al. 1997) and the computational fluid dynamics models (Sharratt 1990; Mann 1993; Seckler, Bruinsma & van Rosmalen 1995; Fox 1998).

Mixing models are generally formulated from either the Lagrangian or Eulerian viewpoints. Tavare (1986b) stated that in the Lagrangian perspective, the changes of the properties of the elementary volumes or clumps are observed as a function of time as they progress through the vessel. On the other hand, in the Eulerian view, the property variation is observed at a fixed point in a stationary coordinate system. Thus, both approaches result in different problem formulations. The Lagrangian system includes those models based on the chemical reaction engineering viewpoint and mechanistic models based on turbulence theory. The Eulerian system is that of classical statistical turbulence theory and computational fluid dynamics models.

The mixing models developed in the literature can be classified into three groups. Firstly, the macromixing models where the system is assumed well micro-mixed (i.e. neglecting micromixing). The second group belongs to that of micromixing models in which the system is assumed well macro-mixed. The third are those models that incorporate interaction between micromixing and macromixing.

This chapter describes briefly the numerous mixing models reported in the literature. A more detailed review on mixing models can be found in Baldyga and Bourne (1986), Villermaux (1983; 1991), Tavare (1986b; 1995b), Baldyga and Pohorecki (1995), and Kuipers and van Swaaij (1998).

10.3 MACROMIXING

10.3.1 Residence Time Distribution

Macromixing is characterised by the residence time distribution (RTD) of the fluid. The RTD concept was introduced by Danckwerts (1953). The term particle is used to represent any conserved entity such as, molecule, elementary fluid volume or clump (Tavare 1986b). Particles have zero age as they enter a continuous flow vessel and acquire age equal to the time they spent in the vessel. The age of a particle at its exit from the vessel is called the residence time. The experimental technique commonly used for determining the RTD of fluid in the vessel is the stimulus-response technique using tracer material in the flow. The stimulus may be pulse, step or periodic injections of tracer, and the response is recorded as the amount of tracer leaving the vessel (Levenspiel 1972).

10.3.2 Macromixing Models

The two extremes of the macroscopic liquid flow pattern in a vessel are represented by the plug flow and completely mixed flow. Plug flow has only radial mixing, and is characterised by an identical residence time for all particles within the vessel. The completely mixed flow is characterised by an exponential RTD function, and has the same composition within the vessel and at the exit of the vessel. Most real vessels exhibit macromixing behaviour between these two extremes. The likely causes of deviation from these idealised extreme flows as suggested by Tavare (1986b) are velocity fluctuations due to turbulent diffusion, bypassing and channelling of suspension, short-circuiting, stagnant regions of fluid or recycling within the vessel. The non-ideal flows within a vessel have been described by the dispersion model, the tank-in-series model and the mixed model (Levenspiel 1972; Tavare 1986b; Villermaux 1991).

10.3.2.1 Dispersion Model

The dispersion model is characterised by the dispersion number, D/ux, that measures the extent of axial dispersion and the characteristic mixing state in the vessel, where D is the axial dispersion coefficient, u is the fluid velocity and x is the distance along the axial direction. D/ux approaching zero indicates negligible dispersion, and the

vessel will behave like a plug flow vessel. As D/ux approaches infinity, implies large dispersion, and hence, mixed flow is achieved.

10.3.2.2 Tanks-in-Series Model

Tanks-in-series model has been proposed to model non-ideal flows in crystallisers by Randolph (1965), Abegg and Balkrishnan (1971) and Nývlt (1971). The approach is to divide an imperfectly mixed suspension into a number of equal volume, perfectly mixed compartments in series. The number of compartments is the model parameter, if each is assumed to have identical independent attributes (Tavare 1986b).

10.3.2.3 Mixed Model

The dispersion and tank-in-series models can account for non-ideality in flows that do not deviate greatly from their corresponding ideal flow patterns. For flows that deviate significantly from the ideal flow pattern, a mixed model is required. The mixed model considers the vessel as consisting of different regions i.e. plug, mixed or dead-water, which are interconnected in different arrangements, i.e. bypassing, cross-flow or recycle. A detailed description of the mixed model is given in Levenspiel (1972), Ritchie and Tobgy (1978) and Tavare (1986b).

10.4 MICROMIXING

10.4.1 Micromixing - Chemical Reaction Engineering Approach

The concepts of the degree of segregation and mixing earliness defined by Danckwerts (1958) and Zwietering (1959) are particularly useful in developing micromixing models. The degree of segregation is concerned with whether mixing occurs on macroscopic or microscopic levels. On the other hand, mixing earliness is concerned with whether the fluid particles of different ages mix with each other early or late as it flows through the vessel.

10.4.1.1 Degree of Segregation

There are two extremes of the degree of segregation, which represent the limits of micromixing, and are called the completely segregated and maximum mixedness states. According to Danckwerts (1958), if individual clumps flow through a vessel

without mixing on molecular scale (i.e. no micromixing), such system is said to be completely segregated. In this situation, an individual clump travels through the vessel according to the RTD. The contents of the vessel are then said to behave as a macrofluid, and each clump acts as a small batch vessel, with same entering conditions, but different exit conditions (Tavare 1986b). The other limit corresponds to the complete molecular mixing, and referred to as the maximum mixedness. In this case, the entering clump mixes immediately with clumps already in the vessel. The vessel contents are then said to behave as a microfluid. The fluid is considered completely segregated as it enters the vessel. If it mixes completely during its time in the vessel, then a maximum mixedness state is achieved, otherwise, it will be either partially segregated, which is the usual case in large scale vessels, or remain completely segregated.

Mixing in real systems are generally partially segregated. To describe such state of micromixing, Danckwerts (1958) defined a measure of the degree of segregation, J, based on age as

$$J = \frac{\mathrm{var}\,\alpha_p}{\mathrm{var}\,\alpha} = \frac{\overline{(\alpha_p - \overline{\alpha})^2}}{\overline{(\alpha - \overline{\alpha})^2}} \tag{10.1}$$

where α is the age of a molecule, $\overline{\alpha}$ is the mean age of all molecules in the vessel, and α_p is the mean age of the molecules at a point. The value of J lies between $J_{\min}$, the maximum mixedness state, and $J = 1$, the completely segregated state. However, $J_{\min}$ depends on the RTD, and is zero only for an exponential RTD (i.e. a MSMPR system). Baldyga and Bourne (1986) stated that this definition is not a useful measure of the level of partial segregation, because it cannot be directly measured.

Brodkey (1981) utilised the concentration fractions to define the intensity of segregation. For mixing of two non-reacting species A and B, the intensity of segregation, I_s, is

$$I_s = \frac{\overline{C_A'^2}}{\overline{C}_{Ao}\overline{C}_{Bo}} = \frac{\overline{C_B'^2}}{\overline{C}_{Ao}\overline{C}_{Bo}} \tag{10.2}$$

where the concentration fraction fluctuation is defined as $C_i' = C_i - \overline{C}_i$, and C_i and $\overline{C}_i$ are the instantaneous and averaged concentration fractions of species i (where i = A or B), at any time instant. The intensity has the value of unity for completely segregated fluid and zero for maximum mixedness (i.e. concentration fluctuation is zero). Brodkey (1981) further stated that the intensity of segregation is a good measure of the diffusional process. Hiby (1981) discussed various definitions and measurements of the degree of mixing in liquid mixtures.

Villermaux and David (1983) introduced an alternative measure of fluid segregation, in which a vessel is considered to have a mixture of macrofluid of υ fraction and microfluid of (1-υ) fraction. A micromixedness ratio, I_υ, can be defined as a simple empirical measure of segregation state,

$$I_\upsilon = \frac{(1-\upsilon)}{\upsilon} \tag{10.3}$$

The value of υ can be determined by reactive or non-reactive tracer systems as described by Villermaux and David (1983).

10.4.1.2 Micromixing Models

Tavare (1986b) provided a clear description of the notation used in developing the micromixing models. According to Danckwerts (1958), a point is defined as an element of a suspension, that is small compared to the volume of the vessel, but large enough to have an average value of intensive properties such as, concentration and population density. Zwietering (1959) defined the age, α, and a residual lifetime, λ, for a point in the system as

$$\alpha + \lambda = 6 \tag{10.4}$$

where θ is the dimensionless residence time for a point. A point enters the system with $\alpha = 0$ and $\lambda = \theta$, and leaves with $\alpha = \theta$ and $\lambda = 0$.

10.4.1.2.1 Completely Segregated Model

The concepts of the degree of segregation and mixing earliness have been utilised to develop models to describe the extreme states of micromixing by Zwietering (1959). In a completely segregated vessel, the mixing between points of different ages takes place only at the vessel outlet where the points have a residual life, $\lambda = 0$. The mixing occurs when $\alpha = \theta$ for all points, but different points will have different values of $\alpha = \theta$. The completely segregated system can be represented schematically by a plug flow reactor with side exits as shown in Figure 10.1,

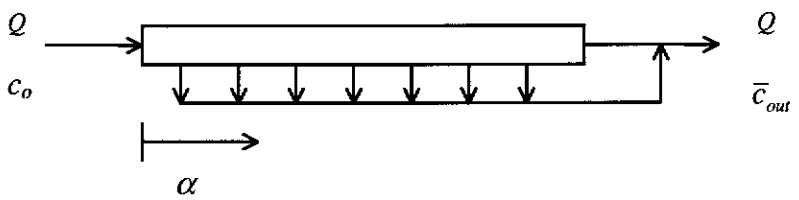

Figure 10.1. A plug flow representation of the completely segregated system (following Zwietering 1959).

where Q is the volumetric flow in and out of the reactor and c_o is the initial concentration. The age α axis is along the longitudinal direction. The side streams represent mixing between points with the same age and same attributes. The mixing between points with different ages is possible only at the vessel outlet, where they merge to form an outlet stream. The average outlet concentration, $\overline{c}_{out}$, is given as

$$\overline{c}_{out} = \int_0^\infty c(\alpha) f(\alpha) d\alpha \qquad (10.5)$$

where $c(\alpha)$ is the concentration in a completely segregated point at time α, which is equal to that in a batch reactor after time α, and $f(\alpha)$ is the residence time distribution function.

10.4.1.2.2 Maximum Mixedness Model

In the maximum mixedness vessel, the mixing between points with different ages takes place immediately once they enter the vessel. When mixing occurs between two points with different ages, one of the points will have $\alpha = 0$ and they have the same residual life. The maximum mixedness system can be represented with a plug flow reactor with side entries shown in Figure 10.2.

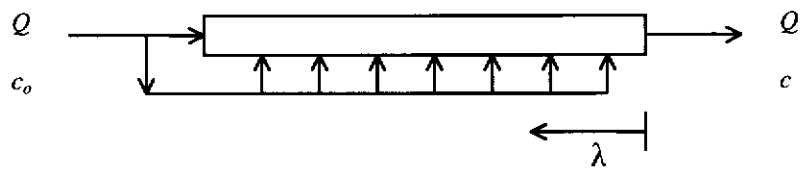

Figure 10.2. A plug flow representation of the maximum mixedness system (following Zwietering 1959).

The side streams represent mixing between points with different ages, but the same residual life. The product concentration, c, can be obtained by solving

$$\frac{dc}{d\lambda} = \frac{f(\lambda)}{1-F(\lambda)}(c - c_o) - R \tag{10.6}$$

where R is the generation term due to reaction, which is a function of concentration only, and

$$F(\lambda) = \int_0^{\lambda} f(\lambda')d\lambda' \tag{10.7}$$

The concentration at the outlet is the value of c for $\lambda = 0$. The appropriate boundary condition is

$$\left.\frac{dc}{d\lambda}\right|_{\lambda \to \infty} = 0 \tag{10.8}$$

10.4.1.2.3 Models for Unpremixed Systems

Models for premixed systems are the aforementioned models, while unpremixed models will be discussed below. Treleaven and Tobgy (1971) have shown that the micromixing effect is different in both cases. Consider two feed streams, each containing a single reactant species fed to the vessel, with a chemical reaction occurring upon mixing between these two reactants. Clearly, if no mixing occurs between the reactants, then no reaction takes place. Two terms are used for the unpremixed feed system, which are known as species mixedness and age mixedness. Two models for unpremixed systems have been proposed (Garside and Tavare 1985). The first of these is for the case of maximum species and age mixedness, where all points with the same residual lifetime mix together as early as possible. The second model is for the case of maximum species but minimum age mixedness, where each point entering at the same time and having the same residual lifetime mix immediately, but does not mix with other points having the same residual lifetime until they exit the vessel. Thus, total age segregation exists within the points. Garside and Tavare (1985) showed that there are only small differences in the conversion between these two unpremixed models, but completely different CSD are obtained. The maximum species and age mixedness model can be represented schematically as shown in Figure 10.3.

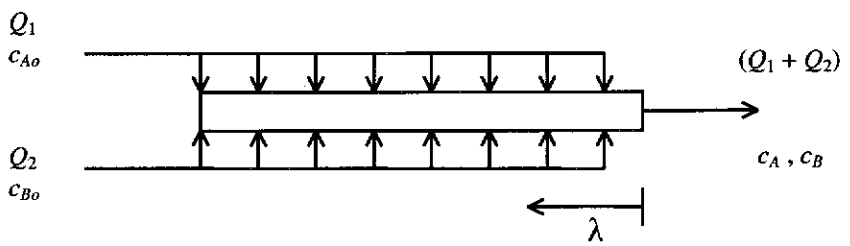

Figure 10.3. A plug flow representation of the maximum species and age mixedness system. (following Treleaven and Tobgy 1971).

Treleaven and Tobgy (1971) showed that the outlet concentration of component i, c_i, is given as

$$\frac{dc_i(\lambda)}{dt} = R_i + \frac{f(\lambda)c_i - f_j(\lambda)\bar{c}_{io}}{1 - F(\lambda)} \qquad (10.9)$$

where i refers to component A or B, and j refers to the inlet stream 1 or 2, and the average initial concentration of component i, $\bar{c}_{io}$, is determined from

$$\bar{c}_{io} = \frac{Q_j}{Q_1 + Q_2} c_{io} \tag{10.10}$$

The appropriate boundary conditions are similar to that in Equation (10.8).

The maximum species and minimum age mixedness model can be represented by the bundle of parallel tubes structure as shown in Figure 10.4. In this structure, the fluid is assumed to flow at constant velocity in small tubes whose length is proportional to the residence time in the vessel.

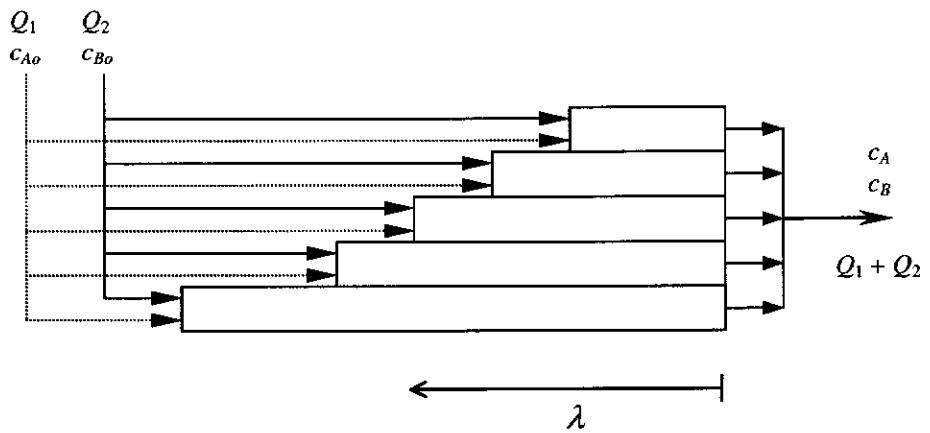

Figure 10.4. The bundle of parallel tubes representation of maximum species and minimum age mixedness system (following Treleaven and Tobgy 1971).

Treleaven and Tobgy (1971) reported that the outlet concentration, c_i, in this case can be expressed as

$$c_i = \int_0^\infty c_{i,batch}(\lambda) f(\lambda) d\lambda \tag{10.11}$$

where $c_{i,batch}$ corresponds to the concentration in a batch reactor with holding time, t.

10.4.1.2.4 Coalescence and Redispersion Model

In the coalescence and redispersion model, fluid clumps are assumed to coalesce randomly at some characteristic frequency, ω. This model assumes coalescence between two clumps is followed by instantaneous homogenisation of concentration, and then redispersion into separate clumps of the same composition (Villermaux 1991). Between interactions, each clump is assumed to behave as a batch vessel. The model is described by an integro-differential equation, derived from the material balance between a concentration interval, c to $c + dc$, of the concentration frequency function, $p(t,c)$, as

$$\frac{\partial p(t,c)}{\partial t} + \frac{\partial (rp(t,c))}{\partial c} = \frac{1}{\tau}\left[p_o(t,c) - p(t,c)\right] + \omega\left[4\int_0^{\infty} p(t,c+\alpha)p(t,c-\alpha)d\alpha - p(t,c)\right] \quad (10.12)$$

where r is the rate of production by chemical reaction per unit volume, τ is mean residence time, $p_o(t,c)$ is the inlet stream frequency function and α is a dummy variable. However, the resulting integro-partial differential equation is difficult to solve.

10.4.1.2.5 Environment Models

Environment models assume that the vessel consists of two or more separate environments (eg. entering and leaving environments) having extreme states of micromixing (i.e. completely segregated and maximum mixedness). The material is transferred from the entering environment to the leaving environment through a transfer function, sometimes referred to as segregation function, $T(\alpha,\lambda)$, which can be a function of age, α, only or both α and residual life, λ.

Several variations of the environment models have been proposed in the literature, which differ in structure, (i.e. plug flow with side entries or exits or bundle of parallel tubes), differ in the environment interaction, (i.e. in series or parallel) or in terms of the transfer rates (Villermaux 1983; 1991).

The vessel may be modelled by considering the entering environment as completely segregated, and transferring it to a "maximum mixedness" leaving environment. Depending on the number of feed streams, various environment models have been proposed, these include the two environment model (Ng and Rippin 1965), the three environment model (Ritchie and Tobgy 1979), and the four environment model (Mehta and Tarbell 1983a; 1983b). Ritchie (1980) extended the coalescence and redispersion model into a form in which it can be applied as an environment model. Tavare (1986b) compiled a list of such models reported in the literature.

The single feed two-environment model proposed by Ng and Rippin (1965) is considered here, other environment models are an extension of this original model. The residence time distribution, $f(t)$, is defined as

$$f(t) = \frac{dF(t)}{dt} \tag{10.13}$$

where $F(t)$ is the volume fraction of the fluid entering the vessel that remains in the vessel between time 0 to t. Conversely, $f(t)dt$ is the volume fraction of material in the outlet stream having an age between t and $t + dt$. Zwietering (1959) showed that the volume fraction of material in the vessel having age between $\alpha + d\alpha$ and residual life of $\lambda + d\lambda$ is given by

$$g(\alpha,\lambda)d\alpha d\lambda = \frac{1}{\tau} f(\alpha+\lambda)d\alpha d\lambda \tag{10.14}$$

where $g(\alpha,\lambda)$ is a frequency function of α and λ.

Ng and Rippin (1965) proposed the rate of transfer of material from the entering environment to the leaving environment is proportional to the amount of material remaining in the entering environment. The rate of transfer of material, m, into the leaving environment is given by

$$-\frac{dm}{dt} = mR_s \tag{10.15}$$

and R_s is the constant transfer coefficient. By solving Equation (10.15) with appropriate initial conditions, gives

$$m = m_o \exp(-R_s t) \tag{10.16}$$

where m_o is the material at $t = 0$. From Equation (10.16), the fraction of material of age α remaining in the entering environment is $\exp(-R_s\alpha)$. Thus, the fraction in the leaving environment will be $1-\exp(-R_s\alpha)$. Ng and Rippin (1965) determined the mean outlet concentration, $\bar{c}$, as

$$\bar{c} = \int_0^\infty [1-\exp(-R_s\alpha)c_L + \exp(-R_s\alpha)c(\alpha)]f(\alpha+\lambda)d\alpha\Big|_{\lambda=0} \tag{10.17}$$

where c_L is the concentration in the leaving environment, and is determined as a function of λ, its value can be obtained by solving the material balance equation in the leaving environment. For further details see Ng and Rippin (1965). It should be mentioned that by setting the values of $R_s = 0$ (no transfer) and $R_s = \infty$ (maximum transfer), the expression of the outlet concentration reduces to that of the completely segregated and maximum mixedness models, respectively.

Mehta and Tarbell (1983a; 1983b) showed that the parameter, R_s, of the three environment model is related to turbulence properties as

$$R_s = \frac{1}{\tau_m} \tag{10.18}$$

where τ_m is the characteristic turbulent mixing time, which may be estimated according to the expression derived by Corrsin(1964) and Rosensweig(1964).

10.4.1.2.6 Interaction by Exchange with the Mean Model

Costa and Trevissoi (1972) and Villermaux and Devillon (1972) suggested that it is the mass transfer between clumps and a fictitious average concentration in the vessel

that accounts for multiple contacts between clumps. The average concentration of the vessel contents is determined by summing the product of the age α and concentration in the clump at any time over all clumps. The basic equation for the change in the concentration in a clump of age α is

$$\frac{dc}{d\alpha} = \frac{\bar{c} - c}{t_m} + R \tag{10.19}$$

where $\bar{c}$ is the average concentration of the environment, t_m is the micromixing time constant and R is the reaction term. If t_m approaches zero, maximum mixedness state is achieved, and as it approaches infinity, the vessel is completely segregated.

10.4.2 Micromixing - Turbulence Theory Approach

The RTD modelling approach described previously uses the Lagrangian viewpoint. In contrast, the classical statistical turbulence theory of mixing takes the Eulerian or fixed frame perspective. Baldyga and Bourne (1986) stated that in the Lagrangian approach, the history of the fluid element is followed, which enables the elementary processes (i.e. deformation and molecular diffusion) responsible for micromixing to be identified, but the spatial distribution in the system is unknown. In the Eulerian approach, on the other hand, the information on the local mixing and age distribution is unavailable due to the averaging procedure.

The turbulent theory based micromixing models discussed in the following sections follow the Lagrangian interpretation. Villermaux (1983) and Baldyga and Bourne (1986) proposed that mixing mechanisms consist of the following three consecutive stages:

(1) spatial distribution of the completely segregated blobs;
(2) reduction of the scale of the completely segregated blobs by deformation; and
(3) mixing by molecular diffusion.

Stage 1 is obviously macromixing, stage 2 is sometimes called turbulent diffusion and stage 3 is molecular diffusion. Hence, a complete mixing model should be able

to describe all the above stages. In developing micromixing models based on turbulence theory, perfect macromixing is usually assumed. Hence, the proposed models describe only the deformation of the completely segregated zone and molecular diffusion.

10.4.2.1 Modelling of the Decay of the Completely Segregated Zone

Villermaux and David (1983) proposed that the deformation of the completely segregated zone is by erosive or laminar mixing, while Baldyga and Bourne (1986) described the deformation process based on the concentration spectral information available in the fluid mechanics literature.

10.4.2.1.1Erosive Mixing

Villermaux and David (1983) derived the "Shrinking Aggregate" model to describe erosive mixing. According to them, mixing consists of peeling off small fragments from the lumps of fluid by turbulent action at their external surface. The peeling off process is characterised by a mass transfer coefficient, h. For a spherical shape, they stated that the erosion rate can be expressed as

$$-\frac{dV_a}{d\alpha} = h\pi \tag{10.20}$$

where V_a is the aggregate volume, α is the aggregate age and π is the aggregate external surface area. They further stated that the rate of shrinking is

$$-\frac{dl}{d\alpha} = 2h \tag{10.21}$$

where l is the diameter of the shrinking aggregate.

According to them a linear decrease of aggregate size with age can be expressed as

$$l = l_o\left(1-\frac{\alpha}{t_e}\right) \tag{10.22}$$

where l_o is the initial size of fluid elements and t_e is the characteristic erosion time constant, given as

$$t_e \equiv l_o \nu^{5/12} D^{-2/3} \varepsilon^{-1/4} \tag{10.23}$$

where ν is the kinematic viscosity, D is the molecular diffusivity and ε is the energy dissipation rate.

10.4.2.1.2 Laminar Mixing

Villermaux and David (1983) suggested that in the absence of turbulent shear, the volume of the aggregates are gradually stretched out and folded up under the action of viscous friction, in a process called laminar stretching. The fluid eventually ends up with a lamellar or striated texture. The thickness of the aggregate decreases with its age. The characteristic time, t_L, for such a process is given as

$$t_L \geq \left(\frac{2\nu}{\varepsilon_v} \right)^{1/2} \tag{10.24}$$

where ε_v is the rate of viscous dissipation per unit mass.

10.4.2.1.3 Concentration Spectral Interpretation

Based on the concentration spectral interpretation, Baldyga and Bourne (1986) proposed that the rate of decrease of the completely segregated fluid volume, V_s, as

$$-\frac{dV_s}{dt} = \frac{V_s}{t_s} \tag{10.25}$$

where t_s is the characteristic time constant. Baldyga and Bourne (1986) reported that the rate of decay of the completely segregated volume in a batch vessel is

$$V_s = V_o \exp(-\frac{t}{t_s}) \tag{10.26}$$

where V_o is the initial volume of fluid considered, and in a well-mixed continuous stirred reactor, the rate of decrease of the completely segregation volume can be expressed as

$$V_s = q_o \tau \left(\frac{1}{1+\tau/t_s} \right) \tag{10.27}$$

where q_o is the volumetric flow from the completely segregated volume to the maximum mixedness zone, and τ is the residence time.

10.4.2.2 Molecular Diffusion

Baldyga and Bourne (1986) reported that when the size of segregated domains is small enough to cause steep concentration gradients, molecular diffusion can take place between clumps of different compositions. This is the only process that results in molecular mixing. The characteristic time for molecular diffusion is expressed as

$$t_D = \frac{l_\infty^2}{D} \tag{10.28}$$

where l_∞ is the average segregated domain size at this stage and D is the molecular diffusivity of the species. In turbulent media, several microscales have been proposed for l_∞, namely, the Kolmogorov microscale, λ_k, the Batchelor microscale, λ_B, and the Corrsin microscale, λ_C, which are defined as

$$l_\infty = \lambda_k = \left(\frac{\nu^3}{\varepsilon} \right)^{1/4}; l_\infty = \lambda_B = \left(\frac{\nu D^2}{\varepsilon} \right)^{1/4}; \text{and } l_\infty = \lambda_C = \left(\frac{D^3}{\varepsilon} \right)^{1/4} \tag{10.29}$$

10.4.2.3 Engulfment-Deformation-Diffusion Model (EDD)

Following the reduction in the size of completely segregated regions by the subdivision of turbulent eddies. Baldyga and Bourne (1986) proposed that three additional mechanisms take place leading to micromixing. The first of these is the engulfment of fluid from the bulk into vortices. The vortices are generated by the stretching of fluid particles. Secondly, deformation of the "engulfed fluid" by further

stretching, produces bursts of vorticity in series at progressively smaller scales, and gives a "sandwich" of heterogeneous material. Finally, molecular diffusion takes place when the striated structures resulting from the deformation process are sufficiently thin (i.e. in the order of Kolmogorov microscale). Baldyga and Bourne (1986) called this model as the EDD model, which requires the solution of coupled, non-linear parabolic partial differential equations

$$\frac{\partial c_i}{\partial t} + u(t,x)\frac{\partial c_i}{\partial x} = D_i \frac{\partial^2 c_i}{\partial x^2} + R_i(t,x) \tag{10.30}$$

where c_i is the concentration of component i, t is time, u is the shrinkage velocity, x is the Cartesian coordinate, D is the diffusivity coefficient, and R is the specific reaction rate. This equation describes the unsteady diffusion and reaction within a deforming vortex. Complete micromixing requires several vortex generations (eg. N times), and hence, it is necessary to solve the equations N times.

Baldyga and Bourne (1989a; 1989b) found that in the case of a Schmidt number, Sc, much less than 4000, the engulfment is the rate-determining step in micromixing. They simplified the EDD model and the micromixing calculations. They considered the growth of spots of substance "i" as

$$\frac{dV_i}{dt} = EV_i \tag{10.31}$$

where V_i is the volume of i rich region, and E is the engulfment rate which is given as

$$E \approx 0.058\left(\frac{\varepsilon}{\nu}\right)^{1/2} \tag{10.32}$$

Baldyga and Bourne (1989a) further stated that in mixing two reactants, the engulfment of the same fluid elements are ineffective for mixing, thus, Equation (10.31) can be extended to give,

$$\frac{dV_i}{dt} = EV_i(1 - X_i) \tag{10.33}$$

where X_i is the volume fraction of i rich region. The concentration of substance i in this zone changes according to

$$\frac{dc_i}{dt} = E(1 - X_i)\left[\langle c_i \rangle - c_i\right] + R - Q \tag{10.34}$$

where $\langle c_i \rangle$ is the concentration of reagent i in environment, R and Q are the rate of generation and consumption of component i.

10.4.2.4 Shrinkage Slab Model

Li, Chen & Chen (1996) showed physical pictures of micromixing and macromixing taken by high-speed microphotography. Instead of a lamellar structure proposed by Ottino, Ranz & Macosko (1979) or the marble-like structure of Baldyga and Bourne (1986) generated from eddy engulfment, the fluid exhibits slice-like laminae (2-D) and stripe-like strands (1-D) during turbulent mixing with $Sc >> 1$. They proposed the shrinkage slab model for micromixing,

$$\frac{\partial c_i}{\partial t} = sx\frac{\partial c_i}{\partial x} + D\frac{\partial^2 c_i}{\partial x^2} \tag{10.35}$$

with

$$c_i(x,0) = \begin{cases} 1 & |x| < \lambda_k / 2 \\ 0 & |x| \geq \lambda_k / 2 \end{cases} \tag{10.36}$$

where s is the shrinkage strain rate, D is the molecular diffusivity and x is the spatial coordinate.

10.5 INTERACTION BETWEEN MACROMIXING AND MICROMIXING

A number of models that account for mixing at various scales have been proposed recently (Bourne and Dell'ava 1987; David and Villermaux 1987; Ranade and

Bourne 1991; Thoma, Ranade & Bourne 1991; Ranade 1992, Bakker and van den Akker 1994; Chen, Zheng & Chen 1996; Li and Chen 1996; Phillips, Rohani & Baldyga 1999).

Baldyga (1989) stated the importance of both macromixing and micromixing on the selectivity, and proposed a model to incorporate interaction between macro- and micromixing. Baldyga and Bourne (1992) and Baldyga (1993) defined the term mesomixing to describe the disintegration of large eddies and interaction of the plume of fresh feed with its surroundings, i.e. turbulent dispersion of the plume. The scale of mesomixing is coarse relative to microscale, but fine relative to the scale of the vessel. The mesomixing concept is introduced to account for mixing in the region near the feed inlet; if mesomixing is slower than micromixing, then the reaction becomes localised.

Baldyga, Podgorska & Pohorecki (1995) and Baldyga, Bourne & Hearn (1997) considered the interaction between macro, meso and micromixing in precipitation systems. They derived the following equations to describe such processes,

$$\frac{dX_i}{dt} = E(\varepsilon)X_i(t')[1 - X_i(t')] \tag{10.37}$$

$$\frac{dc_{ij}(t',t)}{dt'} = E(\varepsilon)[1 - X_i(t')]\left[\left\langle c_{ij}(t',t)\right\rangle - c_{ij}(t',t)\right] - \frac{\rho_s G}{2M_T} A_T \tag{10.38}$$

$$\frac{\partial n_j(L,t',t)}{\partial t'} + G\frac{\partial n_j(L,t',t)}{\partial L} = E(\varepsilon)\left[\left\langle n_j(L,t',t)\right\rangle - n_j(L,t',t)\right] \tag{10.39}$$

Equation (10.37) describes the micromixing in the plume of the mixing zone, equations (10.38) and (10.39) describe the change of concentration and crystal size distribution in the plume of the mixing zone. The term c_{ij} is the concentration of species "i" in the species "j" rich zone, t is the operation time, t' is the time of travel from the feed point. ρ_s is the crystal density, A_T and M_T are the total crystal surface area and mass, respectively. Mesomixing affects the environment concentrations,

$\langle c_{ij} \rangle$, and volume fraction, X_i, whereas macromixing convects material through zones of different energy dissipation, ε, changing local values of engulfment parameter $E(\varepsilon)$.

10.6 COMPARTMENTAL MODELS

The compartmental models have been utilised to account for mixing effects in the modelling of flocculation systems (Koh 1984; Koh, Andrews & Uhlherr 1984; 1987), precipitation systems (Bohlin and Rasmuson 1996; Bermingham, Kramer & van Rosmalen 1998), and suspension polymerisation system (Vivaldolima et al. 1998). The essence of the compartmental model is to divide the vessel volume into a number of compartments. The sizes of the compartments depend on the vessel geometry and operating conditions. Bermingham, Kramer & van Rosmalen (1998) stated that the compartmentals must be chosen such that

(1) they represent the overall flow pattern within the precipitator;
(2) there is negligible local energy dissipation gradient in each compartment;
(3) there is negligible supersaturation gradient in each compartment; and
(4) uniform distribution of the solids suspension in each compartment.

If particle segregation or a non-uniform distribution of the solids phase exists, then a classification function needs to be determined. They also stated that the homogeneity of energy dissipation, supersaturation and solids suspension in the vessel is determined by the precipitator geometry, material properties, operating conditions and precipitation kinetics. Hence, the compartmental model is not universal, and requires reformulating if there is deviation from above conditions. Bermingham, Kramer & van Rosmalen (1998) further emphasised that the gradients in the supersaturation are negligible if the residence time within a compartment is short compared to the time required to deplete the supersaturation by growth and nucleation. As a general rule, the residence time should be at least one order of magnitude lower than the half-life for supersaturation depletion. This type of model

10.7 NETWORK-OF-ZONES MODEL

The network-of-zones model has been developed to simulate single liquid phase systems (Kynsh and Mann 1984; Wang and Mann 1992), precipitation systems (Mann 1993; Wei, Garside & Mann 1996), gas-liquid systems (Mann 1986), and solid-liquid systems (Brucato and Rizzuti 1988). The basic zone or cell in this model is assumed to have perfect micromixing, a direct through flow of fluid and lateral equal and opposite exchange flows between cells adjacent to each other. This is shown in Figure 10.5. The cell (i,j) has a through flow of q and exchange flow of βq, and β is the fractional flow factor. The network is constructed of nested flow loops around foci of circulation above and below the impeller, each flow loop introduces an element of circulatory mixing. See Knysh and Mann (1984) for further network construction details.

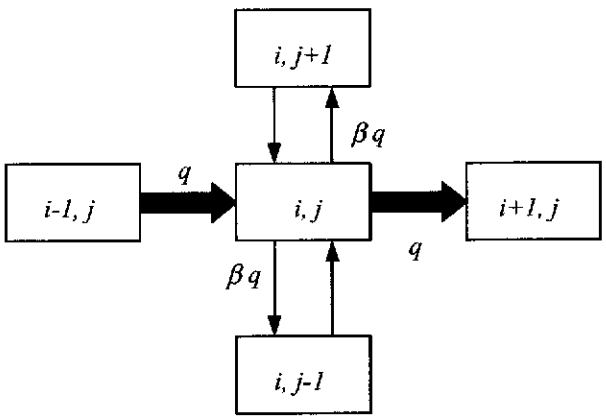

Figure 10.5. A schematic representation of the network-of-zones model; illustration of the main and turbulent diffusive flows between adjacent cells (following Knysh and Mann 1984).

The unsteady material balance in the cell (i,j) is expressed as

$$\frac{dc_{i,j}}{dt} = \frac{q}{V_{i,j}}\left[c_{i-1,j} + \beta(c_{i,j-1} + c_{i,j+1}) - (1+2\beta)c_{i,j}\right] \qquad (10.40)$$

where c is the concentration of the reactant species, V is the cell volume, q is evaluated from $q = Q/N$, where Q is the total internal flow rate generated by the impeller and N is an even number for a $2(N \times N)$ network configuration. The network-of-zones model has the advantages of being simple, and only requires moderate computing effort compared to computational fluid dynamics model. Mann, Ying & Edwards (1994) and Dudczak (1994) further derived a three-dimensional network-of-zones model. The weakness of this approach is that it oversimplifies fluid mechanics, although a good approximation of the overall convective flow is imposed on the mixing process.

10.8 COMPUTATIONAL FLUID DYNAMICS

Computational fluid dynamics (CFD) is a powerful technique, which enables a complete flow pattern to be visualised (Perron and Larocque 1994; Al-Rashed et al. 1996; Ranade 1997; Wei and Garside 1997; Kuipers and van Swaaij 1998; Derksen and van den Akker 1999; Sahu et al. 1999). The use of empirical micromixing or macromixing models described previously do not reflect details of the actual flow patterns within the vessel, whereas, CFD allows complex flow situations to be modelled with reasonable detail and accuracy. In general, the vessel is divided into a large number of cells, and the partial differential equations describing turbulent fluid flow need to be solved for each cell. In turbulent mixing modelling, the basic Navier Stokes relations for incompressible fluid flow in the i^{th} direction are:

Momentum balance:

$$\frac{\partial u_i}{\partial t} = -u_j \frac{\partial u_i}{\partial x_j} - \frac{1}{\rho_L}\frac{\partial p}{\partial x_i} + \nu \frac{\partial^2 u_i}{\partial x_j^2} + g_i \qquad (10.41)$$

Continuity (overall mass balance):

$$\frac{\partial u_i}{\partial x_i} = 0 \qquad (10.42)$$

The terms on the right hand side of Equation (10.41) describe the rate of change in the momentum due to convective transport, pressure, p, viscous and gravitational, g, forces, respectively. u_i and x_i are the velocity and spatial coordinate in the i^{th} direction, respectively. ν is the kinematic viscosity and ρ_L is the liquid density. For further details see Bird, Stewart & Lightfoot (1960).

These equations can be solved by different techniques, either by direct numerical simulation, i.e. solving the equations without approximations, Reynolds-Averaged Navier Stokes (RANS) technique, or Large eddies simulation (Eggels 1996). However, to date it is still not possible to solve these equations by direct numerical simulation, due to the high computer capacity needed for solving these equations in such a huge number of cells (Kuipers and van Swaaij 1998).

The most widely employed technique to solve the Navier Stokes equations is the RANS method. In this technique, the velocity components, pressure, and scalars, ϕ, are decomposed into the mean and fluctuating components. van Leeuwen (1998) showed that the Reynolds-averaged equation for the momentum balance in Equation (10.41) is

$$\frac{\partial \overline{u}_i}{\partial t} = -\overline{u}_j \frac{\partial \overline{u}_i}{\partial x_j} - \frac{\partial \left(\overline{u_i' u_j'}\right)}{\partial x_j} - \frac{1}{\rho_L}\frac{\partial \overline{p}}{\partial x_i} + \nu \frac{\partial^2 \overline{u}_i}{\partial x_j^2} \qquad (10.43)$$

where the over-bar denotes mean term and the superscript " ′ " denotes fluctuation term. The equation now contains an unclosed term, i.e. the term $\overline{u_i' u_j'}$, and is referred to as the Reynold stresses. In order to solve this set of partial differential equations describing the process, additional information is necessary. This is called the closure problem. The main research in turbulence modelling has been directed at finding appropriate closures for these Reynold stresses. The most widely used model employed to solve the RANS equations is the k-ε model (Wei and Garside 1997; Kuipers and van Swaaij 1998; van Leeuwen 1998).

van Leeuwen (1998) reported that for systems with chemical reactions, the closure approximation for the reaction term is even more complex. He showed that the Reynolds-averaged equation for a scalar, i.e. concentration of chemical species is

$$\frac{\partial \overline{\phi}}{\partial t} = -\overline{u}_j \frac{\partial \overline{\phi}}{\partial x_j} - \frac{\partial \left(\overline{u_j' \phi'}\right)}{\partial x_j} + D \frac{\partial^2 \phi}{\partial x_j^2} + \overline{R} \tag{10.44}$$

Equation (10.44) contains two unclosed terms, $\overline{u_j' \phi'}$ and $\overline{R}$. The first represents the turbulent transport of the scalar, and is generally closed by

$$\overline{u_j' \phi'} = -\frac{\nu_t}{Sc_t} \frac{\partial \overline{\phi}}{\partial x_j} \tag{10.45}$$

where ν_t is the turbulent kinematic viscosity and Sc_t is the turbulent Schmidt number of the chemical species. The difficulty is to close the reaction term, $\overline{R}$. There are many concepts of closure described in the literature for closing the reaction term (Patterson 1981; Dutta and Tarbell 1989; Fox 1992; Baldyga 1994; Baldyga and Henczka 1995; Baldyga and Orciuch 1997). The most important concepts are the moment closure and the probability density function for concentration. The simplest moment closure procedure is to neglect the influence of fluctuations in the concentration and reaction rate (Brodkey 1981; van Leeuwen 1998), i.e. $\overline{R} = R(\phi)$.

10.9 CFD MODELLING OF THE PRECIPITATION SYSTEM

In modelling precipitation systems, the PBEs and the Navier Stokes equations need to be solved. The PBEs can be solved either using the DPB model or using the moment equations. As noted by Seckler, Bruinsma & van Rosmalen (1995), the first approach is almost computationally impossible, because of the extremely high computer capacity required to solve the equations describing turbulent mixing. The second approach is less computationally demanding, but provides less information on the CSD.

Seckler, Bruinsma & van Rosmalen (1995) and van Leeuwen (1998) used this latter approach with CFD to model precipitation processes. They assumed that the crystals follow the streamlines of the flow field, and only nucleation and growth take place during the precipitation process. The nucleation and growth kinetics were calculated as a function of supersaturation, which was determined from the local concentration of the species. The k-ε model was used to solve the RANS equations.

The microscopic moment equations are given by

$$\nabla u_i \mu_j = 0^j . B + jG\mu_{j-1} \tag{10.46}$$

van Leeuwen (1998) showed that the time-averaged form of Equation (10.46) is

$$\frac{\partial(\overline{u}_i \overline{\mu}_j)}{\partial t} = \frac{\partial(-\overline{u_i' \mu_j'})}{\partial x_j} + D\frac{\partial^2 \overline{\mu}_j}{\partial x_i^2} + j\overline{\mu}_{j-1}\overline{G} + 0^j \overline{B} + j\overline{\mu_{j-1}' G'} + 0^j \overline{B'} \tag{10.47}$$

The term on the left hand side of Equation (10.47) represents the convective transport. The first term on the right hand side refers to the turbulent transport of the moments, the second is the turbulent diffusion term, and the third and fourth terms are the precipitation terms, containing growth and nucleation rates, respectively. The last two terms represent the production of the moment, μ_j, due to turbulence, and are generally neglected as a first approximation. Seckler, Bruinsma & van Rosmalen (1995) reported that the unknown term, $\overline{u_j' \mu_j'}$, can be taken as

$$-\overline{u_i' \mu_j'} = \frac{\mu_t}{Sc}\frac{\partial \overline{\mu}_j}{\partial x_i} \tag{10.48}$$

where μ_t is the turbulent viscosity.

10.10 CONCLUSIONS

The mixing models reported in the literature have been reviewed. The mixing process is characterised by both macromixing and micromixing. Most mixing models developed are generally based on the RTD concept and fluid turbulence theory, others include compartmental, network-of-zones and CFD models. There is however no unique approach for modelling mixing in precipitation system. As a rule of thumb, a simplistic approach should always be given a first priority. CFD has emerged as an attractive approach for modelling mixing in precipitation. In CFD modelling, a set of equations describing fluid flow and the PBEs are required to solve together. To date it is still not feasible to solve these equations simultaneously, due to the intensive computation power requirements.

CHAPTER 11

THE INFLUENCE OF INHOMOGENEOUSLY-MIXED SUSPENSION ON BATCH GIBBSITE PRECIPITATION

11.1 INTRODUCTION

Precipitation processes involve a suspension of solid particles in stirred vessels. Most precipitator hydrodynamics research reported in the literature has focussed on the influence of fluid mixing processes such as, micromixing and macromixing, on precipitation. There are enormous efforts devoted to modelling mixing in precipitation processes via either the Eulerian or Lagrangian approaches or combinations of both, as reviewed in Chapter 10. However, these are generally for reactive precipitation systems and systems where growth and nucleation are occurring. Recent advances in computer technology has enabled the use of CFD techniques to simulate detailed fluid hydrodynamics in a stirred vessel, but their applicability to the precipitation processes is limited to treating the suspension as fluid phase medium (Seckler, Bruinsma & van Rosmalen 1995; van Leeuwen, Bruinsma & van Rosmalen 1996; Wei and Garside 1997).

The homogeneity of the fluid phase affects supersaturation distribution and micro-level processes such as, chemical reactions and precipitation mechanisms, and hence, precipitation product quality. However, there is an increasing awareness that not only fluid phase mixing, but also solid phase mixing may have an important role in suspension precipitation processes, particularly when crystal agglomeration taking place. The state of solids suspension (i.e. segregation of solids and internal classification) may have a significant influence on the precipitation product (Sha and Palosaari 1998; Bermingham et al. 1999). Wynn, Hounslow & Ilievski (1998)

performed a simulation study of mixing effects on gibbsite precipitation, and found that segregation of solids has significant and different effects to that of a segregated fluid in aggregated system. Attempts also have been made recently to simulate classification functions in inhomogeneously-mixed suspension crystallisation with CFD (Sha et al. 1999).

This work is aimed at investigating the influence of an inhomogeneously-mixed suspension (i.e. poor solids phase mixing) on gibbsite precipitation and kinetics estimations An inhomogeneously-mixed vessel will be used to perform batch gibbsite precipitation experiments. These data will be compared to experimental data from the well-mixed precipitation experiments performed under the same operating conditions as described in Chapter 7.

11.2 EXPERIMENTAL PRECIPITATION SYSTEM

11.2.1 Laboratory Precipitator Configuration

A schematic of the laboratory precipitator used in this study is shown in Figure 11.1. A round bottom stainless steel vessel with inside diameter, T, of 134 mm, was fitted with 4 baffles at 90° of width, W, of $0.1T$. The baffles were placed symmetrically around the vessel periphery. A Lightnin A310 axial impeller of diameter, D, of 64 mm, was employed and placed in the axial position with an off bottom clearance, C, of 85 mm. The liquid depth, H, is $2.19T$. A water jacket was built around the vessel to maintain the temperature inside the vessel. The precipitator has a 5-litre capacity, but the nominated working volume was 4 litres.

11.2.2 Hydrodynamics in the Stirred Vessel

The hydrodynamic conditions for the vessel geometry considered was studied visually using a glass vessel. The glass vessel was built to the same dimensions as the stainless steel vessel. Water at 27 °C was used as the test fluid in place of the synthetic liquor at 80 °C, as both have similar kinematic viscosity, $\nu = 0.86$ m^2 s^{-1}. The flow characteristic in the stirred vessel is a function of the vessel configuration, fluid properties, impeller type, impeller position, and impeller power input.

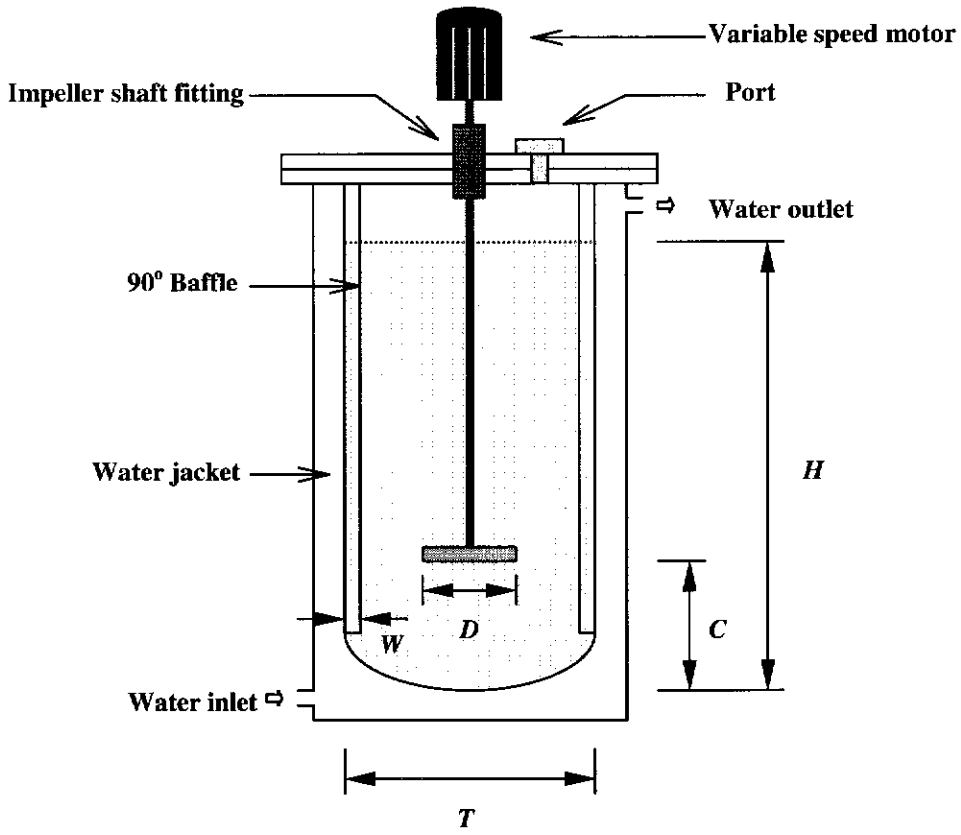

Figure 11.1. A schematic of the laboratory precipitator used in the poorly-mixed suspension batch precipitation experiments, where $C/H = 0.29$; $D/T = 0.48$; $H/T = 2.19$ and $W/T = 0.10$.

A number of dimensionless parameters such as, the Power number, the Reynolds number, and the impeller pumping number are used to characterise the mixing flow in the stirred vessel. The Power number, N_P, is defined as

$$N_P = \frac{P}{\rho_L N^3 D^5} \tag{11.1}$$

which is a function of the impeller power input, P, fluid density, ρ_L, impeller speed, N, and impeller diameter, D. The power input can be determined from

$$P = T\omega \tag{11.2}$$

where T is the torque exerted by the impeller and ω is the angular impeller speed.

The flow regime in a mixing vessel is characterised by the Reynolds number, N_{RE}, and is expressed as

$$N_{RE} = \frac{\rho_L N D^2}{\mu_L} \tag{11.3}$$

where μ_L is the fluid viscosity. The impeller pumping number, N_Q, used to quantify the flow in a mixing vessel is defined as

$$N_Q = \frac{Q}{ND^3} \tag{11.4}$$

N_Q is not only a function of impeller speed, diameter and flow through the impeller, Q, but it is also strongly dependent on the flow regime.

11.2.2.1 Flow Characteristics in the Stirred Vessel

The 64 mm Lightnin A310 impeller used in this experimental study was driven by the Heidolph RZR2101 overhead stirrer. This overhead stirrer provides the stirrer speed and torque readings to an accuracy of ± 3% and ± 5%, respectively. The Power number-Reynolds number curves for both baffled and unbaffled vessels are shown in Figure 11.2.

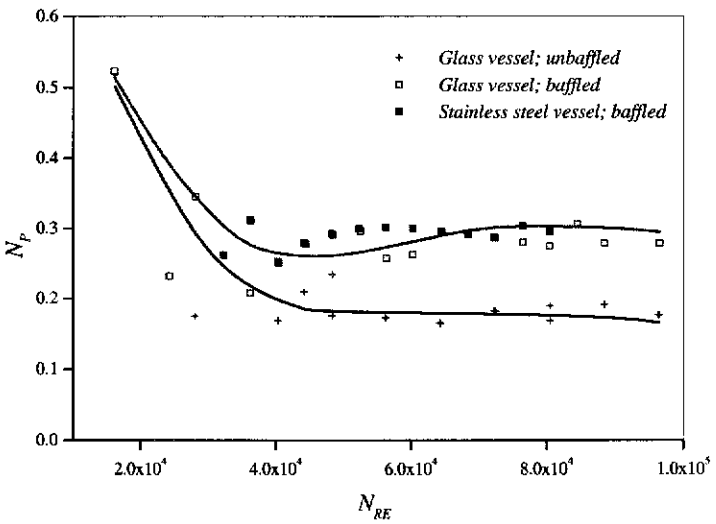

Figure 11.2. The Power number-Reynolds number curves for baffled and unbaffled vessels operated with a 64 mm Lightnin A310 impeller.

The Power number, N_P, is lower in the unbaffled vessel than the baffled vessel, due to the fluid motion being free from the resistance exerted by the baffles, and hence, less power is dissipated moving the fluid around. At low Reynolds number, N_{RE}, a higher Power number is obtained, as high power input is required to initiate and generate fluid motion in the vessel. However, at N_{RE} greater than 4×10^4, N_P remains constant at approximately 0.3 and 0.2, respectively, for baffled and unbaffled vessels, and is independent of the N_{RE}. This result is in agreement with those reported in the literature (Nagata 1975; Oldshue 1983; Shiue and Wong 1984; Sano and Usui 1987). The baffled glass and stainless steel vessels have similar N_P, over the same N_{RE} range. The impeller pumping number for the A310 impeller is assumed to be 0.56 as reported in the literature (Wu et al. 1998).

11.2.2.2 Determination of the Just Suspended Speed

Gibbsite crystals (with mean size of 38 μm) taken from a 2.5-hour run in a well-mixed batch precipitation experiment were suspended in 4 litres of water at 27 °C. The well-mixed precipitation experiment was conducted under the same operating conditions as the precipitation experiment in this study (see section 11.2.3). The solids concentration was 0.06 g solids/ g water.

The just suspended speed, N_{JS}, required to fully suspend the dilute suspension in the glass vessel was found to be 786 ± 5 rpm. It was determined from visual observation of the particle motion on the vessel bottom, using the 1-2 second criterion stated by Zwietering (1958). At the N_{JS} condition, the crystals remain in suspension, but they do not distribute uniformly in the vessel due to the large liquid level to vessel diameter ratio, H/T of 2.19.

Figure 11.3 shows the state of solids suspension achieved at N_{JS}. There are two distinct zones observed in the vessel, a clear liquid zone near the top of the liquid level, and a suspension zone at the bottom of the vessel. Between the two zones, an interface cloud exists. This hydrodynamic condition was used in the poorly-mixed gibbsite precipitation experiments conducted in this experimental work.

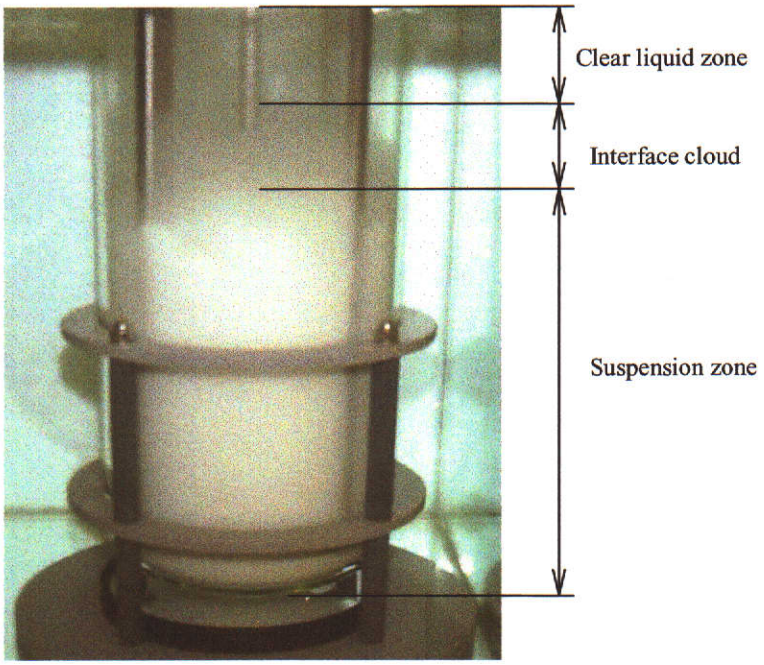

Figure 11.3. Suspension hydrodynamic conditions generated in suspending a solids concentration of 0.06 g solids/ g water in the glass vessel with $H/T = 2.19$, operated at $N_{JS} = 786$ rpm.

11.2.2.3 Axial Solids Concentration

Attempts were made in this study to determine the solids concentration distribution in the vessel operated at N_{JS}. 10 mL slurry samples were taken from various depths in the suspension using a micropipette in the upright position. A plot of the axial solids distribution is shown in Figure 11.4. H' is the normalised height from the bottom of the vessel, and $H' = 1$ refers to the top of the liquid level. The dotted line represents uniform suspension (in the case of well-mixed suspension), where the axial solids concentration is constant. The numbers on the plot indicate roughly the particulate sampling positions employed. However, the solids distribution shown in this figure does not necessarily represent the true solids concentration in the vessel, as the solids may not uniformly suspended radially, and due to the difficulties in obtaining representative samples in this slurry suspension. Nevertheless, it resembles those results reported in the literature, determined using the "wall sampling" withdrawal technique (Einenkel 1980; Barresi and Baldi 1987; MacTaggart, Nasr-el-din & Masliyah 1993; Kuzmanić and Rušić 1999) and from Laser transmitter measurements (Ayazi Shamlou and Koutsakos 1989).

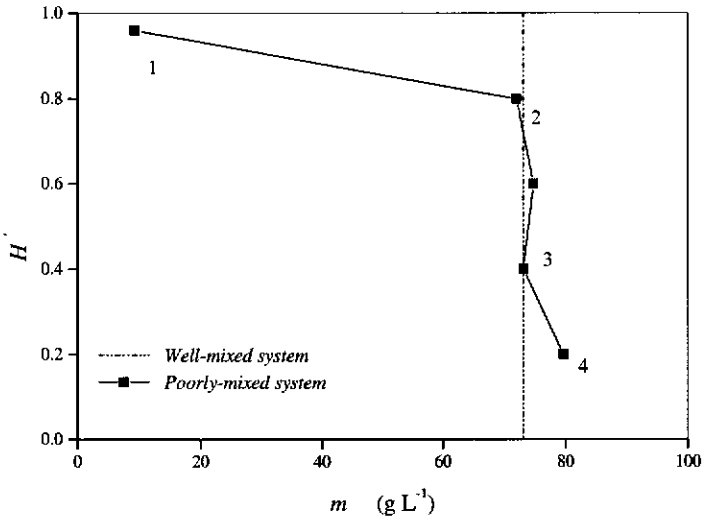

Figure 11.4. Axial solids concentration profile determined using a micropipette sampling technique. 1: clear liquid zone; 2: cloud interface; 3: suspension zone above the impeller; and 4: suspension zone below the impeller.

11.2.3 Poorly-Mixed Batch Gibbsite Precipitation Experiments

Batch gibbsite precipitation experiments were performed isothermally at 80 °C and agitated at 786 rpm. An initial aluminate concentration of 138 ± 1.0 g $L^{-1}Al_2O_3$ and a seed charge of 14.81 ± 0.1 g L^{-1} were used. At this operating temperature, negligible nucleation was expected, and only crystal agglomeration and molecular crystal growth took place.

The precipitation system is well-mixed in liquor phase. Samples were taken for determination of liquor composition. The liquor composition was analysed by the titration method described in Chapter 7. The precipitator's contents were collected at the end of each run, in a plastic container, sodium gluconate was added to halt further precipitation, then the solids were filtered. Solid samples were collected and dried in an oven at 60 °C. The dried samples were weighed and suspended in 4 litres of water. Particulate samples were then taken to determine CSD using Coulter counter multisizer. A check of the mass consistency between the suspended solids and sampled solids was also performed, which was found to be within 4-5 %.

11.3 EXPERIMENTAL PRECIPITATION DATA

Precipitation experiments were conducted for 25, 35, 45, 55, 75, 90 and 120 minutes. Repeats were also performed for the 35, 55 and 75-minute runs, to check the reproducibility of the experimental data. These experiments were performed under the same liquor composition, temperature, seed charge, working volume and mean shear rate (at 459 s^{-1}), as the well-mixed experiments performed in Chapter 7. It should be emphasised that the difference between the two experimental systems are solids phase mixing due to different mixing flows and energy dissipation distributions in the stirred vessels, resulting from differences in the vessel geometry, impeller geometry and agitation rate.

11.3.1 Liquor Composition

Comparison of the aluminate concentration as a function of time in Figure 11.5 shows good agreement between the well-mixed and poorly-mixed experiments. The aluminate concentrations, *A*, from the poorly-mixed experiments are within the 95% confidence limits of those from the well-mixed experiments. This indicates that the desupersaturation rate is similar in both experimental systems.

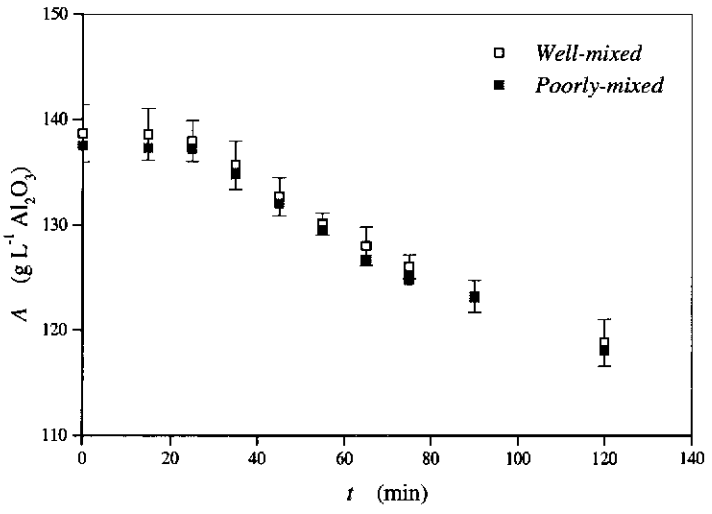

Figure 11.5. Desupersaturation curves for the well-mixed and poorly-mixed batch gibbsite precipitation experiments.

11.3.2 Total Mass Content

The total mass content, m, in this experimental study was determined from solids content, Coulter counter data using Equation (7.1) and titration data using Equation (7.2). The comparison of m determined from the titration data between the well-mixed and poorly-mixed experiments in Figure 11.6(a) shows excellent agreement. This confirms the desupersaturation results in Figure 11.5, as expected from data that is mass balance consistent (Note that crystal agglomeration does not contribute to the total mass content). Figure 11.6(b) shows that good agreement is obtained in m determined from the three techniques for the poorly-mixed experiments.

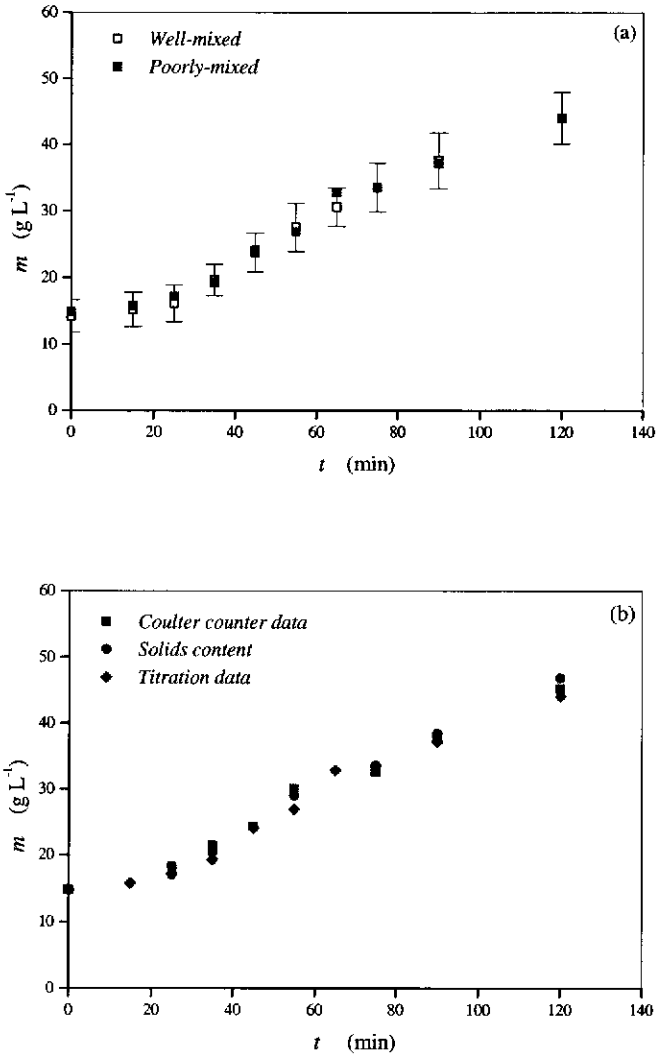

Figure 11.6. Comparisons of the total mass content, m, (a) well-mixed and poorly-mixed experiments determined from the titration data, and (b) poorly-mixed experiments determined from Coulter counter data, solids content and titration data.

11.3.3 Scale Formation

Under the operating conditions considered here, scale formed in the poorly-mixed experiments around the vessel periphery near the top of the liquid level, where the fluid flow is relatively stagnant. Figure 11.7 shows the scale formed after 25 minutes and 35 minutes precipitation runs.

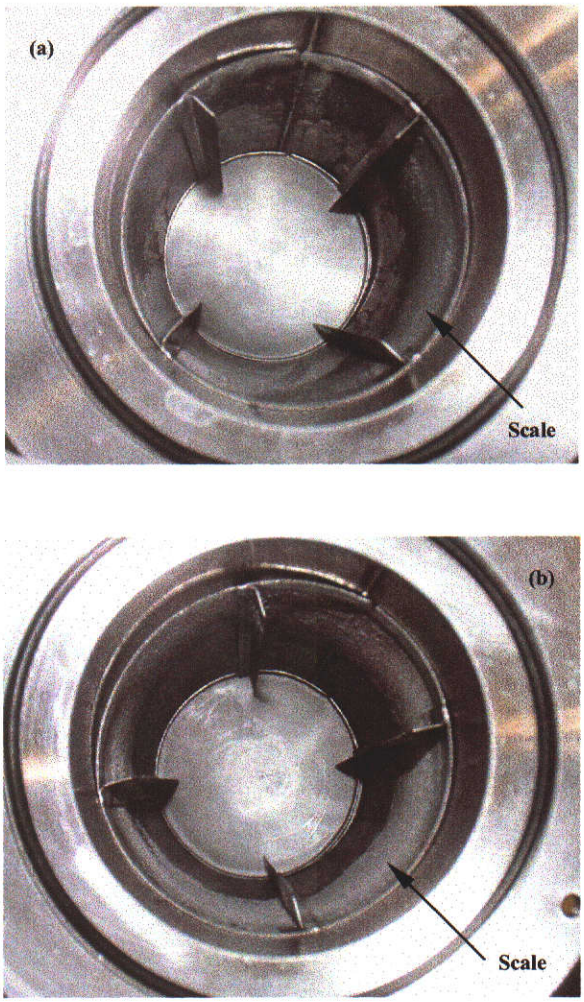

Figure 11.7. Scale formed around the vessel periphery near the top of liquid level after (a) 25 minutes and (b) 35 minutes, batch gibbsite precipitation runs.

Figure 11.8 shows that the scale mass built up rapidly with time after the induction period (approximately 30 minutes) and then slowed down as precipitation run proceeded. The scale mass increases from 2.0 % of the total product mass at 25 minutes to 8.0 % at later times (between 75 to 120 minutes).

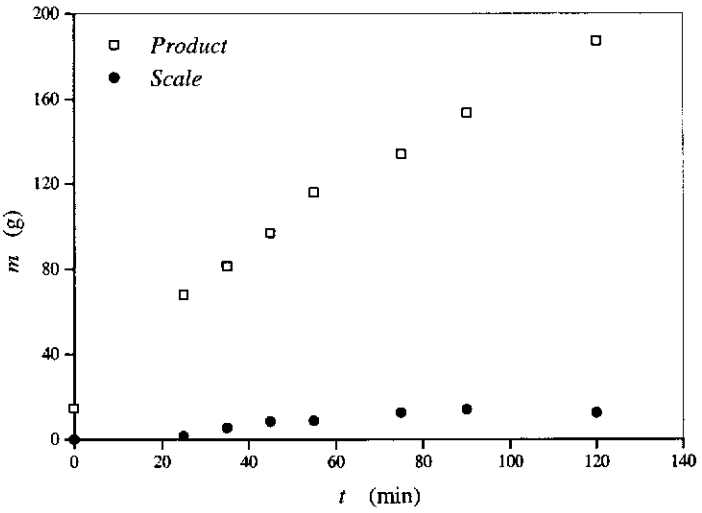

Figure 11.8. Transient total product mass and scale mass obtained in the poorly-mixed batch gibbsite precipitation experiments.

11.3.4 Product Crystal Morphology

The precipitated product samples were analysed using the SEM. Comparison of the SEM images of the product gibbsite for the well-mixed and poorly-mixed experiments after 35 and 90 minutes precipitation runs are given in figures 11.9 and 11.10, respectively. There is no apparent difference in the morphology of the product crystal precipitated under both hydrodynamic conditions.

11.3.5 Crystal Size Distribution

Figure 11.11 shows that reproducible CSD data were obtained from the repeated experiments of the 35, 55 and 75-minute precipitation runs. Comparisons of the transient CSD between the poorly-mixed and the well-mixed experiments in Figure 11.12 show that the poorly-mixed experiments resulted in more fine crystals than the well-mixed experiments. It is interesting to note that the deviations in the CSD between the two experimental systems are reduced as precipitation time increases, but it remains evident that there are more fine crystals in the poorly-mixed experiments. This is likely due to that most fines in the well-mixed experiments have agglomerated during the early stage of the precipitation run, and significantly less fines are available for the agglomeration process at the later stages of the precipitation run, compared to those in the poorly-mixed experiments.

(a)

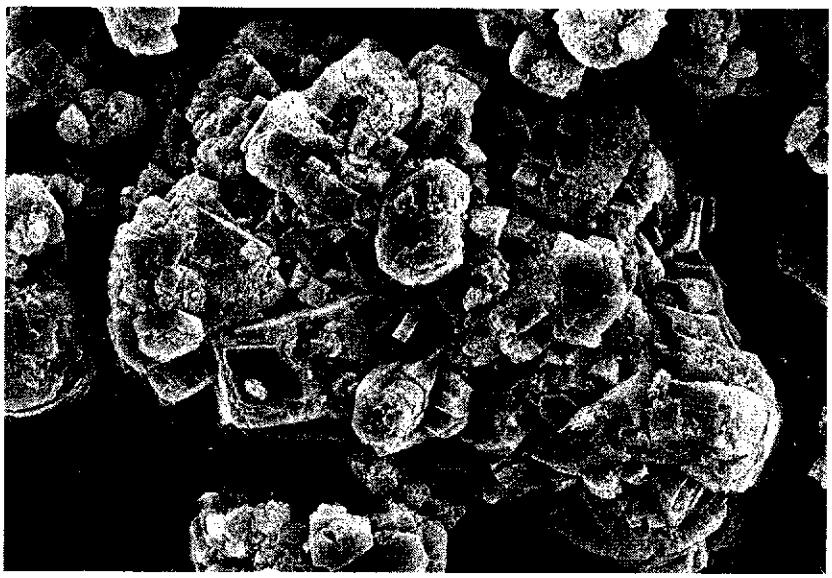

(b)

Figure 11.9. SEM images of gibbsite crystals produced after 35 minutes precipitation run under (a) the well-mixed batch precipitation conditions employed in Chapter 7, and (b) the poorly-mixed batch precipitation conditions employed here.

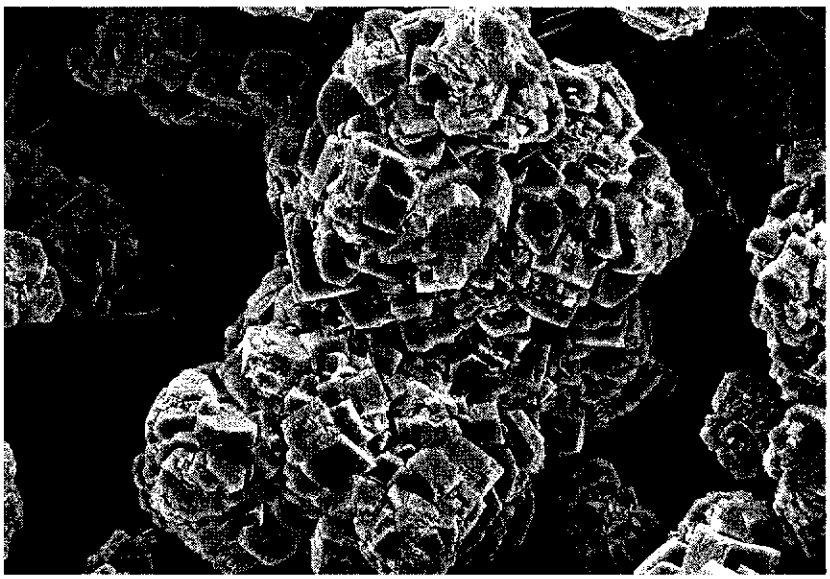

(a)

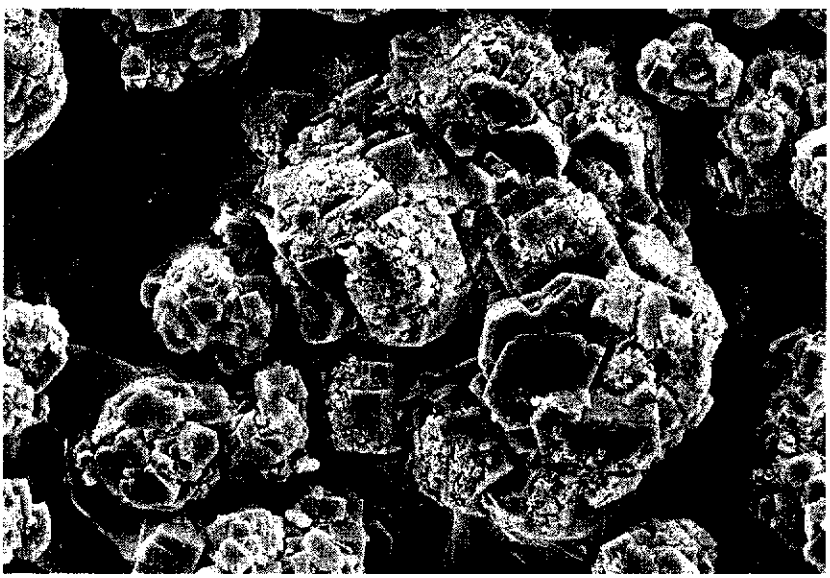

(b)

Figure 11.10. SEM images of the gibbsite crystals produced after 90 minutes precipitation run under (a) the well-mixed batch precipitation conditions employed in Chapter 7, and (b) the poorly-mixed batch precipitation conditions employed here.

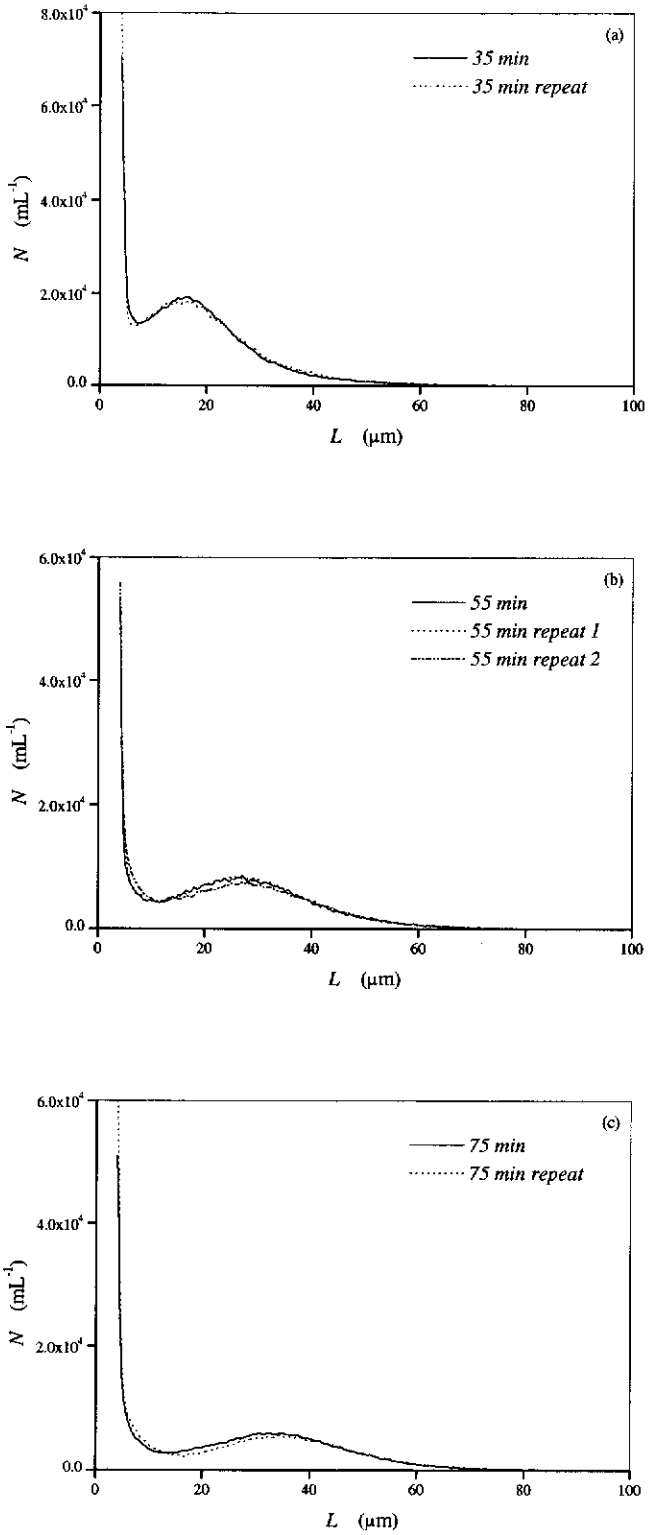

Figure 11.11. Comparisons between the CSDs from repeated poorly-mixed batch gibbsite precipitation experiments. (a) 35-minute; (b) 55-minute; and (c) 75-minute runs.

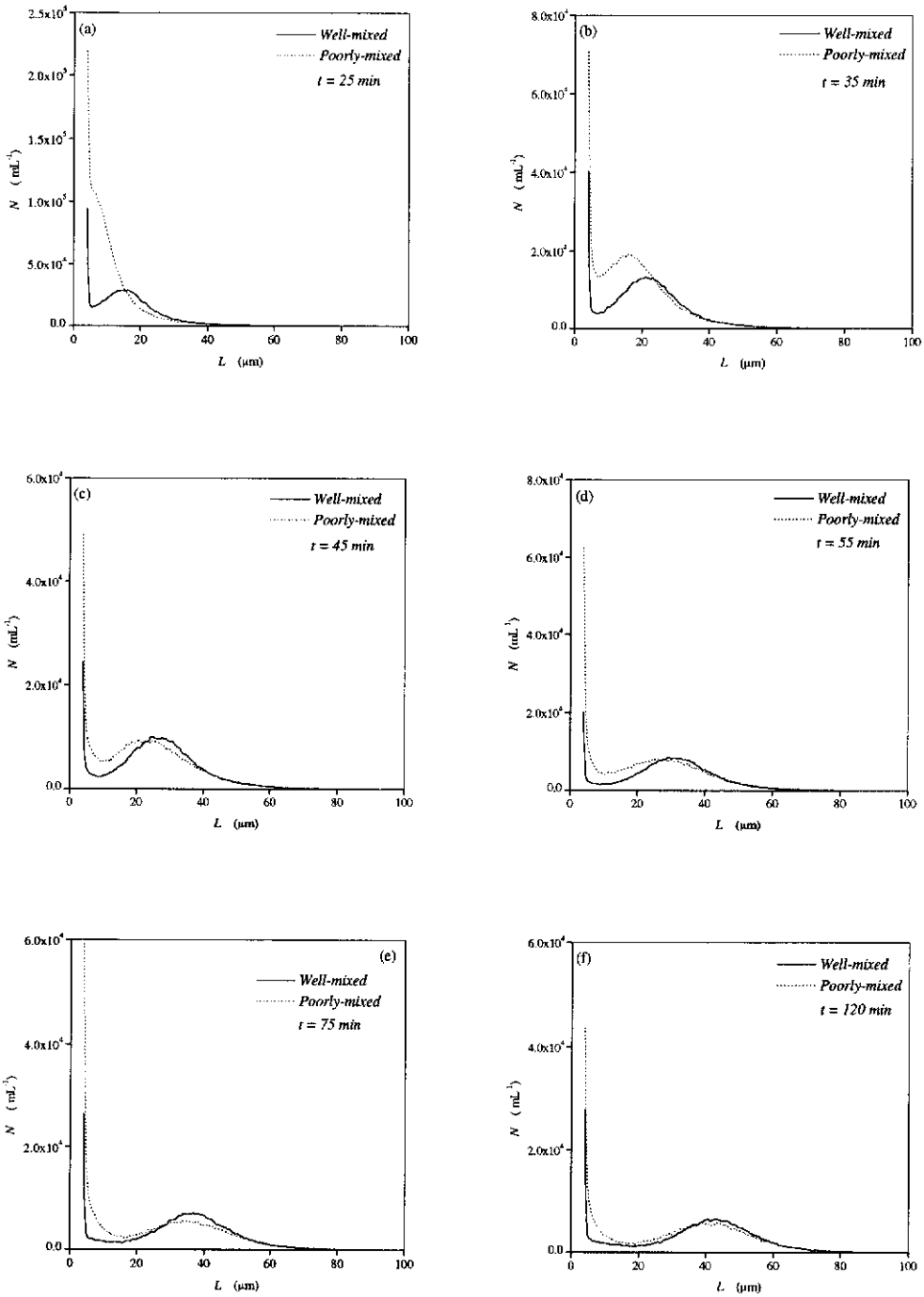

Figure 11.12. Comparisons between the transient CSDs from the well-mixed and the poorly-mixed batch gibbsite precipitation experiments. (a) 25 minutes; (b) 35 minutes; (c) 45 minutes; (d) 55 minutes; (e) 75 minutes; and (f) 120 minutes.

Figure 11.13 shows the total crystal numbers, μ_0, third moment, μ_3, and mean crystal size, μ_1, obtained from both the well-mixed and poorly-mixed experiments. Figure 11.13(a) shows that higher μ_0 were obtained in the poorly-mixed experiments, as a consequence of less crystal agglomeration. The μ_3 in Figure 11.13(b), however, is in good agreement between both experimental systems. This result again strongly suggests that the gibbsite growth rate is similar in both experimental systems, which is in agreement with figures 11.5 and 11.6. It is consistent with previous findings that growth rate is controlled by a surface reaction mechanism and has negligible effects from suspension hydrodynamics (Misra and White 1971a). It can be seen in Figure 11.13(c) that μ_1 in the poorly-mixed system is consistently smaller than and outside the 95% confidence intervals of those obtained from the well-mixed experiments. This suggests that agglomeration kinetics are slow in the poorly-mixed experiments, as it is the main size enlargement process in gibbsite precipitation system and gibbsite molecular growth is very slow. The discrepancies observed in the CSDs between both the well-mixed and poorly-mixed experiments are probably due to the different suspension hydrodynamic effects on the agglomeration process, i.e. different energy dissipation rate distributions (i.e. shear rate) and solids phase mixing. There is strong evidence that gibbsite agglomeration is dependent on fluid shear rate (Ilievski and White 1994b). In addition, Ilievski, Rudman & Metcalfe (1999) reported in their study of well-mixed gibbsite precipitation experiments performed in a high shear turbulent flow stirred vessel and a low shear laminar flow Taylor-Couette precipitator, that the effect of mixing on gibbsite CSD is negligible compared to that of mean shear rate.

In the well-mixed experiments, crystals travel throughout the vessel, carried by fluid flows. They experience different shear rates in their journey around the stirred vessel. Ilievski, Rudman & Metcalfe (1999) stated that it is not the shear distribution that is important to the agglomeration process, but rather, is how long the crystals stay in the shear zones that are favourable to crystal agglomeration and how often the mixing flow brings the crystals into the high shear zone, where crystals may break up. This high shear region in the stirred vessel is usually confined to the regions near the impeller (Koh 1984; Baldyga, Podgorska & Pohorecki 1995).

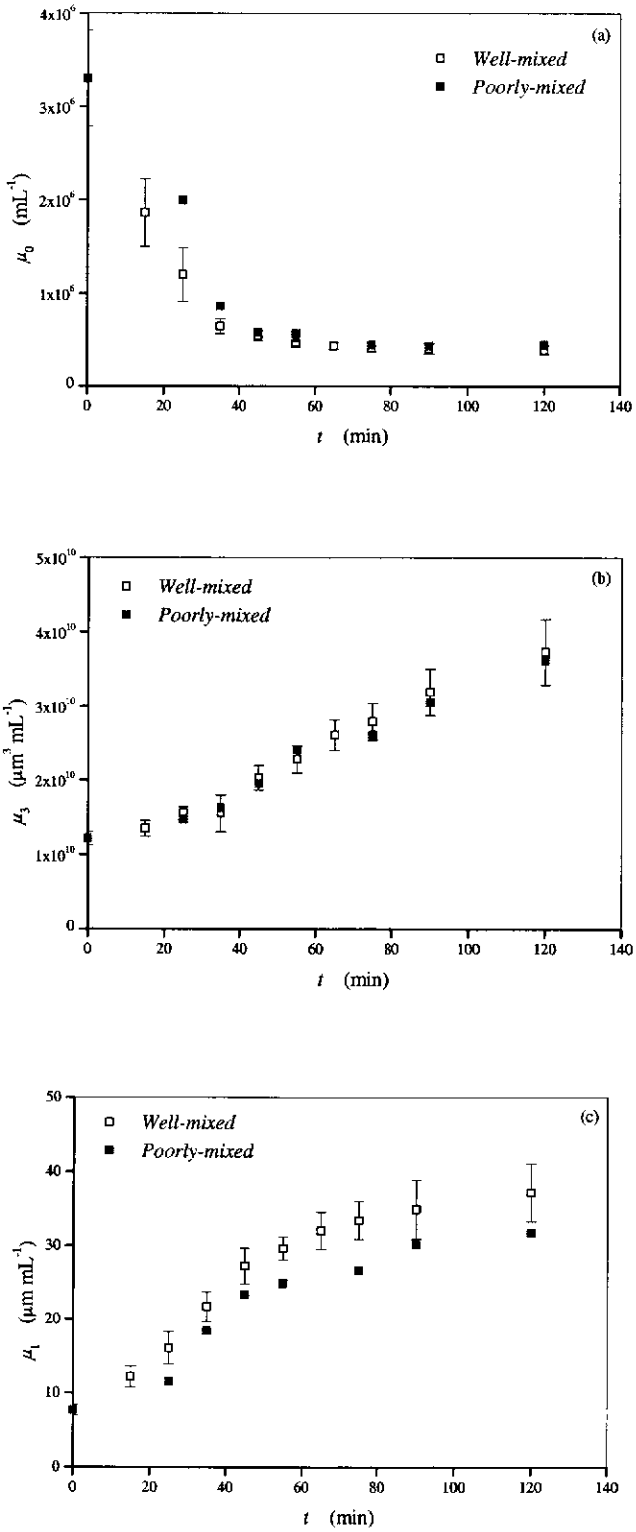

Figure 11.13. Comparisons between the experimental data from the well-mixed and the poorly-mixed batch precipitation experiments. (a) Total crystal numbers, μ_0; (b) third moment, μ_3; and (c) mean crystal size, μ_1.

With that in mind, there should be a range of shear rates that promote crystal agglomeration and a threshold shear rate above which agglomerates are broken in the stirred vessel as suggested by Ilievski, Rudman & Metcalfe (1999). Hence, it is postulated that the poorly-mixed system have a large volume fraction of ineffective shear region in the vessel. In contrast, the well-mixed system may operate under the shear rate ranges that promote agglomeration. Furthermore, in the poorly-mixed system, crystals are not travelling throughout the whole vessel as in the well-mixed case. Hence, there are isolated groups of crystals that remain in different shear zones. It is likely that a high solids concentration remains in the ineffective shear rate regions, and resulting in less crystal agglomeration.

11.4 MODELLING THE POORLY-MIXED BATCH GIBBSITE PRECIPITATION

11.4.1 The State of Mixing in the Precipitator

Modelling of the poorly-mixed suspension precipitation system requires clear knowledge of the state of mixing under the operation conditions considered. The system investigated here is well-mixed with respect to the liquor phase, and there is no mixing of fluid particles of different ages. Hence, the liquor composition should be homogeneous throughout the precipitator at all time. This is demonstrated by the similar desupersaturation rates in both the well-mixed and poorly-mixed experiments in Figure 11.5.

Uniform suspension is not achieved in the vessel when operating at the just suspended speed. Hence, the solids phase is not perfectly mixed. It is assumed that no size dependent classification occurs within the suspension zone, but classification may occur between the cloud interface and suspension zone. It is also assumed that the crystals follow the streamlines of the fluid flow, given that the crystals are smaller than 100 μm. There are no crystals settling at the vessel bottom, as it is free from scale formation at the end of each precipitation run. Under the operating conditions employed in the poorly-mixed suspension precipitation experiments, the parameters that characterise the hydrodynamic conditions are tabulated in Table 11.1.

Table 11.1. Relevant parameters characterising the hydrodynamic conditions generated under the experimental precipitation conditions considered.

Parameters	Values
Reynolds number, N_{RE}	6.26×10^4
Power number, N_P	0.3
Power per unit volume, P/V	221 kg $m^{-1}s^{-3}$
Mean energy dissipation, $\bar{\varepsilon}$	0.180 m^2s^{-3}
Mean shear rate, $\bar{\gamma}$	459 s^{-1}
Impeller pumping number, N_Q	0.56
Impeller pumping flow rate, Q	1.92×10^{-3} m^3 s^{-1}

11.4.2 Preliminary Modelling Approach

An attempt was made to treat the poorly-mixed precipitation system as a well-mixed precipitation system. The "bulk averaged" kinetics were extracted from the experimental CSD using the Bramley's method, and then applied to the DPB model to simulate the product CSD. This approach will help to establish if the "bulk averaged" kinetics can describe the actual kinetics in the poorly-mixed precipitation system satisfactorily. It will indicate the significant of the solids phase mixing in poorly-mixed suspension system. Figure 11.14 shows the comparisons between the experimental and predicted CSD in the poorly-mixed suspension system. The "preceding" approach was used to simulate the CSD with $r = 2^{1/18}$, in order to eliminate or minimise the problem of error propagation initiated from the kinetics estimates uncertainties (see Figure A11.1 in Appendix 11 for the predictions made by the "seed" approach).

The simulation results show that the "bulk averaged" kinetics in the poorly-mixed suspension system resulted in poor CSD predictions. In comparison, the "bulk averaged" kinetics were satisfactory for modelling the well-mixed system in Chapter 7. The discrepancies in the CSD observed in Figure 11.14 may be attributed to

(1) the state of solids phase mixing in the poorly-mixed system, as perfect solids mixing is assumed in the modelling; or

(2) the "bulk averaged" agglomeration kernel estimates are not representing the true agglomeration kinetics, which is likely to be influenced by either the effect of the local energy dissipation rate (i.e. shear rate), or effects associated with the solids phase mixing in the vessel.

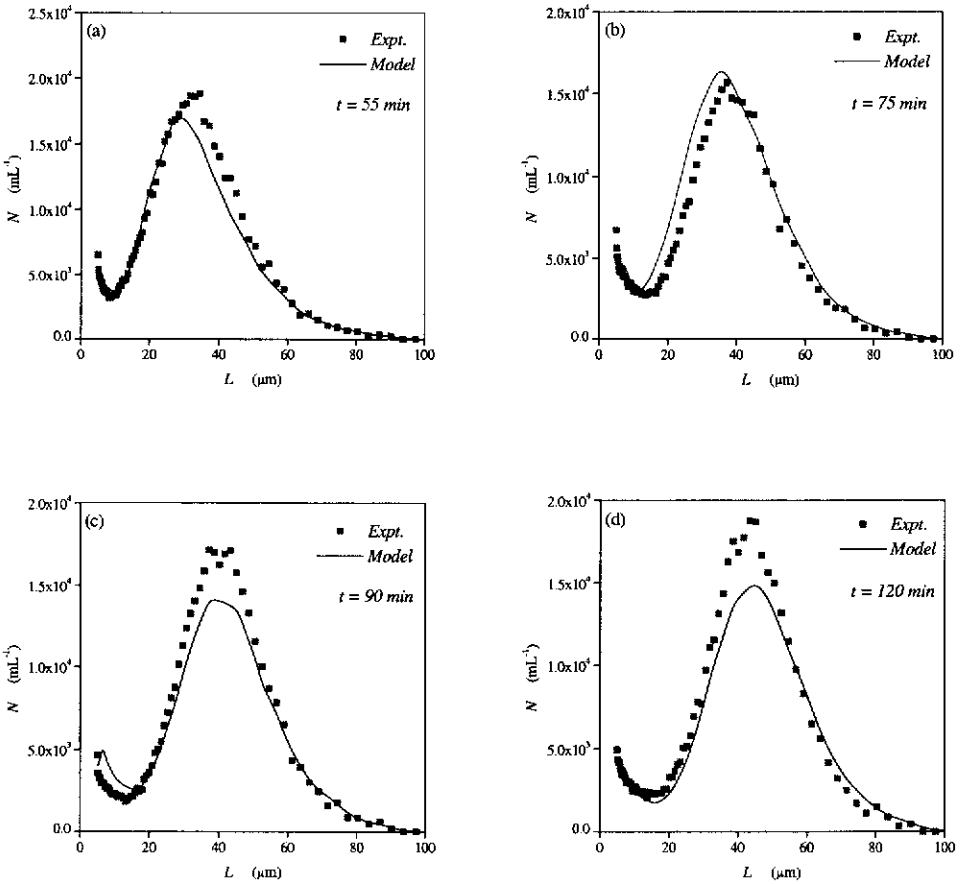

Figure 11.14. Comparisons of the experimental data and model predictions in the poorly-mixed system using the "bulk averaged" kinetics estimates, with the "preceding" approach. (a) 55 minutes; (b) 75 minutes; (c) 90 minutes; and (d) 120 minutes.

11.4.3 Development of a Poorly-Mixed Batch Precipitator Model

11.4.3.1 Compartmental Approach

The compartmental approach is adopted here to model the poorly-mixed batch precipitation system. There are a number of methods reported in the literature reviewed in Chapter 10 that can be classified into this category, which include the compartmental model, network-of-zones model and the CFD model. These approaches vary in model assumptions and complexity, as discussed in the previous

chapter. These types of model assume perfect micromixing, homogeneity of supersaturation and solids concentration, uniform energy dissipation rate and kinetics rates, in each compartment or zone. In addition, each compartment is governed by material balance equations. Hence, the conventional well-mixed model can be considered as a single compartmental model. The number of compartments required to represent the hydrodynamics in the stirred vessel can vary from as little as a few (compartmental model), to hundreds (network-of-zones approach) or even thousands (CFD model). The approach employed here is to simulate the poorly-mixed suspension system with a simplistic compartmental model and increase the number of compartments as necessary to account for the hydrodynamic details. It should be mentioned that full CFD approach is beyond the scope of this work.

11.4.3.2 Compartmental Model Formulation

The hydrodynamic conditions generated in the stirred vessel under the experimental operating conditions is shown in Figure 11.3, which consists of a clear liquor zone, a cloud interface zone and a suspension zone. As an example, the stirred vessel can be divided into 4 compartments as shown in Figure 11.15, each with its intrinsic properties such as, CSD, energy dissipation rate, precipitation kinetics rates, and solids concentration.

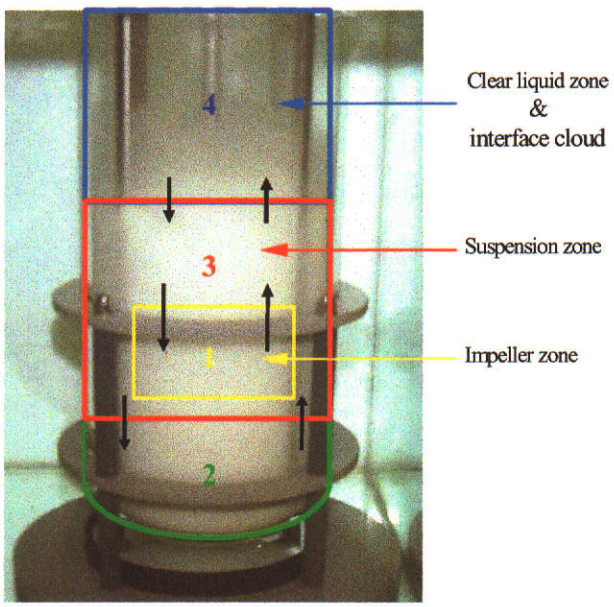

Figure 11.15. A schematic of the division of the stirred vessel into four compartments.

The interchanging flows between each compartment is taken to be some fractional factor, $f_{i,j}$, of the impeller pumping flow rate, Q. Hence, the interchanging flow, $q_{i,j}$, between compartments i and j is

$$q_{i,j} = f_{i,j} Q \tag{11.5}$$

The compartmental PBE considered here has the form in Equation (11.6). The change in the number of crystals, $N_{i,j}$, in the i^{th} size interval at time, t, in the j^{th} compartment that exchanges flows with its k neighbour compartments is

$$\frac{dN_{i,j}}{dt} = \left(\frac{dN_{i,j}}{dt}\right)_A + \left(\frac{dN_{i,j}}{dt}\right)_G + \left(\frac{dN_{i,j}}{dt}\right)_B + \sum_k \frac{q_{k,j}}{V_j}(h_{k,j}N_{i,k} - h_{j,k}N_{i,j}) \tag{11.6}$$

The first three terms on the right hand side of Equation (11.6) are the change in the crystal numbers in the i^{th} size interval as a result of crystal agglomeration, growth and generation (i.e. source term), respectively, i.e. due to the local kinetics rates in the j^{th} compartment. The last term on the right hand side of Equation (11.6) is the change in crystal numbers in the i^{th} size interval resulting from exchanging flows between compartments, and $h_{j,k}$ is the classification function between compartments.

11.4.3.3 Evaluation of the Parameters in the Compartment

11.4.3.3.1 Local Agglomeration Kernel

The gibbsite agglomeration kinetics data published in the open literature is limited. The gibbsite correlation model of Ilievski and White (1994b) is employed here to estimate the agglomeration kernel, β, which is given as

$$\beta = k_H s^4 \left(\frac{P}{V}\right)^{-1.4} \tag{2.13}$$

The above relation can be converted into a function of mean energy dissipation, $\bar{\varepsilon}$, or mean shear rate, $\bar{\gamma}$, according to

$$\bar{\varepsilon} = \frac{P}{V\rho_L} \tag{11.7a}$$

or

$$\bar{\gamma} = \sqrt{\frac{\bar{\varepsilon}}{\nu}} = \sqrt{\frac{P}{V\mu_L}} \tag{11.7b}$$

where ν is the kinematic viscosity of the fluid, ρ_L is the fluid density, and μ_L is the fluid viscosity. Hence, the relation (2.13) becomes

$$\beta = k_H s^4 \rho_L^{-1.4} \bar{\varepsilon}^{-1.4} \tag{11.8a}$$

or

$$\beta = k_H s^4 \mu_L^{-1.4} \bar{\gamma}^{-2.8} \tag{11.8b}$$

The agglomeration correlation in Equation (2.13) is determined in a well-mixed gibbsite precipitation system. The term k_H may not be applicable to the poorly-mixed suspension system, due to the different suspension hydrodynamic effects on k_H. Nevertheless, the value of k_H reported in Equation (2.13) will be used as a first approximation.

The agglomeration kernel in each compartment, β_i, is correlated to the local energy dissipation rate, $\bar{\varepsilon}_i$, which can be related to the mean energy dissipation, $\bar{\varepsilon}$, in the stirred vessel by a factor of η_i

$$\bar{\varepsilon}_i = \eta_i \bar{\varepsilon} \tag{11.9a}$$

By substituting Equation (11.9a) into Equation (11.7b), the mean shear rate in each compartment is

$$\bar{\gamma}_i = \sqrt{\frac{\eta_i \bar{\varepsilon}}{\nu}} = \eta_i^{\frac{1}{2}} \bar{\gamma} \tag{11.9b}$$

Hence, the agglomeration kinetics in each compartment becomes

$$\beta_i = k_H s^4 \rho_L^{-1.4} (\eta_i \bar{\varepsilon})^{-1.4} \tag{11.10a}$$

or

$$\beta_i = k_H s^4 (\eta_i \mu_L)^{-1.4} \bar{\gamma}^{-2.8} \tag{11.10b}$$

The β_i in each compartment is estimated according to

$$\beta_i = 0.05 \times 0.0531 t^{-1.29} \rho_L^{-1.4} (\eta_i \bar{\varepsilon})^{-1.4} \tag{11.11}$$

which shows the kinetic parameters as a function of precipitation time. It should be noted that the supersaturation data generated in the current batch experiments was correlated to the precipitation time as $s^4 = 0.0531 t^{-1.29}$ in Equation (11.11).

11.4.3.3.2 Local Growth Rate

Gibbsite growth rate is affected negligibly by the suspension hydrodynamics. This is confirmed by the match in the desupersaturation curve (Figure 11.5) and the third moment (Figure 11.13(b)) for the well-mixed and the poorly-mixed experiments. Hence, the growth rate in each compartment, G_i, was taken to be the "bulk averaged" growth rate, $\overline{G}$, determined from the poorly-mixed precipitation data, i.e. $G_i = \overline{G}$. For the current batch precipitation data, this was determined to be

$$G_i = 7.28 t^{-0.74} \tag{11.12}$$

11.4.3.3.3 Local Source Term Rate

Nucleation is negligible under the operating conditions of the current batch experiments, but the source term rate needs to be accounted for due to the field of view problem in the Coulter counter multisizer. There is no fundamental understanding of how this term relates to the chemistry environment in the precipitation system, but it is likely to depend on supersaturation and solids content in the vessel. The observed fine crystals in the poorly-mixed experimental data is likely due to two possible sources: (1) seed crystals yet to agglomerate due to poorly-

mixed suspension; and (2) growth and agglomeration of fine crystals into the field of view of the particle size analyser. It is not possible to distinguish their individual contributions. Here, the "bulk averaged" source term rate estimated from the poorly-mixed precipitation data was used as a first approximation, i.e. $B_{u_i} = \overline{B}_u$. For the batch precipitation data, this was correlated to give

$$B_{u_i} = 1.63 \times 10^5 x_i t^{-0.91} \tag{11.13}$$

where x_i is the solids concentration fraction.

11.4.3.3.4 Energy Dissipation Distribution in the Vessel

The energy dissipation rate is an important feature of the turbulent field. It controls the characteristic times of the mixing process. The power input into the vessel by the impeller is not distributed uniformly over the vessel. Hence, the energy dissipation rate is not homogeneous in the vessel. The energy dissipation pattern in a vessel strongly depends on impeller type (Mersmann and Kind 1988). It is possible to calculate the local energy dissipation rate from CFD simulations or measure it from laser doppler anemometry measurements within the vessel (Bertrand, Couderc & Angelino 1980; Wu and Patterson 1989; Armenante and Chou 1996; Zhou and Kresta 1996; Armenante et al. 1997).

Experimental studies using laser detection techniques have shown that the power dissipation rate is highest in the impeller region, and lowest in the bulk region of the vessel. However, considerable differences exist between the various studies, which show the experimental difficulties in obtaining reliable data for the power dissipation rate.

Here, a rough approximation on the energy dissipation distribution in the vessel was made by referring to the published energy dissipation results in the literature (Okamoto, Nishikawa & Hashimoto 1981; Barthole et al. 1982). However, most reported results are for standard vessel geometry with liquid level to vessel diameter ratio, H/T = 1.0 and for different impeller types, rather than the A310 impeller and H/T = 2.19 employed in this work.

11.4.3.3.5 Solids Concentration Distribution in the Vessel

The solids concentration profile obtained previously in Figure 11.4 will be used to describe the system considered. In addition, it is also assumed that solids classification is not significant, and a similar CSD form exists throughout the vessel.

11.4.4 Compartmental Modelling of the Poorly-Mixed Precipitator

Table 11.2 below shows the parameters used in three trials of the compartmental modelling performed. The numbering of the compartment zones in Table 11.2 corresponds to that shown in Figure 11.15.

Table 11.2. Parameter values used in the three trials of the compartmental modelling.

No. Zones	Parameter	COMPARTMENT			
		1	2	3	4
2	v_i		0.85		0.15
	η_i		1.1325		0.25
	x_i		0.85		0.15
	$f_{i,j}$		0.25		0.25
3	v_i		0.3	0.55	0.15
	η_i		1.375	1.0	0.25
	x_i		0.5	0.35	0.15
	$f_{i,j}$		1.0	1.0 / 0.25	0.25
4	v_i	0.1	0.35	0.4	0.15
	η_i	2.25	0.8	1.15	0.45
	x_i	0.1	0.4	0.3	0.2
	$f_{i,j}$	1.0	0.5	1.0 /0.5/ 0.25	0.25
		Impeller zone	Suspension zone		Cloud Interface

The parameters v_i, η_i, x_i and $f_{i,j}$ are volume fraction, proportional factor of the energy dissipation rate, solids concentration fraction and fractional factor of the interchanging flows between compartments, respectively. These are the parameters that need to be determined in the compartmental modelling. It should be noted that the classification function, $h_{i,j}$, is set to 1 in this work. The parameters, v_i, x_i and $f_{i,j}$ should be chosen such that they represent the hydrodynamic conditions in the vessel, however, at this stage they are chosen arbitrarily, due to the difficulties of measuring them accurately.

Both v_i and x_i should satisfy the following conditions:

$$\sum_i v_i = 1 \tag{11.14a}$$

and

$$\sum_i x_i = 1 \tag{11.14b}$$

as they are the volume and mass fraction, respectively. Since the mean energy dissipation rate and mean shear rate is on a volume-averaged basis, the summation of the local energy dissipation rate or shear rate in each compartment should follow

$$\sum_i v_i \frac{\bar{\varepsilon}_i}{\bar{\varepsilon}} = \sum_i v_i \eta_i = 1 \tag{11.15a}$$

or

$$\sum_i v_i \frac{\bar{\gamma}_i}{\bar{\gamma}} = \sum_i v_i \eta_i^{\frac{1}{2}} = 1 \tag{11.15b}$$

where η_i is adjusted to satisfy above condition as the volume fraction v_i are pre-determined.

Figures 11.16(a)-(d) show the comparisons of the experimental and predicted CSDs from the two, three and four compartmental models, respectively. The simulations were carried out between 45 to 120 minutes, and the "preceding" approach and a size discretisation ratio of $2^{1/18}$ were employed. It can be seen that there is virtually no improvement in the CSD predictions, by increasing the number of compartments from two to four. This is further demonstrated in Table 11.3, which shows the SSE between the experimental CSD and model predictions (Note that the SSE values at different times can not be compared as the crystal numbers are changing with time). It should be noted that the contribution of non-ideal solids phase mixing to the discrepancies in the CSD predictions is unknown and not accounted for in the current simulations.

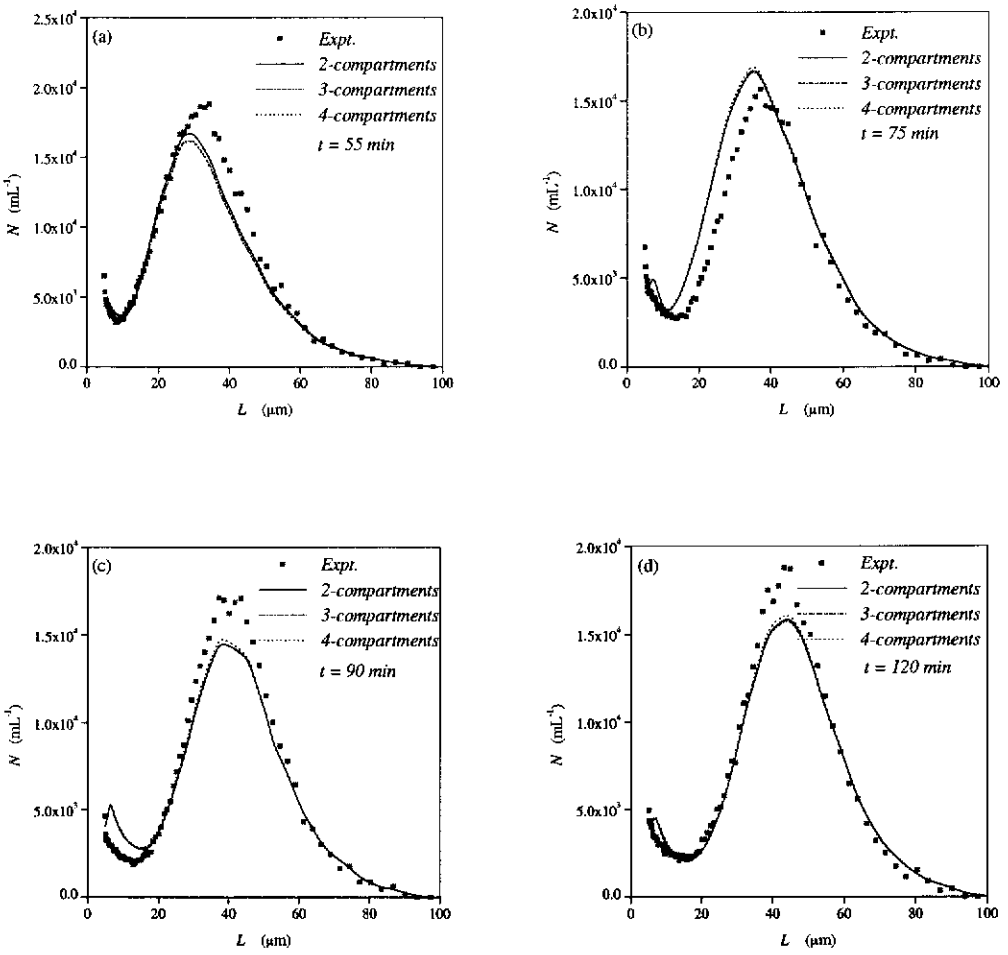

Figure 11.16. Comparisons of the experimental data and the compartmental model predictions in the poorly-mixed system, with the "preceding" approach. (a) 55 minutes; (b) 75 minutes; (c) 90 minutes; and (d) 120 minutes.

Table 11.3. SSE between the experimental data and model predictions for the two, three and four compartmental models.

Modelling Approach	**SSE**			
	t = 55 min	*t = 75 min*	*t = 90 min*	*t = 120 min*
Two Compartments	1.09×10^8	2.16×10^8	1.35×10^8	6.15×10^7
Three Compartments	1.38×10^8	2.14×10^8	1.35×10^8	6.65×10^7
Four Compartments	1.43×10^8	2.42×10^8	1.27×10^8	5.41×10^7

11.5 COMMENTS ON MODELLING THE POORLY-MIXED AGGLOMERATING BATCH GIBBSITE PRECIPITATION SYSTEM

The discrepancies observed in the poorly-mixed precipitator model may be the result of (1) an inaccurate agglomeration model; and (2) complications arising from the large number of adjustable variables in the model such as, number of compartments, interchanging flow rates between compartments, local solids concentration, and local energy dissipation rates. At this stage it is not possible to obtain accurate measurements of these parameters. In addition, assumptions have been made on the CSD form, classification and source term rate. The agglomeration correlation used was found to be unsuitable to describe well-mixed systems in Chapter 5, and no doubt poses a similar problem in the poorly-mixed suspension system.

Due to the poor understanding of the agglomeration mechanism, it is unclear how the agglomeration process behaves in the high turbulence shear regions and in the low shear regions within the stirred vessel. The negative exponent on the mean shear rate in Equation (11.10b) shows that the agglomeration kernel decreases with increasing mean shear rate. If this is the case then the poorly-mixed suspension system should have a faster agglomeration kinetics due to the large volume fraction of the low shear rate region. However, the opposite appears to be true. The other possible explanation is that the low shear region in the poorly-mixed system is lower than the feasible shear rate range that promotes crystal agglomeration. Hence, questions that need to be answered are

(1) if the negative exponent relation between crystal agglomeration kinetics and mean shear rate is applicable to the full shear rate range;
(2) if different agglomeration mechanisms take place in the low and high shear regions in the stirred vessel; and
(3) what is the range of shear rates that promote or retard crystal agglomeration.

Mumtaz et al. (1997) presented a relation for the agglomeration rate constant as a function of shear rate. In the low shear region, agglomeration rate constant increases with shear rate, but in the high shear region, the rate constant quickly drops to zero, due to viscous forces on the agglomerates formed and the decrease in contact time

between primary crystals. However, there is no experimental observation to support this theory yet. Hollander et al. (1999) showed in their simple channel flow simulation study, that the use of a volume averaged agglomeration kernel evaluated from the mean shear rate is inadequate to represent the agglomeration process. They further stated that both the turbulent transport of solids and energy dissipation rate distributions should be accounted to correctly represent the agglomeration process. Finally, the poor CSD predictions in the poorly-mixed suspension system may be also due to the coupled effects of solids phase mixing and shear rate on the agglomeration process. Time constraints prevented these issues being explored further in the current research. Future work may wish to address the importance of the following on modelling poorly-mixed gibbsite precipitators: (1) the number of compartments used in modelling, and (2) determining the energy dissipation rate, the solids concentration in the vessel and classification function.

11.6 CONCLUSIONS

A study on the influence of the suspension hydrodynamics on batch gibbsite precipitation was undertaken. The experimental data was compared to a well-mixed system operating under the same operating conditions. It was found that more fine crystals are produced in the poorly-mixed system, which was attributed to slower agglomeration kinetics. The results suggest that the poor solids phase mixing influences agglomeration kinetics significantly, but have a negligible effect on growth rate. This is expected, as agglomeration kinetics is dependent on fluid shear, whereas growth is not influenced by suspension hydrodynamics. Although the mean shear rate in both experimental systems was equivalent, the shear distributions within the vessels and suspension hydrodynamics are completely different. These factors are seen to have a strong influence on the product CSD. Compartmental modelling was employed to simulate the poorly-mixed suspension system. Poor agreement was obtained between the experimental CSD and model predictions. It is believed that the poor CSD predictions in the poorly-mixed suspension system are due to current inability to correctly account for the coupled effects of local energy dissipation rate and solids phase mixing on agglomeration process. This work highlights that a better understanding of agglomeration mechanism is required.

CHAPTER 12

CONCLUSIONS AND RECOMMENDATIONS

The modelling and kinetics estimation aspects of the gibbsite precipitation system were investigated in this research. This chapter draws important findings from the current research and provides some recommendations for future study in this area.

12.1 CONCLUSIONS

12.1.1 Modelling Well-Mixed Gibbsite Precipitation Systems

The PB theory was used to derive models of the well-mixed, semi-batch constant composition and batch gibbsite precipitation systems. The model predictions of the precipitator models were validated with their corresponding experimental gibbsite precipitation data. It was found that

(1) the PB theory is applicable to model well-mixed precipitation systems;
(2) kinetics rates from the method of moments matching and the Bramley's method both describe the precipitation data satisfactorily; and
(3) the literature correlation models are unsuitable to describe the precipitation data.

12.1.2 Error Propagation in the PB Models

Modelling of non-stationary constant composition and batch precipitation systems showed that the model predictions of the CSD are in good agreement with the experimental CSDs initially but progressively drift apart with time. The cause of this deviation was identified as error propagated in the computation of the DPB model.

The source of the propagated error in modelling the constant composition system was investigated. It was concluded that

(1) the main contribution to the observed error is from the uncertainty in the estimates of the agglomeration kernel and growth rate parameters, which are estimated from experimental data and used in the simulation;
(2) care is required when simulating the CSD of non-stationary precipitators over longer time scales, which may have implications for precipitator start-up simulations; and
(3) more precise kinetics estimation procedures are needed.

12.1.3 Uncertainty in Batch Experimental Precipitation Data

The study on the uncertainty in batch gibbsite precipitation data from repeated experiments showed that

(1) poor CSD reproducibility was obtained during the induction period of the precipitation process;
(2) the poor reproducibility over the induction period may be due to the complex mechanistic activities affecting the process kinetics;
(3) reproducible CSD data was obtained after the induction period;
(4) the uncertainties in total crystal numbers and third moment were within 5%; and
(5) the uncertainty for crystal numbers in the first size interval was significantly higher, around 20-30%.

These results should not be extrapolated to other operating conditions that are significantly different to the conditions employed in the reproducibility study.

12.1.4 Uncertainties in Batch Kinetics Estimates

Following the reproducibility study, the uncertainties in the kinetics estimates from the Bramley's method were determined using Monte Carlo simulations. It was found that

(1) the uncertainties in the estimates of the agglomeration kernel, growth and source term rates increase with time, and are within 30%; and

(2) the uncertainties in the kinetics estimates strongly depend on the magnitude of kinetics values, and the change in the total crystal numbers and the third moment.

12.1.5 The Influence of the Experimental Design on Kinetics Estimates

The importance of experimental design on the accuracy and precision of estimates of the agglomeration, growth and nucleation kinetics for the gibbsite system was investigated. Three different precipitator configurations were considered, which were (1) batch, (2) semi-batch at constant composition with representative solids removal and (3) semi-batch at constant composition with classified solids removal. The Bramley's method was employed to estimate the kinetics from each set of experimental data. The results showed that

(1) differences exist in the kinetics estimates between the different configurations;
(2) the observed differences in the agglomeration kernel and growth rate can be explained by the uncertainties in the kinetics estimates;
(3) the differences in the nucleation source term may also attribute to differences in suspension density between the experiments;
(4) operating conditions have a greater impact on the uncertainties in the estimated kinetics than the precipitator configuration; and
(5) both high supersaturation conditions and a large number of measurements taken favour more precise kinetics estimates.

12.1.6 The Influence of the Kinetics Estimation Technique on Kinetics Estimate Uncertainties

The differential and integral techniques were employed to estimate gibbsite precipitation kinetics in a batch and a constant composition with solids retention precipitation systems. It was found that

(1) kinetics estimates obtained by the integral method describe the experimental CSD data better than those obtained by the differential method;
(2) the kinetics estimates from the differential and integral methods have significant uncertainties; and

(3) the sources of the uncertainty originate from the errors in the experimental data, numerical differentiation scheme used and the nature of the optimisation method employed.

12.1.7 Investigation on the Poorly-Mixed Batch Gibbsite Precipitation System

A study on poorly-mixed suspension batch gibbsite precipitation was undertaken. The experimental data was compared to a well-mixed system operated under the same operating conditions (i.e. supersaturation, seed charge, seed type, mean shear rate and temperature). It was found that

(1) the CSD were different at the same precipitation time and the poorly-mixed system showed more fine crystals;
(2) scale formed around the stagnant region (top of the liquid level) of the poorly-mixed vessel;
(3) suspension hydrodynamics influences the product CSD significantly;
(4) suspension mixing appears to influence the gibbsite agglomeration kinetics significantly but has negligible effect on gibbsite growth rate; and
(5) the agglomeration correlation based on volume averaged shear rate is unsuitable to describe the poorly-mixed gibbsite precipitation system.

12.2 RECOMMEDATIONS

12.2.1 Field of View Problem

The issue of field of view in the Coulter counter multisizer needs to be addressed. This problem arises as the particle size analyser is limited by the minimum detectable size of the orifice tube used, and the continuous movement of the crystals into the field of view of the particle size analyser. It is postulated that this phenomena occurs mainly due to nuclei and seed crystals agglomerate and grow into the field of view of the particle size analyser.

A possible approach that may overcome or minimise the effect of the field of view problem is to remove the fine crystals from the seed used in the experiments, i.e. use large seed crystals in the precipitation experiments. The fine crystals can be removed

via cyclone sizer, wet sieving, decantation or other efficient solids classification techniques.

A decantation procedure for removing the fines has been established in the current research. The decantation procedure and the form of the decanted seed CSD are attached in Appendix 14. The decantation procedure is very time consuming. Due to time constraints in the current research, precipitation experiments with the decanted seed crystals to investigate the field of view problem were not conducted.

12.2.2 Gibbsite Kinetic Rate Correlations

This study has helped to clarify and quantify the influences of the uncertainty in experimental data, operating conditions, precipitator configuration and kinetics estimation technique on the accuracy and precision of the kinetics estimates. There is a need for more reliable kinetic rate correlations, in particular, the agglomeration and nucleation that can be applied to wider range of precipitation conditions. To ensure accurate estimation of the kinetics rates, it is recommended to

(1) perform the gibbsite precipitation experiments at the operating conditions that promote precipitation kinetics rates (high supersaturation and temperature); and
(2) collect large number of sampling data at any given operating conditions.

12.2.3 Modelling Inhomogeneously-Mixed Gibbsite Precipitation System

Modelling of the inhomogeneously-mixed gibbsite precipitator is still at an early stage of the development. Modelling precipitation systems involving agglomeration is much more complex compared to systems involving growth and nucleation only. As demonstrated in this research, the local variation of the agglomeration kinetics cannot be accounted for by means of relating the agglomeration kinetics to the volume averaged shear rate. The compartmental model is an attractive approach to account for the inhomogeneously-mixed system due to its simplicity, but it relies on large number of assumptions and rough estimates of the operating variables. Future research in this area should perform the following tasks:

(1) estimate the energy dissipation rate profile in the operating vessel, either from experimental measurement or CFD simulation;

(2) accurate determination of the solids concentration profile in the vessel;

(3) determine the classification function if the solids loading is high; and

(4) establish the relationships between the local energy dissipation rate and local agglomeration kinetics. This last point is likely the key to the success of any poorly-mixed models.

NOMENCLATURE

ACRONYMS

CCCSR	constant composition classified solids removal
CCRSR	constant composition representative solids removal
CCSR	constant composition solids retention
CFD	computational fluid dynamics
CModel	precipitator model using the kinetics estimates from correlation models
CSD	crystal size distribution
DAModel	discretised agglomeration model
DGModel	discretised growth model
DPB	discretised population balance
EDD	engulfment-deformation-diffusion
MModel	precipitator model using the kinetics estimates from moments matching method
MSMPR	mixed suspension mixed product removal
PB	population balance
PBE	population balance equation
PSP	problem specified polynomial
RANS	Reynolds-averaged Navier Stokes
RTD	residence time distribution
SEM	scanning electron microscopy
SSE	sum of squares error
SMM	simplified moments matching
UV-Vis	ultra-violet-visible

GREEK

α	age of a molecule or aggregate
α	parameter in Equation (6.5)
β	agglomeration kernel, mL hr^{-1}
β	fractional flow factor in the network-of-zones model

β_o	size independent term of the agglomeration kernel
δ	estimate of the 95% confidence interval on parameter
$\delta(L\text{-}L_o)$	Dirac delta function
Δc	solute concentration, kg/ kg solvent
ΔE	activation energy, kJ mol^{-1}
ΔG	Gibb free energy of dissolution, kJ mol^{-1}
ΔL	lateral shift in size due to growth, μm
Δt	time increment, min
$\Delta\mu_3$	change in the third moment due to growth, μm^3
ε	solids free volume of solution per volume of slurry
$\bar{\varepsilon}$	mean energy dissipation rate, m^2s^{-3}
$\bar{\varepsilon}_i$	local energy dissipation rate, m^2s^{-3}
ε_v	viscous dissipation per unit mass
ϕ	conversion factor from Al_2O_3 to $Al(OH)_3$
ϕ	scalars used in the CFD models
Φ	objective function of the optimisation problem
Φ_j	parameters in the method of Bramely, Hounslow & Ryall (1996)
γ	parameter in equations (6.8) to (6.10)
$\bar{\gamma}$	mean shear rate, s^{-1}
$\bar{\gamma}_i$	local shear rate, s^{-1}
η	aggregation collision efficiency factor
η_i	proportional factor of mean energy dissipation rate
η_r	growth rate effectiveness factor
φ	ratio of the uncertainties in the experimental data from different size discretisation resolutions
$\varphi_{j,q}$	over prediction factor of the j^{th} moment with size resolution q by the two-term growth discretised model
κ	slurry turbidity
λ	crystal size, μm
λ	residual life of a molecule
λ_B	Batchelor microscale
λ_C	Corrsin microscale

λ_k	Kolmogorov microscale
μ_L	fluid viscosity, kg m^{-1} s^{-1}
μ_j	j^{th} moment of the CSD, μm^j
ν	fluid kinematic viscosity, $m^2 s^{-1}$
ν_t	turbulent kinematic viscosity
π	aggregate external surface area
θ	dimensionless residence time for a point
θ	induction time, min
θ	denotes kinetic parameters, eg. β, G and B_u
ρ_L	density of the liquor, g L^{-1}
ρ_s	density of the crystals, g L^{-1}
σ	standard deviation or uncertainty
σ_A	standard deviation in the agglomeration parameter estimate
σ_G	standard deviation in the growth rate parameter estimate
τ	dimensionless time
τ	mean residence time, hr
τ_m	turbulent characteristic mixing time
υ	macrofluid volume fraction
ω	angular impeller speed, rad s^{-1}
ω	dispersed phase mixing frequency in the coalescence and redispersion model
ω_i	weighting function
ξ	crystal volume
ψ	denotes measured parameters, eg. μ_j and N_1

ROMAN

A	aluminate concentration, g L^{-1} Al_2O_3
A^*	equilibrium aluminate concentration, g L^{-1} Al_2O_3
A_o	total seed surface area, μm^2 mL^{-1}
A_T	total crystal surface area, μm^2 mL^{-1}
B	birth function, μm^{-1} mL^{-1}
B^o	nucleation rate, mL^{-1} hr^{-1}

B_u	source term rate, $mL^{-1}\ hr^{-1}$
c	concentration
C	concentration fraction
C	caustic concentration, g L^{-1} Na_2O or g L^{-1} Na_2CO_3
C	off-bottom clearance, mm
$C(I)$	function of impurity type and concentration in the induction time model of Brown (1977)
COS	cumulative oversize distribution function
CUS	cumulative undersize distribution function
CV	coefficient of variance
D	death function, $\mu m^{-1}\ mL^{-1}$
D	impeller diameter, mm
D	diffusion coefficient
E	engulfment rate in the EDD model
$f(t)$	residence time distribution function
$f(\nu,\xi)$	size dependency term of the agglomeration kernel
$f_{i,j}$	fractional factor of the interchanging flow between compartments i and j
$F(t)$	cumulative residence time distribution function
FC	free caustic concentration
g	gravitational force in the Navier Stokes equations
$g(\alpha,\lambda)$	frequency function in the environment model
G	growth rate, $\mu m\ hr^{-1}$
G_o	initial growth rate, $\mu m\ hr^{-1}$
G_v	volumetric growth rate
h	measured size width, μm
h	mass transfer coefficient in the "Shrinking Aggregate" model
$h_{i,j}$	classification function between compartments i and j
$h(L)$	classification function
H	liquid level, mm
I	intensity of undiffracted light
I	ionic strength
I_{Agg}	Index of aggregation
I_o	intensity of the incident light

I_v	micromixedness ratio
I_s	intensity of segregation
J	degree of segregation
k_a	surface area shape factor
k_A	agglomeration rate constant
k_β	agglomeration rate constant
k_b	nucleation rate constant
k_g	growth rate constant
k_G	growth rate constant
k_H	agglomeration rate constant
k_v	volume shape factor
K	aggregation parameter
K_θ	induction time constant
K_g	induction time constant
l	diameter of the shrinking aggregate
l_o	initial size of fluid elements
l_∞	average segregated microscale
L	crystal size, μm
L_i	lower bound on the i^{th} size interval, μm
L_{i+1}	upper bound on the i^{th} size interval, μm
L_o	mean seed size, μm
L_T	total crystal length, μm mL^{-1}
m	total mass content, g L^{-1}
m_j	j^{th} moment about the mean, μm^j
M_T	total crystal mass
n	number density function, μm^{-1} mL^{-1}
n_i	number density in the i^{th} size interval, μm^{-1} mL^{-1}
n_{seed}	seed number density function, μm^{-1} mL^{-1}
N	impeller speed, rpm or rps
N_1	number of crystals in the first size interval, mL^{-1}
N_o	total number of seed crystals, mL^{-1}
N_i	number of crystals in the i^{th} discretised size interval, mL^{-1}
N_{JS}	just suspended speed, rpm

N_P	Power number
N_Q	impeller pumping flow number
N_{RE}	Reynolds number
N_T	total number of crystals, mL^{-1}
P/V	power per unit volume, kg s^{-3} m^{-1}
$p(t,c)$	concentration frequency function in the coalescence and redispersion model
p	parameter in the induction time model of Ilievski, Zheng & White (1989)
q	adjustable parameter determining size discretisation resolution
q	interchanging flow in the network-of-zones model
$q_{i,j}$	interchanging flow between compartments i and j, mL hr^{-1}
q_o	volumetric flow from the completely segregated volume to the maximum mixedness zone
Q	volumetric flow rate, mL hr^{-1} or m^3 s^{-1}
Q	consumption rate
r	size discretisation ratio
r	rate of production in the coalescence and redispersion model
R	reaction term or generation term
R	gas constant, J K^{-1} mol^{-1}
R_s	constant transfer coefficient in the environment model
s	supersaturation term
s	shrinkage strain rate in the shrinkage slab model
Sc	Schmidt number
SC	sodium carbonate concentration, g L^{-1} Na_2CO_3
t	time, min or hr
t_D	molecular diffusion time constant
t_e	erosion time constant
t_L	stretching time constant
t_m	micromixing time constant
t_s	micromixing time constant
T	temperature, °C or K
T	precipitator diameter, mm

T	torque, Nm
u	shrinkage velocity in the EDD model
v	crystal volume, μm^3
v_i	volume fraction of compartment i
v_o	mean seed volume, μm^3
V	precipitator volume, L or m^3
V_a	aggregate volume in the "Shrinking Aggregate" model
V_i	volume of species i rich region
V_o	initial fluid volume
V_s	volume of completely segregated fluid
V_T	total crystal volume, $\mu m^3\ mL^{-1}$
W	baffle width, mm
x	spatial coordinate
x_i	solids fraction in compartment i
x_j	j^{th} linear size interval, μm
X	volume fraction
Y_j	number of crystals in the j^{th} measured size interval, mL^{-1}
z	random number

SUBSCRIPT

A	denotes agglomeration
B	denotes nucleation and source term
F	denotes net flow in and out of the system
G	denotes growth
i	denotes the i^{th} size interval
i	denotes the i^{th} compartment, zone or cell
j	denotes the species group in mixing models
j	denotes the j^{th} moment
j	denotes the j^{th} compartment, zone or cell
m	denotes the species group in mixing models
p	denotes the points in macromixing and micromixing models
t	denotes turbulent term
β	denotes agglomeration kernel

ψ	denotes measured parameters

SUPERSCRIPT

$'$	denotes normalised term or fluctuation term
b	supersaturation dependency order of nucleation rate
g	supersaturation dependency order of growth rate

SYMBOL

$\langle\rangle$	denotes environment quantities in equations (10.37)-(10.39)
∇	vector operator, called "divergence"

OVERHEAD

$\bar{}$	denotes mean values or moment transformed quantities
$\bullet$	denotes time derivatives term
$\hat{}$	denotes normalised term

REFERENCES

Abegg, C.F., Stevens, J.D. and Larson, M.A. 1968, 'Crystallization size distribution in continuous crystallizers when growth rate is size dependent', *AIChE Journal*, vol. 14, no. 1, pp118-122.

Abegg, C.F. and Balakrishnan, N.S. 1971, 'The tanks-in-series concept as a model for imperfectly mixed crystallizers', *Chemical Engineering Progress Symposium Series*, vol. 67, no. 110, pp88-96.

Allen, T. 1981, *Particle size measurement*, 3rd ed., Chapman and Hall, London.

Al-Rashed, M.H., Jones, A.G., Hannan, M. and Price, C. 1996, 'CFD modelling of a precipitation mixing vessel', in the proceedings of the *13th Symposium on Industrial Crystallization*, Toulouse, France, vol. 2, pp419-424.

Angst, W., Bourne, J.R. and Sharma, R.N. 1982a, 'Mixing and fast chemical reaction. IV', *Chemical Engineering Science*, vol. 37, no. 4, pp585-590.

Angst, W., Bourne, J.R. and Sharma, R.N. 1982b, 'Mixing and fast chemical reaction. V', *Chemical Engineering Science*, vol. 37, no. 4, pp1259-1264.

Aoun, M., Plasari, E., David, R. and Villermaux, J. 1999, 'A simultaneous determination of nucleation and growth rates from batch spontaneous precipitation', *Chemical Engineering Science*, vol. 54, pp1161-1180.

Armenante, P.M. and Chou, C.C. 1996, 'Velocity profiles in a baffled vessel with single or double pitched-blade turbines', *AIChE Journal*, vol. 42, no. 1, pp42-54.

Armenante, P.M., Luo, C.G., Chou, C.C., Fort, I. and Medek, J. 1997, 'Velocity profiles in a closed, unbaffled vessel - comparison between experimental LDV data and numerical CFD predictions', *Chemical Engineering Science,* vol. 52, no. 20, pp3483-3492.

Audet, D.R. and Larocque, J.E. 1988, 'Development of a model for prediction of productivity of alumina hydrate precipitation', in *Light metals 1989*, ed. P.G. Campbell, The Minerals, Metals & Materials Society, pp21-26.

Ayazi Shamlou, P. and Koutsakos, E. 1989, 'Solids suspension and distribution in liquids under turbulent agitation', *Chemical Engineering Science*, vol. 44, no. 3, pp529-542.

Bakker, R.A. and van den Akker, H.E. 1994, 'A computational study of chemical reactors on the basis of micromixing models', *Institution of Chemical Engineers Symposium Series*, no. 136, pp259-266.

Baldyga, J. and Bourne, J.R. 1986, 'Principles of micromixing', in *Encyclopedia of fluid mechanics*, vol. 1, Gulf Publishing, Houston, pp147-201.

Baldyga, J. and Bourne, J.R. 1988, 'Calculation of micromixing in inhomogeneous stirred tank reactors', *Chemical Engineering Research and Design,* vol. 66, pp33-38.

Baldyga, J. 1989, 'Turbulent mixer model with application to homogeneous, instantaneous chemical reaction', *Chemical Engineering Science*, vol. 44, no. 5, pp1175-1182.

Baldyga, J. and Bourne, J.R. 1989a, 'Simplification of micromixing calculations: I. Derivation and application of new model', *The Chemical Engineering Journal*, vol. 42, pp83-92.

Baldyga, J. and Bourne, J.R. 1989b, 'Simplification of micromixing calculations: II. New applications', *The Chemical Engineering Journal*, vol. 42, pp93-101.

Baldyga, J. and Bourne, J.R. 1992, 'Interactions between mixing on various scales in stirred tank reactors', *Chemical Engineering Science*, vol. 47, no. 8, pp1839-1848.

Baldyga, J. 1993, 'Micromixing and precipitation', in the proceedings of the *12th Symposium on Industrial Crystallization*, Warsaw, Poland, vol. 1, pp2-003-2-014.

Baldyga, J., Bourne, J.R. and Yang, Y. 1993, 'Influence of feed pipe diameter on mesomixing in stirred tank reactors', *Chemical Engineering Science,* vol. 48, no. 19, pp3383-3390.

Baldyga, J. 1994, 'A closure for homogeneous chemical reactions', *Chemical Engineering Science,* vol. 49, no. 12, pp1985-2003.

Baldyga, J. and Henczka, M. 1995, 'Closure problem for parallel chemical reactions', *The Chemical Engineering Journal*, vol. 58, pp161-173.

Baldyga, J. and Pohorecki, R. 1995, 'Turbulent micromixing in chemical reactors - A review', *Chemical Engineering Journal and the Biochemical Engineering Journal*, vol. 58, no. 2, pp183-195

Baldyga, J., Podgorska, W. and Pohorecki, R. 1995, 'Mixing-precipitation model with application to double feed semibatch precipitation', *Chemical Engineering Science*, vol. 50, no. 8, pp1281-1300.

Baldyga, J. and Orciuch, W. 1997, 'Closure problem for precipitation', *Transactions of the Institution of Chemical Engineers*, vol. 75, pp160-170.

Baldyga, J., Bourne, J.R. and Hearn, S.J. 1997, 'Interaction between chemical reactions and mixing on various scales', *Chemical Engineering Science*, vol. 52, no. 4, pp457-466.

Bard, Y. 1974, *Nonlinear parameter estimation*, Academic Press, New York.

Barresi, A. and Baldi, G. 1987, 'Solid dispersion in an agitated vessel', *Chemical Engineering Science,* vol. 42, no. 12, pp2949-2956.

Barthole, J.P., Maisonneuve, J., Gence, D., David, R., Mathieu, J. and Villermaux, J. 1982, 'Measurement of mass transfer rates, velocity and concentration fluctuations in an industrial stirred tank', *Chemical Engineering Fundamentals*, vol. 1, no. 1, pp17-26.

Batterham, R.J., Hall, J.S. and Barton, G. 1981, 'Pelletizing kinetics and simulation of full scale balling circuit', in the proceedings of the *3rd International Symposium on Agglomeration*, Nümberg, West Germany, A136-150.

Becker, G.W. and Larson, M.A. 1969, 'Mixing effects in continuous crystallization', *Chemical Engineering Progress Symposium Series*, vol. 65, no. 95, pp14-23.

Beigler, L.T., Damiano, J.J. and Blau, G.E. 1986, 'Nonlinear parameter estimation: A case study comparison', *AIChE Journal*, vol. 32, pp29-45.

Bermingham, S.K., Kramer, H.J.M. and van Rosmalen, G.M. 1998, 'Towards on-scale crystalliser design using compartmental models', *Computers Chemical Engineering*, vol. 22, Supplementary, ppS335-S362.

Bermingham, S.K., Neumann, A.M., Verheijen, P.J.T. and Kramer, H.J.M. 1999, 'Measuring and modelling the classification and dissolution of fine crystals in a DTB crystalliser', in the proceedings of the *14th International Symposium on Industrial Crystallisation*, Cambridge, UK, paper 62.

Berry, E.X. 1967, 'Cloud droplet growth by collection', *Journal of Atmospheric Science*, vol. 24, pp688-701.

Bertrand, J., Couderc, J.P. and Angelino, H. 1980, 'Power consumption, pumping capacity and turbulence intensity in baffled stirred tanks: comparison between several turbines', *Chemical Engineering Science*, vol. 35, pp2157-2163.

Bhatia, S.K. and Chakraborty, D. 1992, 'Modified MWR approach: Application to agglomerative precipitation', *AIChE Journal*, vol.38, no. 6, pp868-878.

Bird, R.B., Stewart, W.E. and Lightfoot, E.N. 1960, *Transport phenomena*, John Wiley and Sons, New York.

Bohlin, M. and Rasmuson, A.C. 1996, 'Importance of macromixing in batch cooling crystallization', *AIChE Journal*, vol. 42, no. 3, pp691-699.

Bourne, J.R. 1983, 'Mixing on the molecular scale (micromixing)', *Chemical Engineering Science*, vol. 38, no. 1, pp5-8.

Bourne, J.R. and Dell'ava, P. 1987, 'Micro- and macro-mixing in stirred tank reactors of different sizes', *Chemical Engineering Research and Design*, vol. 65, pp180-186.

Bourne, J.B. and Tovstiga, G. 1988, 'Micromixing and fast chemical reactions in a turbulent tubular reactor', *Chemical Engineering Research and Design,* vol. 66, pp26-32.

Bourne, J.R., Gholap, R.V. and Rewatkar, V.B. 1995, 'The influence of viscosity on the product distribution of fast parallel reactions', *Chemical Engineering Journal and the Biochemical Engineering Journal*, vol. 58, no. 1, pp15-20.

Bramley, A.S., Hounslow, M.J. and Ryall, R.L. 1996, 'Aggregation during precipitation from solution: A method for extracting rates from experimental data', *Journal of Colloid and Interface Science*, vol. 183, pp155-165.

Brodkey, R.S. 1981, 'Fundamentals of turbulent motion, mixing and kinetics', *Chemical Engineering Communications*, vol. 8, pp1-23.

Brown, N. 1972a, 'Crystal growth and nucleation of aluminium trihydroxide from seeded caustic aluminate solutions', *Journal of Crystal Growth*, vol. 12, pp39-45.

Brown, N. 1972b, 'Secondary nucleation of aluminium hydroxide in seeded caustic aluminate solutions', *Journal of Crystal Growth*, vol. 16, pp163-169.

Brown, N. 1975, 'A quantitative study of new crystal formation in seeded caustic aluminate solutions', *Journal of Crystal Growth*, vol. 29, pp309-315.

Brown, N. 1977, 'Secondary nucleation of aluminium trihydroxide - Kinetics and mechanism', in *Light metals 1977*, ed. K.B. Higbie, The Metallurgical Society of AIME, New York, vol. 2, pp1-14.

Brucato, A. and Rizzuti, L. 1988, 'The application of the network-of-zones model to solid-liquid suspensions', in the proceedings of the 6^{th} *European Conference on Mixing*, Pavia, Italy, pp273-280.

Budz, J., Jones, A.G. and Mullin, J.W. 1987, 'On the shape-size dependence of potassium sulfate crystals', *Industrial and Engineering Chemistry Research*, vol. 26, pp820-824.

Canning, T.F. and Randolph, A.D. 1967, 'Some aspects of crystallisation theory: Systems that violate McCabe's delta law', *AIChE Journal*, vol.13, no. 1, pp5-10.

Chaubal, M.V. 1990, 'Physical chemistry in aluminium hydroxide precipitation', in *Light metals 1990*, ed. C.M. Bickert, The Minerals, Metals and Materials Society, Pennsylvania, pp85-94.

Chen, J.F., Zheng, C. and Chen, G.T. 1996, 'Interaction of macro- and micromixing on particle size distribution in reactive precipitation', *Chemical Engineering Science,* vol. 51, no. 10, pp1957-1966.

Chistyakova, A.A. 1964, 'Some data on the system Na_2O-Al_2O_3-H_2O', *Tsvetnye Metally*, vol. 37, no. 9, pp58-63.

Clontz, N.A. and McCabe, W.L. 1971, 'Contact nucleation of magnesium sulfate heptahydrate', *AIChE Symposium Series*, vol. 67, no. 111, pp15-34.

Cornell, R.M., Pannett, D.S., Sullivan, N.S., Clake, P.C. and Bailey, C.M. 1999, 'Precipitation of gibbsite: Development of a new rate equation', in the proceedings of the 5^{th} *International Aluminium Quality Workshop*, Bunbury, Australia, vol. 1, pp153-161.

Corrsin, S. 1964, 'The isotropic turbulent mixer: Part II. Arbitrary Schmidt number', *AIChE Journal*, vol. 10, no. 6, pp870-877.

Costa, P. and Trevissoi, C. 1972, 'Reactions with non-linear kinetics in partially segregated fluids', *Chemical Engineering Science*, vol. 27, pp2041-2054.

Curl, R.L. 1963, 'Dispersed phase mixing: I. Theory and effects in simple reactors', *AIChE Journal*, vol. 9, no. 2, pp175-181.

Danckwerts, P.V. 1953, 'Continuous flow systems', *Chemical Engineering Science*, vol. 2, no. 1, pp1-13.

Danckwerts, P.V. 1958, 'The effect of incomplete mixing on homogeneous reactions', *Chemical Engineering Science*, vol. 8, pp93-102.

David, R. and Villermaux, J. 1987, 'Interpretation of micromixing effects on fast consecutive-competing reactions in semi-batch stirred tanks by a simple interaction model', *Chemical Engineering Communications*, vol. 54, pp333-352.

David, R., Marchal, P., Klein, J.P. and Villermaux, J. 1991, 'Crystallisation and precipitation engineering. III. A discrete formulation of the agglomeration rate of crystals in a crystallisation process', *Chemical Engineering Science*, vol. 46, no. 1, pp205-213.

David, R., Marchal, O. and Marcant, B. 1995, 'Modelling of agglomeration in industrial crystallization from solution', *Chemical Engineering Technology*, vol. 18, pp302-309.

Derksen, J. and van den Akker, H.E.A. 1999, 'Large eddy simulations on the flow driven by a rushton turbine', *AIChE Journal*, vol. 45, no. 2, pp209-221.

Drake, R.L. 1972, 'A general mathematical survey of the coagulation equation', in *Topics in current aerosol research*, Part 2, ed. G.M. Hidy, and J.R. Brock, Pergammon Press, New York.

Dudczak, J. 1994, 'A modified network-of-zones model of mixing', *Chemical Engineering Research and Design,* vol. 72, no. A5, pp651-656.

Dutta, A. and Tarbell, J.M. 1989, 'Closure models for turbulent reacting flows', *AIChE Journal*, vol. 35, no. 12, pp2013-2027.

Eggels, J.G.M. 1996, 'Direct and large-eddy simulation of turbulent fluid flow using the lattice-Boltzmann scheme', *International Journal of Heat and Fluid Flow*, vol. 17, pp307-323.

Einenkel, W.-D. 1980, 'Influence of physical properties and equipment design on the homogeneity of suspensions in agitated vessels', *German Chemical Engineering*, vol. 3, pp118-124.

Farrell, R.J. and Tsai, Y.C. 1994, 'Modelling, simulation and kinetic parameter estimation in batch crystallization processes', *AIChE Journal*, vol. 40, no. 4, pp586-593.

Felton, P.G. and Brown, D.J. 1980, 'Measurement of crystal growth by laser light diffraction', *Institution of Chemical Engineers Symposium Series*, vol. 59, pp7:1/1-7:1/9.

Fournier, M.-C., Falk, L. and Villermaux, J. 1996a, 'A new parallel competing reaction system for assessing micromixing efficiency – Experimental approach', *Chemical Engineering Science*, vol. 51, no. 22, pp5053-5064.

Fournier, M.-C., Falk, L. and Villermaux, J. 1996b, 'A new parallel competing reaction system for assessing micromixing efficiency – Determination of micromixing time by a simple mixing model', *Chemical Engineering Science*, vol. 51, no. 23, pp5187-5192.

Fox, R.O. 1992, 'Computation of turbulent reactive flow: First principles macro/micro-mixing models using probability density function models', *Chemical Engineering Science*, vol. 47, no. 9-11, pp2853-2858.

Fox, R.O. 1998, 'On the relationship between Lagrangian micromixing models and computational fluid dynamics', *Chemical Engineering and Processing,* vol. 37, no. 6, pp521-535.

Freij, S., Lee, M.Y., Reyhani, M. and Parkinson, G.M. 1999, 'Investigation of the growth of gibbsite crystals by atomic force microscopy and optical microscopy', in the proceedings of the *5th International Aluminium Quality Workshop*, Bunbury, Australia, vol. 1, pp41-50.

Gale, D.J., Rohl, A.L., Watling, H.R. and Parkinson, G.M. 1998, 'Theoretical investigation of the nature of aluminium-containing species present in alkaline solution', *Journal of Physical Chemistry B*, vol. 102, pp10372-10382.

Garside, J. 1971, 'The concept of effectiveness factors in crystal growth', *Chemical Engineering Science*, vol. 26, pp1425-1431.

Garside, J., Phillips, V.R. and Shah, M.B. 1976, 'On size-dependent crystal growth', *Industrial and Engineering Chemistry Fundamentals*, vol. 15, no. 3, pp 230-233.

Garside, J. 1979, 'The growth of small crystals', in *Industrial Crystallisation 78*, ed. E.J. de Jong, and S.J. Jancic, North-Holland Publishing Company, Amsterdam, pp143-151.

Garside, J. and Shah, M.B. 1980, 'Crystallisation kinetics from MSMPR crystallisers', *Industrial and Engineering Chemistry. Process Design and Development*, vol. 19, pp509-514.

Garside, J., Gibilaro, L.G. and Tavare, N.S. 1982, 'Evaluation of crystal growth kinetics from a desupersaturation curve using initial derivatives', *Chemical Engineering Science,* vol. 37, no. 11, pp1625-1628.

Garside, J. and Tavare, N.S. 1985, 'Mixing, reaction and precipitation: Limits of micromixing in an MSMPR crystallizer', *Chemical Engineering Science*, vol. 40, no. 8, pp1485-1493.

Gelbard, F.M. and Seinfeld, J.H. 1978a, 'Numerical solution of the dynamic equation for particulate systems', *Journal of Computational Physics*, vol. 28, pp357-375.

Gelbard, F.M. and Seinfeld, J.H. 1978b, 'Coagulation and growth of a multi-component aerosol', *Journal of Colloid and Interface Science*, vol. 63, no. 3, pp472-479.

Gelbard, F.M., Tambour, Y. and Seinfeld, J.H. 1980, 'Sectional representations for simulating aerosol dynamics', *Journal of Colloid and Interface Science*, vol. 76, no. 2, pp541-556.

Ginsberg, H., Huttig, W. and Stiehl, H. 1962, 'The system H_2O-Al_2O_3. II. The formation of crystalline $Al(OH)_3$ and the conversion of bayerite to hydragrillite', *Zeitschrift fur Inorganische und Allgemeine Chemie*, vol. 318, pp238-256.

Girolami, M.W. and Rousseau, R.W. 1985, 'Size-dependent crystal growth - A manifestation of growth rate dispersion in the potassium alum-water system', *AIChE Journal*, vol. 31, no. 11, pp1821-1828.

Glastonbury, J.R. 1969, 'Nature of sodium aluminate solution', *Chemistry and Industry*, vol. 169, no. 1, pp121-125.

Halfon, A. and Kaliaguine, S. 1976a, 'Alumina trihydrate crystallization Part 1: Secondary nucleation and growth kinetics', *The Canadian Journal of Chemical Engineering*, vol. 54, pp160-167.

Halfon, A. and Kaliaguine, S. 1976b, 'Alumina trihydrate crystallization Part 2: A model of agglomeration', *The Canadian Journal of Chemical Engineering*, vol. 54, pp168-172.

Harris, D.R., Keir, R.I., Prestidge, C.A. and Thomas, J.C. 1999, 'A dynamic light scattering investigation of nucleation and growth in supersaturated alkaline sodium aluminate solutions (synthetic Bayer liquors)', *Colloids and Surfaces A-Physicochemical and Engineering Aspects*, vol. 154, no. 3, pp343-352.

Hartel, R.W. and Randolph, A.D. 1986a, 'Mechanisms and kinetic modelling of calcium oxalate crystal aggregation in urine-like liquors, part 1: Mechanisms', *AIChE Journal*, vol. 32, pp1176-1185.

Hartel, R.W. and Randolph, A.D. 1986b, 'Mechanisms and kinetic modelling of calcium oxalate crystal aggregation in urine-like liquors, part 2: Kinetic Modelling', *AIChE Journal*, vol. 32, pp1186-1195.

Helt, J.E. and Larson, M.A. 1977, 'Effect of temperature on the crystallisation of potassium nitrate by direct measurement of supersaturation', *AIChE Journal*, vol. 23, no. 6, pp822-830.

Hiby, J.W. 1981, 'Definition and measurement of the degree of mixing in liquid mixtures', *International Chemical Engineering*, vol. 21, no. 2, pp197-204.

Hill, P.J. and Ng, K.M. 1996, 'New discretization procedure for the agglomeration equation', *AIChE Journal*, vol. 42, no. 3, pp727-741.

Hollander, E.D., Derksen, J.J., Bruinsma, O.S.L., van den Akker, H.E.A. and van Rosmalen, G.M. 1999, 'A numerical study on the coupling of hydrodynamics and agglomeration', in the proceedings of the *14th International Symposium on Industrial Crystallisation*, Cambridge, UK, paper 16.

Hostomsky, J. and Jones, A.G. 1991, 'Calcium carbonate crystallization, agglomeration and form during continuous from solution', *Journal of Physics D: Applied Physics*, vol. 24, pp165-170.

Hostomsky, J. and Jones, A.G. 1993, 'Modelling and analysis of agglomeration during precipitation from solution', in the proceeding of the *12th Symposium on Industrial Crystallisation*, vol.1, Warsaw, Poland, pp2-037-2-042.

Hounslow, M.J., Ryall, R.L. and Marshall, V.R. 1988, 'A discretized population balance for nucleation, growth and aggregation', *AIChE Journal*, vol. 34, no. 11, pp1821-1832.

Hounslow, M.J. 1990a, 'A discretized population balance for continuous systems at steady state', *AIChE Journal*, vol. 36, no. 1, pp106-116.

Hounslow, M.J. 1990b, 'Nucleation, growth and aggregation rates from steady-state experimental data', *AIChE Journal*, vol. 36, no. 11, pp106-116.

Hounslow, M.J. 1990c, 'A discretized population balance for nucleation, growth and aggregation', *PhD Thesis*, University of Adelaide, Australia.

Hulburt, H.M. and Katz, S. 1964, 'Some problems in particle technology: A statistical mechanical formulation', *Chemical Engineering Science*, vol. 19, pp555-574.

Ilievski, D., Zheng, S.G. and White, E.T. 1989, 'Induction times for growth in seeded supersaturated caustic aluminate solutions', in the proceedings of the *17th Australasian Conference on Chemical Engineering* (*Chemeca 89*), Gold Coast, Australia, pp1012-1019.

Ilievski, D. 1991, 'Modelling $Al(OH)_3$ agglomeration during batch and continuous precipitation in supersaturated caustic aluminate solutions', *PhD Thesis*, University of Queensland, Australia.

Ilievski, D., White, E.T. and Hounslow, M.J. 1993, 'Agglomeration mechanism identification case study: $Al(OH)_3$ agglomeration during precipitation from seeded supersaturated caustic aluminate solutions', in the proceedings of the *6th International Symposium on Agglomeration*, Nagoya, Japan.

Ilievski, D. and White, E.T. 1994a, 'Agglomeration during precipitation: Agglomeration mechanism identification for $Al(OH)_3$ crystals in stirred caustic aluminate solutions', *Chemical Engineering Science*, vol. 49, pp3227-3239.

Ilievski, D. and White, E.T. 1994b, 'Agglomeration mechanisms in $Al(OH)_3$ crystallization from caustic aluminate solutions', in the proceedings of the *1st Particle Technology Forum*, Denver, New York, pp305-310.

Ilievski, D. and Hounslow, M.J. 1995, 'Agglomeration during precipitation: II. Mechanism deduction from tracer data', *AIChE Journal*, vol. 41, pp525-535.

Ilievski, D. and White, E.T. 1995, 'Agglomeration during precipitation: I. Tracer crystals for $Al(OH)_3$ precipitation', *AIChE Journal*, vol. 41, pp518-524.

Ilievski, D. and White, E.T. 1996, 'Methods for estimating the kinetics of precipitation systems', in *Emerging Separation Technologies for Metals II*, ed. R.G. Bautista, The Minerals, Metals and Materials Society, pp299-314.

Ilievski, D., McShane, J. and Rudman, M., 1997, CSIRO Minerals internal report DMR–570.

Ilievski, D., Rudman, M., Bedell, D., Metcalfe, G. and Cukrov, L. 1998, CSIRO Minerals internal report DMR–693.

Ilievski, D., Rudman, M. and Metcalfe, G. 1999, 'The separate roles of shear rate and mixing on gibbsite precipitation', in the proceedings of the *14th International Symposium on Industrial Crystallisation*, Cambridge, UK, paper 15.

Ilievski, D. 2000, 'Development of a constant supersaturation semi-batch crystalliser and its application to investigating agglomeration', submitted to *Journal of Crystal Growth*.

Jager, J., de Wolf, S., Kramer, H.J.M. and de Jong, E.J. 1991, 'Estimation of nucleation kinetics from crystal size distribution transients of a continuous crystalliser', *Chemical Engineering Science*, vol. 46, no. 3, pp807-818.

King, W.R. 1973, 'Some studies in alumina trihydrate precipitation kinetics', *Light Metals*, vol. 2, pp551-563.

Knysh, P. and Mann, R. 1984, 'Utility of interconnected networks of backmixed zones to represent mixing in a closed stirred vessel', *Institution of Chemical Engineers Symposium Series*, no. 89, pp127-145.

Koh, P.T.L. 1984, 'Compartmental modelling of stirred tank for flocculation requiring a minimum critical shear rate', *Chemical Engineering Science*, vol. 39, no. 12, pp1759-1764.

Koh, P.T.L., Andrews, J.R.G. and Uhlherr, P.H.T. 1984, 'Flocculation in stirred tanks', *Chemical Engineering Science*, vol. 39, no. 6, pp975-985.

Koh, P.T.L., Andrews, J.R.G. and Uhlherr, P.H.T. 1987, 'Modelling shear-flocculation by population balances', *Chemical Engineering Science*, vol. 42, no. 2, pp353-362.

Kuipers, J.A.M. and van Swaaij, W.P.M. 1998, 'Computational fluid dynamics applied to chemical reaction engineering', *Advances in Chemical Engineering*, vol. 24, pp227-328.

Kumar, S. and Ramkrishna, D. 1996a, 'On the solution of population balance equations by discretization- I. A fixed pivot technique', *Chemical Engineering Science*, vol. 51, no. 8, pp311-1332.

Kumar, S. and Ramkrishna, D. 1996b, 'On the solution of population balance equations by discretization- II. A moving pivot technique', *Chemical Engineering Science*, vol. 51, no. 8, pp1333-1342.

Kumar, S. and Ramkrishna, D. 1997, 'On the solution of population balance equations by discretization- III. Nucleation, growth and aggregation of particles', *Chemical Engineering Science,* vol. 52, no.24, pp4659-4679.

Kuzmanić, N. and Rušić, D. 1999, 'Solids concentration measurements of floating particles suspended in a stirred vessel using sample withdrawal techniques', *Industrial and Engineering Chemistry Research,* vol. 38, no. 7, pp2794-2802.

Kuznetsov, S.I. 1963, 'New view of the nature of aluminate solutions', *Tsvetnye Metally*, vol. 36, pp45-52.

Landgrebe, J.D. and Pratsinis, S.E. 1990, 'A discrete-sectional model for powder production by gas-phase chemical reaction and aerosol coagulation in the free-molecular regime', *Journal of Colloid and Interface Science*, vol. 139, no. 1, pp63-86.

Lee, H.W. and Saleeby, E.G. 1994, 'Mathematical behaviour of the population balance of a MSMPRC with agglomeration, feed and size-dependent growth rate', *Computers and Chemical Engineering*, vol.18, no. 10, pp.899-907.

Lee, K.W. 1983, 'Change of particle size distribution during Brownian coagulation', *Journal of Colloid and Interface Science*, vol. 92, no. 2, pp315-325.

Lee, M.Y., Parkinson, G.M., Smith, P.G., Lincoln, F.J. and Reyhani, M.M. 1997, 'Characterization of aluminium trihydroxide crystals precipitated from caustic solutions', *ACS Symposium Series*, no. 667, pp123-133.

Lee, M.Y. and Parkinson, G.M. 1999, 'Growth rates of gibbsite single crystals determined using in situ optical microscopy', *Journal of Crystal Growth*, vol. 199, pp270-274.

Lee, M.Y., Parkinson, G.M. and Tsukamoto, K. 1999, 'The use of rapid dynamic light scattering to investigate the kinetics of gibbsite crystal growth', in the proceedings of the *14th International Symposium on Industrial Crystallisation*, Cambridge, UK, paper 154.

Levenspiel, O. 1972, *Chemical reaction engineering*, 2nd ed., John Wiley and Sons, New York.

Li, T.S., Livk, I. and Ilievski, D. 2000a, 'The Influence of crystalliser configuration on the accuracy and precision of gibbsite crystallisation kinetics estimates', *Chemical Engineering Science*, accepted for publication.

Li, T.S., Livk, I. and Ilievski, D. 2000b, 'Influence of the estimation procedure on the accuracy and precision of aluminium trihydroxide crystallisation kinetics from dynamics data', *Industrial and Engineering Chemistry Research*, accepted for publication.

Li, T.S., Rohl, A.L. and Ilievski, D. 2000, 'Modelling non-stationary gibbsite precipitation systems: Sources of error and their propagation', *Chemical Engineering Science*, accepted for publication.

Li, X. and Chen, G. 1996, 'Simplified framework for description of mixing with chemical reactions II. Chemical reactions in the different mixing regions', *Chinese Journal of Chemical Engineering*, vol. 4, no. 4, pp322-332.

Li, X., Chen, G. and Chen, J. 1996, 'Simplified framework for description of mixing with chemical reactions I. Physical picture of micro- and macromixing', *Chinese Journal of Chemical Engineering*, vol. 4, no. 4, pp311-321.

Lippincot, E., Psellos, J. and Tobin, M. 1952, 'The Raman spectra and structures of aluminate and zincate solutions', *Journal of Chemistry and Physics*, vol. 20, p536.

Litster, J.D., Smit, D.J. and Hounslow, M.J. 1995, 'Adjustable discretized population balance for growth and agglomeration', *AIChE Journal*, vol. 41, pp591-603.

Livk, I., Pohar, C. and Ilievski, D. 1999, 'Estimation of batch precipitation kinetics by a simplified differential method', *AIChE Journal*, vol. 45, no. 7, pp1593-1596.

Loh, P.I.W., Ang, H.M. and Kirke, E.A. 1988, 'Secondary nucleation of alumina trihydrate in batch crystalliser', in the proceedings of the *16th Australasian Conference on Chemical Engineering* (*Chemeca 88*), Sydney, Australia, pp304-309.

Low, G.C. 1975, 'Agglomeration effects in aluminium trihydroxide precipitation', *PhD Thesis*, University of Queensland, Australia.

Lui, Y.M. and Thompson, R.W. 1992, 'Analysis of a continuous crystallizer with agglomeration', *Chemical Engineering Science*, vol. 47, pp1897-1901.

MacTaggart, R.S., Nasr-el-din, H.A. and Masliyah, J.H. 1993, 'Sample withdrawal from a slurry mixing tank', *Chemical Engineering Science*, vol. 48, no. 5, pp921-931.

Mann, R. and Mavros, P. 1982, 'Analysis of unsteady tracer dispersion and mixing in a stirred vessel using interconnected networks of ideal flow zones', in the proceedings of the *4th European Conference on Mixing*, Leeuwenhorst, The Netherlands, pp35-47.

Mann, R. 1986, 'Gas-liquid stirred vessel mixers: Towards a unified theory based on networks-of-zones', *Chemical Engineering Research and Design*, vol. 64, pp23-34.

Mann, R. 1993, 'Computational fluid dynamics of mixing in batch stirred vessel used as crystallizers', in the proceedings of the *12th Symposium on Industrial Crystallization*, Warsaw, Poland, vol. 2, pp5-025-5-035.

Mann, R., Ying, P. and Edwards, R.B. 1994, 'Application of 3-D networks-of-zones mixing model to a stirred vessel', *IChemE Symposium Series*, no. 136, pp317-324.

Mann, R., Togatorop, A., Senior, P.R., Graham, P. and Edwards, R.B. 1997, 'Evaluating mixing in stirred reactors by 3-D visualization: Partial Segregation for dual-feed semi-batch operation', *Transactions of the Institution of Chemical Engineers*, vol. 75, pp755-762.

Marchal, P., David, R., Klein, J.P. and Villermaux, J. 1988, 'Crystallization and precipitation engineering: I. An efficient method for solving population balance in crystallization with agglomeration', *Chemical Engineering Science*, vol. 43, no. 1, pp59-67.

McCoy, B.N. and Dewey, J.L. 1982, 'Equilibrium composition of sodium aluminate liquors', in *Light metals 1982*, ed. J.E. Anderson, The Metallurgical Society of AIME, New York, pp173-185.

Mehta, R.V. and Tarbell, J.M. 1983a, 'Four environment model of mixing and chemical reaction: Part I. Model development', *AIChE Journal*, vol. 29, no. 2, pp320-328.

Mehta, R.V. and Tarbell, J.M. 1983b, 'Four environment model of mixing and chemical reaction: Part II. Comparison with experiments', *AIChE Journal*, vol. 29, no. 2, pp329-337.

Mersmann, A. and Kind, M. 1988, 'Chemical engineering aspects of precipitation from solution', *Chemical Engineering Technology*, vol. 11, pp264-276.

Mersmann, A. 1995, *Crystallisation technology handbook*, Marcel Dekker, New York.

Miller, S.M. and Rawlings, J.B. 1994, 'Model identification and control strategies for batch cooling crystallizers', *AIChE Journal*, vol. 40, no. 8, pp1312-1327.

Misra, C. 1970, 'The precipitation of Bayer aluminium trihydroxide', *PhD Thesis*, University of Queensland, Australia.

Misra, C. and White, E.T. 1970, 'A mathematical model of the Bayer precipitation process for alumina production', *Chemeca 70*, Melbourne, Australia, pp52-76.

Misra, C. and White, E.T. 1971a, 'Kinetics of crystallization of aluminium trihydroxide from seeded caustic aluminate solutions', *Chemical Engineering Progress Symposium Series*, vol. 67, no. 110, pp53-65.

Misra, C. and White, E.T. 1971b, 'Crystallization of Bayer aluminium trihydroxide', *Journal of Crystal Growth*, vol. 6, pp172-178.

Moolenaar, R.J., Evans, J.C. and McKeever, L.D. 1970, 'The structure of aluminate ion solutions at high pH', *The Journal of Physical Chemistry*, vol. 74, no. 20, pp3629-3636.

Mordini, J. and Cristol, B. 1982, 'Mathematical model of alumina trihydrate precipitation from Bayer aluminate liquors', in the proceedings of the 4^{th} *Yugoslav International Symposium on Aluminium*, Titograd, Yugoslavia, pp168-185

Muhr, H., Leclerc, J.P., Plasari, E., and Noval-Cattin, F. 1997, 'A rapid method for the determination of growth rate kinetic constant: application to the precipitation of aluminium trihydroxide', *Industrial and Engineering Chemistry Research*, vol. 36, pp675-681.

Mullin, J.W. 1993, *Crystallisation*, 3rd ed., Butterworth-Heinemann, Oxford.

Mumtaz, H.S., Hounslow, M.J., Seaton, N.A. and Paterson, W.R. 1997, 'Orthokinetic aggregation during precipitation: A computational model for calcium oxalate monohydrate', *Transactions of the Institution of Chemical Engineers*, vol. 75, part A, pp152-159.

Muralidar, R. and Ramkrishna, D. 1986, 'An inverse problem in agglomeration kinetics', *Journal of Colloid and Interface Science*, vol. 112, no. 2, pp348-361.

Nagata, S. 1975, *Mixing: Principles and applications*, John Wiley and Sons, New York.

Nallet, V., Mangin, D. and Klein, J.P. 1998, 'Model identification of batch precipitations: Application to salicyclic acid', *Computers and Chemical Engineering*, vol. 22, supplementary, ppS649-652.

Ng, D.Y.C. and Rippin, D.W.T. 1965, 'The effect of incomplete mixing conversion in homogeneous reactions', in the proceedings of the *3rd European Symposium on Chemical Reaction Engineering*, Amsterdam, The Netherlands, pp161-165.

Nicmanis, M. and Hounslow, M.J. 1998, 'Finite-element methods for steady-state population balance equations', *Chemical Engineering Science*, vol. 44, no. 10, pp2258-2272.

Nývlt, J. 1971, *Industrial crystallisation from solutions*, Butterworths, London.

Nývlt, J. and Broul, M. 1982, 'Kinetics exponents in crystallisation and the accuracy of their determination', *International Chemical Engineering*, vol. 22, pp543-548.

Nývlt, J., Söhnel, O., Matuchova, M. and Brool, M. 1985, *Kinetics of industrial crystallisation*, Elsevier Science, Amsterdam.

Okamoto, Y., Nishikawa, M. and Hashimoto, K. 1981, 'Energy dissipation rate distribution in mixing vessels and its effect on liquid-liquid and solid-liquid mass transfer, *International Chemical Engineering,* vol. 21, no. 1, pp88-94.

Oldshue, J.Y. 1983, *Fluid mixing technology*, McGraw-Hill, New York.

Oomes, L.E. de Boer, J.H. and Lippens, B.C. 1961, 'Phase transformation of aluminium hydroxides', in *Reactivity of solids*, ed. J.H. de Boer, Elsevier Publishing Company, Princeton, pp317-320.

Ottino, J.M., Ranz, W.E. and Macosko, C.W. 1979, 'A lamellar model for analysis of liquid-liquid mixing', *Chemical Engineering Science*, vol. 34, pp877-890.

Overbey, T.L. and Scott, C.E. 1978, 'Characterisation of Bayer plant liquors and seeds utilising a mathematical model for precipitation', in *Light metals 1978*, ed. J.J. Miller, The Metallurgical Society of AIME, New York, vol. 2, pp163-178.

Patterson, G.K. 1981, 'Application of turbulence fundamentals to reactor modelling and scaleup', *Chemical Engineering Communications*, vol. 8, pp25-52.

Pearson, T.G. 1955, 'The chemical background to the aluminium industry, lectures, monographs and reports', no. 3, The Royal Institute of Chemistry.

Perron, J. and Larocque, J. 1994, 'Alumina crystalliser mixing using CFD', in *Light Metals 1994*, ed. U. Mannweiler, and J.W. Evans, The Minerals, Metals and Materials Society, Pennsylvania, pp99-105.

Phillips, R., Rohani, S. and Baldyga, J. 1999, 'Micromixing in a single-feed semi-batch precipitation process', *AIChE Journal*, vol. 45, no. 1, pp82-92.

Plasari, E., David, R. and Villermaux, J. 1978, 'Micromixing phenomena in continuous stirred reactors using a Michaelis-Menten reaction in liquid phase', *ACS Symposium Series*, no. 65, pp126-139.

Ploss, R., Tengler, T. and Mersmann, A. 1984, 'Secondary nucleation and crystal growth in continuous cooling crystallizers', in *Industrial crystallisation 84*, ed. S.J. Jancic and E.J. de Jong, Elsevier, Amsterdam, pp271-274.

Pohorecki, R. and Baldyga, J. 1983a, 'The use of a new model of micromixing for determination of crystal size in precipitation', *Chemical Engineering Science*, vol. 38, no. 1, pp79-83.

Pohorecki, R. and Baldyga, J. 1983b, 'New model of micromixing in chemical reactors: II. Application to a stirred tank reactor', *Industrial and Engineering Chemistry Fundamentals*, vol. 22, pp398-405.

Pohorecki, R. and Baldyga, J. 1988, 'The effects of micromixing and the manner of reactor feeding on precipitation in stirred tank reactors', *Chemical Engineering Science*, vol. 43, no. 8, pp1949-1954.

Pulvermacher, B. and Ruckenstein, E. 1974, 'Similarity solutions of population balances', *Journal of Colloid and Interface Science*, vol. 46, no. 3, pp428-436.

Qiu, Y. and Rasmuson, A. 1990, 'Growth and dissolution of succinic acid crystals in a batch stirred crystalliser', *AIChE Journal*, vol. 36, pp665-676.

Qiu, Y. and Rasmuson, A.C. 1991, 'Nucleation and growth of succinic acid in a batch cooling crystalliser', *AIChE Journal*, vol. 37, no. 9, pp1293-1304.

Radnai, T., May P.M., Hefter, G. and Sipos, P. 1998, 'Structure of aqueous sodium aluminate solutions: a solution X-ray diffraction study', *Journal of Physical Chemistry*, vol. 102, no. 40, pp7841-7850.

Ramabhadran, T.E. 1975, 'On the general theory of solid granulation', *Chemical Engineering Science*, vol. 30, pp1027-1033.

Ramabhadran, T.E. and Seinfeld, J.H. 1975, 'Self-preserving theory of particulate systems', *Chemical Engineering Science*, vol. 30, pp1019-1025.

Ramabhadran, T.E., Patterson, T.W. and Seinfeld, J.H. 1976, 'Dynamics of aerosol coagulation and condensation', *AIChE Journal*, vol. 22, no. 5, pp840-851.

Ramkrishna, D. 1973, 'On problem-specific polynomials', *Chemical Engineering Science*, vol. 28, pp1362-1365.

Ramkrishna, D. 1985, 'The status of population balances', *Reviews in Chemical Engineering*, vol. 3, no. 1, pp49-95.

Ranade, V.V. and Bourne, J.R. 1991, 'Reactive mixing in agitated tank', *Chemical Engineering Communications*, vol. 99, pp33-53.

Ranade, V.V. 1992, 'Decoupling of micro- and macromixing in turbulent reacting flow', *AIChE Journal*, vol. 38, no. 3, pp466-470.

Ranade, V.V. 1997, 'An efficient computational model for simulating flow in stirred vessels - A case of Rushton turbine', *Chemical Engineering Science,* vol. 52, no. 24, pp4473-4484.

Randolph, A.D. 1965, 'The mixed-suspension mixed-product removal crystalliser as a concept in crystalliser design', *AIChE Journal*, vol. 11, p423.

Randolph, A.D. and White, E.T. 1977, 'Modelling size dispersion in the prediction of crystal size distribution', *Chemical Engineering Science*, vol. 32, pp1067-1076.

Randolph, A.D., White, E.T. and Low, C.C.D. 1981, 'On-line measurement of fine-crystal response to crystalliser disturbances', *Industrial and Engineering Chemistry. Process Design and Development*, vol. 20, pp496-503.

Randolph, A.D. and Larson, M.A. 1988, *Theory of particulate processes: Analysis and techniques of continuous crystallization*, 2nd ed., Academic Press, New York.

Rawlings, J.B., Witkowski, W.R. and Eaton, J.W. 1992, 'Modelling and control of crystallisers', *Powder Technology*, vol. 69, pp3-9.

Rawlings, J.B., Miller, S.M. and Witkowski, W.R. 1993, 'Model identification and control of solution crystallization processes - A review', *Industrial and Engineering Chemistry Research,* vol. 32, no. 7, pp1275-1296.

Redman, T.P. and Rohani, S. 1994, 'On-line determination of supersaturation of a KCl-NaCl aqueous solution based on density measurement', *The Canadian Journal of Chemical Engineering*, vol. 72, pp64-71.

Remillard, M., Cloutier, L. and Methot, J.C. 1980, 'Crystallisation du tryhidrate d'allumine: effects des conditions d'agitation', *The Canadian Journal of Chemical Engineering*, vol. 58, pp348-356.

Riebel, U., Kofler, V. and Löffler, F. 1990, 'Control of supersaturation in instationary suspension crystallisation', in *Industrial Crystallisation 90*, ed. A. Mersmann, Garmisch-Partenkirchen, FRG, pp595-599.

Ritchie, B.W. and Tobgy, A.H. 1978, 'General population balance modelling of unpremixed feed stream chemical reactors: A review', *Chemical Engineering Communications*, vol. 2, pp249-264.

Ritchie, B.W. and Tobgy, A.H. 1979, 'A three-environment micromixing model for reactors with arbitrary separate feed streams', *The Chemical Engineering Journal*, vol. 17, pp173-182.

Ritchie, B.W. 1980, 'Simulating the effects of mixing on the performance of unpremixed flow chemical reactors', *The Canadian Journal of Chemical Engineering*, vol. 58, pp626-633.

Roach, G.I.D., Cornell, J.B. and Griffin, B.J. 1998, 'Gibbsite growth history – revelations of a new scanning electron microscope technique', in *Light metals 1988*, ed. B. Welch, The Minerals, Metals and Materials Society, Pennsylvania, pp153-158.

Rohani, S. and Baldyga, J. 1987, 'Micromixing described in terms of inertial-convective disintegration of large eddies and viscous-convective interactions among small eddies: II. Semi-batch and continuous stirred tank reactors', *Chemical Engineering Science*, vol. 42, no. 11, pp2611-2619.

Rohani, S. 1993, 'Nucleation, growth and aggregation kinetics of potassium chloride from a continuous mixed-suspension mixed-product removal cooling crystallizer', *Separation Technology*, vol. 3, pp99-105.

Rosenberg, S.P. and Healy, S.J. 1996, 'A thermodynamic model for gibbsite solubility in Bayer liquor', in the proceedings of the *4th International Alumina Quality Workshop*, Darwin, Australia, pp301-310.

Rosensweig, R.E. 1964, 'Idealized theory for turbulent mixing in vessels', *AIChE Journal*, vol. 10, no. 1, pp91- 97.

Rossiter, D.C., Fawell, P.D., Ilievski, D. and Parkinson, G.M. 1998, 'Investigation of the unseeded nucleation of gibbsite, $Al(OH)_3$, from synthetic Bayer liquors', *Journal of Crystal Growth*, vol. 191, pp525-536.

Sahu, A.K., Kumar, P., Patwardhan, A.W. and Joshi, J.B. 1999, 'CFD modelling and mixing in stirred tanks', *Chemical Engineering Science*, vol. 54, no. 12, pp2285-2293.

Sakamoto, K. 1963, 'Mechanism of the decomposition of sodium aluminate solutions', in *The extractive metallurgy of aluminium*, ed. G. Gerard, vol. 1., Interscience Publishers, New York, pp175-189.

Sakamoto, K., Kanehara, M. and Matsushita. 1971, 'Agglomeration of crystalline particles of gibbsite during the precipitation in sodium aluminate solution', *Chemical Engineering Society of Japan*, vol. 35, pp481-487.

Saleeby, E.G. and Lee, H.W. 1994, 'Solution and analysis for crystallisation with agglomeration', *Chemical Engineering Science*, vol.49, no. 12, pp1879-1884.

Saleeby, E.G. and Lee, H.W. 1995, 'On the solution of the PBE with agglomeration and random growth rate dispersion', *Chemical Engineering Science*, vol. 50, no. 12, pp1971-1981.

Sampson, K.J. and Ramkrishna, D. 1985, 'A new solution to the Brownian coagulation equation through the use of root-shifted problem-specific polynomials', *Journal of Colloid and Interface Science*, vol. 103, no. 1, pp245-254.

Sano, Y. and Usui, H. 1987, 'Effects of paddle dimensions and baffle conditions on the interrelations among discharge flow rate, mixing power and mixing time in mixing vessels', *Journal of Chemical Engineering of Japan*, vol. 20, no. 4, pp399-404.

Sastry, K.V.S. 1975, 'Similarity size distribution of agglomerates during their growth by coalescence in granulation or green pelletization', *International Journal of Minerals Processing*, vol. 2, pp187-203.

Sastry, K.V.S. and Gaschignard, P. 1981, 'Discretization procedure for the coalescence equation of particulate processes', *Industrial and Engineering Chemistry Fundamentals*, vol. 20, pp355-361.

Sato, T. 1984, 'Precipitation and crystallization of gelatinous aluminium hydroxide from aqueous solutions', in *Industrial crystallization 84*, ed. S.J. Jancic and E.J. de Jong, Elsevier Science Publishers, Amsterdam, pp385-390.

Schoen, R. and Roberson, C.E. 1970, 'Structures of aluminium hydroxide and geochemical implications', *The American Mineralogist*, vol. 55, pp43-77.

Scott, J. 1963, 'Effect of seed and temperature on the particle size and Bayer hydrate', in *The extractive metallurgy of aluminium*, ed. G. Gerard vol. 1, Interscience Publishers, New York, pp203-218.

Seckler, M.M., Bruinsma, O.S.L. and van Rosmalen, G.M. 1995, 'Influence of hydrodynamics on precipitation: A computational study', *Chemical Engineering Communications*, vol. 135, pp113-131.

Seigneur, C., Hudischewskyj, A.B., Seinfeld, J.H., Whitby, K.T., Whitby, E.R., Brock, J.R. and Barnes, H.M. 1986, 'Simulation of aerosol dynamics: A comparative review of mathematical models', *Aerosol Science and Technology*, vol. 5, pp205-222.

Seyssiecq, I., Vessler, S., Boistelle, R. and Lamérant, J.M. 1998, 'Agglomeration of gibbsite $Al(OH)_3$ crystals in Bayer liquors. Influence of the process parameters', *Chemical Engineering Science*, vol. 53, pp2177-2185.

Sha, Z. and Palosaari, S. 1998, 'Size dependent classification function in imperfectly mixed suspension continuous crystallizer', *Mixing and Crystallization*, ed. B. Sen Gupta, and S. Ibrahim, Kluwer Academic Publishers, Dordrecht, pp133-150.

Sha, Z., Louhi-Kultanen, M., Oinas, P. and Palosaari, S. 1999, 'CFD simulation of size-dependent classification in an imperfectly mixed suspension crystallizer', in the proceedings of the *14th International Symposium on Industrial Crystallisation*, Cambridge, UK, paper 83.

Sharratt, P.N. 1990, 'Computational fluid dynamics and its application in the process industries', *Transactions of the Institution of Chemical Engineers*, vol. 68, pp13-18.

Shiue, S.J. and Wong, C.W. 1984, 'Studies on homogenisation efficiency of various agitators in liquid blending', *The Canadian Journal of Chemical Engineering*, vol. 62, pp602-609.

Singh, P.N. and Ramkrishna, D. 1975, 'Transient solution of the Brownian coagulation equation by problem-specific polynomials', *Journal of Colloid and Interface Science*, vol. 53, no. 2, pp214-223.

Sipos, P., Capewell, S.G., May, P.M., Hefter, G., Laurenczy, G., Lukacs, F. and Roulet, R. 1998, 'Spectroscopic studies of the chemical speciation in concentrated alkaline aluminate solutions', *Journal of the Chemical Society-Dalton Transactions*, no.18, pp3007-3012.

Skidar, S.K. and Randolph, A.D. 1976, 'Secondary nucleation of two fast growth systems in a mixed suspension crystallizer: Magnesium sulfate and citric acid water systems', *AIChE Journal*, vol. 22, no. 1, pp110-117.

Skrtic, D., Markovic, E. and Fuerdi-Milhofev, H. 1984, 'Orthokinetic aggregation of calcium oxylate trihydrate', in *Industrial crystallisation 84*, ed. S.J. Jancic and E.L. de Jong, Elsevier Science Publishers, Amsterdam, pp421-424.

Smit, D.J., Hounslow, M.J. and Paterson, W.R. 1994, 'Aggregation and gelation – I. Analytical solutions for CST and batch operation', *Chemical Engineering Science*, vol. 49, no. 7, pp1025-1035.

Smith, P. and Woods, G. 1993, 'The measurement of very slow growth rates during the induction period in aluminium trihydroxide growth from Bayer liquors', in *Light metals 1993*, ed. S.K. Das, The Minerals, Metals and Materials Society, Pennsylvania, pp113-117.

Smith, P., Austin, P. and Ilievski, D. 1995, 'Modelling the induction period in gibbsite precipitation', in *Light metals 1995*, ed. J. Evans, The Minerals, Metals and Materials Society, Pennsylvania, pp45-49.

Smoluchowski, M.V. 1917, 'Mathematical theory of the kinetics of coagulation of colloidal systems', *Zeitschrift fur Phyikalische Chemie*, vol. 92, pp129-168.

Sowul, L. and Epstein, M.A.F. 1981, 'Crystallisation kinetics of sucrose in a CMSMPR evaporative crystalliser', *Industrial and Engineering Chemistry. Process Design and Development*, vol. 20, no. 2, pp197-203.

Swift, D.L. and Friedlander, S.K. 1964, 'The coagulation of hydrosols by Brownian motion and laminar shear flow', *Journal of Colloid Science*, vol. 19, pp621-647.

Tavare, N.S. and Garside, J. 1982, 'Estimation of crystal growth and dispersion parameters using pulse response techniques in batch crystallisers', *Transactions of the Institution of Chemical Engineers*, vol. 60, pp334-344.

Tavare, N.S., Shah, M.B. and Garside, J. 1985, 'Crystallisation and agglomeration kinetics of nickel ammonium sulphate in an MSMPR crystalliser', *Powder Technology*, vol. 44, pp13-18.

Tavare, N.S. 1986a, 'Crystallisation kinetics from transients of an MSMPR crystalliser', *The Canadian Journal of Chemical Engineering*, vol. 64, pp752-758.

Tavare, N.S. 1986b, 'Mixing in continuous crystallizers', *AIChE Journal*, vol. 32, no. 5, pp705-732.

Tavare, N.S. and Garside, J. 1986, 'Simultaneous estimation of crystal nucleation and growth kinetics from batch experiments', *Chemical Engineering Research and Design*, vol. 64, 109-118.

Tavare, N.S. 1989, 'Limits of micromixing in an MSMPR crystallizer', *Chemical Engineering Technology*, vol. 12, pp1-11.

Tavare, N.S. 1991, 'Batch crystallizers', *Reviews in Chemical Engineering*, vol. 7, pp312-355.

Tavare, N.S. 1992, 'Mixing, reaction and precipitation: Environment micromixing models in continuous crystallizers -I. Premixed feeds', *Computers and Chemical Engineering*, vol. 16, no. 10, pp923-936.

Tavare, N.S. and Patwardhan, A.V. 1992, 'Agglomeration in a continuous MSMPR crystalliser', *AIChE Journal*, vol.38, no. 3, pp377-384.

Tavare, N.S. and Garside, J. 1993, 'Silica precipitation in a semi-batch crystallisation', *Chemical Engineering Research and Design*, vol. 48, pp475-488.

Tavare, N.S. 1994, 'Mixing, reaction and precipitation: An interplay in continuous crystallizers', *Chemical Engineering Science*, vol. 49, no. 24, pp5193-5201.

Tavare, N.S. 1995a, *Industrial crystallisation: process simulation analysis and design*, Plenum Press, New York.

Tavare, N.S. 1995b, 'Mixing, reaction and precipitation: Interaction by exchange with mean micromixing models', *AIChE Journal*, vol. 41, no. 12, pp2537-2548.

Thoma, S., Ranade, V.V. and Bourne, J.R. 1991, 'Interaction between micro- and macromixing during reactions in agitated tanks', *The Canadian Journal of Chemical Engineering*, vol.69, pp1135-1141.

Thompson, P.D. 1968, 'A transformation of the stochastic equation for droplet coalescence', in proceedings of the *International Conference on Cloud Physics*, Toronto, Canada, pp115-125.

Treleaven, C.R. and Tobgy, A.H. 1971, 'Conversion in reactors having separate reactant feed streams', *Chemical Engineering Science*, vol. 26, pp1259-1269.

Treleaven, C.R. and Tobgy, A.H. 1972, 'Monte Carlo methods of simulating micromixing in chemical reactors', *Chemical Engineering Science*, vol. 27, p1479.

van Leeuwen, M.L.J., Bruinsma, O.S.L. and van Rosmalen, G.M. 1996, 'Influence of mixing on the product quality in precipitation', *Chemical Engineering Science*, vol. 51, no. 11, pp2595-2600.

van Leeuwen, M.L.J. 1998, 'Precipitation and mixing', *PhD Thesis*, The Technical University of Delft, The Netherlands.

van Straten, H.A. and De Bruyn, P.L. 1984, 'Precipitation from supersaturated aluminate solutions', *Journal of Colloid and Interface Science*, vol. 102, no. 1, pp260-277.

Veesler, S. and Boistelle, R. 1993, 'About supersaturation and growth rates of hydrargillite $Al(OH)_3$ in alumina caustic solutions', *Journal of Crystal Growth*, vol. 130, pp411-415.

Veesler, S. and Boistelle, R. 1994, 'Growth kinetics of hydrargillite $Al(OH)_3$ from caustic soda solutions', *Journal of Crystal Growth*, vol. 142, pp177-183.

Veesler, S., Roure, S. and Boistelle, R. 1994, 'General concepts of hydrargillite $Al(OH)_3$ agglomeration', *Journal of Crystal Growth*, vol. 135, pp505-512.

Villermaux, J. and Devillon, J.C. 1972, 'Representation de la coalescence et de la redispersion. Les domaines de segragation dans un fluide par un modele d'interaction phenomenologique', in the proceedings of the 2^{nd} *International Symposium on Chemical Reactions Engineering*, Amsterdam, The Netherlands.

Villermaux, J. 1983, 'Mixing in chemical reactors', *ACS Symposium Series*, no. 266, pp136-186.

Villermaux, J. and David, R. 1983, 'Recent advances in the understanding of micromixing phenomena in stirred reactors', *Chemical Engineering Communications*, vol. 21, pp105-122.

Villermaux, J. 1991, 'Mixing effects on complex chemical reactions in a stirred reactor', *Reviews in Chemical Engineering*, vol. 7, no. 1, pp51-108.

Vivaldolima, E., Wood, P.E., Hamielec, A.E. and Penlidis, A. 1998, 'Calculation of the particle size distribution in suspension polymerization using a compartment-mixing model', *The Canadian Journal of Chemical Engineering*, vol. 76, no. 3, pp495-505.

Wakao, H., Hiraguchi, H. and Ishii, T. 1987, 'A simulation of crystallisation from aqueous supersaturated solutions in a batch isothermal stirred tank', *Chemical Engineering Journal*, vol. 35, no. 7, pp169-178.

Wang, C.S. and Friedlander, S.K. 1967, 'The self-preserving size distribution for coagulation by Brownian motion', *Journal of Colloid and Interface Science*, vol. 24, pp170-179.

Wang, Y.D. and Mann, R. 1992, 'Partial segregation in stirred batch reactors: Effect of scale-up on the yield of a pair of competing reactions', *Transactions of the Institution of Chemical Engineers*, vol. 70, pp282-290.

Wang, Z.K., Zeng, Q.S. and Qian, R.Y. 1989, 'Precise determination of supersaturation by temperature float method', *AIChE Journal*, vol. 35, no. 4, pp679-682.

Watling, H.R., Fleming, S.D., van Bronswijk, W. and Rohl, A.L. 1998, Ionic structure in caustic aluminate solutions and the precipitation of gibbsite', *Journal of Chemical Society-Dalton Transactions*, pp3911-3917.

Watts, H.L. and Utley, D.W. 1956, 'Sodium gluconate as a complexing agent in the volumetric analysis of aluminium compounds', *Analytical Chemistry*, vol. 28, pp1731-1735.

Wei, H.Y., Garside, J. and Mann, R. 1996, 'Simulation of mixing and precipitation in a batch crystallizer using the network-of zones model', in the proceedings of the *13th International Symposium on Industrial Crystallization*, Toulouse, France, vol. 2, pp669-674.

Wei, H.Y. and Garside, J. 1997, 'Application of CFD modelling to precipitation systems', *Transactions of the Institution of Chemical Engineers*, vol. 75, pp219-227.

White, E.T. 1971, *Industrial crystallization, course notes - Industrial Crystallization Workshop*, University of Queensland, Australia.

White, E.T. and Wright, P.G. 1971, 'Magnitude of size dispersion effects in crystallisation', *Chemical Engineering Progress Symposium Series*, vol. 67, no. 110, pp81-87.

White, E.T. 1988, 'The effect of precipitation conditions on alumina quality', in the proceedings of the *3rd International Aluminium Quality Workshop*, Gladstone, Australia.

White, E.T. and Bateman, S.H. 1988, 'Effect of caustic concentration on growth rate of $Al(OH)_3$ particles', in *Light Metals 1988*, ed. L.G. Boxall, The Metallurgical Society Inc., Pennsylvania, pp257-162.

Wu, H. and Patterson, G.K. 1989, 'Laser-doppler measurements of turbulent-flow parameters in a stirred mixer', *Chemical Engineering Science*, vol. 44, no. 10, pp2207-2221.

Wu, J., Bandopadhayay, P.C., Pullum, L. and Shepherd, I. 1998, 'Fluid dynamics analysis and scale modelling of mixing and agitating vessels', in the proceedings of the *26th Australasian Chemical Engineering Conference* (*Chemeca 98*), Port Douglas, Australia, paper 153.

Wulkow, M., Gerstlauer, A. and Nieken, U. 1999, 'Modelling and simulation of crystallization process using PARSIVAL', in the proceedings of the *14th International Symposium on Industrial Crystallisation*, Cambridge, UK, paper 7.

Wynn, E.J.W. 1996, 'Improved accuracy and convergence of discretized population balance of Litster et al.', *AIChE Journal*, vol. 42, pp2084-2086.

Wynn, E.J.W., Hounslow, M.J. and Ilievski, D. 1998, 'Micromixing of solids and fluid in an aggregating precipitator', *Chemical Engineering Science*, vol. 53, no. 12, pp2187-2194.

Yokota, M. and Kubota, N. 1996, 'Apparent size-dependent growth of potash alum crystals by agglomeration', *AIChE Journal*, vol. 42, no. 4, pp1170-1173.

Yokota, M., Sato, A. and Kubota, N. 2000, 'A simple method for evaluating kinetic parameters in non-isothermal batch crystallisation', *Chemical Engineering Science*, vol. 55, pp717-722.

Zámbó, J. 1986, 'Structure of sodium aluminate liquors; molecular model of the mechanisms of their decomposition', in *Light Metals 1986*, ed. R.E. Miller, The Metallurgical Society Inc., Pennsylvania, pp199-215.

Zhou, G. and Kresta, S. 1996, 'Impact of tank geometry on the maximum turbulence energy dissipation rate for impellers', *AIChE Journal*, vol. 42, no. 9, pp2476-2490.

Zumstein, R.C. and Rousseau, R.W. 1987a, 'Growth rate dispersion by initial growth rate distributions and growth rate fluctuations', *AIChE Journal*, vol. 33, no. 1, pp121-129.

Zumstein, R.C. and Rousseau, R.W. 1987b, 'Utilisation of industrial data in the development of a model for crystalliser simulation', *AIChE Symposium Series*, vol. 83, no. 253, pp130-139.

Zwietering, T.N. 1958, 'Suspending of solid particles in liquid by agitators', *Chemical Engineering Science*, vol. 8, pp244-253.

Zwietering, T.N. 1959, 'The degree of mixing in continuous flow systems', *Chemical Engineering Science*, vol. 11, no. 1, pp1-15.

APPENDIX 1: DERIVATION OF THE ANAYTICAL SOLUTIONS BY THE METHOD OF MOMENTS

1. MSMPR System

In an unseeded steady state MSMPR precipitation system involving simultaneous agglomeration, growth and nucleation, the resulting zeroth moment equation of the PBE can be shown to be:

$$\frac{1}{2}\beta\mu_0^2 + \frac{\mu_0}{\tau} - B^o = 0 \qquad \text{(A1.1)}$$

The solution to Equation (A1.1) can be found by evaluating the roots of the quadratic equation, which yields

$$\mu_0 = \frac{-\frac{1}{\tau} \pm \sqrt{\left(\frac{1}{\tau}\right)^2 + 2\beta B^o}}{\beta} \qquad \text{(A1.2)}$$

However, only one of the roots is feasible, which can be simplified to give,

$$\mu_0 = \frac{\sqrt{1 + 2\beta B^o \tau^2} - 1}{\beta\tau} \qquad \text{(3.28)}$$

2. Dynamic Systems

In a batch system with agglomeration and growth occurring, the zeroth moment form of the PBE is

$$\frac{d\mu_0}{dt} = -\frac{1}{2}\beta\mu_0^2 \qquad \text{(3.30)}$$

For a time invariant agglomeration kernel, the analytical solution to Equation (3.30) can be found with the initial condition, $\mu_0(t)\big|_{t=0} = \mu_0(0)$, i.e. the total seed crystal number, using the method of separation of variables, as shown

$$\int_{\mu_0(0)}^{\mu_0(t)} \frac{d\mu_0}{\mu_0^2} = -\frac{1}{2}\beta \int_0^t dt \tag{A1.3}$$

which gives

$$-\frac{1}{\mu_0}\Bigg|_{\mu_0(0)}^{\mu_0(t)} = -\frac{1}{2}\beta t \tag{A1.4}$$

and yields

$$\frac{1}{\mu_0(t)} = \frac{1}{\mu_0(0)} + \frac{1}{2}\beta t \tag{3.33}$$

In the case of simultaneous agglomeration, growth, and nucleation taking place in a batch system, the zeroth moment equation becomes

$$\frac{d\mu_0}{dt} = B^o - \frac{1}{2}\beta\mu_0^2 \tag{3.32}$$

For the special case of time-invariant agglomeration kernel and nucleation rate in Equation (3.32), the analytical solution can be evaluated as follows,

$$\int_{\mu_0(0)}^{\mu_0(t)} \frac{d\mu_0}{B^o - \frac{1}{2}\beta\mu_0^2} = \int_0^t dt \tag{A1.5}$$

The above integral involves rational fraction, which can be decomposed into two partial fraction terms as

$$\frac{1}{B^o - \frac{1}{2}\beta\mu_0^2} = \frac{A}{\left(\sqrt{B^o} + \sqrt{\frac{1}{2}\beta}\mu_0\right)} + \frac{B}{\left(\sqrt{B^o} - \sqrt{\frac{1}{2}\beta}\mu_0\right)} \tag{A1.6}$$

Clearing the fraction terms in Equation (A1.6), i.e. cross-multiplying both sides with the denominator term on the left hand side of Equation (A1.6),

$$1 = A\left(\sqrt{B^o} - \sqrt{\tfrac{1}{2}\beta}\mu_0\right) + B\left(\sqrt{B^o} + \sqrt{\tfrac{1}{2}\beta}\mu_0\right) \tag{A1.7}$$

Equating the coefficients of the like power of μ_0, and gives

$$A\sqrt{B^o} + B\sqrt{B^o} = 1 \tag{A1.8a}$$

$$-A\sqrt{\frac{\beta}{2}} + B\sqrt{\frac{\beta}{2}} = 0 \tag{A1.8b}$$

By solving equations (A1.8a) and (A1.8b) simultaneously yields

$$A = B = \frac{1}{2\sqrt{B^o}} \tag{A1.9}$$

Hence, Equation (A1.5) becomes

$$\frac{1}{2\sqrt{B^o}} \int_{\mu_0(0)}^{\mu_0(t)} \frac{1}{(\sqrt{B^o} + \sqrt{\tfrac{1}{2}\beta}\mu_0)} + \frac{1}{(\sqrt{B^o} - \sqrt{\tfrac{1}{2}\beta}\mu_0)} d\mu_0 = \int_0^t dt \tag{A1.10}$$

which gives

$$\frac{1}{\sqrt{2B^o\beta}} \left[\ln \frac{\sqrt{B^o} + \sqrt{\frac{\beta}{2}}\mu_0}{\sqrt{B^o} - \sqrt{\frac{\beta}{2}}\mu_0} \right]_{\mu_0(0)}^{\mu_0(t)} = t \tag{A1.11}$$

and

$$\left[\ln \frac{\sqrt{B^o} + \sqrt{\frac{\beta}{2}}\mu_0}{\sqrt{B^o} - \sqrt{\frac{\beta}{2}}\mu_0} \right] - \left[\ln \frac{\sqrt{B^o} + \sqrt{\frac{\beta}{2}}\mu_0(0)}{\sqrt{B^o} - \sqrt{\frac{\beta}{2}}\mu_0(0)} \right] = \sqrt{2B^o\beta}\, t \tag{A1.12}$$

Rearranging Equation (A1.12) gives

$$\frac{\sqrt{B^o} + \sqrt{\frac{\beta}{2}}\mu_0}{\sqrt{B^o} - \sqrt{\frac{\beta}{2}}\mu_0} = \kappa \exp\left(\sqrt{2B^o\beta}\, t\right) \tag{A1.13}$$

where

$$\kappa = \frac{\sqrt{B^o} + \sqrt{\frac{\beta}{2}}\mu_0(0)}{\sqrt{B^o} - \sqrt{\frac{\beta}{2}}\mu_0(0)} \tag{A1.14}$$

Cross-multiplying Equation (A1.14) yields

$$\sqrt{B^o} + \sqrt{\frac{\beta}{2}}\mu_0 = \kappa \exp\left(\sqrt{2B^o\beta}\, t\right)\left(\sqrt{B^o} - \sqrt{\frac{\beta}{2}}\mu_0\right) \tag{A1.15}$$

and collect the coefficient of the term μ_0 gives

$$\mu_0(t) = \sqrt{\frac{2B^o}{\beta}}\left(\frac{\kappa \exp\left(\sqrt{2B^o\beta}t\right) - 1}{1 + \kappa \exp\left(\sqrt{2B^o\beta}t\right)}\right) \tag{3.34}$$

Checking the validity of Equation (3.34) with initial condition, $t = 0$, and $\mu_0 = \mu_0(0)$, gives

$$\begin{aligned}
\mu_0(0) &= \sqrt{\frac{2B^o}{\beta}}\left(\frac{\kappa - 1}{1 + \kappa}\right) \\
&= \sqrt{\frac{2B^o}{\beta}}\left(\frac{\sqrt{B^o} + \sqrt{\frac{\beta}{2}}\mu_0(0) - \sqrt{B^o} + \sqrt{\frac{\beta}{2}}\mu_0(0)}{\sqrt{B^o} - \sqrt{\frac{\beta}{2}}\mu_0(0)}\right)\left(\frac{\sqrt{B^o} - \sqrt{\frac{\beta}{2}}\mu_0(0)}{\sqrt{B^o} - \sqrt{\frac{\beta}{2}}\mu_0(0) + \sqrt{B^o} + \sqrt{\frac{\beta}{2}}\mu_0(0)}\right) \\
&= \sqrt{\frac{2B^o}{\beta}}\left(\frac{2\sqrt{\frac{\beta}{2}}\mu_0(0)}{2\sqrt{B^o}}\right) \\
&= \mu_0(0)
\end{aligned} \tag{A1.16}$$

As $t \to \infty$, Equation (3.34) becomes

$$\mu_0(t)\big|_{t\to\infty} \approx \sqrt{2B^o/\beta} \tag{3.36}$$

APPENDIX 2: COMPUTER CODE - BATCH PRECIPITATION KINETICS ESTIMATION

This computer code is written for estimating batch gibbsite precipitation kinetics from experimental data using the method of Bramley, Hounslow & Ryall (1996). The algorithms coded to evaluate the system of linear equations are adopted from Atkinson, Harley & Hudson (1989).

Coder: Tian S. Li
Programming Language: Visual Basic

```
'-----------------------------------------------------------------------------------------------------

Option Explicit

Dim a(1 To 5, 1 To 5), b(1 To 5), u(1 To 5), v(1 To 5) As Double
Dim n, Status As Integer

'-----------------------------------------------------------------------------------------------------

Sub Kinesti()

Dim i, j, k, lm, Neqn, p, q, S(1 To 10), Sq, z As Integer
Dim c, d, r, denom, B1, B2, B3, B4, D1, D2, Phi0, Phi1, Phi2, Phi3 As Double
Dim agg(1 To 50, 1 To 50), L(1 To 50), y(1 To 50) As Double
Dim dN1, dmu0, dmu3 As Double

'-----------------------------------------------------------------------------------------------------
'
'           Variables Declaration
'
'
'a( )                    n x n matrix element
'b( )                    vector contains the RHS of the kinetics estimation equations
'agg( )                  agglomeration kernel
'B?, D?                  birth and death terms used to evaluate the coefficients Phi0
'c,d,r                   parameters used to evaluate the coefficients Phi2 and Phi3
'denom, p, S( ), Sq, z   parameter used to evaluate the coefficients Phi0
'dmu0                    derivative of zeroth moment
'dmu3                    derivative of third moment
'dN1                     derivative of number in the first size interval
'L( )                    crystal size
'n                       dimension of the n x n matrix
'Neqn                    number of size intervals
'Phi?                    coefficients in the kinetics estimation equations
'q                       parameter used to determine the discretised size ratio
'u( )                    vector contains the kinetic parameter estimates
'v( )                    intermediate vector used to evaluate the system of linear equations
'y( )                    experimental crystal numbers in each size interval
'-----------------------------------------------------------------------------------------------------
```

```
    n = 3
    q = 2
    Neqn = 27

  For k = 1 To 7
      Phi0 = 0
      Phi1 = 0
      Phi2 = 0

'-----------------'
' Read data       '
'-----------------'

      For i = 1 To Neqn
        L(i) = Worksheets("Ratio").Range("AT6").Offset(i, 0)
        y(i) = Worksheets("Ratio").Range("AU6").Offset(i, k)
      Next i

      dmu0 = Worksheets("Ratio").Range("BF4").Offset(k, 0)
      dN1 = Worksheets("Ratio").Range("BH4").Offset(k, 0)
      dmu3 = Worksheets("Ratio").Range("BJ4").Offset(k, 0)

'-----------------------------------------'
' Evaluate agglomeration kernel           '
'-----------------------------------------'

      For i = 1 To Neqn
        For j = 1 To Neqn
          agg(i, j) = 1#
        Next j
      Next i

'-------------------------------------------------------------'
' Evaluate the coefficients Phi0, Phi1, Phi2 and Phi3         '
'-------------------------------------------------------------'

'-------------------------------------------------------------------------------------------------------------------

     For z = 1 To q
        S(z) = Int(1 - q * Log(1 - 2 ^ (-z / q)) / Log(2))
     Next z

     Sq = S(1)
     denom = 2# ^ (1 / q) - 1#

     For i = 1 To Neqn
       B1 = 0#
       If (i - Sq >= 1) Then
         For j = 1 To i - Sq
           B1 = B1 + agg(i - 1, j) * y(i - 1) * y(j) * (2# ^ ((j - i + 1) / q)) / denom
         Next j
       End If

       B2 = 0#
       For p = 2 To q
         lm = i - S(p - 1)
         If (lm >= 1) Then
           For j = lm To i - S(p)
             B2 = B2 + agg(i - p, j) * y(i - p) * y(j) *(2# ^ ((j - i + 1) / q) - 1# + _
             2# ^ (-(p - 1) / q)) / denom
```

```
            Next j
          End If
        Next p
        B3 = 0#
        If (i - q >= 1) Then
          B3 = 0.5 * agg(i - q, i - q) * y(i - q) ^ 2#
        End If

        B4 = 0#
        For p = 1 To q - 1
          lm = i + 1 - S(p)
          If (lm >= 1) Then
            For j = lm To i + 1 - S(p + 1)
              B4 = B4 + agg(i - p, j) * y(i - p) * y(j) * (-2# ^ ((j - i) / q) + 2# ^ (1 / q) _
              - 2# ^ -(p / q)) / denom
            Next j
          End If
        Next p

        D1 = 0#
        If (i - Sq + 1 >= 1) Then
          For j = 1 To i - Sq + 1
            D1 = D1 + agg(i, j) * y(i) * y(j) * (2# ^ ((j - i) / q)) / denom
          Next j
        End If

        D2 = 0#
        If (i - Sq + 2 >= 1) Then
          lm = i - Sq + 2
        Else
          lm = 1
        End If

        For j = lm To Neqn
          D2 = D2 + agg(i, j) * y(i) * y(j)
        Next j

        Phi0 = Phi0 + B1 + B2 + B3 + B4 - D1 - D2

      Next I

'-------------------------------------------------------------------------------------------------------------

      For j = 1 To Neqn
        Phi1 = Phi1 - y(1) * agg(1, j) * y(j)
      Next j

'-------------------------------------------------------------------------------------------------------------

      r = 2# ^ (1# / 6#)
      c = r / (r ^ 2# - 1#)
      d = 2# / (1# + r) / L(1)

      Phi2 = d * ((1 - r * c) * y(1) - c * y(2))

'-------------------------------------------------------------------------------------------------------------

      Phi3 = d * ((1 - r * c) * y(1) - c * y(2)) * 2 ^ (1 / (2 * q)) * L(1) ^ 3
```

```
      For i = 2 To Neqn
         d = 2# / (1# + r) / L(i)
         Phi3 = Phi3 + d * (c * y(i - 1) + y(i) - c * y(i + 1)) * 2 ^ (1 / (2 * q)) * L(i) ^ 3
      Next i
'-------------------------------------------------------------------------------------------------------------------

'-------------------------------------'
' Assemble the n x n matrix    '
'-------------------------------------'

      a(1, 1) = Phi0
      a(1, 2) = 0
      a(1, 3) = 1
      a(2, 1) = 0
      a(2, 2) = Phi3
      a(2, 3) = 2 ^ (1 / (2 * q)) * L(1) ^ 3
      a(3, 1) = Phi1
      a(3, 2) = Phi2
      a(3, 3) = 1

      b(1) = dmu0
      b(2) = dmu3
      b(3) = dN1

'-----------------------------------'
' Calling solver routines    '
'-----------------------------------'

      Call LUDEC(n, a, Status)

          If Status = 1 Then MsgBox "LUDEC fails"

      Call LUSOL(n, a, b, Status, u)

'---------------------'
' Print results    '
'---------------------'

          If Status = 1 Then
             MsgBox " LUSOL fails"
          Else
             Worksheets("Ratio").Range("BL30").Offset(k, 0).Value = phi0
             Worksheets("Ratio").Range("BL30").Offset(k, 1).Value = phi1
             Worksheets("Ratio").Range("BL30").Offset(k, 2).Value = phi2
             Worksheets("Ratio").Range("BL30").Offset(k, 3).Value = phi3

             Worksheets("ratio").Range("BD30").Offset(k, 0).Value = u(1)
             Worksheets("ratio").Range("BD30").Offset(k, 1).Value = u(2)
             Worksheets("ratio").Range("BD30").Offset(k, 2).Value = u(3)
          End If
Next k

End Sub

'
'-------------------------------------------------------------------------------------------------------------------

' This subroutine decomposes the n x n matrix into upper and lower triangular matrices

'
'-------------------------------------------------------------------------------------------------------------------
```

```
Function LUDEC(n, a, Status)

  Dim i, j, k As Integer
  Dim Mult, Pivot As Double

  For i = 1 To n - 1
    Pivot = a(i, i)
    If (Abs(Pivot) > 0.000000000000001) Then
      For k = i + 1 To n
        If (Abs(a(k, i)) > 0.000000000000001) Then
          Mult = a(k, i) / Pivot
          a(k, i) = Mult
          For j = i + 1 To n
            a(k, j) = a(k, j) - Mult * a(i, j)
          Next j
        Else
          a(k, i) = 0
        End If
      Next k
    Else
      Status = 1
      GoTo 40
    End If
  Next i
  Status = 0
40  End Function

'
'-------------------------------------------------------------------------

' This subroutine evaluates the unknown parameters from the upper and lower triangular
' matrices by forward and backward substitutions
'
'-------------------------------------------------------------------------

Function LUSOL(n, a, b, Status, u)

  Dim i, j As Integer
  Dim Sum As Double

  If (Abs(a(n, n)) > 0.000000000000001) Then
    Status = 0

    v(1) = b(1)

    For i = 2 To n
      Sum = b(i)
      For j = 1 To i - 1
        Sum = Sum - a(i, j) * v(j)
      Next j
      v(i) = Sum
    Next i

    u(n) = v(n) / a(n, n)

    For i = n - 1 To 1 Step -1

      Sum = v(i)
      For j = i + 1 To n
        Sum = Sum - a(i, j) * u(j)
      Next j
      u(i) = Sum / a(i, i)
```

```
    Next i
  Else
    Status = 1
  End If

End Function
'
```

REFERENCE

Atkinson, L.V., Harley, P.J. and Hudson, J.D. 1989, *Numerical methods with FORTRAN 77: A practical introduction*, Addison-Wesley Publishing Company, Wokingham.

APPENDIX 3: COMPUTER CODE - BATCH PRECIPITATOR MODEL

This computer code is written for predicting CSD in batch gibbsite precipitation system using the DPB models of Hounslow and Litster. This code can be easily modified for other precipitator configurations.

Coder: Tian S. Li
Programming Language: Visual Basic

```
'
'-------------------------------------------------------------------------------------
Option Explicit

  Dim agg(1 To 100, 1 To 100), d(1 To 100), Bu, cn, cp, G, ka, kb, kg, mu2, x, _
      y(1 To 100), yp(1 To 100) As Double
  Dim Mtd, Neqn As Integer
'
'-------------------------------------------------------------------------------------
Sub BModel()

  Dim beta, co, dy(1 To 100), ENT, h, k1(1 To 100), k2(1 To 100), k3(1 To 100), k4(1 To 100), _
      kc1, kc2, kc3, kc4, MNT, SSE, xe, xf, xi, xo, ye(1 To 100), yn(1 To 100), yo(1 To 100) _
      As Double
  Dim i, i1, i2, j, k, ni, Ndata, Nsize, Nstep As Integer

'-------------------------------------------------------------------------------------
'
'                Variables Declaration
'
'agg( ),beta     agglomeration kernel (mL/hr)
'Bu              source term rate (apparent nucleation rate) (/mL/ hr)
'co              concentration difference (g/L Al2O3)
'cn, cp          calculated concentration difference (g/L Al2O3)
'd( )            particle size (microns)
'G               growth rate (microns/hr)
'h               time step (hr)
'k?( ), kc?      parameters used in RK4 method
'ka              agglomeration rate constant
'kb              nucleation rate constant
'kg              growth rate constant
'mu2             second moment of the CSD
'Ndata           number of data
'Neqn            number of equation
'Nstep           number of time step
'SSE             sum of squares error; dy( ), ENT, MNT are parameters used in SSE evaluation
'x               time (hr)
'xf              final time (min)
'xe, xi          initial time (min)
'xo              simulation time duration (hr)
'yo              seed number within size range (/mL)
'ye              observed number within size range (/mL)
'yn              calculated number within size range (/mL)
'y, yp           parameters used in RK4
'-------------------------------------------------------------------------------------
```

```
'--------------------'
'  Input Data      '
'--------------------'

   Mtd = 2          '(1 for Two-term growth; any number for Three-term growth)
   ni = 1           '(number of simulation steps indicator)
   Ndata = 85
   h = 0.01

'--------------------'
'  Read Data       '
'--------------------'

   co = Worksheets("Batch").Range("BI75").Offset(0, 0)
   ka = Worksheets("Batch").Range("BI75").Offset(0, 1)
   kg = Worksheets("Batch").Range("BI75").Offset(0, 2)
   kb = Worksheets("Batch").Range("BI75").Offset(0, 3)

   xi = Worksheets("Batch").Range("C5").Offset(0, ni)
   x = xi / 60#

   For i = 1 To Ndata
        d(i) = Worksheets("Batch").Range("B5").Offset(i, 0)
       yo(i) = Worksheets("Batch").Range("C5").Offset(i, ni)
     If d(i) = 0# Then Exit For
   Next i

   Nsize = i - 1

   For i = Nsize + 1 To Ndata
       d(i) = d(i - 1) * 2# ^ (1# / 18#)
     yo(i) = 0#
   Next i

   For k = 1 To 4 - ni
     For i = 1 To Ndata
          d(i) = Worksheets("Batch").Range("B5").Offset(i, 0)
         ye(i) = Worksheets("Batch").Range("B5").Offset(i, k + ni + 1)
       If d(i) = 0# Then Exit For
     Next i

     Nsize = i - 1
     For i = Nsize + 1 To Ndata
        d(i) = d(i - 1) * 2# ^ (1# / 18#)
        ye(i) = 0#
     Next i

     xe = Worksheets("Batch").Range("B5").Offset(0, k + ni)
     xf = Worksheets("Batch").Range("B5").Offset(0, k + ni + 1)
     xo = (xf - xe) / 60#

    Nstep = Int(xo / h + 0.1)
    Neqn = Ndata

    For i = 1 To Neqn
        Worksheets("Batch").Range("K5").Offset(i, k).Value = ye(i)
    Next i
```

```
'-------------------------------------------------------------------------'
' Evaluate the derivatives using the fourth order R-K method             '
'-------------------------------------------------------------------------'

    For j = 1 To Nstep

'---------------------------------'
' Evaluate kinetics rates         '
'---------------------------------'

        G = kg * co^2
        Bu = kb * co ^ 2
        beta = ka * co ^ 4

        'OR

        'Insert expressions for Agglomeration, growth and nucleation kinetics

'-----------------------------------------------'
' Assigning agglomeration kernel                '
'-----------------------------------------------'

      For i1 = 1 To Neqn
        For i2 = 1 To Neqn
          agg(i1, i2) = beta
        Next i2
      Next i1

'-----------------------------------'
' Calling the solver routine        '
'-----------------------------------'

      Call f(x, yo, co)
          kc1 = h * cp
           cn = co + kc1 / 2#
          For i = 1 To Neqn
              k1(i) = h * yp(i)
              yn(i) = yo(i) + k1(i) / 2#
          Next i

      Call f(x + h / 2#, yn, cn)
          kc2 = h * cp
           cn = co + kc2 / 2#
          For i = 1 To Neqn
              k2(i) = h * yp(i)
              yn(i) = yo(i) + k2(i) / 2#
          Next i

      Call f(x + h / 2#, yn, cn)
          kc3 = h * cp
           cn = co + kc3
          For i = 1 To Neqn
              k3(i) = h * yp(i)
             yn(i) = yo(i) + k3(i)
          Next i

      Call f(x + h, yn, cn)
          kc4 = h * cp
          For i = 1 To Neqn
              k4(i) = h * yp(i)
```

```
            Next i

        x = x + h

        For i = 1 To Neqn
            cn = co + (kc1 + 2# * kc2 + 2# * kc3 + kc4) / 6#
            co = cn
            yn(i) = yo(i) + (k1(i) + 2# * k2(i) + 2# * k3(i) + k4(i)) / 6#
            yo(i) = yn(i)
        Next i
      Next j

'-----------------------------------------------'
' Evaluate sum of squares error, SSE  '
'-----------------------------------------------'

      ENT = 0#
      MNT = 0#
      For i = 1 To Neqn
        ENT = ENT + ye(i)
        MNT = MNT + yn(i)
      Next i

      SSE = 0#
      For i = 1 To Neqn
        dy(i) = (ye(i) / ENT - yn(i) / MNT) ^ 2
        SSE = SSE + dy(i)
      Next i

'-------------------'
' Print Results  '
'-------------------'

      Worksheets("Batch").Range("T5").Offset(0, k).Value = x * 60#
      Worksheets("Batch").Range("T6").Offset(0, k).Value = cn

      For i = 1 To Neqn
        Worksheets("Batch").Range("K5").Offset(i, 0).Value = d(i)
        If yn(i) < 0 Then yn(i) = 0#
        Worksheets("Batch").Range("T5").Offset(i, k).Value = yn(i)
      Next i

      Worksheets("Batch").Range("T95") = "SSE"
      Worksheets("Batch").Range("T95").Offset(0, k) = SSE

  Next k

End Sub

'-------------------------------------------------------------------------------

This subroutine evaluates the DPB equations using the methods of Hounslow, Marshall
& Ryall (1988) and Wynn (1996).
'
-------------------------------------------------------------------------------

Function f(x, y, cn) As Double

  Dim a, b, r, denom, B1, B2, B3, B4, D1, D2, ya(1 To 100), yg(1 To 100) As Double
  Dim i, j, k, lm, p, q, S(1 To 10), Sq As Integer
```

```
'
'-----------------------------------------------------------------------------'
'  Calculate agglomeration terms using the method of Wynn (1996)  '
'-----------------------------------------------------------------------------'

  q = 6

  For k = 1 To q
    S(k) = Int(1 - q * Log(1 - 2 ^ (-k / q)) / Log(2))
  Next k

  Sq = S(1)
  denom = 2# ^ (1 / q) - 1#

  For i = 1 To Neqn

    B1 = 0#
    If (i - Sq >= 1) Then
      For j = 1 To i - Sq
        B1 = B1 + agg(i - 1, j) * y(i - 1) * y(j) * (2# ^ ((j - i + 1) / q)) / denom
      Next j
    End If

    B2 = 0#
    For p = 2 To q
      lm = i - S(p - 1)
      If (lm >= 1) Then
        For j = lm To i - S(p)
          B2 = B2 + agg(i - p, j) * y(i - p) * y(j) * (2# ^ ((j - i + 1) / q) - 1# + _
               2# ^ (-(p - 1) / q)) / denom
        Next j
      End If
    Next p

    B3 = 0#
    If (i - q >= 1) Then
      B3 = 0.5 * agg(i - q, i - q) * y(i - q) ^ 2#
    End If

    B4 = 0#
    For p = 1 To q - 1
      lm = i + 1 - S(p)
      If (lm >= 1) Then
        For j = lm To i + 1 - S(p + 1)
          B4 = B4 + agg(i - p, j) * y(i - p) * y(j) * (-2# ^ ((j - i) / q) + 2# ^ (1 / q) _
               - 2# ^ -(p / q)) / denom
        Next j
      End If
    Next p

    D1 = 0#
    If (i - Sq + 1 >= 1) Then
      For j = 1 To i - Sq + 1
        D1 = D1 + agg(i, j) * y(i) * y(j) * (2# ^ ((j - i) / q)) / denom
      Next j
    End If

    D2 = 0#
```

```
      If (i - Sq + 2 >= 1) Then
        lm = i - Sq + 2
      Else
        lm = 1
      End If

      For j = lm To Neqn
        D2 = D2 + agg(i, j) * y(i) * y(j)
      Next j

      ya(i) = B1 + B2 + B3 + B4 - D1 - D2

    Next i

'-------------------------------------------------------------------------------------------------------'
'  Calculate growth terms using the method of Hounslow, Ryall & Marshall (1988)  '
'-------------------------------------------------------------------------------------------------------'

    r = 2# ^ (1# / 18#)

    For i = 1 To Neqn
      If y(i) < 0.000000000000001 Then y(i) = 0#
    Next i

    If Mtd = 1 Then

'-----------------------------------'
'  Two-term growth model  '
'-----------------------------------'

      a = G / (r - 1#) / d(1)
      yg(1) = -a * y(1)

      For i = 2 To Neqn
        a = G / (r - 1#) / d(i)
        yg(i) = a * (r * y(i - 1) - y(i))
      Next

    Else

'-------------------------------------'
'  Three-term growth model  '
'-------------------------------------'

      b = r / (r ^ 2# - 1#)
      a = 2# * G / (1# + r) / d(1)

      yg(1) = a * ((1# - r * b) * y(1) - b * y(2))

      For i = 2 To Neqn - 1
        a = 2# * G / (1# + r) / d(i)
        yg(i) = a * (b * y(i - 1) + y(i) - b * y(i + 1))
      Next i

      a = 2# * G / (1# + r) / d(Neqn)
      yg(Neqn) = a * (b * y(Neqn - 1) + y(Neqn))

    End If
```

```
'-------------------------------------------------------------------------------------------------'
' Summation of all contributions to the change in crystal numbers in a size interval '
'-------------------------------------------------------------------------------------------------'

   For i = 1 To Neqn
      If i = 1 Then
         yp(1) = ya(1) + yg(1) + Bu
      Else
         yp(i) = ya(i) + yg(i)
      End If
   Next i

'---------------------------------------'
' Evaluate solute mass balance '
'---------------------------------------'

   mu2 = 0#
   For i = 1 To Neqn
        mu2 = mu2 + 2 ^ (1 / 6) * d(i) ^ 2 * y(i)
   Next i

   cp = -2420 * 3.1416 * 0.654 * kg*cn^2 * mu2 / 2 / 10 ^ 12

End Function

'
```

APPENDIX 4: DERIVATION OF THE ANAYTICAL SOLUTION FOR A CONSTANT SIZE INDEPENDENT AGGLOMERATION PBE

The PBE for a constant supersaturation semi-batch system with size independent agglomeration kernel is

$$\frac{\partial n}{\partial t} = B_A - D_A \tag{6.2}$$

The analytical solution to this equation with the seed CSD of

$$n_{seed} = \frac{N_o}{v_o}\exp\left(-\frac{v}{v_o}\right) \tag{6.3}$$

is shown by Gelbard and Seinfeld (1978a) to be

$$n = \frac{4N_o}{v_o(\tau+2)^2}\exp\left(-\frac{2v/v_o}{\tau+2}\right) \tag{6.4}$$

where N_o is the seed numbers, v_o is the mean seed size (in volume) and $\tau = N_o\beta t$, is the dimensionless time. Integrating Equation (6.4) from v_i to $2^{1/q}v_i$,

$$\int_{v_i}^{2^{1/q}v_i} \frac{4N_o}{v_o(\tau+2)^2}\exp\left(-\frac{2v/v_o}{\tau+2}\right)\,dv \tag{A4.1}$$

Applying the following integration rule for exponential function;

$$\int_0^{\infty} f'(x)\exp(f(x))\,dx = \exp(f(x)) \tag{A4.2}$$

i.e.

$$f(v) = \frac{2v}{v_o(\tau+2)}; \quad f'(v) = \frac{2}{v_o(\tau+2)} \tag{A4.3}$$

Substituting Equation (A4.3) into Equation (A4.1) gives

$$\frac{2N_o}{(\tau+2)} \int_{v_i}^{2^{1/q}v_i} \exp(-f(v)) \quad dv \tag{A4.4}$$

and yields

$$\frac{2N_o}{\tau+2}\left[-\exp(-f(v))\right]_{v_i}^{2^{1/q}v_i} \tag{A4.5}$$

Hence, the number N_i, within size interval v_i to v_{i+1} is

$$N_i = \frac{2N_o}{\tau+2}\left[\exp\left(-\frac{2v_i/v_o}{\tau+2}\right) - \exp\left(-\frac{2^{\alpha}v_i/v_o}{\tau+2}\right)\right] \tag{A4.6}$$

where $\alpha = 1+1/q$.

Noting that

$$\tilde{L}_i^3 = \frac{v_i}{v_o} = \left(\frac{k_v L_i^3}{k_v L_o^3}\right) = \left(\frac{L_i}{L_o}\right)^3 \tag{A4.7}$$

where $\tilde{L}_i$ is the dimensionless length.

Substituting Equation (A4.7) into Equation (A4.6) gives

$$N_i = \frac{2N_o}{\tau+2}\left[\exp\left(-\frac{2\tilde{L}_i^3}{\tau+2}\right) - \exp\left(-\frac{2^{\alpha}\tilde{L}_i^3}{\tau+2}\right)\right] \tag{6.5}$$

APPENDIX 5: DERIVATION OF THE ANAYTICAL SOLUTION FOR A CONSTANT SIZE INDEPENDENT GROWTH PBE

The PBE for the constant supersaturation, semi-batch system with size independent growth only is

$$\frac{\partial n}{\partial t} = -G\frac{\partial n}{\partial L} \tag{6.6}$$

That a solution of the form of

$$n = f(L - Gt) \tag{6.7}$$

satisfies Equation (6.6) can be demonstrated as follows.

Taking the derivative w.r.t time, t, in Equation (6.6), gives

$$\frac{\partial n}{\partial t} = \frac{\partial n}{\partial f}\cdot\frac{\partial f}{\partial t} = \frac{\partial n}{\partial f}\cdot -G = -G\frac{\partial n}{\partial f} \tag{A5.1}$$

Similarly, taking the derivative w.r.t size, L, in Equation (6.6), yields

$$\frac{\partial n}{\partial L} = \frac{\partial n}{\partial f}\cdot\frac{\partial f}{\partial L} = \frac{\partial n}{\partial f}\cdot 1 = \frac{\partial n}{\partial f} \tag{A5.2}$$

Substituting equations (A5.1) and (A5.2) into Equation (6.6) gives

$$-G\frac{\partial n}{\partial f} = -G\frac{\partial n}{\partial f} \tag{A5.3}$$

Hence, $n = f(L - Gt)$ is solution to the Equation (6.6).

For the following seed density function,

$$n = \begin{cases} 0 & L \le Gt \\ \dfrac{\gamma N_o}{L_o}\left(\dfrac{L-Gt}{L_o}\right)^{\gamma-1} \exp\left(-\left(\dfrac{L-Gt}{L_o}\right)^{\gamma}\right) & L > Gt \end{cases} \tag{6.9}$$

where N_o is the total seed crystal numbers and L_o is the seed mean size. γ defines the seed CSD form, i.e. $\gamma = 1$ for the exponential function and $\gamma = 3$ for the bell-shaped Weibull function, respectively. Integrating Equation (6.9) from L_i to L_{i+1},

$$\int_{L_i}^{L_{i+1}} \frac{\gamma N_o}{L_o}\left(\frac{L-Gt}{L_o}\right)^{\gamma-1} \exp\left(-\left(\frac{L-Gt}{L_o}\right)^{\gamma}\right) dL \tag{A5.4}$$

Applying the integration rule for exponential function given in Equation (A4.2) by letting

$$f(L) = \left(\frac{L-Gt}{L_o}\right)^{\gamma} \; ; \quad f'(L) = \frac{\gamma}{L_o}\left(\frac{L-Gt}{L_o}\right)^{\gamma-1} \tag{A5.5}$$

and substituting into Equation (A5.4) and integrating yields

$$-N_o \exp\left(-\left(\frac{L-Gt}{L_o}\right)^{\gamma}\right)\Bigg|_{L_i}^{L_{i+1}} \tag{A4.6}$$

Note that to $L_{i+1} = r\,L_i$. The number, N_i, within size interval of L_i to L_{i+1} at any time instant, t, is

$$N_i = \begin{cases} 0 & L_i \le Gt \\ N_o\left[\exp\left(-\left(\dfrac{L_i-Gt}{L_o}\right)^{\gamma}\right) - \exp\left(-\left(\dfrac{rL_i-Gt}{L_o}\right)^{\gamma}\right)\right] & L_i > Gt \end{cases} \tag{6.10}$$

APPENDIX 6: DERIVATION OF THE GROWTH ADJUSTMENT TERM

In a non-nucleating, non-agglomerating batch precipitation system with size independent growth, the growth shifts the CSD laterally by ΔL over time Δt, and the variance of the CSD remains constant. White (1971) developed a technique to estimate this lateral shift using the moments of the PBE. The change in the third moment with time, for a size independent growth only system is

$$\frac{d\mu_3'}{dt} = 3G\mu_2' \tag{6.11}$$

where $'$ denotes the normalised moment. The normalised second moment, μ'_2, can be expressed in terms of the distribution variance, σ^2 and the mean μ'_1 as

$$\mu_2' = \sigma^2 + \mu_1'^2 \tag{6.12}$$

and the growth rate can be expressed as

$$G = \frac{d\mu_1'}{dt} = \frac{d\overline{L}}{dt} \tag{A6.1}$$

Rearranging equations (6.11), (6.12) and (A6.1) yields

$$\frac{d\mu_3'}{dt} = 3(\sigma^2 + \overline{L}^2)\frac{d\overline{L}}{dt} \tag{A6.2}$$

Applying the product rule of differentiation,

$$\frac{df}{dx} = \frac{df}{dy} \cdot \frac{dy}{dx} \tag{A6.3}$$

i.e.

$$\frac{d(3\sigma^2\overline{L}+\overline{L}^3)}{dt} = 3(\sigma^2+\overline{L}^2)\frac{d\overline{L}}{dt} \tag{A6.4}$$

For σ^2 = constant, Equation (A6.2) becomes

$$\frac{d\mu_3'}{dt} = \frac{d(3\sigma^2\overline{L}+\overline{L}^3)}{dt} \tag{A6.5}$$

Integrating Equation (A6.5) from the time t - Δt to t,

$$\int_{t-\Delta t}^{t} \frac{d\mu_3'}{dt}\,dt = \int_{t-\Delta t}^{t} \frac{d(3\sigma^2\overline{L}+\overline{L}^3)}{dt}\,dt \tag{A6.6}$$

and yields

$$\Delta\mu_3' = \Delta(3\sigma^2\overline{L}+\overline{L}^3) \tag{A6.7}$$

Using finite difference approximation, Equation (A6.7) becomes

$$\begin{aligned}
\Delta\mu'_3 &= 3\sigma^2\overline{L}+\overline{L}^3\Big|_{\overline{L}-\Delta L}^{\overline{L}} \\
&= 3\sigma^2\overline{L}+\overline{L}^3-(3\sigma^2(\overline{L}-\Delta L)+(\overline{L}-\Delta L)^3) \\
&= 3\sigma^2\Delta\overline{L}+\overline{L}^3-(\overline{L}^3-3\Delta L\overline{L}^2+3\Delta L^2\overline{L}-\Delta L^3) \\
&= 3(\mu_2'-\overline{L}^2)\Delta L-(-3\Delta L\overline{L}^2+3\Delta L^2\overline{L}-\Delta L^3) \\
&= 3\mu_2'\Delta L-3\Delta L^2\overline{L}+\Delta L^3 \\
&= 3\mu_2'\Delta L-3\mu_1'\Delta L^2+\Delta L^3
\end{aligned} \tag{A6.8}$$

where $\Delta\mu_3' = \mu_3'\big|_t - \mu_3'\big|_{t-\Delta t}$, is the change in the third moment and $\mu_1' = \overline{L}$.

Hence, the expression for the growth adjustment term ΔL becomes

$$\Delta\mu_3' = \Delta L^3 - 3\mu_1'\Delta L^2 + 3\mu_2'\Delta L \tag{6.13}$$

The growth adjustment term ΔL can be determined by finding the roots of the cubic equation (6.13). The details of evaluating the roots of the cubic equation provided below are extracted from Beyer (1981);

The cubic equation

$$x^3 + bx^2 + cx + d = 0 \tag{A6.9}$$

can be reduced to

$$y^3 + py + q = 0 \tag{A6.10}$$

by substituting

$$x = y - \frac{b}{3} \tag{A6.11}$$

where

$$p = \frac{1}{3}(3c - b^2) \text{ and } q = \frac{1}{27}(27d - 9bc + 2b^3) \tag{A6.12}$$

The roots of the cubic equation (A6.10) are

$$\begin{aligned} y_1 &= A + B, \\ y_2 &= -\frac{(A+B)}{2} + \sqrt{-3}\frac{(A-B)}{2}, \\ y_3 &= -\frac{(A+B)}{2} - \sqrt{-3}\frac{(A-B)}{2} \end{aligned} \tag{A6.13}$$

where

$$A = \sqrt[3]{-\frac{q}{2} + \sqrt{R}}, \quad B = -\sqrt[3]{\frac{q}{2} + \sqrt{R}}, \quad \text{and} \quad R = \left(\frac{q}{2}\right)^2 + \left(\frac{p}{3}\right)^3 \tag{A6.14}$$

If b, c and d are all real, then,

If $R > 0$, there will be 1 real root and 2 conjugate complex roots;

If $R = 0$, there will be 3 real roots and at least 2 are equal;

If $R < 0$, there will be 3 real and unequal roots.

Hence, for the cubic equation (6.13),

$$p = 3(\mu_2' - \mu_1'^2), \tag{A6.15}$$

$$q = (-\Delta\mu_3' + 3\mu_1'\mu_2' - 2\mu_1'^3), \tag{A6.16}$$

and

$$R = (\mu_2' - \mu_1'^2)^3 + (-\tfrac{1}{2}\Delta\mu_3' + \tfrac{3}{2}\mu_1'\mu_2' - \mu_1'^3)^2 \tag{A6.17}$$

The growth adjustment term can be evaluated accordingly.

REFERENCE

Beyer, W.H. 1981, *CRC standard mathematical tables*, 27th ed., CRC Press Inc, Florida.

APPENDIX 7: BATCH PRECIPITATION REPRODUCIBILITY STUDY: CSD DATA AT DIFFERENT SAMPLING TIMES

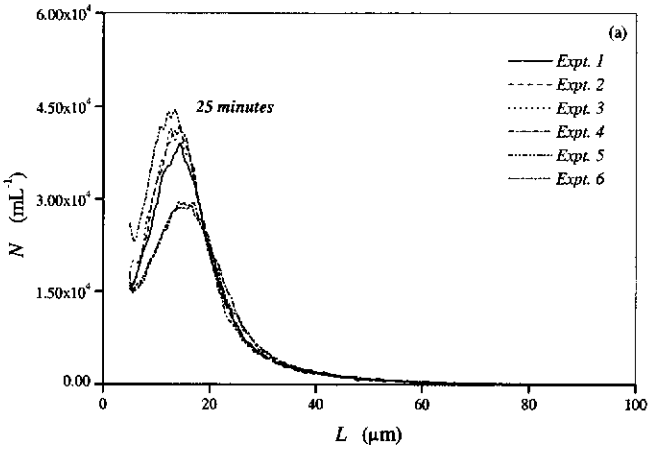

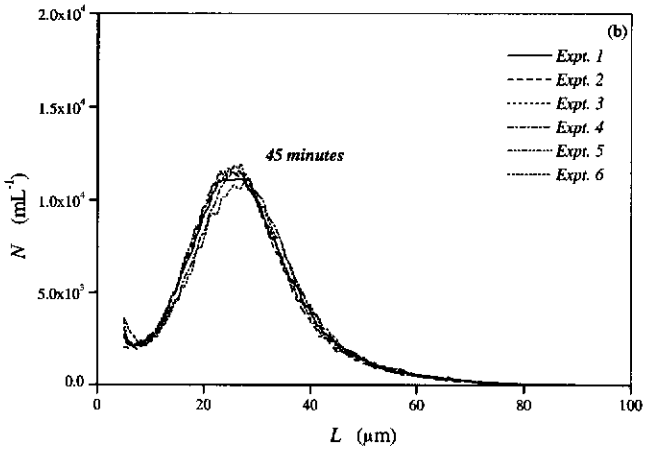

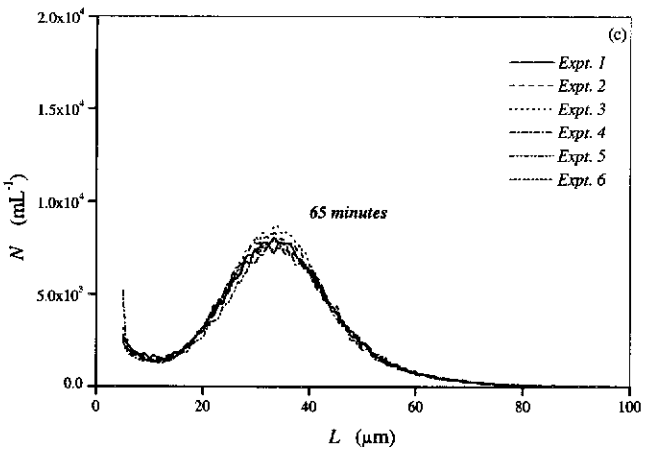

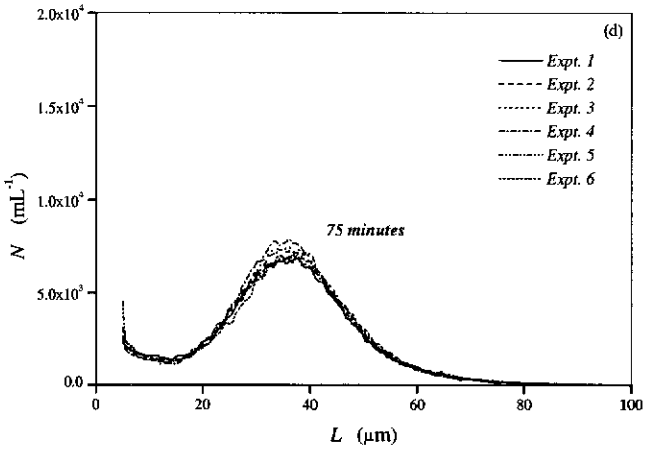
(d)
Expt. 1
Expt. 2
Expt. 3
Expt. 4
Expt. 5
Expt. 6
75 minutes
N (mL-1)
L (μm)

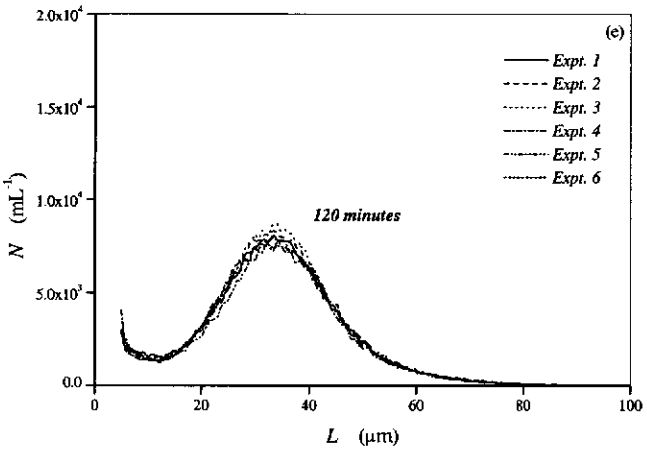
(e)
Expt. 1
Expt. 2
Expt. 3
Expt. 4
Expt. 5
Expt. 6
120 minutes
N (mL-1)
L (μm)

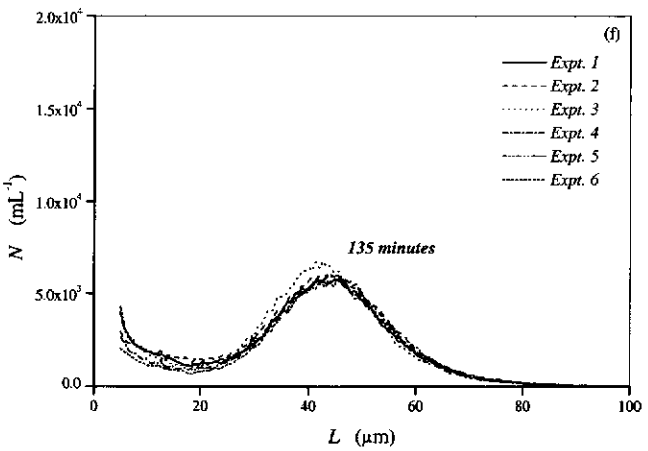
(f)
Expt. 1
Expt. 2
Expt. 3
Expt. 4
Expt. 5
Expt. 6
135 minutes
N (mL-1)
L (μm)

APPENDIX 8: BATCH PRECIPITATION REPRODUCIBILITY STUDY: EXPERIMENTAL DATA

Time	Precipitation Experiment					
min	Batch32	Batch33	Batch34	Batch35	Batch36	Batch37
	Total Crystal Numbers, μ_0 (mL^{-1})					
2	3.59E+06	3.13E+06	3.28E+06	3.27E+06	3.05E+06	3.47E+06
15	1.95E+06	1.90E+06	1.95E+06	1.68E+06	2.01E+06	1.70E+06
25	1.20E+06	1.25E+06	1.27E+06	1.09E+06	1.35E+06	1.05E+06
35	6.55E+05	6.77E+05	6.85E+05	6.26E+05	6.32E+05	6.03E+05
45	5.54E+05	5.43E+05	5.57E+05	5.58E+05	5.64E+05	5.07E+05
55	4.77E+05	4.63E+05	4.67E+05	4.58E+05	4.49E+05	4.58E+05
65	4.37E+05	4.40E+05	4.48E+05	4.58E+05	4.23E+05	4.19E+05
75	3.95E+05	4.13E+05	4.16E+05	4.24E+05	3.96E+05	4.00E+05
90	4.04E+05	4.00E+05	4.22E+05	4.34E+05	3.74E+05	3.94E+05
120	4.04E+05	3.80E+05	3.94E+05	4.11E+05	3.63E+05	4.00E+05
135	3.36E+05	3.68E+05	3.94E+05	3.89E+05	3.54E+05	3.77E+05
	Total Crystal Volume, μ_3 (μm^3 mL^{-1})					
2	1.27E+10	1.19E+10	1.20E+10	1.22E+10	1.18E+10	1.25E+10
15	1.35E+10	1.35E+10	1.38E+10	1.37E+10	1.28E+10	1.38E+10
25	1.53E+10	1.53E+10	1.55E+10	1.60E+10	1.58E+10	1.53E+10
35	1.57E+10	1.54E+10	1.56E+10	1.64E+10	1.37E+10	1.62E+10
45	2.08E+10	1.95E+10	2.02E+10	2.13E+10	2.04E+10	1.99E+10
55	2.35E+10	2.26E+10	2.24E+10	2.24E+10	2.19E+10	2.37E+10
65	2.61E+10	2.61E+10	2.67E+10	2.70E+10	2.47E+10	2.63E+10
75	2.63E+10	2.85E+10	2.90E+10	2.76E+10	2.73E+10	2.85E+10
90	3.11E+10	3.17E+10	3.36E+10	3.25E+10	3.01E+10	3.24E+10
120	3.87E+10	3.50E+10	3.83E+10	3.73E+10	3.54E+10	3.91E+10
135	3.60E+10	3.59E+10	3.91E+10	3.66E+10	3.65E+10	3.83E+10
	Number in the First Discretized Size Interval, N_1 (mL^{-1})					
2	6.05E+05	6.29E+05	6.83E+05	6.41E+05	6.53E+05	7.05E+05
15	9.57E+04	8.73E+04	8.98E+04	7.14E+04	1.15E+05	7.12E+04
25	1.99E+04	1.95E+04	2.25E+04	2.08E+04	3.12E+04	1.88E+04
35	6.23E+03	5.02E+03	6.39E+03	6.81E+03	9.07E+03	5.75E+03
45	3.18E+03	2.47E+03	3.10E+03	3.60E+03	4.04E+03	4.97E+03
55	3.27E+03	2.66E+03	3.71E+03	4.95E+03	4.69E+03	3.11E+03
65	2.97E+03	3.36E+03	3.13E+03	3.77E+03	5.74E+03	2.94E+03
75	2.83E+03	2.98E+03	2.85E+03	3.65E+03	4.93E+03	3.13E+03
90	4.27E+03	3.24E+03	4.62E+03	4.03E+03	5.24E+03	3.00E+03
120	3.59E+03	3.41E+03	3.52E+03	4.09E+03	4.59E+03	3.44E+03
135	2.46E+03	4.73E+03	3.52E+03	4.57E+03	3.22E+03	5.11E+03

Time	Precipitation Experiment					
min	Batch32	Batch33	Batch34	Batch35	Batch36	Batch37
Aluminate Species Concentration, A (g L^{-1} Al_2O_3)						
0	138.1956	138.9189	139.4620	140.1074	138.3668	137.1005
2	138.4869	139.4255	139.4019	140.1886	139.0421	138.5908
15	137.6322	138.6474	139.5669	139.3846	139.0653	137.2832
25	137.4026	138.1790	139.0592	138.1636	138.1723	136.8801
35	134.9350	135.7418	136.9503	136.1047	136.0121	134.4591
45	132.0322	133.1901	132.9944	133.2196	133.2290	131.6155
55	129.5485	130.3886	130.5962	130.1389	130.3704	129.7365
65	127.5943	128.4352	128.2933	128.7408	128.3240	126.8113
75	126.0298	126.4246	126.3861	125.9318	126.2721	125.2454
90	123.3708	124.0609	123.2206	123.1029	123.5072	122.2545
120	118.6313	119.7686	118.4959	119.4597	119.2457	117.3432
135	117.0205	118.0713	117.6844	117.0170	117.1046	116.2996
Caustic Concentration, C (g L^{-1} Na_2CO_3)						
0	194.2481	197.6541	192.9241	198.8457	195.7475	195.4064
2	193.9440	198.5894	194.9407	198.3650	198.1499	196.8972
15	194.6727	198.3369	196.0858	200.8467	198.7402	196.4364
25	194.8885	199.7293	196.5527	199.7021	198.4036	197.7324
35	195.7418	200.0201	195.8546	200.6772	199.8912	198.7077
45	194.0909	199.6387	196.2841	203.0193	199.6362	199.2041
55	196.5256	200.6231	196.7386	201.8644	201.5656	200.1539
65	196.0404	200.8601	198.2501	202.7074	201.0557	200.4480
75	198.5797	202.2367	197.9580	203.3343	202.0131	200.5220
90	197.8812	202.1519	200.7474	202.8258	202.3694	200.3384
120	198.4180	205.0314	200.1094	205.0899	203.1131	200.7050
135	198.6765	202.6279	199.8065	204.4446	204.2832	202.1293
Supersaturation Ratio, A/A^*						
0	1.9714	1.9356	2.0079	1.9363	1.9534	1.9401
2	1.9797	1.9303	1.9791	1.9438	1.9308	1.9411
15	1.9576	1.9228	1.9658	1.9003	1.9233	1.9289
25	1.9514	1.8982	1.9523	1.8983	1.9154	1.9062
35	1.9050	1.8610	1.9320	1.8577	1.8664	1.8600
45	1.8855	1.8308	1.8706	1.7897	1.8313	1.8145
55	1.8191	1.7803	1.8311	1.7620	1.7687	1.7771
65	1.7977	1.7508	1.7803	1.7332	1.7470	1.7335
75	1.7449	1.7074	1.7573	1.6882	1.7079	1.7113
90	1.7163	1.6765	1.6810	1.6560	1.6665	1.6725
120	1.6443	1.5875	1.6236	1.5827	1.6010	1.6013
135	1.6191	1.5904	1.6158	1.5571	1.5599	1.5718

Time	Precipitation Experiment					
min	Batch32	Batch33	Batch34	Batch35	Batch36	Batch37
Solids Content, m (g L^{-1} $Al(OH)_3$)						
2	14.8635	14.7624	15.2679	15.7735	14.9646	14.9646
15	15.8746	15.9757	16.2791	16.7846	15.6724	15.9757
25	17.5935	17.2902	17.7958	18.8069	16.8857	17.7958
35	21.5369	21.5369	21.9414	23.8625	21.0313	22.2447
45	26.5925	26.6936	27.4014	28.6148	25.4803	28.1092
55	31.0415	31.5470	31.3448	33.3670	30.9403	30.7381
65	34.7826	34.2770	35.5915	37.0071	34.3782	36.4004
75	38.0182	37.8160	38.9282	40.3438	38.1193	40.1416
90	42.6694	43.3771	44.4894	44.9949	43.0738	44.7927
120	50.5561	50.5561	51.5672	N/A	52.0728	49.8483
135	53.3873	53.6906	55.1062	56.0162	54.4995	47.8261
Coulter Counter Data, m (g L^{-1} $Al(OH)_3$)						
2	16.2722	15.3085	15.4565	15.6979	15.1844	16.0941
15	17.1285	17.1346	17.4946	17.4454	16.1952	17.5324
25	19.3194	19.3679	19.6194	20.3352	20.0373	19.4495
35	19.9149	19.5037	19.8021	20.7656	17.3868	20.5950
45	26.2798	24.6611	25.5639	26.9894	25.8676	25.2418
55	29.7438	28.6534	28.4425	28.3534	27.7185	30.0990
65	33.0407	33.0502	33.8347	34.2622	31.2655	33.3643
75	33.3632	36.1394	36.7094	34.9945	34.5979	36.1220
90	39.4097	40.1221	42.6408	41.2339	38.2135	41.1115
120	49.0050	44.3941	48.5563	47.3024	44.8645	49.4606
135	45.6695	45.5765	49.5202	46.3418	46.2406	48.5096
Titrator Data, m (g L^{-1} $Al(OH)_3$)						
2	14.3609	14.1225	15.1561	14.9359	14.3778	12.4760
15	15.6270	15.4398	15.2085	16.7832	14.0779	14.2484
25	16.0717	16.1173	16.1526	18.1207	15.4126	14.9900
35	19.8015	19.9279	19.1704	21.2454	19.0432	18.6837
45	23.8099	23.5698	24.5951	25.4939	22.6958	22.5520
55	27.1659	27.3671	28.3264	29.8958	26.8882	25.7625
65	30.2992	30.3548	31.7424	32.1831	29.3968	29.6496
75	33.1893	32.9675	34.4951	36.0120	32.5752	32.1876
90	36.8112	36.7921	39.2200	40.1471	36.4120	36.2423
120	43.2940	43.4459	46.1187	45.9091	42.6116	43.1727
135	46.1224	45.4526	46.9181	49.2126	45.9817	44.6996

Time	Precipitation Experiment					
min	Batch32	Batch33	Batch34	Batch35	Batch36	Batch37
Agglomeration Kernel, β (mL hr^{-1})						
35	2.76E-06	2.40E-06	2.30E-06	2.38E-06	3.15E-06	2.36E-06
45	2.36E-06	2.35E-06	2.17E-06	1.83E-06	2.30E-06	2.36E-06
55	2.48E-06	2.50E-06	2.52E-06	2.40E-06	2.91E-06	2.02E-06
65	2.34E-06	2.32E-06	2.11E-06	1.81E-06	2.76E-06	1.94E-06
75	2.42E-06	2.12E-06	2.03E-06	1.78E-06	2.53E-06	1.85E-06
90	2.00E-06	1.85E-06	1.80E-06	1.40E-06	2.37E-06	1.55E-06
120	1.33E-06	1.48E-06	1.42E-06	1.16E-06	1.72E-06	1.14E-06
Source Term Rate, B_u (mL^{-1} hr^{-1})						
35	1.53E+05	1.22E+05	1.49E+05	1.48E+05	1.96E+05	1.40E+05
45	5.45E+04	4.79E+04	5.94E+04	5.74E+04	6.44E+04	9.53E+04
55	5.05E+04	4.29E+04	6.44E+04	7.68E+04	6.66E+04	5.14E+04
65	4.09E+04	4.72E+04	4.45E+04	4.94E+04	6.77E+04	4.17E+04
75	3.96E+04	3.55E+04	3.84E+04	4.38E+04	5.33E+04	4.14E+04
90	4.84E+04	3.51E+04	5.32E+04	4.03E+04	5.40E+04	3.62E+04
120	3.29E+04	3.22E+04	3.83E+04	3.54E+04	3.93E+04	3.42E+04
Growth Rate, G (μm hr^{-1})						
35	1.47E+01	1.44E+01	1.53E+01	1.42E+01	1.59E+01	1.53E+01
45	1.14E+01	1.17E+01	1.24E+01	1.09E+01	1.13E+01	1.27E+01
55	1.01E+01	1.02E+01	1.14E+01	1.04E+01	1.08E+01	1.06E+01
65	9.10E+00	8.89E+00	9.71E+00	8.52E+00	9.56E+00	9.67E+00
75	8.88E+00	8.10E+00	9.03E+00	8.17E+00	8.72E+00	8.90E+00
90	7.45E+00	7.19E+00	7.77E+00	6.77E+00	7.91E+00	7.74E+00
120	5.82E+00	6.22E+00	6.69E+00	5.69E+00	6.54E+00	6.24E+00

APPENDIX 9: EVALUATION OF THE FLOW CHARACTERISTIC PARAMETERS OF THE POORLY-MIXED BATCH PRECIPITATION SYSTEM

Operating Parameters

Synthetic liquor density @ 80 °C, $\rho_L = 1225$ kg m^{-3}

Synthetic liquor viscosity @ 80 °C, $\mu_L = 1.05 \times 10^{-3}$ kg m^{-1} s^{-1}

Impeller diameter, $D = 6.4 \times 10^{-2}$ m

Impeller speed, $N = 786$ rpm = 13.1 rps

Impeller pumping number, $N_Q = 0.56$

Power number, $N_p = 0.3$

Precipitator working volume, $V = 4 \times 10^{-3}$ m^3

Impeller Power Input,

$$\begin{aligned} P &= N_P \rho_L N^3 D^5 \\ &= 0.3(1225)(13.1)^3(0.064)^5 \\ &= 0.8871 \text{ kg m}^2\text{s}^{-3} \end{aligned} \tag{A9.1}$$

Power per unit volume,

$$\frac{P}{V} = \frac{0.8871}{0.004} = 221.8 \text{ kg m}^{-1}\text{s}^{-3} \tag{A9.2}$$

Reynolds number,

$$\begin{aligned} N_{RE} &= \frac{\rho_L N D^2}{\mu_L} \\ &= \frac{1225(13.1)(0.064)^2}{1.05\times10^{-3}} \\ &= 6.26\times10^4 \end{aligned} \tag{A9.3}$$

Impeller pumping flow,

$$\begin{aligned} Q &= N_Q N D^3 \\ &= 0.56(13.1)(0.064)^3 \\ &= 1.92\times10^{-3} \text{m}^3\text{s}^{-1} \end{aligned} \tag{A9.4}$$

Volume averaged energy dissipation rate,

$$\begin{aligned}\bar{\varepsilon} &= \frac{P}{V\rho_L} \\ &= \frac{221.8}{1225} \\ &= 0.180\ \mathrm{m^2 s^{-3}}\end{aligned} \tag{A9.5}$$

Volume averaged shear rate,

$$\begin{aligned}\bar{\gamma} &= \sqrt{\frac{\bar{\varepsilon}}{\nu}} = \sqrt{\frac{\bar{\varepsilon}\rho_L}{\mu_L}} \\ &= \sqrt{\frac{0.180(1225)}{(0.00105)}} \\ &= 459\ \mathrm{s^{-1}}\end{aligned} \tag{A9.6}$$

APPENDIX 10: POORLY-MIXED BATCH PRECIPITATION EXPERIMENTAL DATA

Time t (min)	μ_0 (mL^{-1})	N_1 (mL^{-1})	μ_1 ($\mu m\ mL^{-1}$)	μ_3 ($\mu m^3\ mL^{-1}$)
2	3.59E+06	6.05E+05	7.65	1.24E+10
25	2.34E+06	1.10E+05	11.56	1.47E+10
35	9.73E+05	1.90E+04	18.43	1.62E+10
35	9.84E+05	1.40E+04	18.70	1.73E+10
45	6.48E+05	1.21E+04	23.31	1.95E+10
55	6.56E+05	1.43E+04	24.50	2.24E+10
55	6.26E+05	1.05E+04	24.90	2.25E+10
55	6.31E+05	1.23E+04	24.90	2.25E+10
75	5.32E+05	1.45E+04	26.60	2.61E+10
75	5.35E+05	1.23E+04	27.50	2.64E+10
90	5.02E+05	9.32E+03	30.14	3.05E+10
120	5.10E+05	1.10E+04	31.73	3.63E+10

Time t (min)	A ($g\ L^{-1}\ Al_2O_3$)	Titration Data m ($g\ L^{-1}\ Al(OH)_3$)	Solids Content m ($g\ L^{-1}\ Al(OH)_3$)	CC Data m ($g\ L^{-1}\ Al(OH)_3$)
2	137.53	14.81	14.81	14.81
15	137.28	15.75	N/A	N/A
25	137.23	17.23	17.00	18.34
35	134.95	19.40	20.35	21.43
35	135.08	19.09	21.02	20.33
45	132.05	24.07	24.21	24.49
55	129.55	26.91	28.98	30.40
55	130.03	26.90	30.45	27.80
55	129.07	26.34	29.92	27.94
65	126.73	32.82	N/A	N/A
75	125.28	33.49	33.53	32.92
75	125.12	33.23	33.40	33.16
90	123.16	37.21	38.40	38.10
120	118.06	44.06	46.82	45.26

Time t min	Product (g)	Scale (g)	β ($mL\ hr^{-1}$)	G ($\mu m\ hr^{-1}$)	B_n ($mL^{-1}\ hr^{-1}$)
25	68.00	1.62	N/A	N/A	N/A
35	81.42	5.50	8.47E-06	1.07E+01	3.13E+05
45	96.82	8.55	2.65E-06	9.20E+00	1.98E+05
55	115.90	8.91	2.27E-06	7.27E+00	1.79E+05
75	134.12	12.61	2.96E-06	6.60E+00	1.71E+05
90	153.60	14.16	2.00E-06	5.39E+00	9.07E+04
120	187.27	12.59	1.54E-06	4.25E+00	8.81E+04

APPENDIX 11: SIMULATION RESULTS: POORLY-MIXED BATCH GIBBSITE PRECIPITATION

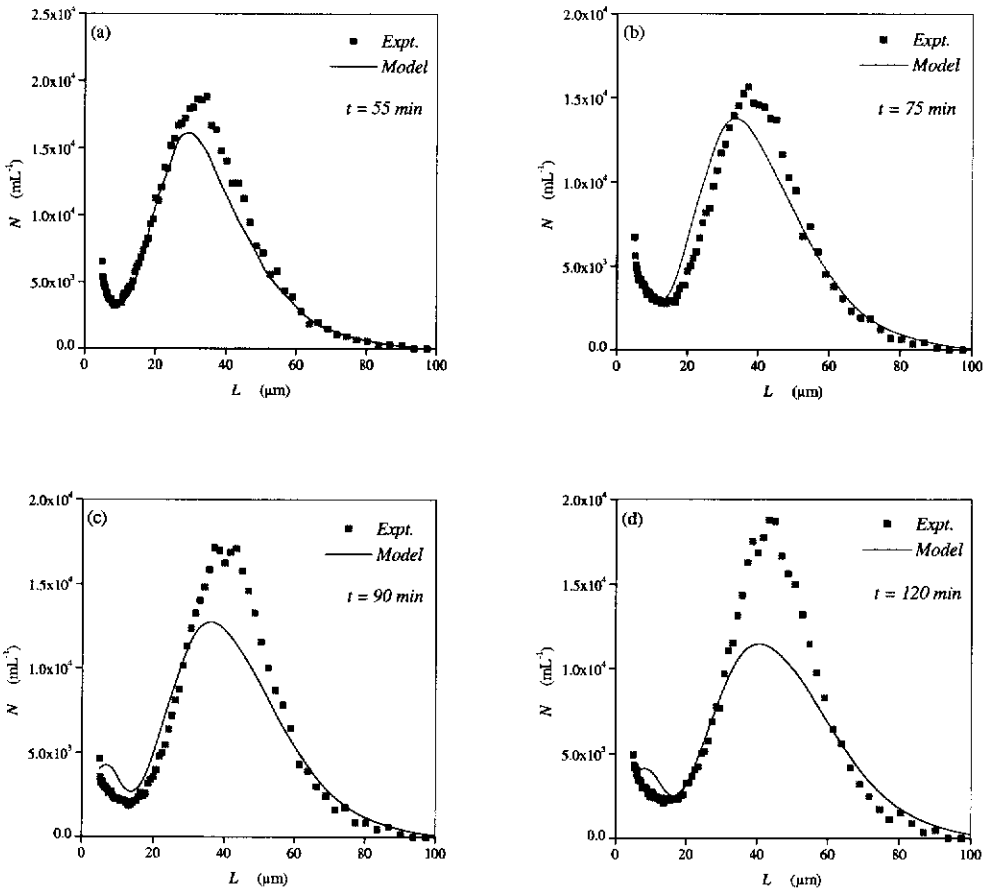

Figure A11.1. Comparisons of the experimental data and model predictions, by the "seed" approach with "bulk averaged" kinetics estimated from the poorly-mixed precipitation data.
(a) 55 minutes; (b) 75 minutes; (c) 90 minutes; and (d) 120 minutes.

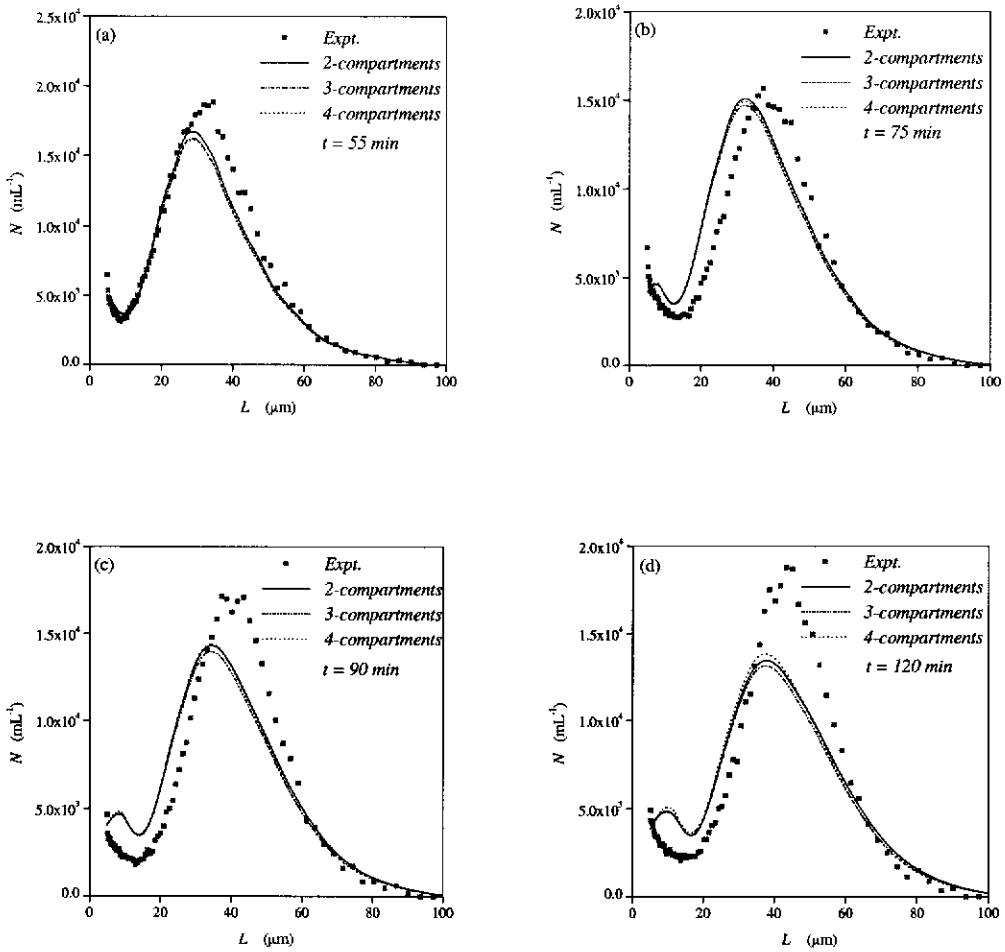

Figure A11.2. Comparisons of the experimental data and model predictions, by the compartmental models with the "seed" approach. (a) 55 minutes; (b) 75 minutes; (c) 90 minutes; and (d) 120 minutes.

Table A11.1. SSE between the experimental data and model predictions for the two, three and four compartmental models, using the "seed" approach.

Modelling Approach	**SSE**			
	t = 55 min	***t = 75 min***	***t = 90 min***	***t = 120 min***
Two Compartments	1.09×10^8	2.85×10^8	3.63×10^8	4.08×10^8
Three Compartments	1.38×10^8	2.72×10^8	3.83×10^8	4.45×10^8
Four Compartments	1.43×10^8	2.84×10^8	3.89×10^8	4.36×10^8

APPENDIX 12: COMPUTER CODE - COMPARTMENTAL MODEL

This computer code is written for simulating inhomogeneous batch gibbsite precipitation system using the compartmental model. The DPB models of Hounslow, Ryall & Marshall (1988) and Litster, Smit & Hounslow (1995) were employed to predict the CSD.

Coder: Tian S. Li
Programming Language: Visual Basic

```
'
'-------------------------------------------------------------------------------
Option Explicit

  Dim agg(1 To 100, 1 To 100), d(1 To 100), Bo(1 To 10), Bu(1 To 100, 1 To 10), flow_
      fv(1 To 10), G, Vc, x, y(1 To 100, 1 To 10), yp(1 To 100, 1 To 10) As Double
  Dim Mtd, Neqn, nz As Integer
'
'-------------------------------------------------------------------------------
Sub Hydro()

  Dim beta(1 to 10), fn(1 to 10), fs(1 To 10), h, k1(1 To 100), k2(1 To 100), _
      k3(1 To 100), k4(1 To 100), RPM, STRD, xe, xf, xi, xo, yn(1 To 100, 1 To 10), _
      yo(1 To 100, 1 To 10), ys(1 To 100), yt(1 To 100) As Double
  Dim i, i1, i2, j, k, ni, nzones, Ndata, Nsize, Nstep As Integer

'-------------------------------------------------------------------------------
'
'                Variables Declaration
'
'agg( ),beta( )    agglomeration kernel (mL/hr)
'Bo ( ), Bu ( )    source term rate (apparent nucleation rate) (/mL/ hr)
'd( )              particle size (microns)
'flow              interchanging flowrate between compartments (mL /hr)
'fn( )             solids fraction in each compartment
'fs( )             energy dissipation rate proportional factor
'fv( )             volume fraction of each compartment
'G                 growth rate (microns/hr)
'h                 time step (hr)
'k?( )             parameters used in RK4 method
'Ndata             number of data
'Neqn              number of equation
'Nstep             number of time step
'nzones            number of compartments
'RPM               stirrer speed (rpm)
'STRD              stirrer diameter (m)
'Vc                precipitator working volume (mL)
'x                 time (hr)
'xf                final time (min)
'xe, xi            initial time (min)
'xo                simulation time duration (hr)
'yo, ys            seed number within size range (/mL)
'yn                calculated number within size range (/mL)
'y, yp             parameters used in RK4
'-------------------------------------------------------------------------------
```

```
'--------------------'
'   Input Data     '
'--------------------'

   Mtd = 2          '(1 for Two-term growth; any number for Three-term growth)
   ni = 4           '(number of simulation steps indicator)
   h = 1/60#
   Ndata = 85
   nzones = 4
   Vc = 4000#
   STRD = 0.064
   RPM = 786

   flow = 0.56*RPM*60*STRD^3*(1000000)

'--------------------'
'   Read Data      '
'--------------------'

   xi = Worksheets("Batch").Range("C5").Offset(0, ni)
   x = xi / 60#

   For k = 1 To ni
      For i = 1 To Ndata
         d(i) = Worksheets("Batch").Range("B5").Offset(i, 0)
        ys(i) = Worksheets("Batch").Range("B5").Offset(i, k+2)
       If d(i) = 0# Then Exit For
      Next i

      Nsize = i - 1

      For i = Nsize + 1 To Ndata
         d(i) = d(i - 1) * 2# ^ (1# / 18#)
        ys(i) = 0#
      Next i

      Neqn = Ndata

      For nz = 1 To nzones
          fn(nz) = Worksheets("Batch").Range("BI75").Offset(0, nz)
          fs(nz) = Worksheets("Batch").Range("BI76").Offset(0, nz)
          fv(nz) = Worksheets("Batch").Range("BI77").Offset(0, nz)
         For i = 1 To Neqn
             yo(i, nz) = fv(nz)*ys(i)
         Next i
      Next nz

      xe = Worksheets("Batch").Range("B5").Offset(0, k + ni)
      xf = Worksheets("Batch").Range("B5").Offset(0, k + ni + 1)
      xo = (xf - xe) / 60#

     Nstep = Int(xo / h + 0.1)


     For i = 1 To Neqn
         yt(i) = 0#
     Next i
```

```
'-------------------------------------------------------------------------'
' Evaluate the derivatives using the fourth order R-K method '
'-------------------------------------------------------------------------'

    For j = 1 To Nstep

'---------------------------------'
' Evaluate kinetics rates '
'---------------------------------'

        For nz = 1 To nzones
            beta(nz) = 0.05*0.0531*x^-1.29*1225^-1.4*(fs(nz)*0.1804)^-1.4/fv(nz)
            Bo(nz) = 163000*fn(nz)*x^-0.91
            G = 7.28*x^-0.74

'-------------------------------------------------------------------------'
' Assigning agglomeration kernel and source term rate '
'-------------------------------------------------------------------------'

          For i1 = 1 To Neqn
              If i1 = 1 Then
                 Bu(i1, nz) = Bo(nz)
              Else
                 Bu(i1, nz) = 0#
              Endif
              For i2 = 1 To Neqn
                  agg(i1, i2) = beta(nz)
              Next i2
          Next i1

'---------------------------------'
' Calling the solver routine '
'---------------------------------'

          Call f(x, yo, nz)
              For i = 1 To Neqn
                  k1(i) = h * yp(i, nz)
                  yn(i, nz) = yo(i, nz) + k1(i) / 2#
              Next i

          Call f(x + h / 2#, yn, nz)
              For i = 1 To Neqn
                  k2(i) = h * yp(i, nz)
                  yn(i, nz) = yo(i, nz) + k2(i) / 2#
              Next i

          Call f(x + h / 2#, yn, nz)
              For i = 1 To Neqn
                  k3(i) = h * yp(i, nz)
                  yn(i, nz) = yo(i, nz) + k3(i)
              Next i

          Call f(x + h, yn, nz)
              For i = 1 To Neqn
                  k4(i) = h * yp(i, nz)
              Next i
```

```
            For i = 1 To Neqn
                yn(i, nz) = yo(i, nz) + (k1(i) + 2# * k2(i) + 2# * k3(i) + k4(i)) / 6#
                yo(i, nz) = yn(i, nz)
            Next i
        Next nz

        x = x + h

        Next j

'-------------------'
' Print Results     '
'-------------------'

        Worksheets("Batch").Range("T5").Offset(0, k+1).Value = x * 60#

        For i  = 1 To Neqn
            For nz = 1 To nzones
                If yn(i, nz) < 0 Then yn(i, nz) = 0#
                  yt(i) = yt(i) +yn(i, nz)
            Next nz
        Next i

        For i  = 1 To Neqn
            Worksheets("Batch").Range("T5").Offset(i, 0).Value = d(i)
            Worksheets("Batch").Range("T5").Offset(i, k+1).Value = yt(i)
        Next i
    Next k

End Sub

'
```

This subroutine evaluates the DPB equations using the methods of Hounslow, Marshall & Ryall (1988) and Wynn (1996).

```
'
```

```
Function f(x, y, nz) As Double

    Dim a, b, r, denom, B1, B2, B3, B4, D1, D2, ya(1 To 100, 1 To 10), _
        yg(1 To 100, 1 To 10) As Double
    Dim i, j, k, lm, p, q, S(1 To 10), Sq As Integer

'
```

```
'-------------------------------------------------------------------------------'
'  Calculate agglomeration terms using the method of Wynn (1996)               '
'-------------------------------------------------------------------------------'

    q = 6

    For k = 1 To q
      S(k) = Int(1 - q * Log(1 - 2 ^ (-k / q)) / Log(2))
    Next k

    Sq = S(1)
    denom = 2# ^ (1 / q) - 1#
```

```
For i = 1 To Neqn
   B1 = 0#
   If (i - Sq >= 1) Then
      For j = 1 To i - Sq
         B1 = B1 + agg(i - 1, j) * y(i – 1, nz) * y(j, nz) * (2# ^ ((j - i + 1) / q)) / denom
      Next j
   End If

   B2 = 0#
   For p = 2 To q
      lm = i - S(p - 1)
      If (lm >= 1) Then
         For j = lm To i - S(p)
            B2 = B2 + agg(i - p, j) * y(i – p, nz) * y(j, nz) * (2# ^ ((j - i + 1) / q) - 1# + _
                 2# ^ (-(p - 1) / q)) / denom
         Next j
      End If
   Next p

   B3 = 0#
   If (i - q >= 1) Then
      B3 = 0.5 * agg(i - q, i - q) * y(i – q, nz) ^ 2#
   End If

   B4 = 0#
   For p = 1 To q - 1
      lm = i + 1 - S(p)
      If (lm >= 1) Then
         For j = lm To i + 1 - S(p + 1)
            B4 = B4 + agg(i - p, j) * y(i – p, nz) * y(j, nz) * (-2# ^ ((j - i) / q) + 2# ^ (1 / q) _
                 - 2# ^ -(p / q)) / denom
         Next j
      End If
   Next p

   D1 = 0#
   If (i - Sq + 1 >= 1) Then
      For j = 1 To i - Sq + 1
         D1 = D1 + agg(i, j) * y(i, nz) * y(j, nz) * (2# ^ ((j - i) / q)) / denom
      Next j
   End If

   D2 = 0#
   If (i - Sq + 2 >= 1) Then
      lm = i - Sq + 2
   Else
      lm = 1
   End If

   For j = lm To Neqn
      D2 = D2 + agg(i, j) * y(i, nz) * y(j, nz)
   Next j

   ya(i, nz) = B1 + B2 + B3 + B4 - D1 - D2

Next i
```

```
'-------------------------------------------------------------------------------------------------------'
' Calculate growth terms using the method of Hounslow, Ryall & Marshall (1988) '
'-------------------------------------------------------------------------------------------------------'

  r = 2# ^ (1# / 18#)

  For i = 1 To Neqn
    If y(i, nz) < 0.000000000000001 Then y(i,nz) = 0#
  Next i

  If Mtd = 1 Then

'-----------------------------------'
' Two-term growth model '
'-----------------------------------'

    a = G / (r - 1#) / d(1)
    yg(1, nz) = -a * y(1, nz)

    For i = 2 To Neqn
      a = G / (r - 1#) / d(i)
      yg(i, nz) = a * (r * y(i – 1, nz) - y(i, nz))
    Next

  Else

'-----------------------------------'
' Three-term growth model '
'-----------------------------------'

    b = r / (r ^ 2# - 1#)
    a = 2# * G / (1# + r) / d(1)

    yg(1, nz) = a * ((1# - r * b) * y(1, nz) - b * y(2, nz))

    For i = 2 To Neqn - 1
      a = 2# * G / (1# + r) / d(i)
      yg(i, nz) = a * (b * y(i – 1, nz) + y(i, nz) - b * y(i + 1, nz))
    Next i

    a = 2# * G / (1# + r) / d(Neqn)
    yg(Neqn, nz) = a * (b * y(Neqn – 1, nz) + y(Neqn, nz))

  End If


'-------------------------------------------------------------------------------------------------------'
' Summation of all contributions to the change in crystal numbers in a size interval '
'-------------------------------------------------------------------------------------------------------'

  For i = 1 To Neqn
    If nz = 1 Then
      yp(i, nz) = ya(i, nz) + yg(i, nz) + Bu(i, nz) _
          + flow * (y(i, 3) / (fv(3) * Vc) - y(i, 1) / (fv(1) * Vc))
    ElseIf nz = 2 Then
      yp(i, nz) = ya(i, nz) + yg(i, nz) + Bu(i, nz) _
          + 0.5 * flow *(y(i, 3) / (fv(3) * Vc) - y(i, 2) / (fv(2) * Vc))
```

```
        ElseIf nz = 3 Then
            yp(i, nz) = ya(i, nz) + yg(i, nz) + Bu(i, nz) + 0.25 * flow * y(i, 4) / (fv(4) * Vc) _
                      + flow * y(i, 1) / (fv(1) * Vc) + 0.5 * flow * y(i, 2) / (fv(2) * Vc)_
                      - 1.75 * flow * y(i, 3) / (fv(3) * Vc)
        ElseIf nz = 4 Then
            yp(i, nz) = ya(i, nz) + yg(i, nz) + Bu(i, nz) _
                      + 0.25 * flow * (y(i, 3) / (fv(3) * Vc) - y(i, 4) / (fv(4) * Vc))
        End If
    Next i

End Function

'
```

APPENDIX 13 : LABORATORY BATCH PRECIPITATION UNIT FOR THE POORLY-MIXED GIBBSITE PRECIPITATION SYSTEM

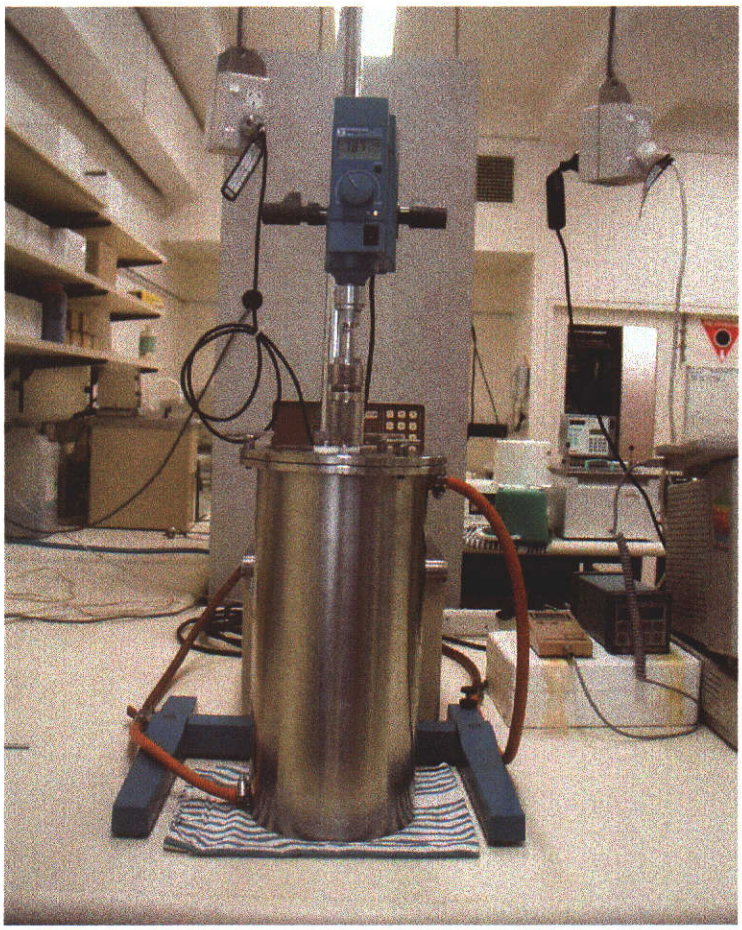

Figure A13. 1. Picture of the poorly-mixed batch gibbsite precipitation experiment in operation.

APPENDIX 14: DECANTATION PROCEDURE FOR REMOVING FINE GIBBSITE CRYSTALS

The decantation procedure employed in the current research to remove fines from the Alcoa C31 gibbsite crystals is outlined as follows;

(1) Select a crystal size to be cut (cut size), i.e. crystals smaller than the nominated size will be removed during the decantation run. A cut size of 20 μm was chosen in the current research.

(2) Determine the time required for crystals to settle at a nominated liquid height using the Stoke's law. A liquid height of 20 cm was used.

(3) Standard 5 litre laboratory glass beakers were used in the decantation runs. For an efficient cut, it is recommended that the crystal's settling height (i.e. liquid height), H, should be greater than the diameter of the beaker, T, used to carry out the decantation, i.e. $H/T > 1.0$.

(4) The solids mass suspended in the liquid should not more than 10% of the liquid mass. 50 g of gibbsite crystals was used in each decantation run in this work.

(5) Suspend the solids with a plunger and ensure that there are no crystal settle at the bottom of the beaker.

(6) Repeat each decantation run at least 4 times.

(7) The speed of the decantation procedure can be improved by carrying out the procedure using a number of beakers in series. In the current research, 5 beakers were used in series.

(8) The recovery of the loading of 50g gibbsite crystals from every four repeated decantations was approximately 75%, i.e. 37.5 g.

Figure A14.1 shows the CSD of the original Alcoa C31 gibbsite seed and the decanted seed produced by the decantation procedure employed. It can be seen that the CSD of the seed has undergone a dramatic changes from an exponential distribution in Figure A14.1(a) to the decanted CSD in Figure A14.1(b). This shows that the decantation procedure is efficient in removing the fine crystals and generating reproducible CSD.

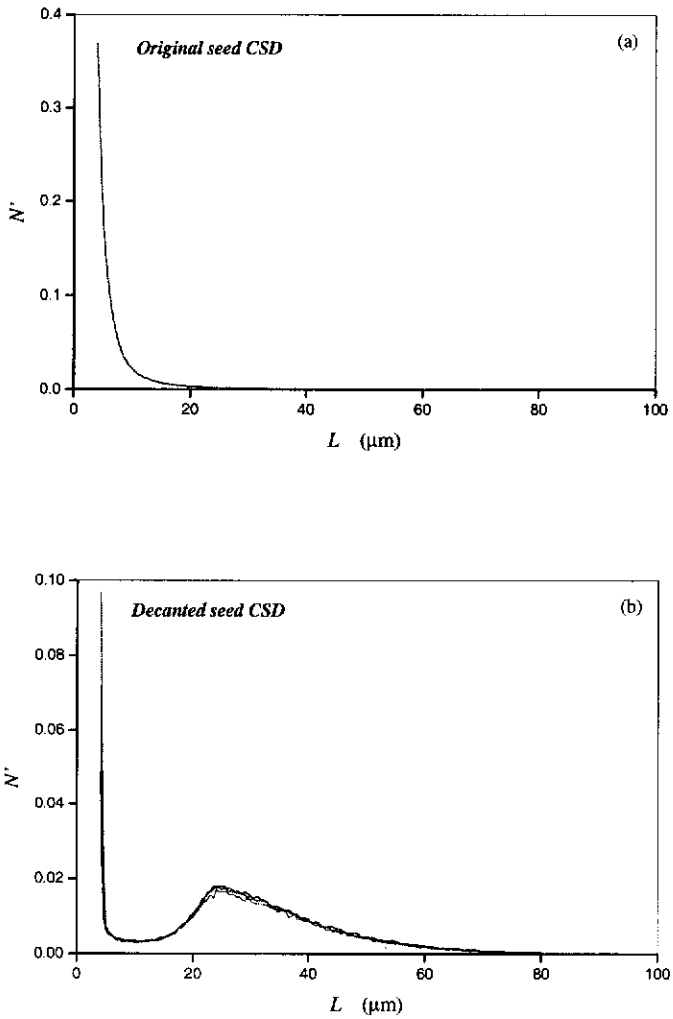

Figure A14.1. (a) Gibbsite seed CSD and (b) decanted seed CSD produced by the decantation procedure employed.